CROSS SECTIONS AND ANALYZING POWERS IN THE 8- TO 17-MeV RANGE FOR NEUTRON SCATTERING FROM $^{54,56}Fe$, $^{58,60}Ni$, ^{93}Nb, AND ^{120}Sn

by

Ronald Scott Pedroni

Department of Physics
Duke University

Date: June 27, 1986

Approved:

Richard L Walter
Richard L. Walter, Supervisor

Edward G. Bilpuch

Harold W. Lewis

Mary Hall

Dissertation submitted in partial fulfillment of the requirements for the degree of Doctor of Philosophy in the Department of Physics in the Graduate School of Duke University

1986

Abstract

(Physics-Nuclear)

CROSS SECTIONS AND ANALYZING POWERS IN THE 8- TO 17-MeV RANGE FOR NEUTRON SCATTERING FROM $^{54,56}Fe$, $^{58,60}Ni$, ^{93}Nb, AND ^{120}Sn

by

Ronald Scott Pedroni

Department of Physics
Duke University

Date: June 27, 1986

Approved:

Richard L. Walter

Richard L. Walter, Supervisor

Edward G. Bilpuch

Harold W. Lewis

[signature]

[signature]

An abstract of a dissertation submitted in partial fulfillment of the requirements for the degree of Doctor of Philosophy in the Department of Physics in the Graduate School of Duke University

1986

ABSTRACT

CROSS SECTIONS AND ANALYZING POWERS
IN THE 8- TO 17-MeV RANGE FOR NEUTRON SCATTERING
FROM $^{54,56}Fe$, $^{58,60}Ni$, ^{93}Nb, AND ^{120}Sn

by

Ronald Scott Pedroni

Using standard time-of-flight techniques, differential cross section $\sigma(\theta)$ and/or analyzing power $A_y(\theta)$ data have been acquired in the 20^o to 160^o angular range for: $^{54,56}Fe$ and $^{58,60}Ni$, for neutron elastic scattering and inelastic scattering to the first 2^+ excited states, and for ^{93}Nb and ^{120}Sn, for neutron elastic scattering. For ^{54}Fe and ^{58}Ni, $\sigma(\theta)$ data were measured at 17 MeV, and $A_y(\theta)$ data were measured at 10, 14, and 17 MeV. For ^{56}Fe and ^{60}Ni, $A_y(\theta)$ measurements were made at 10 MeV. The inelastic scattering $A_y(\theta)$ data for the Fe and Ni isotopes are for only a few selected angles. For ^{93}Nb, $\sigma(\theta)$ data were measured at 8, 10, 12, 14, and 17 MeV, and $A_y(\theta)$ data were measured at 10 and 14 MeV. Also, for ^{93}Nb, nine $\sigma(\theta)$ measurements have been made at 10 MeV for neutron elastic scattering at "small-angles" (1.8^o to 15.9^o). For ^{120}Sn, $A_y(\theta)$ data were measured at 17 MeV.

The absolute normalizations for the $\sigma(\theta)$ measurements are made using n-p scattering measurements. The $\sigma(\theta)$ and $A_y(\theta)$ data are corrected for finite geometry, attenuation, relative efficiency, and multiple scattering effects using Monte Carlo calculations.

The data for $^{54,56}Fe$ and $^{58,60}Ni$ are combined with existing data for these isotopes to expand and refine previous coupled-channel analyses performed using the vibrational model with the ground and first excited states coupled. The ^{93}Nb data are examined using a spherical optical model analysis, and comparisons are made to previous spherical optical model studies. The data for ^{120}Sn are compared only to predictions of a previous coupled-channel analysis.

Also, for incident neutron energies from 2 to 18 MeV, the first multi-bias absolute efficiency measurements are reported for the two main neutron detectors used in measuring the $\sigma(\theta)$ and $A_y(\theta)$ data. The neutron detectors are filled with NE-213 and NE-218 liquid scintillator.

ACKNOWLEDGMENTS

There are many people who have aided me in this work through their knowledge, experience, time, and effort. I hope that I do not inadvertently leave out anyone in acknowledging his participation and in thanking him. First, of course, I would like to thank my research advisor, Dr. Richard L. Walter, for all of his help and understanding and for the guidance he has given me throughout my graduate career, and especially in this work. I am indebted to Dr. Jean-Paul Delaroche for his direction of the coupled-channel analyses of this work. I am also indebted to Dr. Werner Tornow for our discussions of detector efficiencies and for the insight and knowledge that I have gained from him.

The data measurements for this work were made in a series of experiments over a period of several years. I would like to thank the members of the neutron time-of-flight group who participated in these experiments and who insured that the highest possible quality was obtained and without whom the experiments could not have been undertaken: Dr. Calvin Howell, Dr. Roger Byrd, Dr. Gerry Honoré, Harold Pfützner, Mark Roberts, Dr. Garry Tungate, Dr. Kim Murphy, Dr. Carey Floyd, and Dr. Paul Guss. I would also like to thank Dr. F.O. Purser, Dr. L.W. Seagondollar, Dr. C.R. Gould, Dr. Gail Glendinning, Dr. Al Beyerle, and Dr. Sadiq El-Kadi, previous members of the neutron time-of-flight group, who aided me in learning the ropes in my early years in graduate school. I am also grateful to the participants of the of the small-angle scattering measurements: Dr. R.E. Anderson, Dr. C.R. Gould, Dr. B.C. Karp, K.E. Nash, and H.G. Pfützner.

A special thanks goes to Mike Bailey who made all the drawings and diagrams in this work. Thanks also go to Pat Gibson and Pauline McCrary the

secretaries of TUNL, Bob Rummel and Paul Carter who keep the accelerator and laboratory equipment running, Sidney Edwards and the electronics shop staff, Al Lovett and the machine shop staff, the library staff, and the secretaries of the Physics Department.

I would also like to thank Dr. Gerry Honoré, Dr. Philippe Martin, Harold Pfützner, and my mother for proofreading the various iterations of this work.

Finally, and most importantly, I would like to thank my mother and father and my brother, Gary, who made this work possible through their love, understanding, support, and encouragement through many adversities.

Work supported by the U.S. Department of Energy Director of Energy Research, Office of High Energy and Nuclear Physics, under Contract No. DE-AC05-76ER01067.

T.G.B.T.G.

TABLE OF CONTENTS

LIST OF FIGURES

LIST OF TABLES

CHAPTER 1

INTRODUCTION

Neutrons are a unique probe of the nuclear force, since the neutron-nucleus interaction is not complicated by the effects of the Coulomb force, as is the proton-nucleus interaction. Also, knowledge of the neutron-nucleus interaction is important because there are many technological and theoretical applications for differential cross section $\sigma(\theta)$ data for neutron scattering. For example, one important application today is in the construction of fusion power generators. The neutron cross sections of the materials used in the construction of such devices must be known at energies below 20 MeV in order to determine the structural radiation damage and contamination due to the high flux of neutrons emitted from the fusion reaction . In this dissertation, $\sigma(\theta)$ data are presented for neutron elastic scattering from ^{93}Nb and for neutron elastic and inelastic scattering for ^{54}Fe and ^{58}Ni, all of which are important in fusion reactor design studies. The data for ^{54}Fe and ^{58}Ni are extensions to 17 MeV of measurements made by Guss et al. (Guss 1985) and by El-Kadi et al. (El-Kadi 1982), as explained later.

Theoretical applications for the $\sigma(\theta)$ data are for testing the predictions of various nuclear models and for developing refinements to these models based on the results of such tests. One importance of the new $\sigma(\theta)$ data is the ability to determine better the energy dependencies of the surface and volume absorptive potentials in optical model studies.

In conjunction with model tests, data for the analyzing power $A_y(\theta)$ for neutron scattering are very important, since these types of data give us

information about the spin-orbit interaction associated with the nuclear force. Also, $A_y(\theta)$ data place additional constraints on models developed on only $\sigma(\theta)$ information. The $A_y(\theta)$ measurements reported in this work are for neutron elastic scattering for ^{93}Nb and ^{120}Sn and for neutron elastic and inelastic scattering for $^{54,56}Fe$ and $^{58,60}Ni$. Here, too, the data for $^{54,56}Fe$, $^{58,60}Ni$, and ^{120}Sn are extensions of previous measurements (Guss 1982b, 1985, and 1986; El-Kadi 1982; and Floyd 1983). For ^{93}Nb, the $A_y(\theta)$ measurements are the first ever made.

Although the present work had two main goals -- the determination of differential cross section and/or analyzing power data and the use of the acquired data in model analyses for neutron elastic and inelastic scattering, the project is composed of many diverse parts. The data were acquired using time-of-flight techniques at the Triangle Universities Nuclear Laboratory (TUNL) located at Duke University. A brief outline of this dissertation follows.

The first multi-bias measurements at TUNL of the detection efficiencies of the two main neutron detectors used for measuring $\sigma(\theta)$ and $A_y(\theta)$ data are described in chapter 3. These measurements used the calibrated $^{2}H(d,n)^{3}He$ neutron source reaction and covered the neutron energy range from 2 to 18 MeV. The data are compared to efficiency calculations based in part on known n-p and n-^{12}C interaction cross sections. The measurements for an energy bias corresponding to recoil proton energies of about 2 MeV are compared with those of El-Kadi (El-Kadi 1981), which were the previous standard calibration at TUNL. Problems concerning the new measurements are discussed, and recommendations are made for future extensions of similar measurements at TUNL.

The experimental equipment and procedures used in taking most of the $\sigma(\theta)$ and $A_y(\theta)$ data are briefly described in chapter 2. The data stripping, normalization, and correction procedures for $\sigma(\theta)$ and $A_y(\theta)$ data are discussed in chapter 4. The final corrected $\sigma(\theta)$ data are shown with Legendre polynomial fits, and the final corrected $A_y(\theta)$ data are displayed with fits derived from associated Legendre polynomial fits to the product $A_y(\theta) \times \sigma(\theta)$. The $\sigma(\theta)$ data reported in the present work are for elastic scattering at 8, 10, 12, 14, and 17 MeV for ^{93}Nb and for elastic and inelastic scattering at 17 MeV for ^{54}Fe and ^{58}Ni. The $A_y(\theta)$ measurements are for elastic scattering at 10 and 14 MeV for ^{93}Nb; for elastic and inelastic scattering at 10, 14, and 17 MeV for ^{54}Fe and ^{58}Ni; for elastic and inelastic scattering at 10 MeV for ^{56}Fe and ^{60}Ni; and for elastic scattering at 17 MeV for ^{120}Sn. With our technique and for the accelerator time devoted to these projects, it was only possible to obtain significant data for inelastic scattering to the lowest-lying excited state, which happens to be the first 2^+ state for the Fe and Ni nuclei. Also, for these four nuclei, $A_y(\theta)$ data for inelastic scattering were measured at only a few selected angles as a complement to the earlier studies of Guss et al. (Guss 1982b).

The level schemes of the six nuclei for which data were obtained and the related nucleus ^{116}Sn are given in figure 1.1. The Q-values, spins and parities, and level diagrams used in this work are taken from the information in the text of Browne et al. (Browne 1978). As can be seen from figure 1.1, inelastic scattering measurements for ^{93}Nb would be very difficult due to the density and spacing of the excited states; no such data are reported here. However, the elastic scattering data reported in the

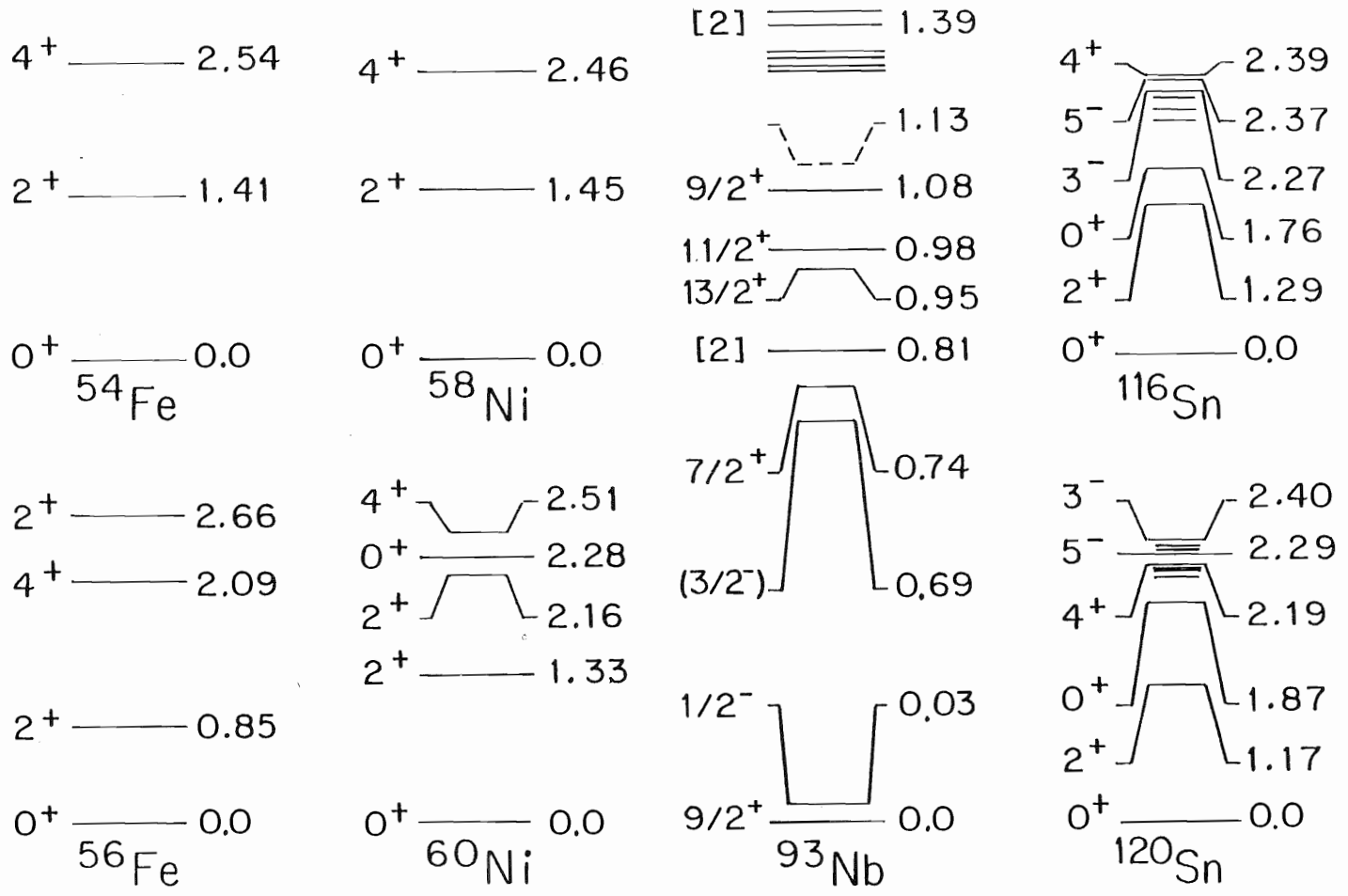

Figure 1.1. Level diagrams for $^{54,56}Fe$, $^{58,60}Ni$, ^{93}Nb, and $^{116,120}Sn$. The information for the diagrams comes from Browne 1978. Note that the levels given are only some of the lower lying levels.

present work for ^{93}Nb have a small contaminant contribution from inelastic scattering to the first excited state of ^{93}Nb; unfortunately, this state at 0.03 MeV is too close to resolve from the ground state with the present level of technology for neutron scattering experiments.

Additional $\sigma(\theta)$ data were obtained as a by-product of an unfinished development project at TUNL to obtain data for neutron scattering at small angles, that is, in the angular range between 0° and 16°. The technique utilized the unique small-angle collimator of Bucher and Hollandsworth (Bucher 1973), which is presently located at TUNL. A discussion of the specialized experimental equipment and procedures for small-angle $\sigma(\theta)$ measurements is contained in chapter 5. The system was used to obtain data for ^{93}Nb at nine angles between 1.8° and 15.9° for neutron elastic scattering at 10 MeV.

Briefly summarizing, there were several reasons for the decision to measure the broad range of data contained in this work. The data for the Fe and Ni isotopes were taken as an extension of previous work at TUNL for ^{54,56}Fe and ^{58,60}Ni (El-Kadi 1982, Floyd 1983, and Guss 1982b and 1985). The $\sigma(\theta)$ and $A_y(\theta)$ data for ^{54}Fe and ^{58}Ni at 17 MeV are the first at this energy for these isotopes; they help to fill the gaps in existing data between 14 and 20 MeV for ^{54}Fe and between 14 and 24 MeV for ^{58}Ni. As indicated above, the new $A_y(\theta)$ data for ^{54}Fe and ^{58}Ni at 10 and 14 MeV, as well as the new $A_y(\theta)$ data at 10 MeV for ^{56}Fe and ^{60}Ni, represent an attempt to obtain several high quality measurements to supplement those of Guss et al. (Guss 1982b). The data for ^{93}Nb, together with the companion data for ^{89}Y of Honoré (Honoré 1986a), fill a gap in the mass range between ^{60}Ni and ^{116}Sn in the extensive neutron scattering measurements that have been

carried out at TUNL in the past. The $A_y(\theta)$ data at 17 MeV for ^{120}Sn complement the $\sigma(\theta)$ data of Guss (Guss 1986) for ^{120}Sn at the same energy, as well as his 10 and 14 MeV distributions of $\sigma(\theta)$ and $A_y(\theta)$ data for $^{116,120}Sn$. All of these new data will assist in the ongoing program at TUNL to obtain an understanding of neutron-nucleus scattering for nuclei throughout the entire periodic table.

The optical model analyses of the data followed several approaches, each specific to the structure of the individual nuclei. For ^{93}Nb, spherical optical model (SOM) calculations are presented in chapter 6. The $\sigma(\theta)$ and $A_y(\theta)$ data for ^{93}Nb are first compared to predictions from calculations using the global SOM parameters of Walter and Guss (Walter 1985) and Rapaport, Kulkarni, and Finlay (Rapaport 1979) and the SOM parameters of Lagrange and Lejeune (Lagrange 1982) for ^{93}Nb. Then, using the global parameters of Walter and Guss as a starting point, searches of the ^{93}Nb data are performed to obtain optimum energy-dependent SOM parameters for the 7- to 20-MeV range, which are specific to ^{93}Nb.

The optical model analyses of the Fe, Ni, and Sn data use the coupled-channel (CC) approach. Such calculations for $^{54,56}Fe$, $^{58,60}Ni$, and ^{120}Sn are described in chapter 7. An introduction to the CC calculations is given in the section 7.1. Calculations for ^{58}Ni are explored in section 7.2. This analysis of ^{58}Ni is an extension of the CC analysis for $^{58,60}Ni$ of Guss et al. (Guss 1985) and includes the new ^{58}Ni data with the data base used by Guss. The main aim of this analysis is to explore further the energy dependencies of the imaginary surface and volume potentials, W_D and W_V, respectively. The final parameters derived in section 7.2 for ^{58}Ni are used as a starting point for determining parameters for ^{54}Fe in section 7.3. The

calculations for ^{54}Fe are based on the data of this work, as well as the $\sigma(\theta)$ data of El-Kadi et al. (El-Kadi 1982) and of Mellema (Mellema 1983a), and the $A_y(\theta)$ data of Floyd et al. (Floyd 1983). The total cross sections of Larson et al. are also included in the analysis. The new $A_y(\theta)$ data for inelastic scattering for all four isotopes are compared to CC calculations in section 7.4. These calculations explore the relationship between the spin-orbit deformation lengths δ_{SO} and the central potential deformation lengths δ_C. The study of this relationship is an extension of the work of Guss et al. (Guss 1982b). Comparisons of $A_y(\theta)$ data for the elastic scattering of 17 MeV neutrons from ^{120}Sn and predictions from calculations using the CC parameters of Guss et al. (Guss 1986) are presented in section 7.5. Time constraints prohibited new CC or SOM analyses for ^{116,120}Sn from being made for this dissertation.

There are five appendices to this work. Tabulations of the $\sigma(\theta)$ data and associated experimental parameters, together with the coefficients and parameters from Legendre polynomial fits to the data, are presented in appendix A. Tabulations of the $A_y(\theta)$ data and associated experimental parameters, together with the coefficients and parameters from associated Legendre polynomial fits to the data, are given in appendix B. New tabulations of the $\sigma(\theta)$ and $A_y(\theta)$ data for ^{116,120}Sn obtained at TUNL by Guss (Guss 1982a) are presented in appendix C. The data of Guss had to be revised due to an error in the number of nuclei per volume used in the multiple scattering corrections. As with appendices A and B, Legendre polynomial fits for the data distributions are presented for the Sn isotopes in appendix C. An explanation of the procedures used to calculate the "polyethylene correction factors", which are needed for the normalization of

the $\sigma(\Theta)$ data, is given in appendix D. Finally, tabulations of the multi-bias efficiency data for the two main neutron detectors are presented in appendix E.

CHAPTER 2

EXPERIMENTAL TECHNIQUE

2.1 Introduction

Neutron time-of-flight methods have long been employed at the Triangle Universities Nuclear Laboratory in making neutron cross section measurements and, in recent years, in making analyzing power measurements. For the most part, both types of measurements are made using the same equipment and following similar procedures, the main exceptions being in the production of the neutron beams. Most of the time-of-flight equipment and procedures used have been extensively documented in dissertations and publications: Beyerle 1981, Bucher 1973, Byrd 1978, El-Kadi 1981 and 1982, Floyd 1981 and 1983, Glendinning 1980, Guss 1982a, Hogue 1977a, Howell 1984, and Lisowski 1973 and 1975. In this work, descriptions will only be given for techniques that are either essential or new.

The floor plan of the accelerator laboratory is shown in figure 2.1. The neutron time-of-flight target room appears in the lower right corner of the figure. The two main detectors are the most prominent features in the target room.

The data measured in the $\sigma(\theta)$ and $A_y(\theta)$ experiments are in the form of time-of-flight spectra. A time-of-flight spectrum is a histogram of the number of neutrons detected versus the time-of-flight as represented by channel numbers. The channels correspond to time bins of equal widths into which events are sorted. The channels are typically about 0.017 ns for the $\sigma(\theta)$ experiments and 0.35 ns for the $A_y(\theta)$ experiments. Scattering to a discrete state of a nucleus produces a peak in the time-of-flight spectrum

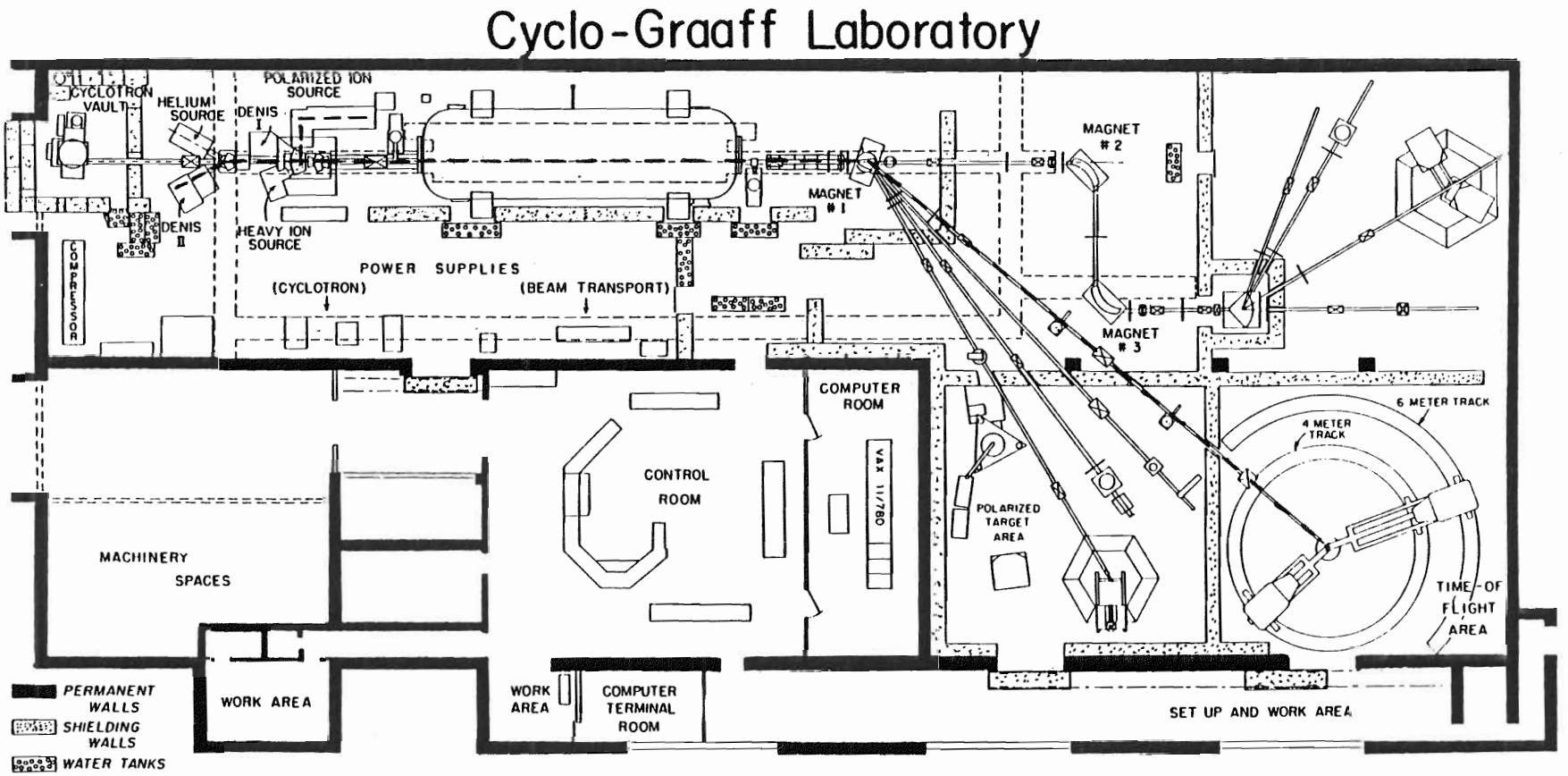

Figure 2.1. Floor plan of the accelerator laboratory. The heavy dashed lines represent the paths from the two ion sources used in the neutron time-of-flight experiments.

at the time-of-flight corresponding to the energy of the scattered neutron. The separation between peaks representing scattering to different nuclear states is determined by the full-width-at-half-maximum (FWHM) of the beam bursts, the flight paths of the detectors, and the excitation energies of the states of the target nucleus.

2.2 Neutron Beam Production

2.2.1 Cross Section Measurements

In taking $\sigma(\theta)$ data for neutron scattering, a 50 keV d.c. beam of deuterons is produced using a direct extraction negative ion source (DENIS-II)(see figure 2.1). This beam is then chopped and bunched to produce a pulsed beam having a repetition rate of 2 MHz. The chopping and bunching techniques are described in detail in Howell 1984. The beam is injected into a FN tandem Van de Graaff accelerator where it is accelerated to the required energy. After exiting the accelerator, the beam is steered into the neutron time-of-flight target room where it bombards a deuterium-filled gas cell. This results in a high intensity cone of nearly mono-energetic neutrons centered at 0^{o}, since the cross section for the $^{2}H(d,n)^{3}He$ reaction is very forward-peaked. One advantage of using the $^{2}H(d,n)^{3}He$ reaction is that the neutrons emitted have energies higher than the bombarding deuterons, since the reaction has a Q-value of +3.269 MeV. The choice of the $^{2}H(d,n)^{3}He$ reaction as the best source of neutrons for $\sigma(\theta)$ (and $A_{y}(\theta)$) experiments in the 8- to 17-MeV energy range is explained in both Guss 1982a and Howell 1984. Deuteron-beam currents of about 2 μA are incident on the gas cell for most $\sigma(\theta)$ experiments.

2.2.2 Analyzing Power Measurements

A Lamb-shift polarized ion source (see figure 2.1) is used to produce a polarized beam of deuterons that is bunched to form a pulsed beam with a repetition rate of 4 MHz. The bunching is done with the three-stage buncher system described in Howell 1984. This beam is accelerated to the proper energy by the tandem Van de Graaff accelerator and steered into the neutron time-of-flight target room, where it enters a deuterium-filled gas cell. The $^{2}H(\vec{d},\vec{n})^{3}He$ polarization-transfer reaction yields a polarized beam of nearly mono-energetic neutrons at 0^{o}. The beam of deuterons typically has an intensity of about 150 nA and a polarization of 60%, of which approximately 90% is transferred to the neutron beam (Lisowski 1975).

2.2.3 Deuterium Gas Cells

Three gas cells were used in taking the data contained in this work: gas cells A and B (shown in Guss 1982a) and gas cell C (shown in figure 2.2). The gas cells are electrically isolated from the beam pipe so that beam-current integration can be used as a monitor of the number of deuterons incident on the gas targets. For $A_{y}(\theta)$ measurements, beam-current integration is used for normalization purposes. The outer walls of all three cells are constructed of stainless steel. The side walls of the cells are lined with 0.38 mm thick tantalum sleeves. The beam stops or liners for the exit walls of the cells are made of 0.51 mm thick tantalum. The tantalum sleeves and beam stops prevent deuterons from escaping the gas cell, a requirement for good beam-current integration, and also prevent (d,n) reactions in the stainless steel walls and the air immediately surrounding the gas cells.

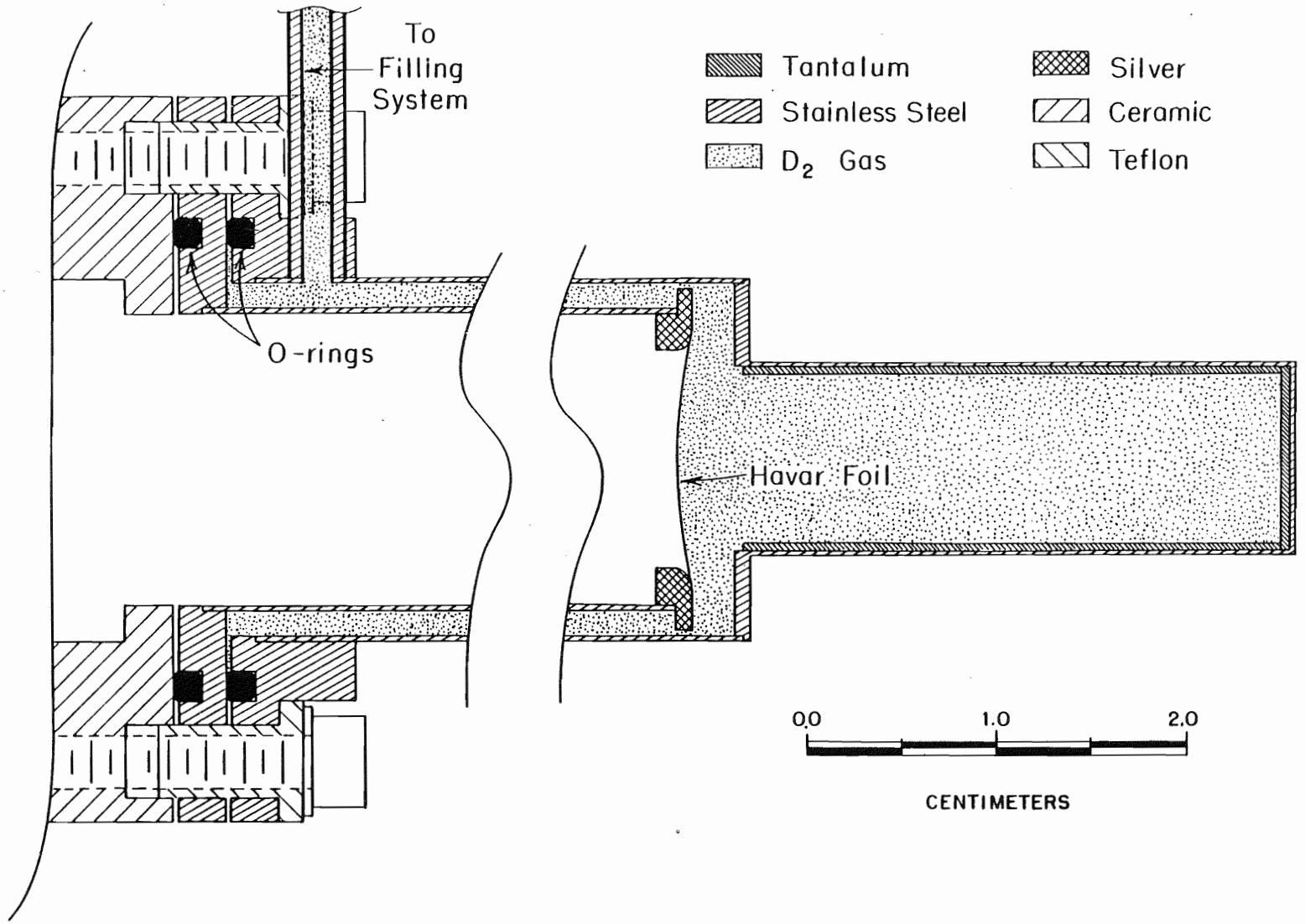

Figure 2.2. Longitudinal view of gas cell C.

Gas cell A, which has a 2.92 cm long gas volume and can be pressurized to a maximum of 3.0 bar, was used for $\sigma(\theta)$ measurements made before the spring of 1981. A deuterium gas pressure of only 2.0 bar is needed in gas cell A in order to produce reasonable neutron counting rates when using a 2 μA intensity deuteron beam. A 3.5 μm thick molybdenum foil is used as the entrance wall that retains the gas in the cell.

Gas cell B, which has a 5.08 cm long gas volume and can be pressurized to a maximum of 6.1 bar, was used for $A_y(\theta)$ measurements made prior to the spring of 1981. With cell B, a gas pressure of 4.1 bar is required to produce enough neutrons for reasonable counting rates when using polarized beams of deuterons, which have average intensities of only 150 nA. The entrance wall for gas cell B is 6.35 μm thick Havar foil.

In the spring of 1981, a decision was made to use one gas cell for both types of measurements, thus facilitating the change from one type of experiment to the other. Neither gas cell A nor B could be used to do this, since their physical specifications limited their use to the experiments for which they were designed. Therefore, G. Tungate designed gas cell C to replace the other cells. This cell has a 3.16 cm long gas volume and can be pressurized to a maximum of about 3.5 bar when using a 3.5 μm thick molybdenum foil and to a maximum of over 15.2 bar when using a 6.35 μm thick Havar foil. The gas cell is usually pressurized to 2.0 bar for $\sigma(\theta)$ experiments (using either a molybdenum or a Havar foil) and to 7.9 bar for $A_y(\theta)$ experiments (using a Havar foil). The thinner molybdenum foil is more desirable than the Havar foil due to energy-spread considerations.

2.3 Neutron Time-of-Flight Spectrometer Facility

The time-of-flight spectrometer facility (see figures 2.3 and 2.4) consists of two main detectors, the right (4-m) and left (6-m) detectors. Directions are as seen by the beam incident on the scattering sample. In addition, there are two detectors that are used to monitor the pulse timing and the neutron flux. Note that in later references to the scattering plane, we mean the horizontal plane (the X-Z plane of figure 2.4) defined by the axes of the right and left detectors and the deuteron beam. Note also that the direction of travel of the deuteron beam defines 0^{o} (the Z-axis of figure 2.4), and left and right directions are defined relative to 0^{o}.

All of the detectors are liquid organic scintillators contained in cylindrical glass housings and coupled to photomultiplier tubes. The liquid scintillator used in the right detector and neutron flux monitor detectors is NE-218, while the scintillator used in the other two detectors is NE-213. Both types of scintillators provide good pulse-shape-discrimination (PSD) between γ-rays and neutrons (see chapter 3 and Howell 1984).

The right and left detectors are mounted inside massive shields located on movable carts that give both detectors angular ranges from 0^{o} to 162^{o}. These detectors both have adjustable flight paths, defined to be the straight line distances from the center of the scattering sample to the centers of the liquid scintillators. The range of flight paths for the right detector is from 2.77 to 3.76 m, while that for the left detector is from 3.76 to 5.70 m. Most of the data in this work were taken at the maximum detector flight paths. Note that with the detectors at their longest flight paths, the minimum angle for simultaneous measurements with both detectors at equal angles is 16^{o}. The scintillator volumes of both the

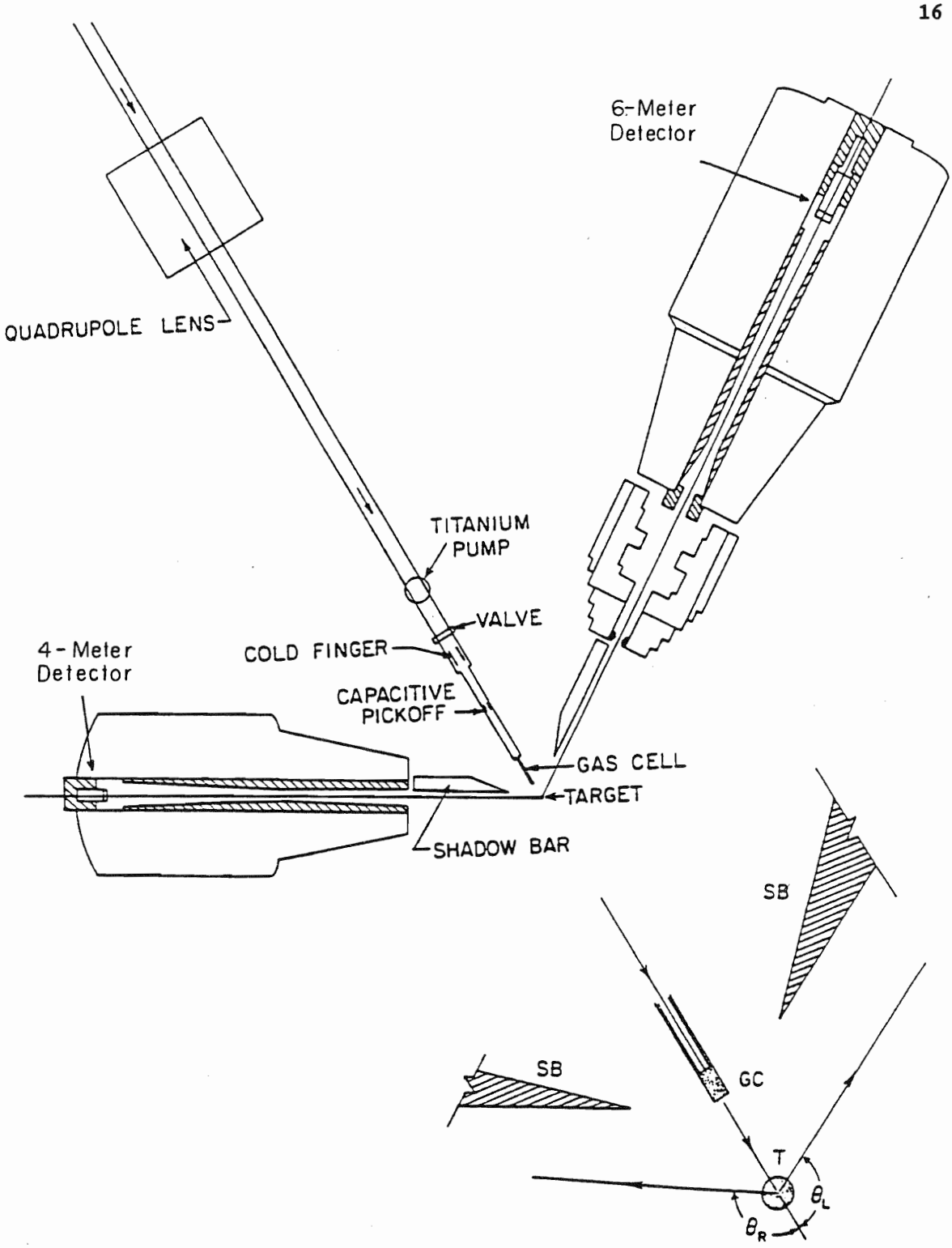

Figure 2.3. Arrangement of the neutron time-of-flight spectrometer facility.

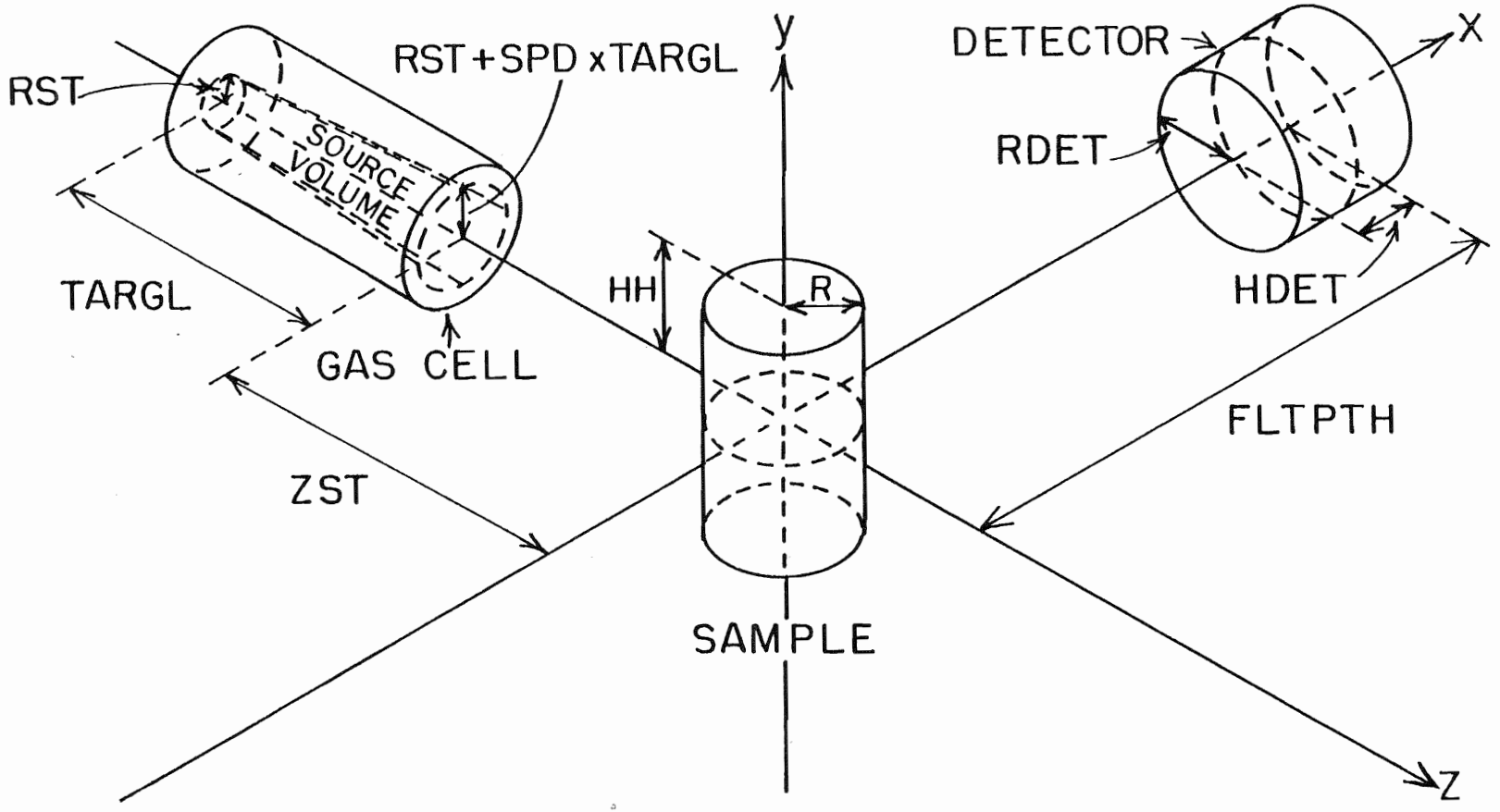

Figure 2.4. Schematic of the gas cell, sample, and detector geometries. The labeled parameters are used in multiple scattering calculations. RST is the radius of the beam at the entrance to the gas volume. SPD is the increase in the radius per unit length of the gas volume. TARGL is the length of the gas volume. ZST is the distance from the end of the gas volume to the center of the sample. R and HH are the radius and half height of the scattering sample, respectively. FLTPTH is the flight path of the detector. RDET and HDET are the radius and half thickness of the detector, respectively.

right and left detectors are 5.08 cm thick, and they have radii of 4.44 and 6.35 cm, respectively. The symmetry axes of these cylindrical volumes point in the direction of the vertical axis of rotation of the carts (see figure 2.4). The outer casings for the detector shields are modified storage containers for jet aircraft engines. The casings are filled with paraffin loaded with lithium carbonate and have large copper collimators at their front faces. The detectors are located inside the shields at the ends of long double-truncated conical throats. The left detector also has an additional collimator pre-shield made of copper. The purpose of the shields is to block background radiation, such as air- and wall-scattered neutrons, from the detectors. Both detector carts have tungsten shadow bars mounted near the pivot points. These shadow bars are used to hide the direct flux of neutrons from the organic scintillators, and also to shield the detector casing.

The timing monitor is located near 0^{o} in the scattering plane with its cylindrical axis pointing at the gas cell and has a flight path of about 4 m. This detector is used as a monitor of the time widths of the beam bursts. The buncher and chopper are tuned to produce the most narrow full-width-at-half-maximum (FWHM) possible for the neutron peak in the time-of-flight spectra of the timing monitor. Also, tails on the right and left of this neutron peak are minimized using the chopper and buncher system. The beam bursts typically have FWHM of 2 ns, although FWHM of 1.5 ns have been obtained (Howell 1984).

The neutron flux monitor is suspended from the ceiling of the target room and is used to monitor the direct neutron flux from the gas cell for normalization purposes in cross section experiments. This detector is

housed in a massive copper shield that has a narrow double-truncated conical throat. The detector is suspended from the ceiling of the target room above the radial axis of the scattering plane at left 15^{o}. The cylindrical axis of this detector points directly at the gas cell and has an angle of inclination with the scattering plane of about 50^{o}. The detector has a flight path of about 2 m.

Another important part of the spectrometer facility is a cylindrical capacitive pick-off, located in the beam pipe about 46 cm before the gas cell (see figure 2.3). See section 2.1.5 of Howell 1984 for a description of the pick-off system.

The scattering samples used in the spectrometer facility are right circular cylinders (see figure 2.4), oriented so that their axes of symmetry are perpendicular to the scattering plane. The samples are suspended by thin wires so that their axes coincide with the axis of the pivot point of the right and left detectors. The samples are positioned so that they are vertically centered in the neutron flux from the gas cell (the X-Z plane splits the sample in half).

2.4 Electronics

The electronics used for each detector is shown in figure 2.5. Descriptions of the detector electronics are given by Howell (Howell 1984) and Beyerle (Beyerle 1981). The input and output signals from the various electronic modules are shown in Beyerle 1981.

The electronics are used to set two conditions on events before they are included in the time-of-flight spectra. First, the energy deposited in the detector due to the event must be greater than an energy bias. The

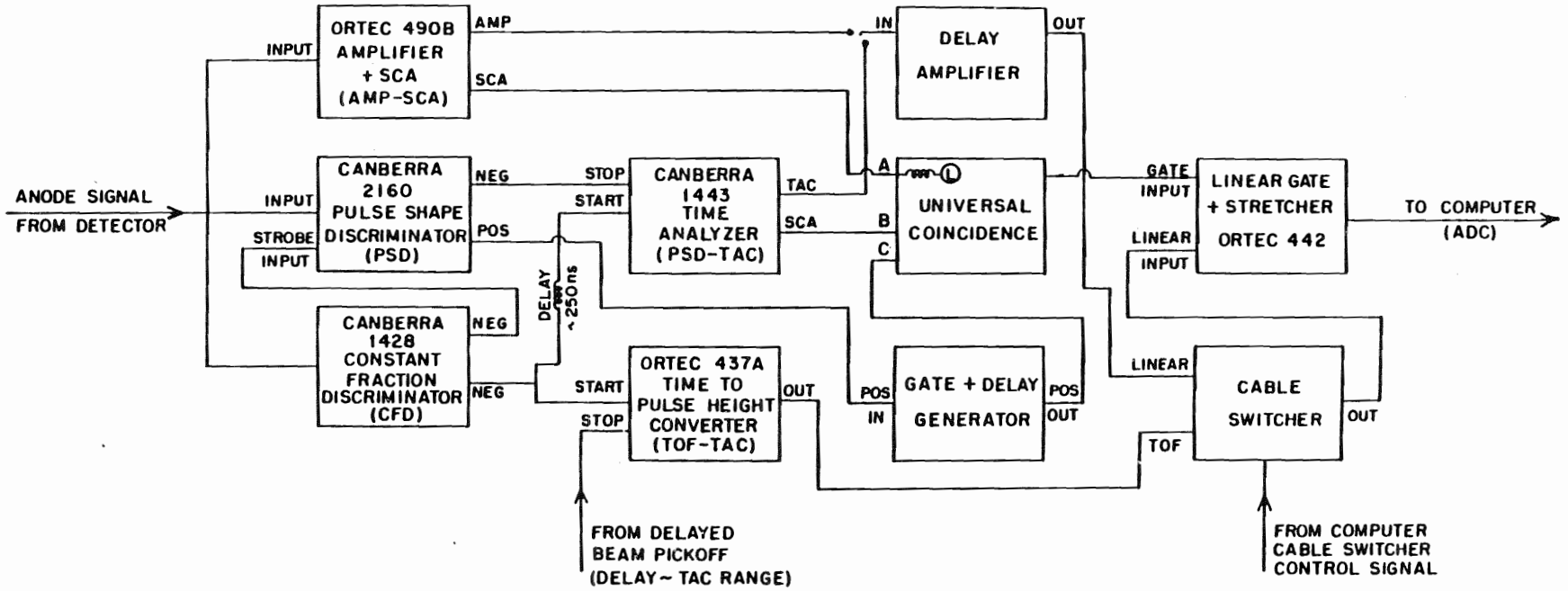

Figure 2.5. Diagram of the detector electronics.

energy bias is set by placing a ^{137}Cs source (γ-ray source) next to the scintillator and looking at the recoil-energy spectrum that results from Compton scattering from electrons (see the ungated spectra of figure 2.6). Then, the lower-level discriminator of the amplifier and SCA (AMP-SCA) box is adjusted so that events to the left of 1/2 the maximum height of the Compton recoil edge are eliminated (see the gated spectra of figure 2.6). Note that the energy increases from left to right for the recoil-energy spectra. According to TUNL convention, an energy bias set in the above fashion is called a 1×Cs bias. This energy bias corresponds to recoil protons in the scintillator of about 2 MeV. More detailed discussions of energy bias settings will be given in chapter 3, which deals with the efficiency measurements for the left and right detectors.

The second condition imposed by the electronics is that the event must be caused by a neutron and not by a γ-ray. This is accomplished with standard pulse-shape-discrimination (PSD) techniques. In the ungated PSD spectra of figure 2.7, the γ-ray associated events give rise to the narrow peaks on the left, while the broad peaks on the right are due to neutron associated events. Note that the peaks due to neutrons and γ-rays overlap. To set the PSD bias, the lower level discriminator of the PSD time-to-amplitude converter (PSD-TAC) is adjusted so that most of the γ-rays are eliminated, but no neutron events are excluded (see the gated spectra of figure 2.7). Many of the γ-rays events are from neutron induced reactions in the sample and neutron and deuteron induced reactions in the material of the beam pipe. Gamma-ray events of this type that are included in the PSD setting will be eliminated from consideration due to their location in the time-of-flight spectra, since the flight times of these γ-rays to the

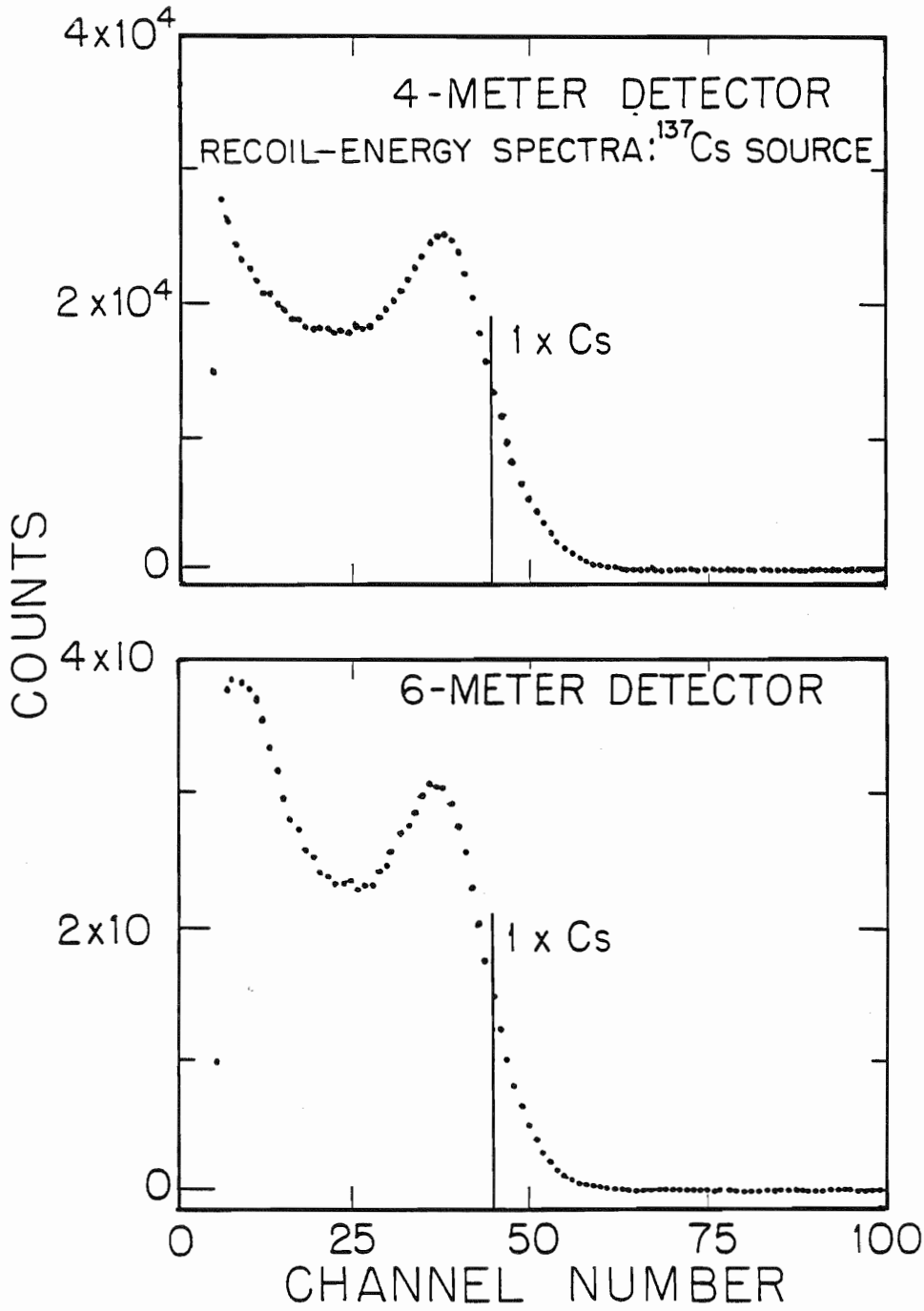

Figure 2.6. Recoil-energy spectra for electrons from Compton scattering in the scintillators of the right (4-m) and left (6-m) detectors due to γ-rays from ^{137}Cs. The solid vertical lines indicate the bias set within the detector electronics for 1×Cs biases.

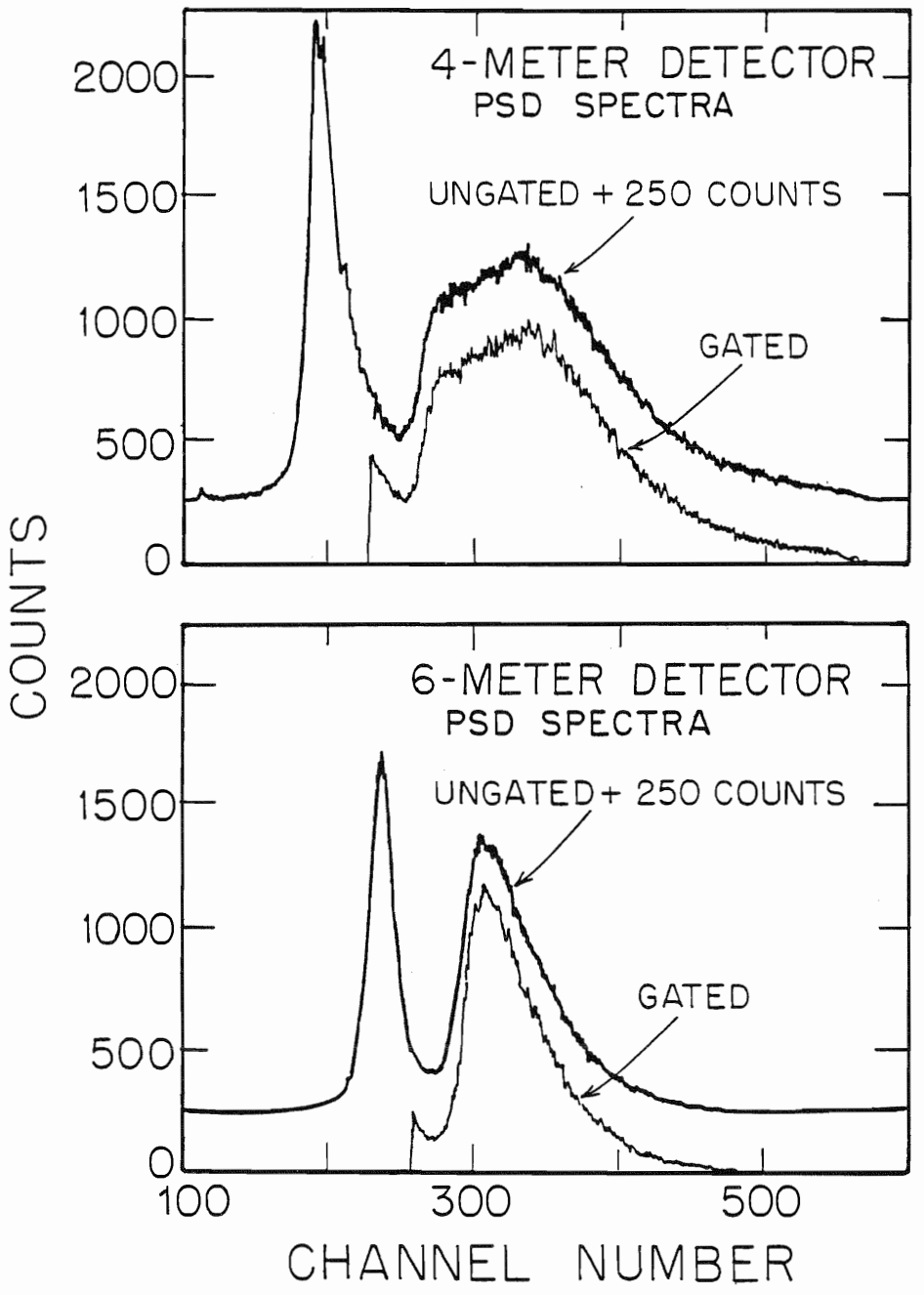

Figure 2.7. PSD spectra used to discriminate between neutrons and γ-rays. Typical gated and ungated PSD spectra for the right (4-m) and left (6-m) detectors are shown in this figure. The broad peaks on the right are due to neutrons, and the narrow peaks on the left are from γ-rays. Note that the bias is set where the γ-ray events rise to about twice the height of the valley between the peaks.

detector are much shorter than the flight times of neutrons to the detector.

Some of the γ-ray events that are allowed through the PSD setting will not be eliminated through time-of-flight considerations. First, there is a constant background level of γ-rays incident on the detector all the time. These γ-rays are primarily due to neutron interactions with various materials in the target room. Second, a few neutrons may interact through (n,γ) reactions with the material immediately adjacent to the scintillator, and the γ-rays from these interactions may then enter the scintillator and be detected. These two types of γ-ray events appear in the same time-of-flight interval as a normal good neutron event, and will result in a small level of γ-ray events underlying the neutron events in the time-of-flight spectra. Since the efficiency of the detectors for counting neutrons must be known for the PSD bias used in the measurements, it is important always to count the same fraction of these two types of γ-ray events as were counted in the efficiency calibration measurements for the detectors.

Events that meet the energy bias and PSD requirements are sorted into time-of-flight spectra. The time-of-flight is determined from the time difference between start and stop signals. The start signals are the anode signals from the photomultiplier tubes of the detectors. The stop signals are produced by the deuteron beam bursts passing through the pick-off and are purposely delayed so that they reach the detector electronics after the start signals. The time difference between the start and stop signals is determined by the time-of-flight-time-to-amplitude converter (TOF-TAC). The sorting of events into the proper channel of the time-of-flight spectrum is done with an analog-to-digital converter (ADC) and a computer (see figure 2.5). All of the data in this work except the $\sigma(\Theta)$ data for ^{93}Nb at 14 MeV,

which were taken using an older DDP-224, were taken using a VAX-11/780 computer.

Examples of time-of-flight spectra for various experiments are shown later in figures 3.2, 4.1-4.3, 4.8-4.10, and D.1. The time-of-flight spectra for $\sigma(\theta)$ measurements are 1024 channels wide; those for $A_y(\theta)$ measurements are 512 channels wide. Note that since the pick-off signal is delayed and used as the stop and not the start signal, the time-of-flight in the spectra decreases from left to right, i.e., the higher energy neutron events will be to the right in the spectra.

2.5 Data Acquisition

Various physical parameters of the $^{54,56}Fe$, $^{58,60}Ni$, ^{93}Nb, and ^{120}Sn samples are given in table 2-1. All of the samples except Nb, for which ^{93}Nb is the only naturally occurring isotope, are isotopically enriched from their natural abundance. The physical parameters of the polyethylene (assumed to be $(CH_2)_n$ in chemical composition) and carbon (graphite) samples used in the normalization measurements for the $\sigma(\theta)$ data are listed in table D-1.

2.5.1 Cross Section Measurements

The procedure for obtaining $\sigma(\theta)$ data is straightforward. First, an "in spectrum" (sample in place) and then, an "out spectrum" (sample replaced by only a sample-support wire) are accumulated at each desired angle for each detector. Both in and out spectra are accumulated for the neutron flux monitor concurrently. The out spectra for the left and right detectors are subtracted from the in spectra, removing background events that were not

TABLE 2-1

Sample Parameters[a)]

Parameter	^{54}Fe	^{56}Fe	^{58}Ni	^{60}Ni	^{93}Nb	^{116}Sn	^{120}Sn
mass (g)	50.9	63.4	34.7	38.7	120.	42.6	45.0
diameter (cm)	1.90	1.90	1.54	1.55	2.57	1.59	1.59
height (cm)	2.40	2.91	2.41	2.41	2.71	3.02	3.08
volume (cm^3)	6.80	8.25	4.49	4.52	14.1	6.00	6.12
number of nuclei ($\times 10^{23}$ nuclei)	5.68	6.83	3.59	3.89	7.79	2.21	2.26
density of nuclei ($\times 10^{22}$ nuclei/cm^3)	8.45	8.27	7.98	8.59	5.54	3.69	3.69
isotopic purity (%)	97.6	99.9	99.9	99.8	99.5	95.7	98.4

a) Although no new data is presented for the ^{116}Sn sample, the sample parameters were needed for the corrected data reported in appendix C.

caused by scattering from the sample but that reached the detector by some other mechanisms. The spectra formed by subtracting the out spectra (normalized to the same monitor counts) from the in spectra are referred to as "difference spectra". Typical in, out, and difference spectra are shown later in figure 4.2 for the left detector at one angle and energy (see also figure D.1). The term "angle pair" will be used to refer to measurements made simultaneously with the right and left detectors, i.e., for data that have the same monitor spectrum in common. Various neutron flux monitor spectra are shown later in figure 4.1; examples of timing monitor spectra are shown later in figure 4.10.

The $\sigma(\theta)$ measurements are normally made in 5° increments. Usually, both detectors are used to measure the same angle simultaneously in the 20° to 40° angular range. Then, measurements are made in the 45° to 160° angular range. In the angular range from 45° to 160°, one or two overlap angles are measured using both detectors. The remaining angles are measured by either alternating the detectors every 5° or by measuring the forward half of the angular range with the left detector and the backward half of the angular range with the right detector. The latter procedure is used when the nucleus for which the measurements are being made has low-lying excited states, which are more easily resolved by using the left detector with the 6-m flight path at forward angles where the strong elastic scattering peak dominates over the inelastic scattering in the time-of-flight spectra.

All of the data measured with both detectors are used to check for shifts in the scattering angle and normalization differences between the two detectors. The angle shifts are caused by the steering of the deuteron beam

and/or a misalignment of equipment in the target room, such as the sample hanger. The forward angle pairs are especially useful in determining angle shifts, since at these angles the cross sections can change by an order of magnitude in only 5^{o}. In this region, a slight angle shift between the two detectors will give noticeably different measured cross sections.

The $\sigma(\theta)$ measurements are normalized to absolute cross section values by making measurements of the reaction $^{1}H(n,n)^{1}H$, i.e., n-p scattering. The normalization measurements are made by measuring scattering from a polyethylene sample (in) and then a carbon sample (out). The difference spectra for these measurements are the spectra for n-p scattering. See figure D.1 for an example of an in, out, and difference spectra from n-p scattering measurements. The measurements are made at an optimum angle, chosen so that the hydrogen scattering peak is resolved as well as possible from the elastic and inelastic scattering peaks for carbon, ensuring good subtraction of carbon scattering events from the region of the hydrogen scattering peak. The usual procedure for the normalization measurements is to average the results of three measurements that are made at the start, middle, and end of a data-taking session for any given energy setting. The absolute normalization is made by scaling the measured values for the scattering sample by the ratio of "standard known n-p scattering cross section values to the values measured for n-p scattering. The standard values used in normalizing the $\sigma(\theta)$ data of this work are the well-known n-p scattering values of Hopkins and Breit (Hopkins 1971).

The spectra at each angle are accumulated until the statistical uncertainty desired for the peaks of interest are obtained. Usually, data with statistical uncertainties of 1% are obtained for elastic scattering

measurements, and uncertainties of 2% to 3% are accepted for inelastic scattering. The out spectra are accumulated for somewhat less time than the in spectra. The time required is dependent on the amount of structure in the out spectra; a lot of structure in the out spectra requires longer counting time than the presence of a flat background.

2.5.2 Analyzing Power Measurements

The procedure for obtaining $A_y(\theta)$ data is somewhat more complex than that for $\sigma(\theta)$ data. An excellent discussion of the theory and experimental technique for $A_y(\theta)$ measurements is given by Byrd (Byrd 1978). There are several conventional methods for taking $A_y(\theta)$ data. The first, the one-detector, spin-flip method, basically uses two measurements made with a single detector to determine the analyzing power at an angle. In this method, one measurement is made while bombarding the sample with a polarized beam of one spin direction, and the other is made for the same amount of time or monitor counts as the first with the spin direction aligned in the opposite direction. The second, the two-detector non-spin-flip method, uses both a left and a right detector to make simultaneous measurements at equal angles with a polarized beam of only one spin direction to determine the analyzing power at an angle.

The method usually employed at TUNL, the two-detector, spin-flip method, combines both of the above methods, using two detectors and also alternating the spin direction of the beam. This procedure minimizes asymmetries introduced by instrumental effects (Byrd 1978). The present measurements were usually made from 20° to 160° in 10° steps, and then at any intermediate angles needed to fill in or confirm the structure of the

angular distribution. The quantity BCI (taken from a beam-current integrator) is a measure of the charge deposited on the gas cell by the deuteron beam while spectra are accumulated. The spectra are accumulated for both spin-up and spin-down by using the same preset value for the BCI alternating between spin-up and spin-down until the uncertainty in the $A_y(\theta)$ is within an acceptable absolute range. As with the $\sigma(\theta)$ measurements, both in and out spectra are accumulated, but for both spin-up and spin-down. In order to normalize the out spectra to their corresponding in spectra, they are multiplied by the ratio of BCI-IN to BCI-OUT. Also, as with the $\sigma(\theta)$ data, the out spectra are accumulated for somewhat less time than the in spectra. At the end of each measurement in one spin direction, the polarization of the deuteron beam is measured using the quench ratio method (Ohlsen 1973, Guss 1982a). Since $A_y(\theta)$ can be computed from the ratio of yields, the measurements of absolute $\sigma(\theta)$ are not necessary, and so no normalization measurements of n-p scattering are needed. Examples of difference spectra for the various $A_y(\theta)$ measurements are shown later in figures 4.8 and 4.9. The experimental uncertainties for elastic scattering data are usually $\pm$ 0.02 to 0.05; those for inelastic scattering data are usually $\pm$ 0.05 to 0.10.

CHAPTER 3

NEUTRON DETECTOR EFFICIENCY MEASUREMENTS

3.1 Introduction

Neutrons, having no charge, must be detected by indirect methods. The detection methods are indirect because they must occur via the nuclear interaction of the neutrons with the nuclei of some material in the detector, and the subsequent detection of charged particles emitted through this interaction. The efficiencies of the detection methods are dependent on the quantity $1-\exp(-\rho t\sigma_T(E))$, the probability of the interaction of neutrons with the nuclei of the material. That is, the efficiency depends on the following properties of the material: ρ the density of nuclei, t the thickness, and $\sigma_T(E)$ the total neutron cross section at incident neutron energy E. The efficiency of a method of neutron detection is not 100%, since this would require that ρ, t, or $\sigma_T(E)$ be infinite. To correct neutron-scattering data properly for the neutron flux lost in the detection process, the efficiency of the detection method must be determined.

Neutrons are detected at TUNL using time-of-flight techniques with organic liquid scintillators. These scintillators are composed primarily of liquid hydrocarbons with trace amounts of activators and spectrum shifters. As stated in chapter 2, the types of scintillators employed are NE-218 (right detector and neutron flux monitor) and NE-213 (left detector and timing monitor), which have hydrogen-to-carbon ratios of 1.28 and 1.21, respectively.

Neutron detection using liquid organic scintillators works in the following manner: neutrons enter the scintillator and scatter from the

hydrogen or carbon nuclei of the scintillator, transferring some energy to the nuclei. The recoiling nuclei lose their acquired energy through ionization in the scintillator, and photons are emitted when the freed electrons and cations recombine. The photons eventually exit the scintillator and bombard a photomultiplier tube, which generates an electric signal proportional to the energy lost by the recoiling nuclei. If the light output due to a recoiling nucleus is larger than that of a proton with an energy equivalent to the bias energy, then the event will be counted.

The light output of the scintillator, and thus the signal from the photomultiplier tube, is dependent on the type of recoiling nuclei. The light output due to recoiling protons (^{1}H nuclei) in NE-218 and NE-213 is high, while that due to ^{12}C nuclei is often negligible. Generally, at incident neutron energies below about 12 MeV, the efficiency of the detectors is primarily due to $^{1}H+n$ interactions and depends mainly on the total cross sections for $^{1}H+n$.

There are, however, $^{12}C+n$ nuclear reactions that can result in significant light output. These reactions involve the emission of a proton, deuteron, or one or more α-particles, since the scintillators can have significant light output for all three of these lighter particles. Dietze and Klein (Dietze 1982) give functions for calculating the light output of various recoiling particles and nuclei in NE-213. As can be seen from their discussion, the light output for deuterons is less than that for protons, and the light output for α-particles is less than that for deuterons. For instance, for NE-213, a 2.6 MeV deuteron and a 5.6 MeV α-particle have the same light output as a 2.0 MeV proton, while a 9.7 MeV deuteron and a 21.3 MeV α-particle have the same light output as a 8.0 MeV proton.

Reactions involving the elastic or inelastic scattering of neutrons from ^{12}C do not directly result in any significant light output. However, scattered neutrons from these reactions that subsequently scatter from ^{1}H do appreciably affect the measured efficiency.

Below incident neutron energies of 18 MeV, the following neutron-carbon reactions require consideration: $^{12}C(n,n_0)^{12}C$, $^{12}C(n,n_1)^{12}C$ (Q = -4.44 MeV), $^{12}C(n,\alpha)^{9}Be$ (Q = -5.70 MeV), $^{12}C(n,n')3\alpha$ (Q = -7.28 MeV), $^{12}C(n,p)^{12}B$ (Q = -12.9 MeV), and $^{12}C(n,d)^{11}B$ (Q = -13.7 MeV). The $^{12}C(n,n_0)^{12}C$ reaction followed by neutron-hydrogen interactions is the dominant process involving ^{12}C below 5.70 MeV, while the $^{12}C(n,n')3\alpha$ reaction is the dominant process above 14.0 MeV, comprising more than 20% of the neutron total cross section for carbon above this energy (Antolkovic 1983). The light outputs for the emitted ^{9}Be, ^{11}B, and ^{12}B nuclei are negligible compared to the light output for the lighter reaction products.

Detector efficiencies can be determined either by calculation or by direct measurement, but neither is easy. Calculating the detector efficiencies is generally difficult due to the complexities involved in accounting for the various ^{12}C+n interactions. These calculations are also limited by the uncertainties of the measured cross sections for the ^{12}C+n reactions; for instance, the uncertainties for the $^{12}C(n,n')3\alpha$ reaction are on the order of 20% (Antolkovic 1983). Some success has been achieved using Monte Carlo codes to calculate efficiencies. One such code, NEFF4, from the Physikalisch-Technische Bundesanstalt (PTB) at Braunschweig, West Germany (Dietze 1982), can require up to 100 hours of central processing unit (CPU) time to achieve good statistical results, but again the results are only as good as the measured cross sections used for the calculations.

Traditionally, the efficiencies of the detectors at the neutron time-of-flight facility at TUNL are measured rather than calculated, because of the difficulties and inaccuracies involved in calculating them. To make these measurements, neutron producing reactions having well determined or "standard" differential cross sections are remeasured. Preferably, the efficiencies of the detectors should be measured over the entire energy range in small energy intervals and for each bias at which it might be used.

There are two types of measured efficiencies, absolute and relative. The absolute efficiency of a detector can be defined as the measured yield (normalized to an absolute value) divided by the known cross section. In absolute efficiency measurements, the shape and normalization of the efficiency function over an energy range are determined. Absolute efficiencies are required when measurements are not made relative to known cross sections, such as in (p,n) scattering measurements. Relative measurements determine the shape of the efficiency function, but not the absolute normalization. This type of measurement is sufficient for correcting data that were measured relative to known cross sections, such as the n-p normalization measurements used at TUNL.

The efficiency measurements presented in this work are absolute measurements for both the right and left detectors at multiple energy-bias settings. These are the first such multi-bias efficiency measurements for these detectors. The most recent prior measurement was by El-Kadi (El-Kadi 1981) at a bias of 1×Cs for both detectors. In the present measurements, the efficiencies of the detectors were determined by measuring the neutron cross sections from the $^{2}H(d,n)^{3}He$ reaction. The values for the $^{2}H(d,n)^{3}He$

reaction measured by M. Drosg (Drosg 1978) at Los Alamos National Laboratory (LANL) were used as the standard values. The experimental details, data analysis, and corrections to the data are dealt with in section 3.2; various attempts to fit the data are outlined in section 3.3; and conclusions and specific suggestions are given in section 3.4 for improving future efficiency measurements for these detectors. Note that the efficiencies of the neutron flux and timing monitors were not measured, since these efficiencies are not needed for either our $\sigma(\theta)$ or $A_y(\theta)$ measurements.

There were several reasons for the decision to measure the efficiency data presented in the present work. First, it is wise to measure the efficiencies of detectors periodically to ensure that the detectors are still functioning properly and that the light-output qualities have not become degraded. Second, there are some problems in data from El-Kadi's previous measurement: the scatter and uncertainties of the data are larger than desired. Also, the data between 14 and 17 MeV for the left detector and his fit in the region of this data disagree. In addition, El-Kadi's fit to the data of the right detector is used in the data correction codes for both detectors, since his measurement indicates close agreement between the efficiencies of the right and left detectors. Thus, it is important to check this apparent agreement more carefully. Third, at the higher neutron energies available at TUNL, that is $E \geq 14$ MeV, higher bias settings would improve the signal-to-noise ratio in the time-of-flight spectra. Therefore, new measurements were indicated to obtain higher-quality data at $1 \times Cs$, especially in the 14- to 17-MeV region, and to obtain data for higher biases.

3.2 Method, Corrections, and Results

3.2.1 Experimental Procedure

The data-taking procedures used in the efficiency measurements were only slightly different from those used for the neutron cross section measurements. One difference in the arrangement was that the gas cell (cell C) was moved so that the center of the gas volume was located over the pivot point of the detectors. In this case, when the primary reaction is viewed directly, the acquisition of data in the angular range from 0^{o} to 160^{o} is possible. Second, the efficiency measurements required a special data-taking code, prepared by C.R. Howell. In the measurements, data were accumulated simultaneously for many bias settings. This was made possible through the software selection of bias levels; the code sorted events for the various biases into separate time-of-flight spectra for each bias. Unlike the usual $\sigma(\Theta)$ measurements, BCI (instead of monitor) normalizations were used so that absolute normalizations could be obtained for the data, through the known absolute $^{2}H(d,n)^{3}He$ cross sections (Drosg 1978). For all of the efficiency measurements, both detectors were placed at their full flight paths, even though the detector efficiencies are independent of flight path to first order.

The procedure used to set the multiple biases was another difference between the efficiency measurements and the usual cross section measurements. Since some difficulties arose in doing these efficiency measurements with this new technique, the method will be carefully detailed here. In fact, a repeat measurement was required to salvage the data recorded for the biases other than 1 X Cs. First, an ungated recoil energy

spectrum for the ^{137}Cs source (γ-decay) was accumulated. The signal from a precision pulser, modified to simulate an anode signal, was then run through a precision attenuator and substituted for the anode signal (refer to figure 2.5). The pulse-shape modification was accomplished by using a delay line with a short to reduce the pulse width. The attenuator was fine tuned to line up the pulser signal with the channel of the recoil-energy spectrum corresponding to the 1×Cs setting, as in figure 2.6. Then, the precision attenuator was used to multiply or divide the signal amplitude to obtain the other desired bias settings, e.g., twice the attenuation would put the pulser signal at the proper channel for a 2×Cs setting. As stated in chapter 2, a 1×Cs setting, according to the TUNL convention and that of Drosg (Drosg 1972), corresponds to the channel number at which the spectrum near the Compton recoil edge falls to 1/2 of the maximum height. Note that the definition of 1×Cs may differ from lab to lab, and one must be careful in making efficiency comparisons. Recoil-energy spectra are shown in figure 3.1 for the $^{2}H(d,n)^{3}He$ reaction for the right and left detectors with various bias settings indicated. In the figure, the Compton recoil spectra for the ^{137}Cs source are superimposed on the spectra for the $^{2}H(d,n)^{3}He$ reaction.

The absolute efficiencies of the right and left detectors were measured in two separate experiments. In the first experiment (data set 1), the efficiencies of the detectors were measured at several biases ranging from 1/8×Cs to 9×Cs for neutron energies ranging from 2.0 to 18.0 MeV. However, useful data were acquired only at 0.5, 1, 2, 3, 4, and 7×Cs biases. First, measurements were made for incident deuteron energies from 5.6 to 15.2 MeV in 0.2 MeV steps for the right detector at 0^{o} and the left

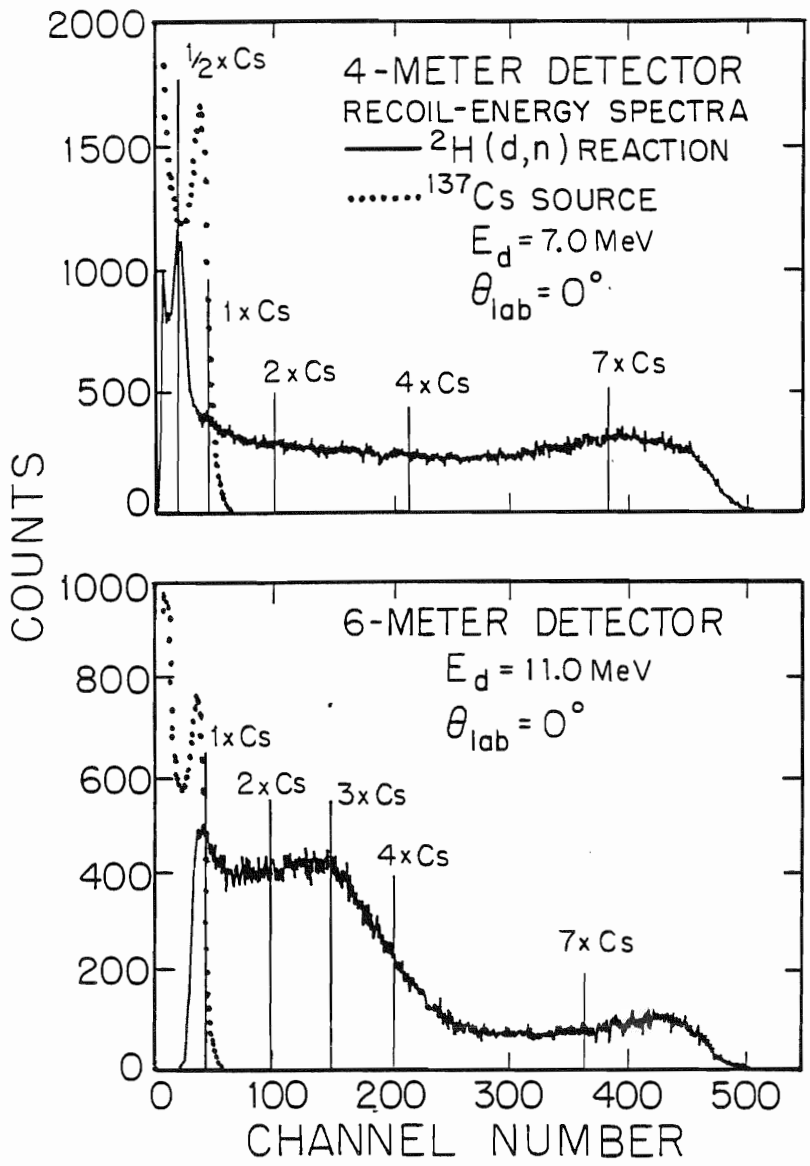

Figure 3.1. Recoil-energy spectra for the $^{2}H(d,n)^{3}He$ reaction from the right (4-m) and left (6-m) detectors. The dotted lines represent recoil-energy spectra for electrons from Compton scattering of the γ-rays from ^{137}Cs that were used to set the 1X Cs biases. The vertical lines indicate various other biases. As discussed later in the text, the bias settings for the left detector are not the true settings, since there was a zero-offset in the electronics of this detector. These spectra are from the first efficiency experiments reported in this work.

detector at 60^{o}, and then with detector angles interchanged. The 60^{o} measurements were intended to be used as a check for the 0^{o} energy distributions, but were not of sufficient statistical accuracy to be included in the final data sets. Also as a check of the 0^{o} data, several repeat measurements were made at various energies. The 0^{o} measurements provided data for neutron energies from 8.8 to 18.1 MeV. To provide data from 2.0 to 9.2 MeV, angular distributions of the $^{2}H(d,n)^{3}He$ reaction were measured at an incident deuteron energy of 6.0 MeV in 10^{o} steps from 0^{o} to 140^{o} for both detectors; measurements were made at several additional angles for each detector. Time-of-flight spectra are shown in figure 3.2 for both detectors at various bias settings.

The second experiment was required because the results of the first experiment indicated two problems, neither of which was noticed during the first experiment. The first problem was that the 1×Cs data were approximately 15% lower than that previously measured by El-Kadi (El-Kadi 1981). The second problem was that while the bias energies for the right detector at 0.5, 1, 2, 3, and 4×Cs bias settings, 1.3, 2.0, 3.1, 4.0, and 5.10 MeV, respectively, and the left detector at 0.5, 1, 2, and 3×Cs bias settings, 1.2, 2.0, 3.2, and 4.4 MeV, respectively, were in good agreement with those of Drosg, 1.3, 2.0, 3.2, 4.2, and 5.1 MeV, respectively, that for the left detector at a 4×Cs settings, 5.8 MeV, was not (Drosg's highest bias setting was 5×Cs). Also, for the 7×Cs setting, the bias energy for the right detector was 8.2 MeV, while that for the left detector was 10.30 MeV.

For the second experiment, it was decided not to repeat the entire first experiment, but to obtain only a fraction of the amount of original

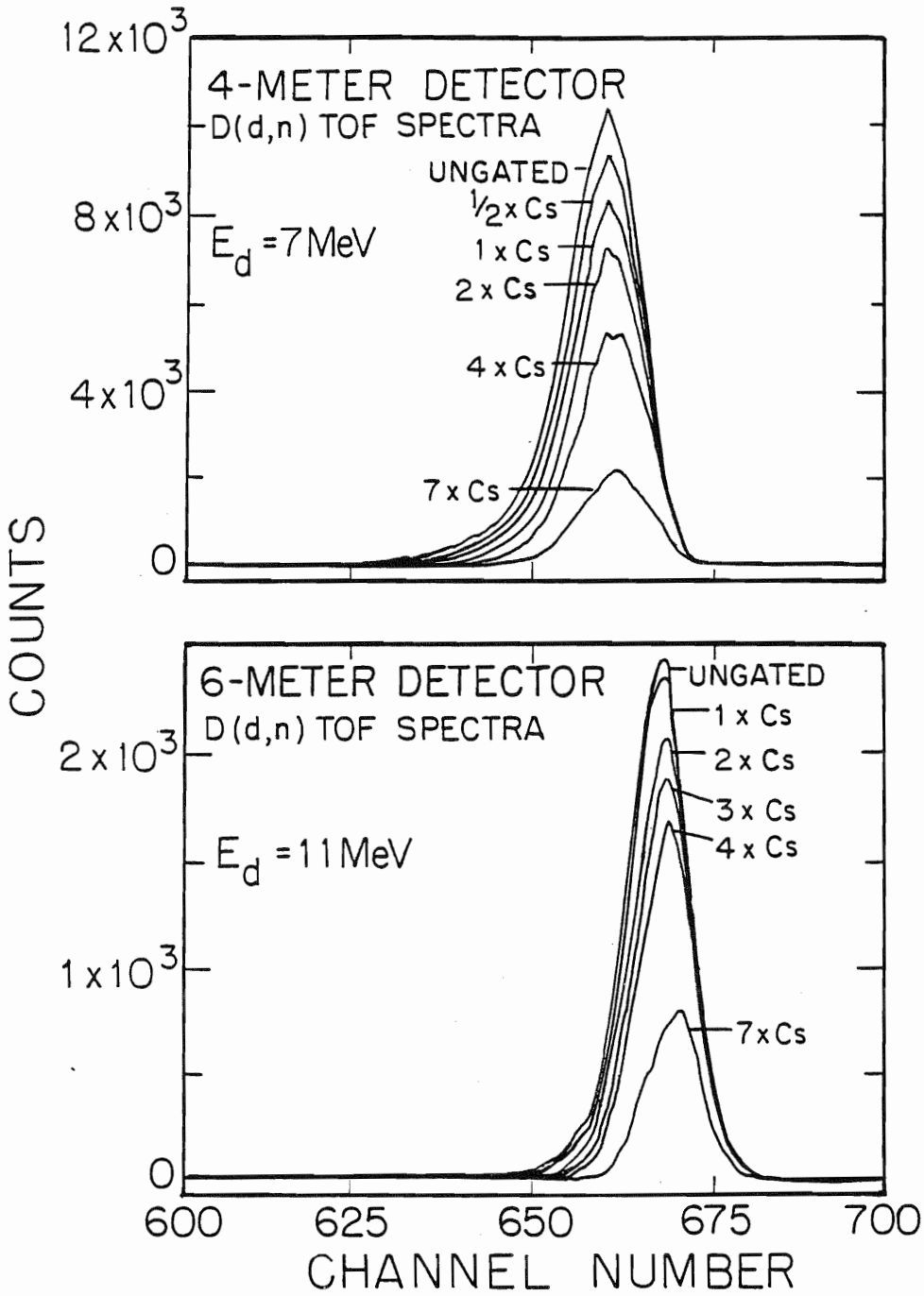

Figure 3.2. Time-of-flight spectra for the $^{2}H(d,n)^{3}He$ reaction from the right (4-m) and left (6-m) detectors. Spectra are overlaid for several biases. These spectra are from the first efficiency experiments reported in this work.

data and then to combine the two data sets in a consistent way. (This approach turned out to be a time-consuming mistake; in retrospect, it would have been much wiser to discard the first set and repeat the whole first experiment.) Therefore, in the second experiment (data set 2), measurements were made at 0^{o} for each detector for incoming deuteron energies from only 4.0 to 11.0 MeV in only 1.0 MeV steps. The experimental conditions were the same as those for the first, except that a new bottle of deuterium gas was used to fill the target cell, and as discussed later, more care was followed in determining the zero bias of the amplifiers.

3.2.2 Data Reduction and the Extraction of Efficiencies

The time-of-flight spectra of sets 1 and 2 were stripped in a manner similar to that for the $\sigma(\Theta)$ data, which will be described in chapter 4. The yields obtained from stripping the spectra were scaled by the number of BCI instead of the yield of the neutron flux monitor. There were no target out spectra to subtract as the yields typically observed when the gas is removed from the target cell are less then 1% of the yield with the gas in, and so, they were not measured for the present data. The following equation was used to convert the yields into efficiencies:

$$\varepsilon(E_n) = NF \times \frac{1}{T_{GC}(E_n,\Theta)} \times \frac{1}{T_D(E_n)} \times \frac{Y_G(E_d,\Theta)}{\sigma_G(E_n,\Theta)}, \qquad (3.1)$$

where E_d is the bombarding deuteron energy, E_n is the outgoing neutron energy, and Θ is the reaction angle in the lab system. The symbol $Y_G(E_d,\Theta)$ is the experimental neutron yield per BCI. The quantity $\sigma_G(E_n,\Theta)$ is the known $^{2}H(d,n)^{3}He$ cross section in the lab system.

The quantity $T_D(E_n)$ in equation 3.1 is the transmission probability through the entrance face of the detector for a neutron of energy E_n and is calculated using the fact that the entrance faces in front of the organic scintillators of both the right and left detectors are made of 0.16 cm thick aluminum. The transmissions were calculated using σ_T values for aluminum from ENDF/B-V. Neutrons enter the detectors essentially perpendicular to the aluminum faces due to the flight paths used, so the neutron path lengths L_D, which are also used to calculate the transmissions, through the aluminum faces are just the thicknesses of the faces. The values of $T_D(E_n)$ calculated for the data range from 97.0 to 98.4%, with the majority being close to the latter value. Typical transmissions through the aluminum are listed in table 3-1. The efficiency values calculated from equation 3.1 slightly overestimate the true efficiency because of the use of the full value for σ_T in the calculation of $T_D(E_n)$ for the aluminum face. Since much of the total cross section for aluminum is due to neutron elastic and inelastic scattering, some of the neutrons that interact with Al nuclei will be scattered into the organic scintillator and detected. However, since $T_D(E_n)$ is typically over 98%, the overestimation of the attenuation effect should be less than 25% of this 2% loss. The error introduced here should be within the 0.45% maximum uncertainty assigned for the $T_D(E_n)$ values, which was included in the relative uncertainties for the data.

The value $T_{GC}(E_n,\Theta)$ in equation 3.1 is the product of the transmission probabilities $T_{Ta}(E_n)$ and $T_{SS}(E_n)$ through the liner and wall of the gas cell for a neutron of energy E_n. This quantity is angle-dependent because the path lengths of neutrons through the wall and liner of the gas cell depend on the emission angle. The walls of the gas cell C are made of 0.25 mm

TABLE 3-1

Transmissions T_{Ta}, T_{SS}, and T_D
Used in Corrections to the Efficiency Data

θ_{lab}	E_d	E_n	L_{Ta}	T_{Ta}	L_{SS}	T_{SS}	T_{GC}	T_D	T_{TOT}
0°	14.0	16.8	0.0508	98.5	0.0254	99.5	98.0	98.3	96.4
0°	12.0	14.9	0.0508	98.5	0.0254	99.5	98.0	98.3	96.3
0°	10.0	13.0	0.0508	98.5	0.0254	99.4	97.9	98.4	96.3
0°	8.0	11.1	0.0508	98.6	0.0254	99.4	98.0	98.3	96.3
0°	6.0	9.21	0.0508	98.6	0.0254	99.3	97.9	98.4	96.3
20°	6.0	8.77	0.1114	97.0	0.0743	97.9	95.0	98.4	93.4
40°	6.0	7.61	0.0593	98.4	0.0395	98.8	97.2	98.2	95.4
60°	6.0	6.08	0.0440	98.7	0.0293	99.1	97.8	98.0	95.8
80°	6.0	4.59	0.0387	98.7	0.0258	99.2	97.9	98.0	96.0
100°	6.0	3.39	0.0387	98.6	0.0258	99.2	97.8	97.3	95.2
120°	6.0	2.55	0.0440	98.3	0.0293	99.0	97.3	96.9	94.3
140°	6.0	2.04	0.0593	97.7	0.0395	98.6	96.3	96.9	93.4

The transmissions given are for neutrons emitted by the $^2H(d,n)^3He$ reaction at various lab angles and incident deuteron energies. The transmissions for neutrons through the tantalum liners and stainless steel walls of gas cell C and through the aluminum entrances to the detectors are T_{Ta}, T_{SS}, and T_D, respectively. The total transmission through gas cell C is T_{GC}, and the total transmission through the gas cell and entrance to the detector is T_{TOT}. The neutron path lengths through the tantalum liners and the #304 stainless steel walls of gas cell C are L_{Ta} and L_{SS}, respectively. The units for E_d and E_n are MeV those for L_{Ta} and L_{SS} are cm; and those for T_{Ta}, T_{SS}, T_{GC}, and T_D are percent. The neutron path lengths L_D through the aluminum faces of the right and left detectors are 0.159 cm. For θ_{lab} larger than 141.6°, neutrons will encounter part of the base of gas cell C (see related table 3-2).

thick #304 stainless steel, and the end (beam stop) and side liners are 0.51 mm and 0.38 mm thick tantalum, respectively (see figure 2.2). For the gas cell, the relations for determining the neutron path lengths L_{Ta} and L_{SS}, which are used to calculate the corresponding transmissions, through the tantalum liner and beam stop and the stainless steel cylindrical containment vessel, respectively, are given in table 3-2. The composition of #304 stainless steel is approximately 18% chromium, 71% iron, 2% manganese, 8% nickel, 1% silicon, and trace amounts of other elements (primarily carbon). The transmissions were calculated using σ_T values for elemental Cr, Fe, Mn, Ni, and Si from ENDF/B-V. (We note that the use of the full values of σ_T for the calculation of $T_{Ta}(E_n)$ and $T_{SS}(E_n)$ are proper, since the detectors are far from the gas cell and the neutrons that scatter upon exiting the gas cell have a negligible chance of reaching the detector.) The values of $T_{GC}(E_n,\Theta)$ calculated for the data range from 94.9 to 98.0%, with the majority being close to the latter value. Typical values of the transmissions through the tantalum and stainless steel are listed in table 3-1. A maximum uncertainty of 0.34% has been assigned for the $T_{GC}(E_n,\Theta)$ values and is included in the relative uncertainties for the data.

The factor NF in equation 3.1 is the normalization factor used to convert the yields per BCI to cross sections and is calculated with the following equation:

$$NF = \frac{1}{NI} \times \frac{1}{NT} \times \frac{1}{\Omega}, \qquad (3.2)$$

where NI is the number of deuterons per BCI incident on the gas cell, NT is the number of target nuclei per cm^2 in the gas cell, and Ω is the solid

TABLE 3-2

Neutron Path Lengths L_{Ta} and L_{SS} Used in Corrections to the Efficiency Data

$L_{Ta} = 0.0508/\cos\theta$	$0.0^{o} \leq \theta_{lab} \leq 15.5^{o}$
$L_{Ta} = 0.0508/\cos\theta + \{[(1.5800 \cdot \tan\theta) - 0.4382]/\sin\theta\}$	$15.5^{o} \leq \theta_{lab} \leq 16.3^{o}$
$L_{Ta} = 0.0381/\sin\theta$	$16.3^{o} \leq \theta_{lab} \leq 141.6^{o}$
$L_{SS} = 0.0254/\cos\theta$	$0.0^{o} \leq \theta_{lab} \leq 16.5^{o}$
$L_{SS} = 0.0254/\cos\theta + \{[(1.6308 \cdot \tan\theta) - 0.4826]/\sin\theta\}$	$16.5^{o} \leq \theta_{lab} \leq 17.1^{o}$
$L_{SS} = 0.0254/\sin\theta$	$17.1^{o} \leq \theta_{lab} \leq 141.6^{o}$

The neutron path lengths through the tantalum liners and the #304 stainless steel walls are L_{Ta} and L_{SS}, respectively. The units for L_{Ta} and L_{SS} are cm. For θ_{lab} larger than 141.6^{o}, neutrons will encounter part of the base of gas cell C (i.e., the area near the foil). Note, see related table 3-1 and figure 2.2.

angle subtended by the detector. The quantity NI is calculated from:

$$NI = FS \times \frac{CF}{CD}, \tag{3.3}$$

where FS is the full-scale current setting of the beam-current integrator, CF is the scale factor for the beam-current integrator (0.01 s), and CD is the charge of a deuteron. The quantity NT is calculated from:

$$NT = \frac{P \times L \times NM}{R \times T}, \tag{3.4}$$

where P is the pressure of the gas target in bar (1.02±2%)), L is the length of the gas target in cm (3.16±1.6% for gas cell C), NM is the number of nuclei in the target gas per mole (12.05×10^{23} nuclei/mole), R is the universal gas constant (83.15 cm^3-bar/mole-Kelvin), and T is the temperature of the gas in Kelvin (296±2%).

The final data of set 2 at the 1×Cs setting for both detectors were in good agreement with those of El-Kadi and with calculations using the following semi-empirical equation, which had been used previously by Drosg to normalize his efficiency data (Drosg 1972):

$$\varepsilon(E) = \left[1 - \frac{B}{E}\right]\left[1 - e^{-\rho_H t \sigma_H(E)}\right]\left[1 + \frac{B}{E'}(1 - e^{-\rho_H t \sigma_H(E')})\right]. \tag{3.5}$$

This equation considers only scatterings from hydrogen and includes an approximation for double-scattering. In this relation, the first two sets of brackets account for detection of single scattering events, with the quantity enclosed in the first pair being an approximation for light output, and the quantity enclosed in the second pair the attenuation for neutrons through the scintillator (only considering hydrogen). The second term enclosed by the third pair of brackets is the double-scattering

approximation. The quantities used in this equation are: ρ_H, the density of ^1H nuclei; t, the thickness of the detector; σ_H, the ^1H total neutron cross section; E, the incident neutron energy; B, the bias energy; E', the energy of the "effective neutrons" after the first scattering; and B', the effective bias energy for neutrons that scatter a second time.

The effective neutrons are those that originally have an energy greater than the bias B, but lose an energy less than B in the first scattering, and then are still counted, providing that they lose an energy greater than B' in a second scattering. In other words, these neutrons contribute to the detector efficiency if the combined light outputs due to the first and second scatterings are greater than the light output for the bias energy. The effective neutrons, on the average, lose an energy of B/2 in the first scattering, so that E' is equal to E-B/2. Clearly then, the effective bias B' is equal to B-B/2, the original bias energy minus the average energy lost by the effective neutrons. If a neutron loses an energy greater than B on the first scattering, and then scatters a second time, it will be included through the first two set of brackets in equation 3.5, and so it does not enter into the enhancement factor in the third set.

The data of set 2, the data of set 1 renormalized by 1.15 and the calculations from equation 3.5 are shown in figures 3.3 and 3.4 for the right and left detectors, respectively. The data of El-Kadi are also shown in these figures. Note that the calculations are lower than El-Kadi's data at the higher energies, since Drosg's equation only considers the presence of hydrogen in the scintillator, that is, it ignores interactions with carbon. This is appropriate at the low energies, but at energies above about 12 MeV the $^{12}C+n$ interactions can no longer be ignored.

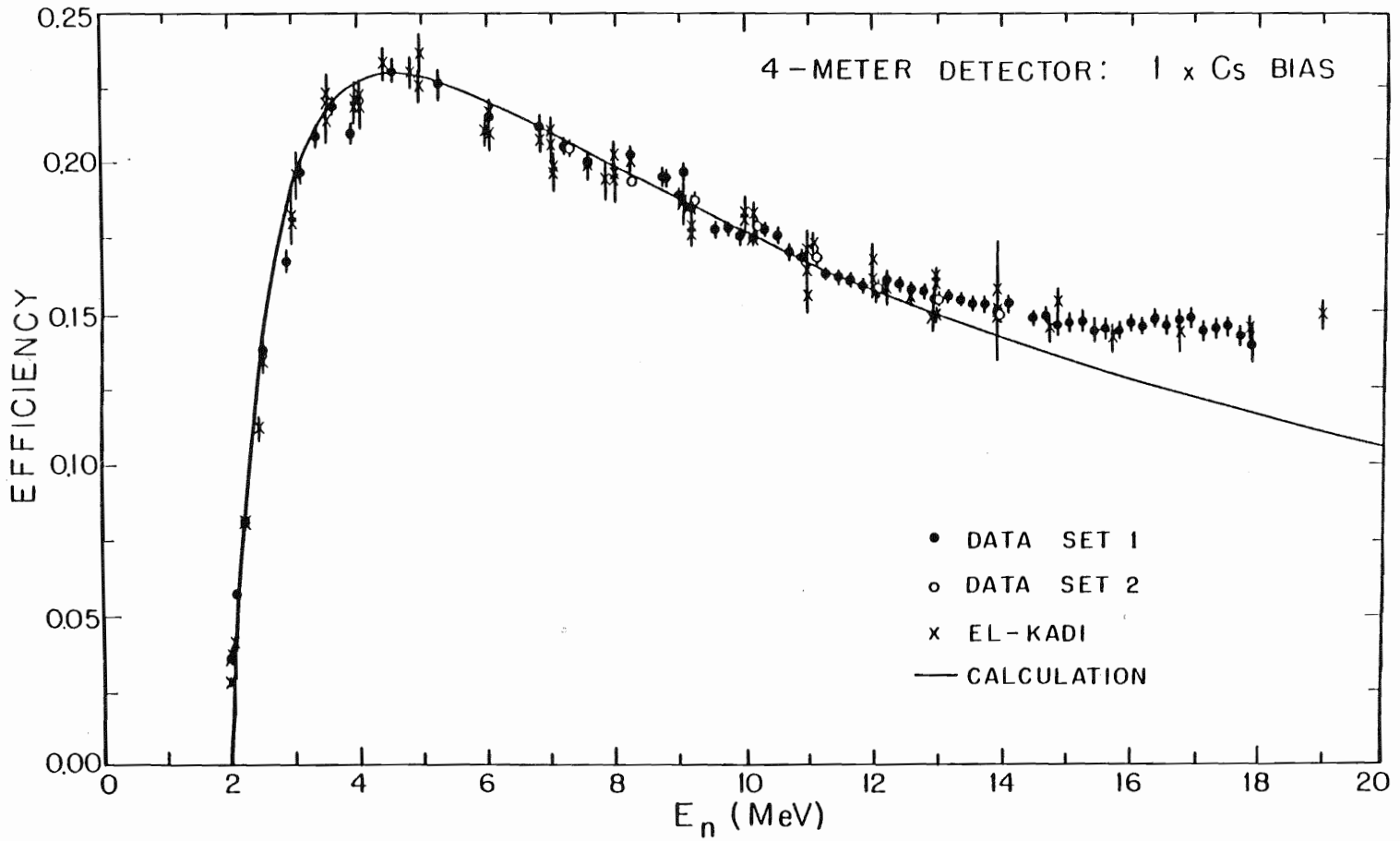

Figure 3.3. Efficiency data for the right (4-m) detector for an energy bias of 1×Cs. The data of set 1 (renormalized by 1.15) are from the first experiment for this work; those of set 2 are from the second. The El-Kadi data are from El-Kadi 1981. The calculation was made using equation 3.5, which was taken from Drosg 1972.

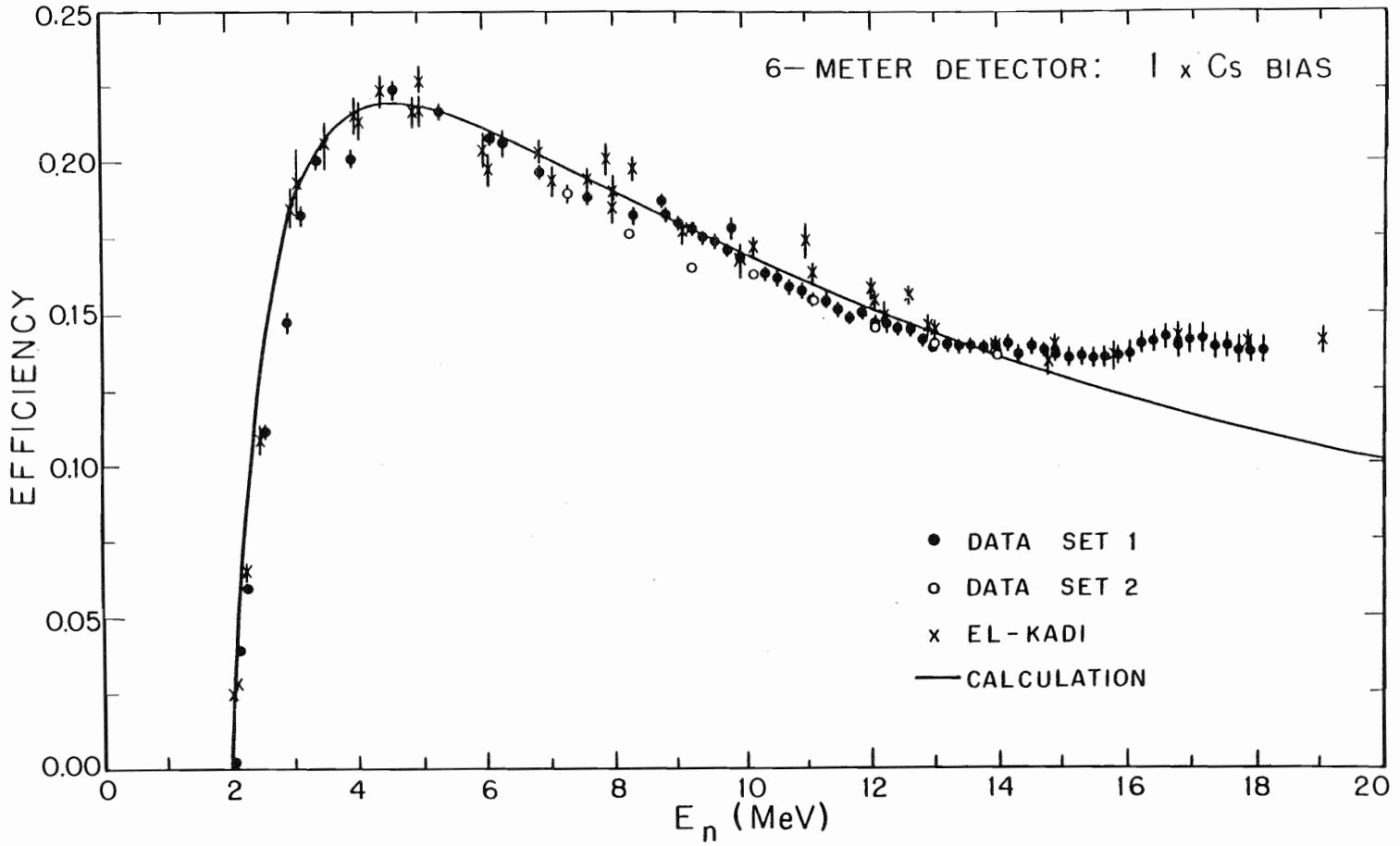

Figure 3.4. Efficiency data for the left (6-m) detector for an energy bias of 1×Cs. The data of set 1 (renormalized by 1.15) are from the first experiment for this work; those of set 2 are from the second. The El-Kadi data are from El-Kadi 1981. The calculation was made using equation 3.5, which was taken from Drosg 1972.

The only known difference between the first and second experiments was a different source of deuterium. This fact, coupled with the agreement between the data of set 2, El-Kadi's data, and the portion of the calculation below 12 MeV, strongly suggests that the gas used in the first experiment was contaminated. By comparison of the relevant data of sets 1 and 2, the renormalization factor necessary to correct the data of set 1 was determined to be 1.15 ± 0.03.

The problem with the left-detector bias energies from data set 1 appears to be the result of a voltage-offset (zero-offset) associated with the anode signal before it entered the detector electronics. This offset was in the direction of subtracting from the amplitude of the signal, making it smaller than the actual pulse. The effect of the offset can be seen by comparing the recoil-energy spectra for the $^{2}H(d,n)^{3}He$ reaction shown in figure 3.1. The recoil edges for the spectra of the right and left detectors are near the same channel (about 500), but the spectrum for the right detector is for 7.0 MeV deuterons and that of the right detector is for 11 MeV deuterons. This means that with the method used to set the biases, only the $1 \times Cs$ bias would be correct. Biases below a $1 \times Cs$ setting would actually be lower than intended (as set with the pulser), with the deviation between the intended and actual settings increasing with decreasing setting; the reverse is true for biases above $1 \times Cs$. The effect is the same as if the pulser signal had an offset that decreased the amplitude of the signal. However, this possibility seems unlikely, since the same pulser system was used in setting the biases of both detectors and since the system was switched back and forth between the detectors throughout the experiment.

The data of set 1 were taken with great care. Therefore, it was desirable to determine the actual bias settings for the left detector so that the data can be made useful. This can be done by determining the light output or bias setting versus bias-energy function from the data of set 2 for the left detector, and then determining the bias settings for the data of set 1 from their bias energies and this first function. If the bias energy for a setting cannot be determined from the data, then for incident neutron energies below 12 MeV, equation 3.5 can be used to make an approximate determination. The determination with equation 3.5 is made by varying B to find the range of possible bias energies for each bias setting. After the bias energies have been found, the bias setting versus bias energy is plotted.

The top curve in figure 3.5 shows the light-output function determined in the above way for the combined data of sets 1 and 2 for the right detector. The data points indicate the mean bias energies for the bias settings, and the horizontal error bars indicate the ranges of bias energies for the settings. The linear part of the function is a fit to the data and is

$$L(E) = -0.94 + 0.97E \qquad E \geq 2.0 \text{ MeV} , \tag{3.6}$$

where L(E) represents the bias setting or light output (units of 1×Cs) at energy E. The non-linear portion of the function was determined by assuming a polynomial form of even powers of E up to the 4^{th} order, and requiring that L(0.0) = 0.0 and that the slopes of the linear and non-linear functions match at E = 2.0 MeV. This gave

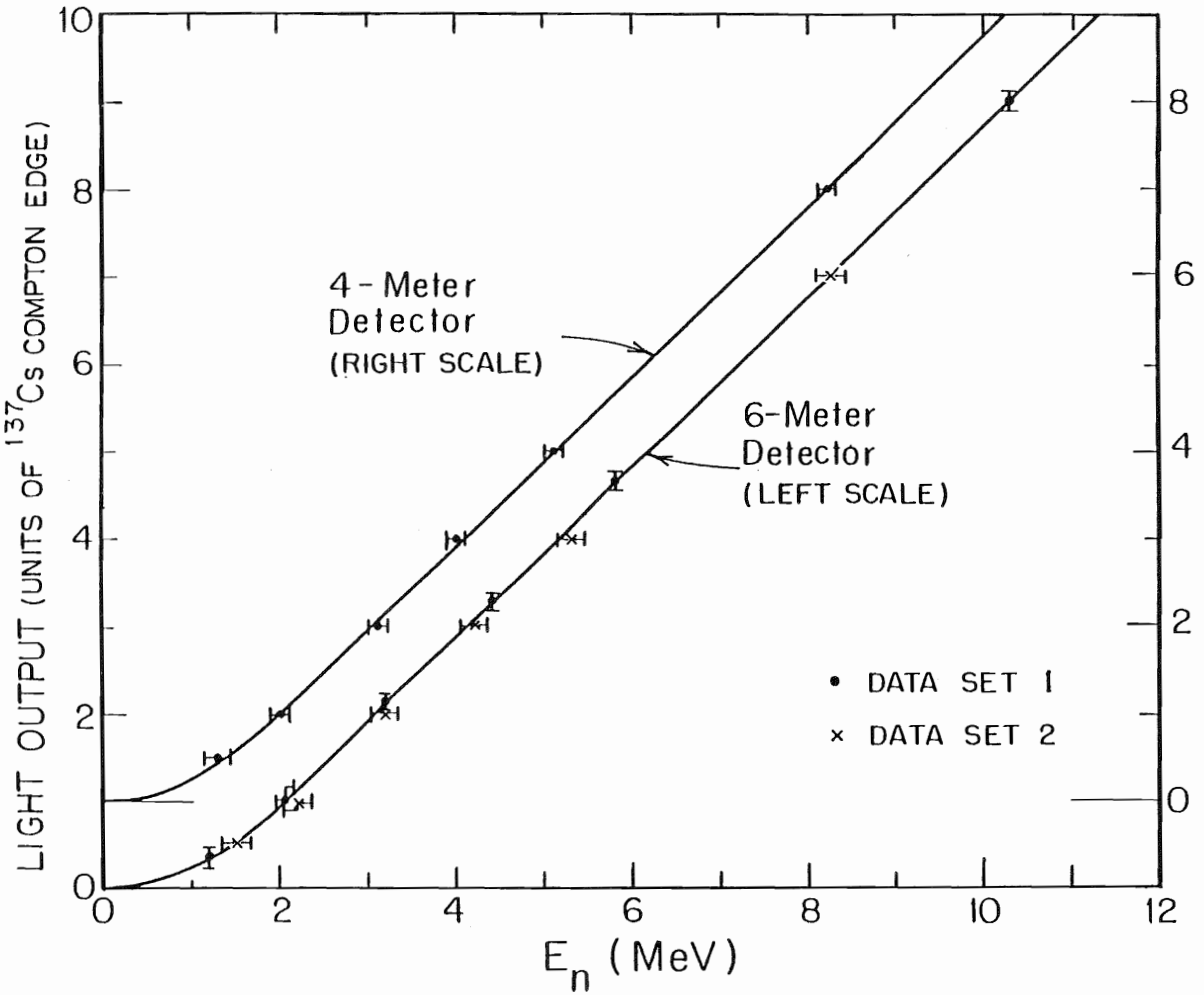

Figure 3.5. Light-output functions for the right (4-m) and left (6-m) detectors. The data of set 1 are from the first experiment for this work; those of set 2 are from the second. See text for discussions of the horizontal and vertical error bars.

$$L(E) = 0.25E^2 - 1.46\times10^{-3}E^4 \qquad E \leq 2.0 \text{ MeV} . \tag{3.7}$$

After repeating the above process for the left detector data of set 2, it was realized that the data for the 0.5, 1, 2, 3, and 4×Cs bias settings were not taken at energies low enough to determine accurately the bias energies. Fortunately, this was not the case for the 7×Cs setting, and the range of bias energies could be determined for this setting. Also, since the data of set 1 at the 1×Cs bias for the left detector had to be at the correct bias setting, this bias information could be used to determine the range of bias energies for the 1×Cs bias setting. The mean bias energies determined for the 1×Cs setting of set 1 and the 7×Cs setting of set 2 were used to determine the light-output function for the left detector, assuming a linear dependence from the 1 to 7×Cs setting and a non-linear function below 1×Cs, with the constraints similar to those used to determine equation 3.7 for the right detector. For the lower curve of figure 3.5, the linear portion is given by

$$L(E) = -0.98 + 0.97E \qquad E \geq 2.05 \text{ MeV} , \tag{3.8}$$

and the non-linear portion is given by

$$L(E) = 0.24E^2 - 4.59\times10^{-4}E^4 \qquad E \leq 2.05 \text{ MeV} . \tag{3.9}$$

As a check on the linear portion, the ranges of bias energies for the 0.5, 2, 3, and 4×Cs biases of data set 2 were determined using equation 3.5 and added to the plot (horizontal error bars). While the ranges for these setting are not completely reliable, since the efficiency data of set 2 is too high in energy, as explained above, the agreement with the calculation is good. The ranges of bias energies for the 0.5, 2, 3, 4, and 7×Cs bias

settings of data set 1 for the left detector were then determined and used to plot the ranges for their true bias settings (vertical error bars). Instead of 0.5, 2, 3, 4, and 7×Cs the actual bias settings were approximately 0.35, 2.2, 3.3, 4.7, and 9.0×Cs. The uncertainties for all five settings are estimated to be ±0.10×Cs.

The data for all of the bias settings for sets 1 and 2 are listed in appendix E and are shown later in figures 3.6 and 3.7. The relative uncertainties for the data were determined by combining in quadrature the uncertainties for TGCEN, $T_D(E_n)$, $Y_G(E_d,\theta)$, and $\sigma_G(E_n,\theta)$ (see equation 3.1). The uncertainties for Drosg's tabulations of the $\sigma(\theta)$ data for the $^2H(d,n)^3He$ reaction range from 1% (E_d=5 MeV) to 4% (E_d=17 MeV). The overall normalization uncertainties for the data are determined by combining in quadrature the uncertainties for NI, NT, and Ω (see equation 3.2). The uncertainties for NI and Ω are negligible. The uncertainty for NT is calculated by combining in quadrature the uncertainties for P, L, and T (see equation 3.4) and a 1% overall normalization uncertainty for Drosg's tabulations. The overall normalization uncertainty for data set 2 is 3.4%. The overall normalization uncertainty for data set 1 includes an additional factor for the uncertainty of the renormalization factor and is 4.1%.

3.3 Fitting Function

A reasonably simple function that fits the efficiency data is needed for use in the Monte Carlo codes used to correct the scattering data in the $\sigma(\theta)$ and $A_y(\theta)$ experiments. "Reasonably simple" means a function that takes only a few seconds of CPU time at most to calculate, since this quantity needs to be calculated for every neutron "detected" in the Monte Carlo

simulation. The number of such detected events is typically greater than 10^4 per angle investigated. An added advantage of being able to parametrize the efficiency systematically and properly is that it should be possible to predict accurately the efficiencies at biases not measured in the present work. Several simple functions based on the physics of the detection processes were explored in trying to fit the efficiency data of this work. No function, so based, was found that could be used to fit systematically all the data, much less produce accurate fits at the individual biases. Not even a purely mathematical function which ignored the physics could by found. The reason for this is the structure in the detector efficiency produced by the various $^{12}C+n$ reactions mentioned in section 3.1. Most of the functions tried were based in part on equation 3.5. In fact, some of the functions were fairly successful for describing the data at bias settings greater than $2\times Cs$, but not for the data at bias settings below $2\times Cs$. The disagreement between the data and the calculations becomes more pronounced as the biases decrease. This is due to the increasing structure caused by the $^{12}C+n$ reactions.

The best results were obtained with the following function, which though complicated in full written form, runs quickly, but requires large amounts of input:

$$\begin{aligned}\varepsilon(B_p,E) = C(B_p) \times \Big[&\varepsilon(^1H(n,n)^1H) + \varepsilon(^{12}C(n,n_0)^{12}C) + \varepsilon(^{12}C(n,n_1)^{12}C) \\ &+ \varepsilon(^{12}C(n,\alpha)^9Be) + \varepsilon(^{12}C(n,n')3\alpha) \\ &+ \varepsilon(^{12}C(n,p)^{12}B) + \varepsilon(^{12}C(n,d)^{11}B)\Big] . \qquad (3.10)\end{aligned}$$

At proton bias energy B_p, the detector efficiency for a neutron of energy E

is $\varepsilon(B_p,E)$. The factor $C(B_p)$ is a coefficient determined from a least-squares fit to the data. The remaining terms are: $\varepsilon(^1H(n,n)^1H)$, the contribution to the efficiency due to neutrons scattering up to three times from ^1H; $\varepsilon(^{12}C(n,n_0)^{12}C)$, the contribution to the efficiency due to neutrons elastically scattering first from ^{12}C and then up to twice from ^1H; $\varepsilon(^{12}C(n,n_1)^{12}C)$, the contribution to the efficiency due to neutrons inelastically scattering first to the first excited state of ^{12}C and then scattering up to twice from ^1H; $\varepsilon(^{12}C(n,\alpha)^9Be)$, the contribution to the efficiency due to the α-particle produced in the the $^{12}C(n,\alpha)^9Be$ reaction; $\varepsilon(^{12}C(n,n')3\alpha)$, the contribution to the efficiency due to the three α-particles produced in the $^{12}C(n,n')3\alpha$ reaction; $\varepsilon(^{12}C(n,p)^{12}B)$, the contribution to the efficiency due to the proton produced in the $^{12}C(n,p)^{12}B$ reaction; and $\varepsilon(^{12}C(n,d)^{11}B)$, the contribution to the efficiency due to the deuteron produced in the $^{12}C(n,p)^{12}B$.

The terms of equation 3.10 are expanded to their full form below. First, it is important to define some of the symbols and concepts to be employed. All the terms in equation 3.10 are dependent on the total probability $P_X(E)$ for the reaction X, which is the total cross section for the reaction divided by the total cross section for the scintillator times the attenuation in the scintillator. The attenuation A(E) is determined from $1 - \exp(-\rho_C t\sigma_{SC}(E))$ where ρ_C is the density of ^{12}C nuclei for the scintillator, t is the thickness of the scintillator, and $\sigma_{SC}(E)$ is the total microscopic neutron cross section of the scintillator $(\sigma_H\rho_H/\rho_C + \sigma_C)$ at neutron energy E. Note, as stated above, ρ_H is the density of ^1H nuclei for the scintillator. It is assumed for equation 3.10 that for second and third scatterings A(E) is calculated using t/2 and t/4, respectively, i.e.,

the scintillator thickness seen after a scattering is on an average one half of that before the scattering. Also, for each scattering or reaction, there is a factor that depends on the solid angle in the center-of-mass system through which the reaction X will result in light output greater than the bias setting. This factor $R_X(B_p,E)$ is the ratio of this solid angle to the total 4π solid angle in the center-of-mass system. For calculating this ratio, it was assumed that the process resulted in isotropic distributions in the center-of-mass system. This simplifying assumption is satisfactory for n-p scattering and was necessary for the reactions on ^{12}C for which little angular information is known. For $^{12}C(n,n_0)^{12}C$ and $^{12}C(n,n_1)^{12}C$, the assumption is recognizably crude. The quantities $R_X(B_p,E)$ replace the $1-B_p/E$ factors in equation 3.5.

The first term in equation 3.10 is then,

$$\varepsilon(^1H(n,n)^1H) = \varepsilon(H) + \varepsilon(HH) + \varepsilon(HHH) \ , \tag{3.11}$$

with

$$\varepsilon(H) = R_{Hnn}(B_p,E)P_{Hnn}(E) \ , \tag{3.12}$$

$$\varepsilon(HH) = [1 - R_{Hnn}(B_p,E)]P_{Hnn}(E)R_{Hnn}(B_p',E')P_{Hnn}(E') \ , \tag{3.13}$$

and

$$\varepsilon(HHH) = [1 - R_{Hnn}(B_p,E)]P_{Hnn}(E)[1 - R_{Hnn}(B_p',E')] \times P_{Hnn}(E')R_{Hnn}(B_p'',E'')P_{Hnn}(E'') \ , \tag{3.14}$$

where $E' = E-B_p/E$ and $B_p' = B_p-B_p'/2$, as in equation 3.5, and $E'' = E-3B_p/4$ and $B_p'' = B_p-3B_p/4$.

The second term in equation 3.10 is

$$\varepsilon(^{12}C(n,n_0)^{12}C) = \varepsilon(C) + \varepsilon(CH) + \varepsilon(CHH) \quad , \tag{3.15}$$

with $\varepsilon(C)$ approximately zero,

$$\varepsilon(CH) = P_{Cnn_0}(E)R_{Hnn}(B_p',E')P_{Hnn}(E') \quad , \tag{3.16}$$

and

$$\varepsilon(CHH) = P_{Cnn_0}(E)[1 - R_{Hnn}(B_p',E')]P_{Hnn}(E')R_{Hnn}(B_p'',E'')P_{Hnn}(E'') \quad , \tag{3.17}$$

where the average energy E' of the neutron after the first scattering is estimated to be 0.95E, $B_p' = B_p$, $E'' = E'-B_p/2$, and $B_p'' = B_p-B_p/2$.

The third term in equation 3.10 is

$$\varepsilon(^{12}C(n,n_1)^{12}C) = \varepsilon(C^*) + \varepsilon(C^*H) + \varepsilon(C^*HH) \quad , \tag{3.18}$$

with $\varepsilon(C^*)$ approximately zero,

$$\varepsilon(C^*H) = P_{Cnn_1}(E)R_{Hnn}(B_p',E')P_{Hnn}(E') \quad , \tag{3.19}$$

and

$$\varepsilon(C^*HH) = P_{Cnn_1}(E)[1 - R_{Hnn}(B_p',E')]P_{Hnn}(E')R_{Hnn}(B_p'',E'')P_{Hnn}(E'') \quad , \tag{3.20}$$

where $B_p' = B_p$, $EE'' = E'-B_p/2$, $B_p'' = B_p-B_p/2$, and the average energy E' of the neutron after the first scattering is estimated to be 0.85(E+Q).

The fourth term in equation 3.10 is

$$\varepsilon(^{12}C(n,\alpha)^{9}Be) = R_{Cn\alpha}(B_\alpha,E)P_{Cn\alpha}(E) \quad , \tag{3.21}$$

where B_α is the α-particle bias energy at which a recoiling α-particle will

have the same light output as a proton recoiling with energy B_p.

The fifth term in equation 3.10 is

$$\varepsilon(^{12}C(n,n')3\alpha) = R_{Cnn'3\alpha}(B_\alpha,E)P_{Cnn'3\alpha}(E) \ . \qquad (3.22)$$

For this fifth term, unlike the other terms, $R_{Cnn'3\alpha}(B_\alpha,E)$ is estimated to be of the form $1-(B_\alpha-Q)/E$. This form is used since there are far too many processes (several of which involving two step reactions) for the breakup of $^{12}C+n$ into three α-particles to try calculations of the type used for the other reaction mechanisms of equation 3.10. The choice of this form is somewhat arbitrary, but it is similar to the form $1-B_p/E$ for recoil protons in equation 3.5, and it is a reasonable one to use for the present purpose. Some of the complexity comes from the fact that the $^{12}C(n,n')3\alpha$ reaction is dominated by sequential decays with $^{12}C(n,\alpha')^9Be^*$ ($Q = -2.9$ MeV and higher magnitudes) and $^{12}C(n,n')^{12}C^*$ ($Q = -7.65$ MeV and higher magnitudes) being the dominant first reaction steps.

The sixth term in equation 3.10 is

$$\varepsilon(^{12}C(n,p)^{12}B) = R_{Cnp}(B_p,E)P_{Cnp}(E) \ . \qquad (3.23)$$

The seventh term in equation 3.10 is

$$\varepsilon(^{12}C(n,d)^{11}B) = R_{Cnd}(B_d,E)P_{Cnd}(E) \ , \qquad (3.24)$$

where B_d is the deuteron bias energy at which a recoiling deuteron will have the same light output as a proton recoiling with energy B_d.

The best fits obtained with equation 3.10 are plotted as solid lines in figures 3.6 and 3.7 for the efficiency data of all of the bias settings for the right and left detectors, respectively. The bias energies for protons,

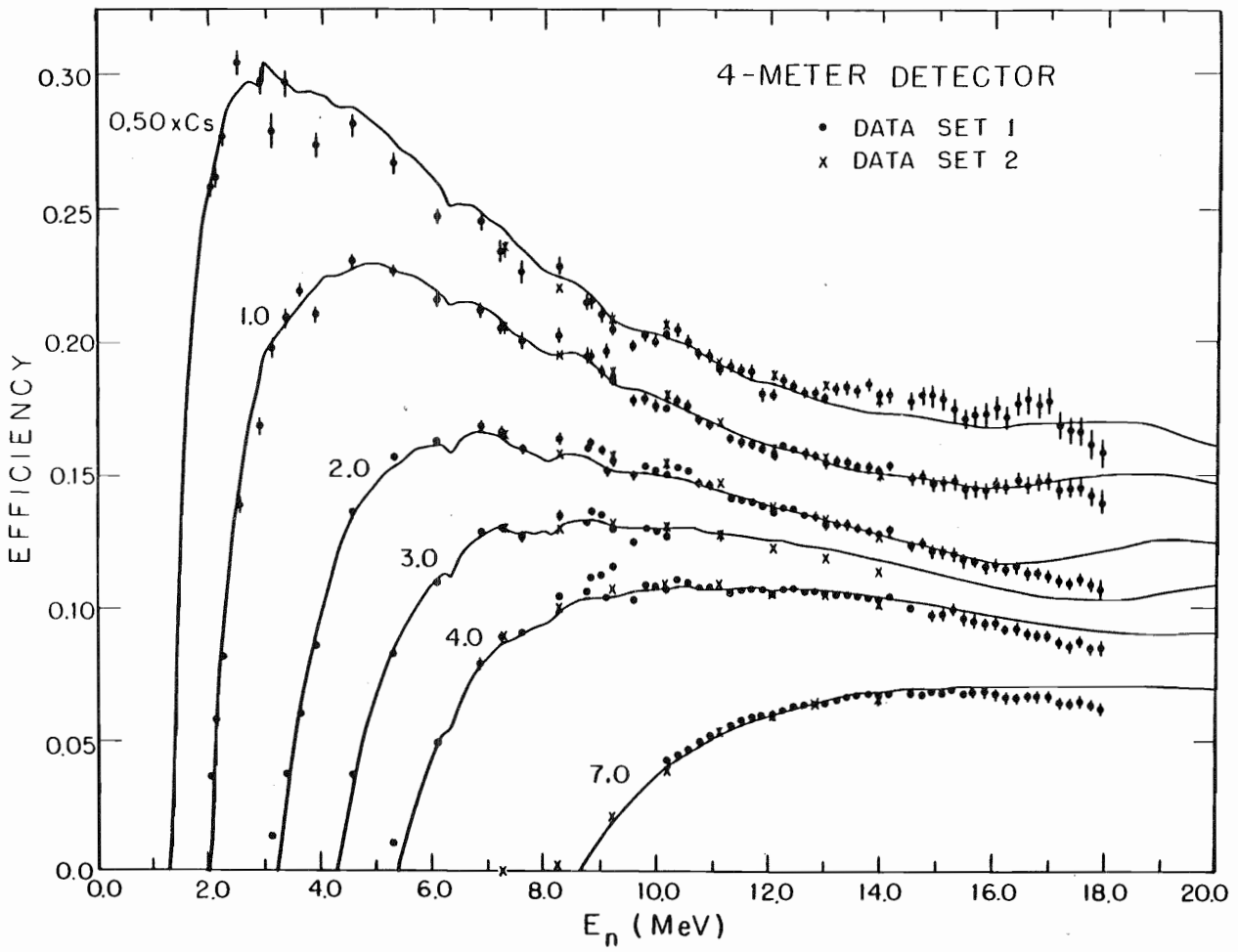

Figure 3.6. Multi-bias efficiency data and fits for the right (4-m) detector. The data of set 1 are from the first experiment for this work; those of set 2 are from the second. The fits were calculated using equation 3.10.

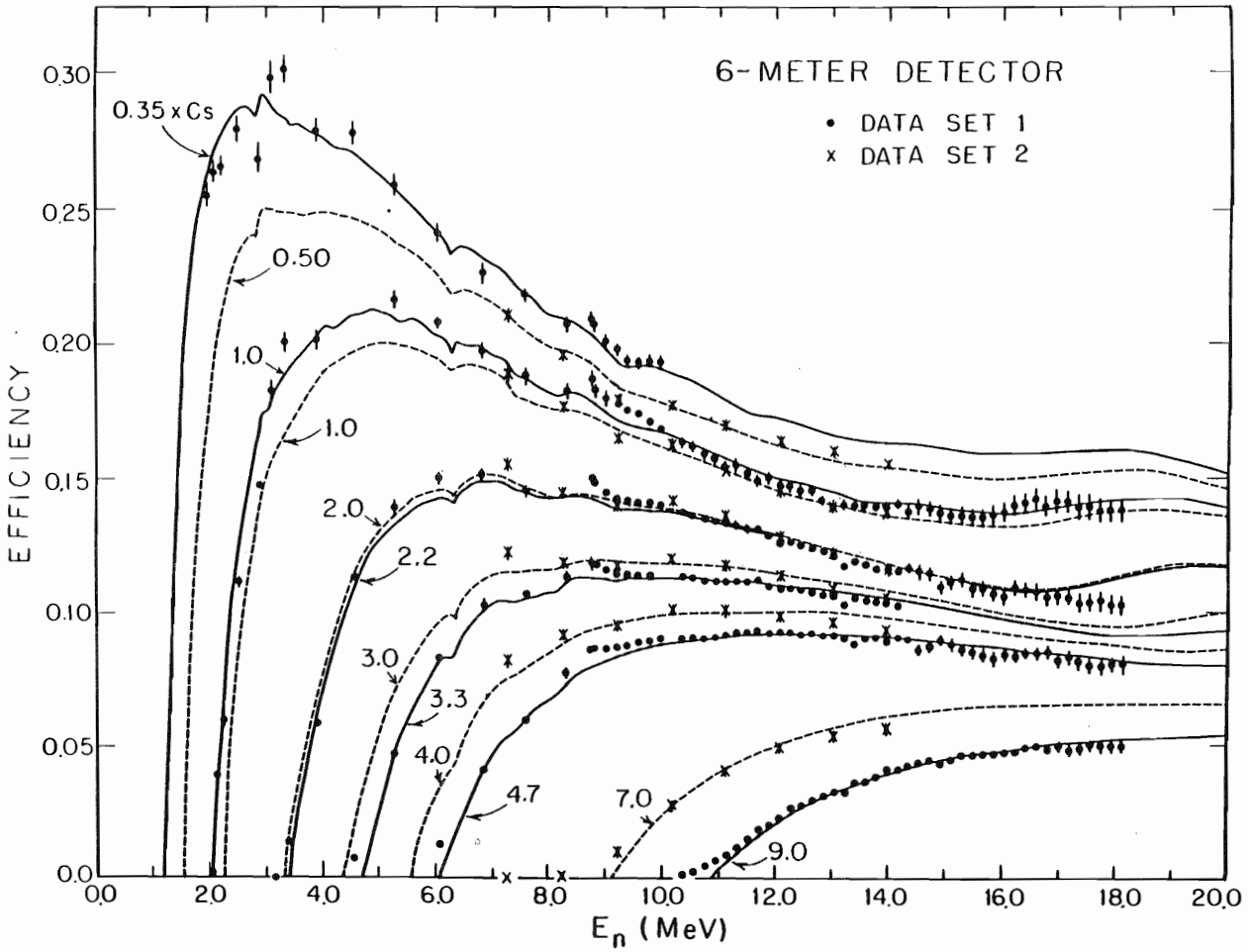

Figure 3.7. Multi-bias efficiency data and fits for the left (6-m) detector. The data of set 1 are from the first experiment for this work; those of set 2 are from the second. The fits were calculated using equation 3.10.

α-particles, and deuterons and the $C(B_p)$ coefficients used to make the fits are given in table 3-3. The bias energies for α-particles and deuterons is based on information from Dietze and Klein (Dietze 1982). The sources of the cross sections used in calculating the fits are listed in table 3-4. As can be seen from figures 3.6 and 3.7, with the exceptions of the 0.5×Cs setting for the right detector and all the data above 16 MeV, the fits to the data are quite good. The discrepancies between the data and fits above 16 MeV seem to be due to the overestimation of the contributions of the ^{12}C+n reactions. The discrepancies between the fit and the 0.5×Cs data of the right detector indicated that the structure of the ^{12}C+n reactions has important effects on the efficiency. The discrepancies for 0.5×Cs could probably be removed if the $^{12}C(n,n_0)^{12}C$ and $^{12}C(n,n_1)^{12}C$ reactions were handled more exactly and the cross sections for the other ^{12}C+n reactions were better determined. Presumably, if there were more detailed data for the left detector at the 0.35 and 0.5×Cs setting, then there would a lot of structure in the data.

3.4 Conclusions

Several important results can be drawn from the data obtained in the multi-bias efficiency measurements. The first is a much more detailed knowledge of the shapes of the efficiency functions for the detectors between 9.2 and 18.0 MeV than was obtained from El-Kadi's measurements. The second is that a close inspection of the 1×Cs and 2×Cs data for the right and left detectors shows noticeable differences between the data for the two detectors. The data at the other biases are not easily compared, due to the zero-offset.

TABLE 3-3

Parameters Used in Equation 3.10 for the Fits to the Efficiency Data

	Bias Energy (× Cs)	B_p (MeV)	B_α (MeV)	B_d (MeV)	$C(B_p)$
Right Detector Data Sets 1 and 2	0.50	1.30	3.87	1.69	1.07 ± 0.35%
	1.0	2.00	5.58	2.58	1.03 ± 0.84%
	2.0	3.20	8.19	4.00	1.01 ± 0.58%
	3.0	4.28	10.8	5.30	1.04 ± 0.78%
	4.0	5.35	13.6	6.56	1.03 ± 0.92%
	7.0	8.60	23.1	10.3	1.05 ± 0.58%
Left Detector Data Set 1	0.35	1.20	3.62	1.56	1.03 ± 0.61%
	1.0	2.05	5.60	2.60	1.02 ± 1.49%
	2.2	3.38	8.61	4.21	1.01 ± 0.57%
	3.3	4.70	11.9	5.80	1.02 ± 0.65%
	4.7	6.05	15.6	7.39	1.03 ± 1.01%
	9.0	10.9	29.9	12.8	1.07 ± 2.52%
Left Detector Data Set 2	0.50	1.50	4.38	1.96	1.02 ± 0.96%
	1.0	2.20	6.03	2.83	1.01 ± 0.43%
	2.0	3.30	8.42	4.12	1.00 ± 0.86%
	3.0	4.35	11.0	5.39	1.01 ± 1.25%
	4.0	5.50	14.1	6.75	1.03 ± 1.71%
	7.0	9.05	24.5	10.8	1.07 ± 13.3%

TABLE 3-4

References for the Total Cross Sections

Used in Equation 3.10 for the Fits to the Efficiency Data

Reaction	Q-Value	Reference
$^{1}H(n,n)^{1}H$		Gammel 1963
$^{12}C+n$		ENDF/B-V
$^{12}C(n,n_0)^{12}C$		ENDF/B-V
$^{12}C(n,n_1)^{12}C$	-4.44 MeV	ENDF/B-V
$^{12}C(n,\alpha)^{9}Be$	-5.70 MeV	Dietze 1982
$^{12}C(n,n')3\alpha$	-7.28 MeV	Antolkovic 1983
$^{12}C(n,p)^{12}B$	-12.59 MeV	Garber 1976
$^{12}C(n,d)^{11}B$	-13.73 MeV	Garber 1976

One important conclusion of the efficiency analysis is that there is no simple systematic way to fit the data when the $^{12}C+n$ interactions are important. The method of using equation 3.10 to fit the data is more time consuming than is desirable for use in the Monte Carlo codes that are employed to make corrections to neutron scattering data. For the Monte Carlo codes used to correct the $\sigma(\theta)$ and $A_y(\theta)$ data at TUNL, a simple interpolation of the experimental data may be necessary.

There are several steps that should be taken if the efficiencies of the detectors are ever measured again. The overall normalization uncertainty could be reduced by measuring the deuterium gas pressure more precisely than was possible with the gauge used in the present case. Also, several angular distributions of the $^2H(d,n)^3He$ reaction with smaller angle increments should be measured, so that the efficiencies at energies below 9.2 MeV can be determined as well as were those above 9.2 MeV in the present measurement. However, the accuracy of such angular distribution data is limited by the uncertainties of the cross sections in Drosg's (Drosg 1978) definitive compilation of values for the $^2H(d,n)^3He$ reaction. Finally, special care should be taken to guarantee that the efficiencies of both detectors are determined at identical bias settings.

One additional point should be mentioned. After the efficiency analysis was completed, it was realized that there is a problem with some of the data from the angular distribution measurement for the $^2H(d,n)^3He$ reaction at an incident deuteron energy of 6 MeV. The information given in tables 3-1 and 3-2 is for the ideal case of a neutron emitted from a reaction at the center of the gas cell. For this ideal case the largest θ_{lab} allowable -- without a neutron encountering the base of the gas cell

(i.e., the area near the foil) -- is 141.6°. However, we now realize that for neutrons emitted in reactions in the first half of the gas volume, some of the neutrons will encounter the base of the gas cell starting with $\theta_{lab} = 90^{\circ}$. Therefore, for all of the data taken for θ_{lab} greater than 90° (i.e., for neutrons with energies lower than about 4 MeV in our efficiency measurement), there is an additional attenuation effect. The precise magnitude of this effect is difficult to calculate, since it varies from angle to angle, and since it also varies according to the site where the neutrons are emitted in the gas cell. Our estimate for the worst case, where θ_{lab} is equal to 140°, gives a maximum effect of about 5%. For any future efficiency measurements at TUNL, it is suggested that for angular distributions for the $^{2}H(d,n)^{3}He$ reaction, θ_{lab} should not be greater than 90° with the present design of the gas cell.

CHAPTER 4

EXPERIMENTAL DATA: CORRECTIONS AND RESULTS

4.1 Introduction

The method of reduction of the spectra at TUNL for the $\sigma(\theta)$ and $A_y(\theta)$ experiments into usable data and the procedures for correcting the data are discussed extensively in Howell 1984 and Guss 1982a. Therefore, the descriptions given in this chapter will be as brief as possible. However, special problems were encountered with the 17 MeV data for ^{54}Fe and ^{58}Ni and some of the ^{93}Nb data due to inelastic scattering states lying close to the ground states, because of the resolution properties of the spectrometer facility. The methods for dealing with these problems will be described in detail. Codes for stripping the data with the VAX-11/780 were written by C.R. Howell.

4.2 Cross Section Measurements

4.2.1 Data Stripping

The first step in analyzing the $\sigma(\theta)$ data deals with the monitor spectra. Examples of spectra for the neutron flux monitor are shown in figure 4.1; the information given in the figure and caption will be explained below. First, a "monitor window" -- designated by two channels in the time-of-flight spectrum -- is set on the narrow peak of good neutron events in the spectrum (see figure 4.1). The "good" events in the neutron peaks are due to neutrons that come directly from the $^{2}H(d,n)^{3}He$ ground state reaction in the gas cell. The window excludes from consideration any

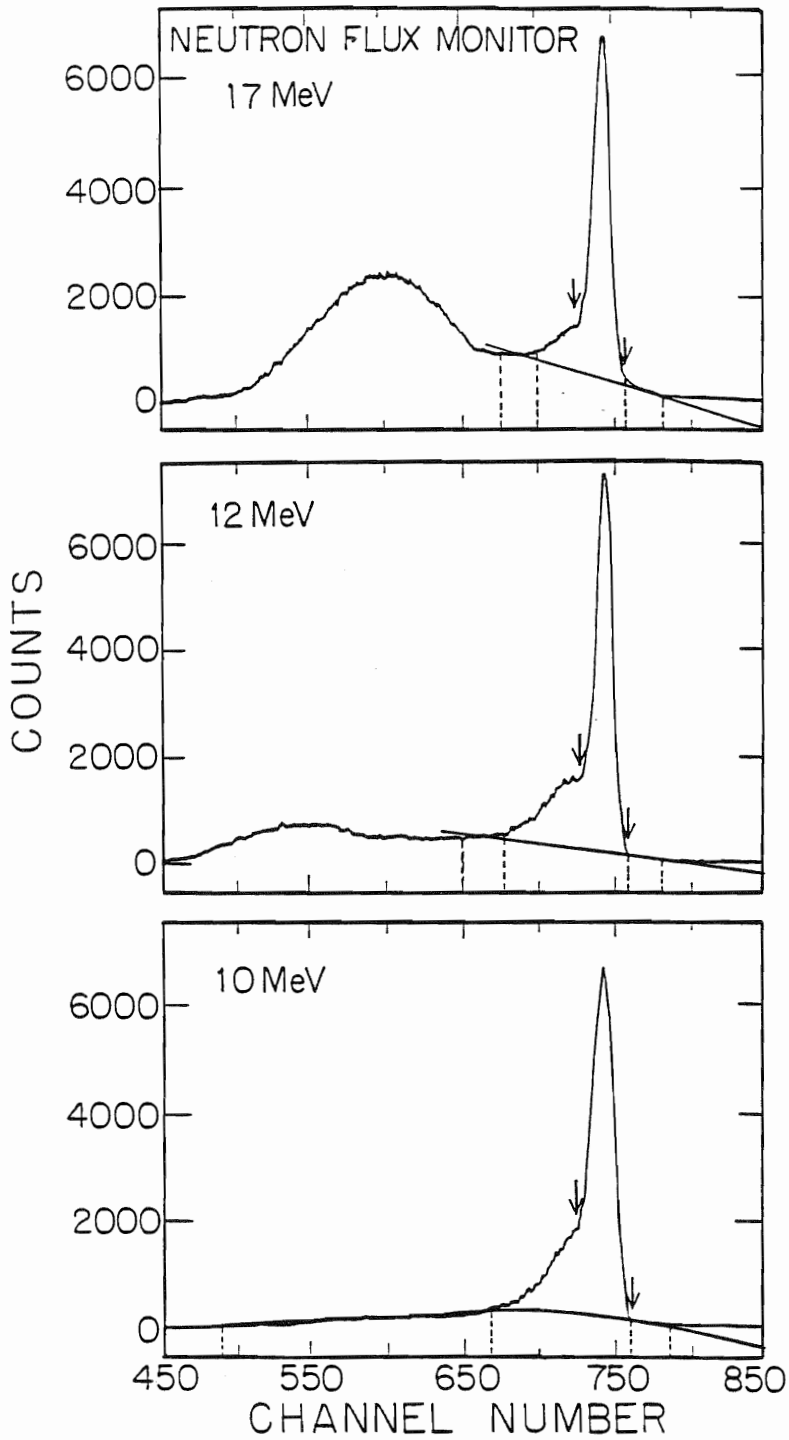

Figure 4.1. Spectra from the neutron flux monitor at 10, 12, and 17 MeV. The smooth solid lines are the background estimates for the region or the peaks, and the vertical short dashed lines indicate the two windows selected for the backgrounds. The arrows indicate the limits of the windows chosen about the neutron peaks.

high- and low-energy neutrons to the left and right of the discrete neutron peak. Also excluded from consideration, are the "break-up" neutrons at the lower energies to the left of the discrete peak. "Break-up" neutrons are produced in the breakup of two deuterons colliding in the gas cell, resulting in the reaction $^{2}H(d,np)d$ (Q = -2.23 MeV) or $^{2}H(d,np)np$ (Q = -4.45 MeV).

After the monitor window is selected, a "monitor background" is selected through the regions to the left and right of the peak to estimate the level of background neutron events lying under the discrete peak (see figure 4.1). Note that to insure a proper normalization of the entire data set, the same window and similar backgrounds must be used for all of the in and out spectra from the neutron flux monitor including the spectra for the polyethylene and carbon normalization measurements. Occasional shifts in timing, due to changes in the operating conditions of the various particle-beam related equipment, required shifting the monitor windows one or more channels, but care was used to guarantee that the widths of the windows were held constant.

After the background and windows are set, the neutron events inside the monitor windows and above the backgrounds are summed to obtain the monitor yields for both in and out spectra. Then the ratio of the in to out yields is calculated.

The second step in analyzing the $\sigma(\theta)$ data is to calculate difference spectra for the right and left detectors. The out spectra for the right and left detectors are scaled by the above ratio for the neutron flux monitor. Then, the scaled out spectra must be subtracted from their corresponding in spectra, yielding difference spectra for the right and left detectors.

Examples of in, out, and difference spectra for the left detector for ^{58}Ni+n at 17 MeV are shown later in figure 4.2.

The next step after the difference spectra for the right and left detectors have been formed is the calculation of the yields for the various discrete peaks of interest in the difference spectra. First, backgrounds are drawn in the difference spectra to remove from consideration the residual background -- still existing after the subtraction of the out spectra -- that lies under the peaks of interest. Then, as with the monitor, windows are chosen about the peaks of interest. Care must be taken to include <u>all</u> of the good neutron events in this case, as opposed to the monitor case where only a relative number is required. The yield designated as $Y(\theta_{lab})$ is defined as the number of counts in a window after the subtraction of the background. The "high-low" background method (yields are obtained with high and low background estimations and then averaged) is employed when the selection of backgrounds is ambiguous. The high- low background procedure is documented in Guss 1982a. Note that the yields for the difference spectra for n-p scattering from the normalization measurements are averaged for use in the normalization procedure -- one average yield for the right detector and one for the left detector. In figure 4.2, background estimates and window settings for the elastic scattering peak (0^+) and for scattering to the first excited state (2^+) are displayed for ^{58}Ni+n.

Corrections, due to tails of the peaks for elastically scattered neutrons that extend under the inelastic peaks, were required for the inelastic scattering data for ^{54}Fe and ^{58}Ni at 17 MeV. The tailing problem is due to the limitations of the chopping and bunching system at TUNL and

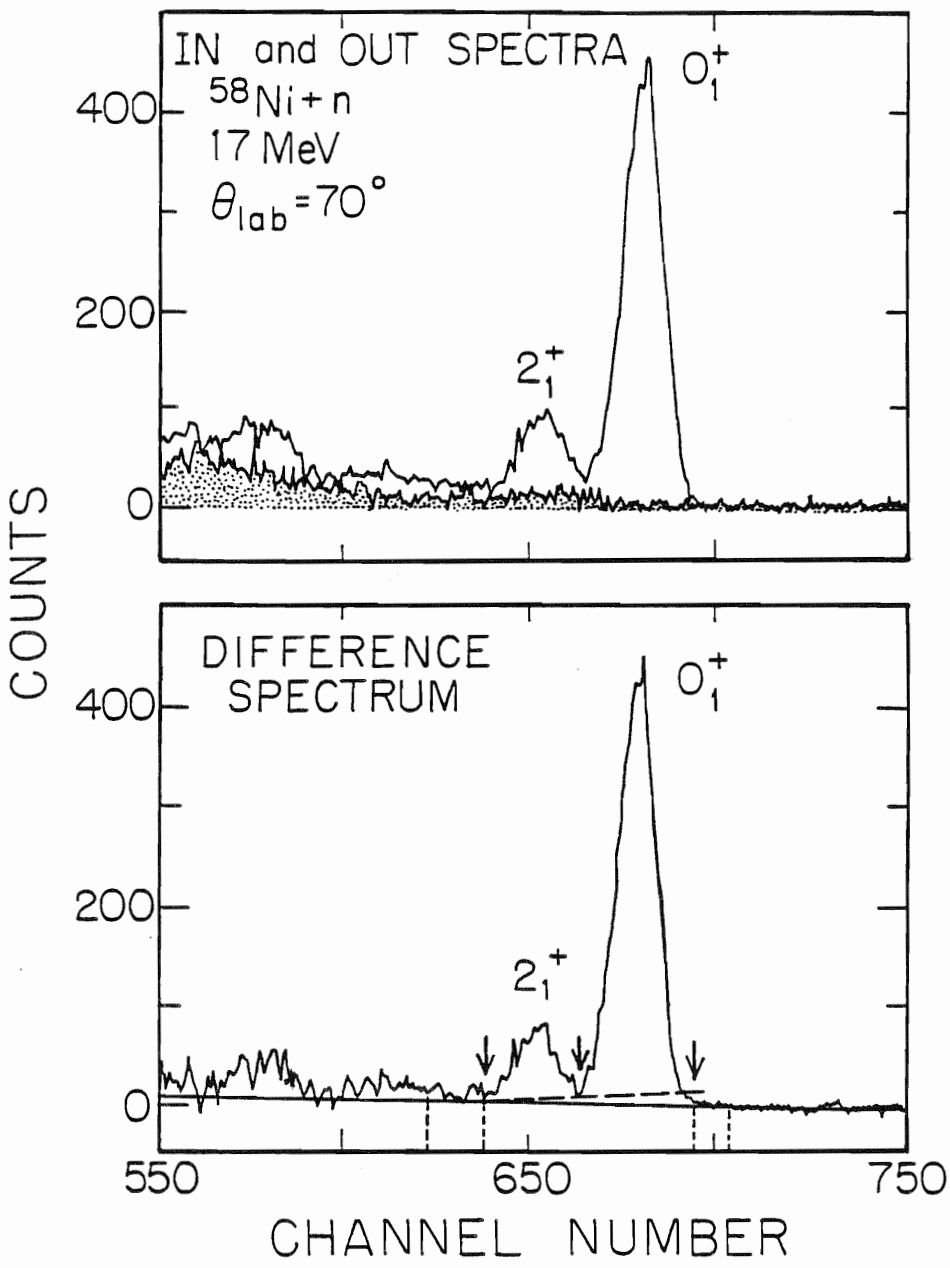

Figure 4.2. In, out, and difference spectra from the left detector for ^{58}Ni+n at 17 MeV. The shaded region in the top plot is the out spectrum. The elastic and inelastic scattering peaks are labeled 0^+ and 2^+, respectively. In the difference spectrum, the smooth solid line is the background for the 0^+ peak, the vertical short dashed lines indicate the windows for this background, and the long dashed line indicates the background for the 2^+ peak. The arrows indicate the windows chosen about the neutron peaks.

the short flight path of the right detector. Evidence of the existence of tails due to the chopping and bunching system can be seen in the line shape of the timing monitor shown later in figure 4.10. The tail is visible starting near channel 465 and extending on down to channel 375 where the deuteron break-up reaction becomes visible. Note that the the right side of the neutron peak drops quickly to zero near channel 490, while the left side drops off more gradually and reaches a minimum level near channel 450. The magnitude of the tail for this particular angle pair is not large compared to the peak height. However, at forward angles where inelastic scattering is small compared to elastic scattering, the tail may be equal in magnitude or larger than the magnitude of good neutron events in an inelastic scattering peak.

Corrections for the tails were made by making estimates of their contributions from the line shape of the timing monitor spectra. This was done by scaling the peak in the timing monitor to overlay the elastic peaks in the difference spectra of the right and left detectors. For ^{93}Nb, the line shape of the timing monitor was also used to make estimates of the contributions of low-lying excited states ($Q \geq 0.69$ MeV) to the elastic scattering peaks in the difference spectra. There is, of course, no way at present to remove any contribution from scattering to the first excited state of ^{93}Nb that has a Q-value of 30 keV. The procedure employed for ^{93}Nb was required primarily at the higher scattering energies (14 and 17 MeV). Typical ^{93}Nb+n difference spectra are shown in figure 4.3 for the right detector.

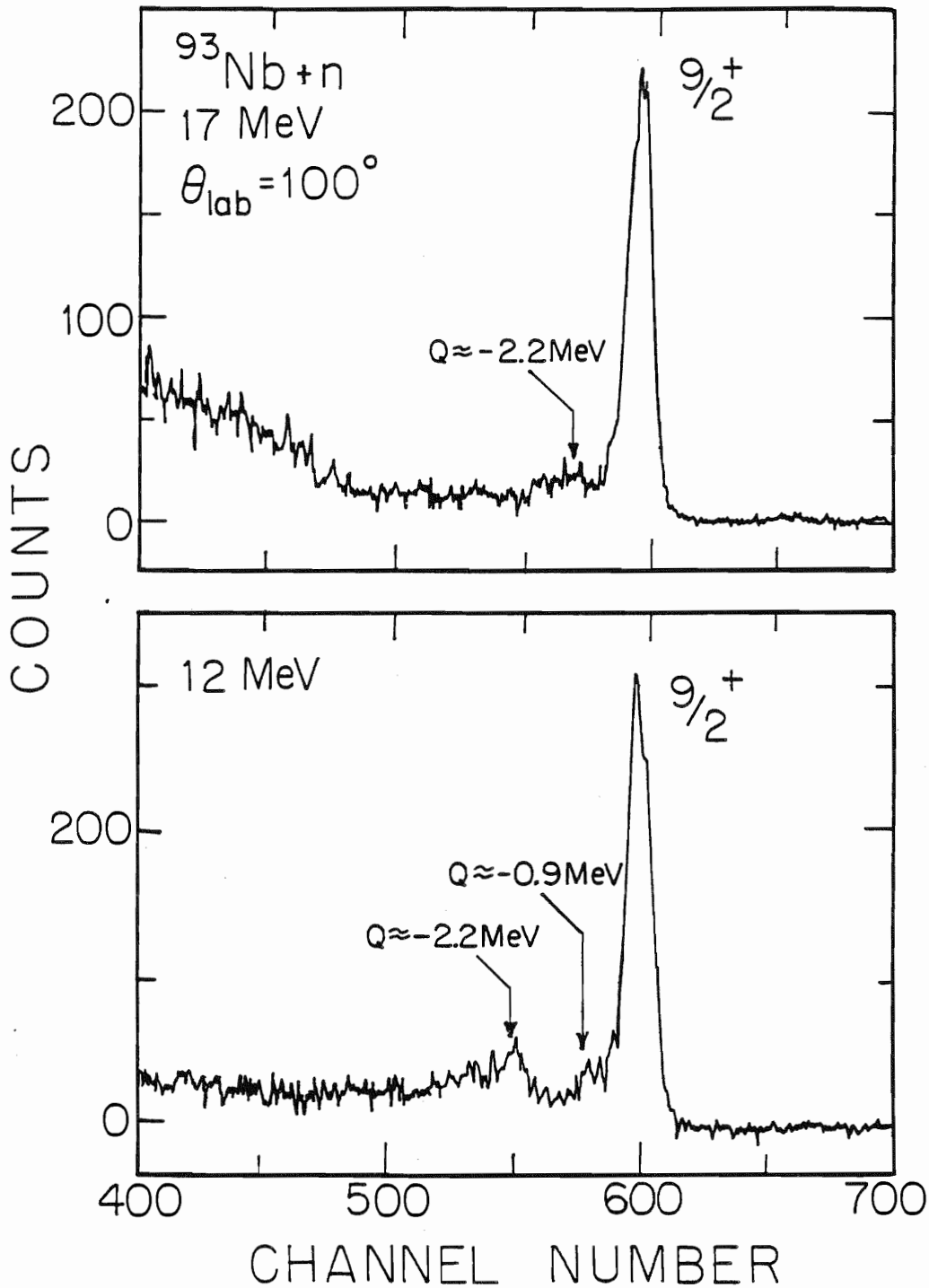

Figure 4.3. Difference spectra from the right detector for ^{93}Nb+n at 12 and 17 MeV.

4.2.2 Data Normalization

The next stage in the data reduction procedure after all the yields $Y(\theta_{lab})$ for a sample are extracted is to normalize and correct the $Y(\theta_{lab})$ using the following equation:

$$\sigma_S(\theta_{lab}) = F_{norm} \times M_S(\theta_{lab}) \times Y_S(\theta_{lab}) , \qquad (4.1)$$

In this equation, the subscript S denotes values associated with the scattering sample, F_{norm} is the constant normalization factor, which will be discussed in this section, and $M_S(\theta_{lab})$ is a correction factor to be discussed in section 4.2.3.

The quantity F_{norm} is calculated from the formula:

$$F_{norm} = \frac{n_H}{n_S} \times \frac{1}{PCF(\theta_H)} \times \frac{\sigma_H(\theta_H)}{Y_H(\theta_H)} , \qquad (4.2)$$

where the subscript H denotes values associated with the normalization measurement for n-p scattering in which polyethylene and carbon scattering samples are used. The quantity θ_H is the angle at which the normalization measurement was made. The ratio n_H/n_S is the number of ^1H nuclei in the polyethylene sample divided by the number of nuclei in the scattering sample. The quantity $PCF(\theta_H)$ is a correction factor for relative efficiency, attenuation, finite geometry, and multiple scattering effects that is applied to $Y_H(\theta_H)$, the averaged yield for ^1H+n at θ_H. The calculation of the PCF factors are fully explained in appendix D. Finally, $\sigma_H(\theta_H)$ is the known n-p scattering cross section; the values used are the well-determined values of Hopkins and Breit (Hopkins 1971). Note, the $\sigma(\theta)$ data for each detector is normalized relative to the normalization measurements made with the detector, leading to a normalization uncertainty

for each detector; the larger of which is reported for the entire $\sigma(\theta)$ distribution.

4.2.3 Multiple Scattering, Finite Geometry, and Attenuation Corrections

The factor $M_S(\theta_{lab})$ of equation 4.1 is a correction factor for attenuation, finite geometry, relative efficiency and multiple scattering effects in the scattering sample. These correction factors are calculated and applied to the normalized data ($F_{norm} \times Y_S(\theta_{lab})$) by using the Monte Carlo code EFFIGY15 (Pedroni 1984). EFFIGY15 is the current version of the code EFFIGY written by H.H. Hogue (Hogue 1977b). In the evolution process that produced EFFIGY15, there were several intermediate versions of the code including numerous modifications and corrections. The production of EFFIGY15 and the writing of a user's manual, "EFFIGY15 Manual," (Pedroni 1984) was one of the major projects leading up to the present work. This manual describes in detail the procedure for using EFFIGY15 to correct data.

The code EFFIGY15 simulates the experiment in the lab system and obtains corrections for the data using an iterative procedure. In each iteration of the correction process, the experiment is simulated by using a library of cross sections and the physical parameters of the experiment (i.e., the characteristics of the deuteron beam, gas cell, scatterer, and the detector) to generate time-of-flight spectra at each angle for which measurements were made.

The initial cross section library contains coefficients from a Legendre polynomial fit made to the current experimental $\sigma(\theta)$ data. If only $\sigma(\theta)$ data for elastic scattering is being corrected, then the library only needs

coefficients for elastic scattering. If $\sigma(\theta)$ data for inelastic scattering is being corrected, then the library needs coefficients for elastic scattering and for inelastic scattering to the state under consideration, as well as for inelastic scattering to any states with Q-values less than the Q-value of the state under consideration. The initial library, besides coefficients from a fit to the experimental data, should also contain coefficients at energies other than the experimental energy if $\sigma(\theta)$ data is available. The library also needs the total cross sections for the scatterer.

The simulation is done by following individual neutron histories through the production at the gas cell and the scattering and detection processes. Weights or probabilities are calculated for the neutron histories for each process involved. The source, scattering, and detection sites of the neutron are chosen randomly inside the gas cell, sample, and detector volumes (see figure 2.4). The first scattering is forced, and a weighted random selection process is used to decide whether or not the neutron scatters more than once, and, if so, by what process. The term Monte Carlo comes from this use of random selections. As with the experiment, the statistical accuracies of the peaks of interest in the simulated time-of-flight spectra are checked periodically to determine when sufficient neutron histories have been run. Yields are calculated from the simulated time-of-flight spectra and used with values generated from the current $\sigma(\theta)$ parameters in the cross section library at the experimental energy to calculate correction factors. The correction factors are applied to the experimental data to obtain the corrected $\sigma(\theta_{lab})$ values.

At this stage, the calculated yields are compared to the experimental values to check for the convergence of the calculation. Convergence is achieved when the calculated yields and the experimental values agree to within a set percentage. If convergence is not achieved for an iteration, then the cross section library is updated with coefficients from Legendre polynomial fits to the corrected experimental data of the present iteration. The parameters from the fit become the new current values in the cross section library at the energy of the data being corrected, and a new iteration is begun. The iteration process terminates when convergence is achieved. The corrected experimental $\sigma(\theta_{lab})$ data of the converged iteration are converted to the center-of-mass system to obtain the final reported $\sigma(\theta_{c.m.})$ data.

Several other features of the code are noteworthy. Corrections are calculated simultaneously for both elastic and inelastic scattering to all of the states for which data is input. The mean energy of the incident neutrons and the mean scattering angles are also obtained from the simulation. Furthermore, all of the data for an entire measured angular distribution are calculated in the same Monte Carlo run.

The significance of the multiple scattering corrections for $\sigma(\theta)$ data for the ^{93}Nb sample at 10 MeV is shown in figure 4.4. The normalized data (open circles) and corrected data (closed circles) are shown together with data corrected only for attenuation (crosses) by using the "disc approximation" of Kinney (Kinney 1970). The dominant correction is for the attenuation of scattered neutrons as they traverse the scattering sample. This effect causes a lowering of the experimental yields by approximately the same factor across the entire distribution. The effect of the

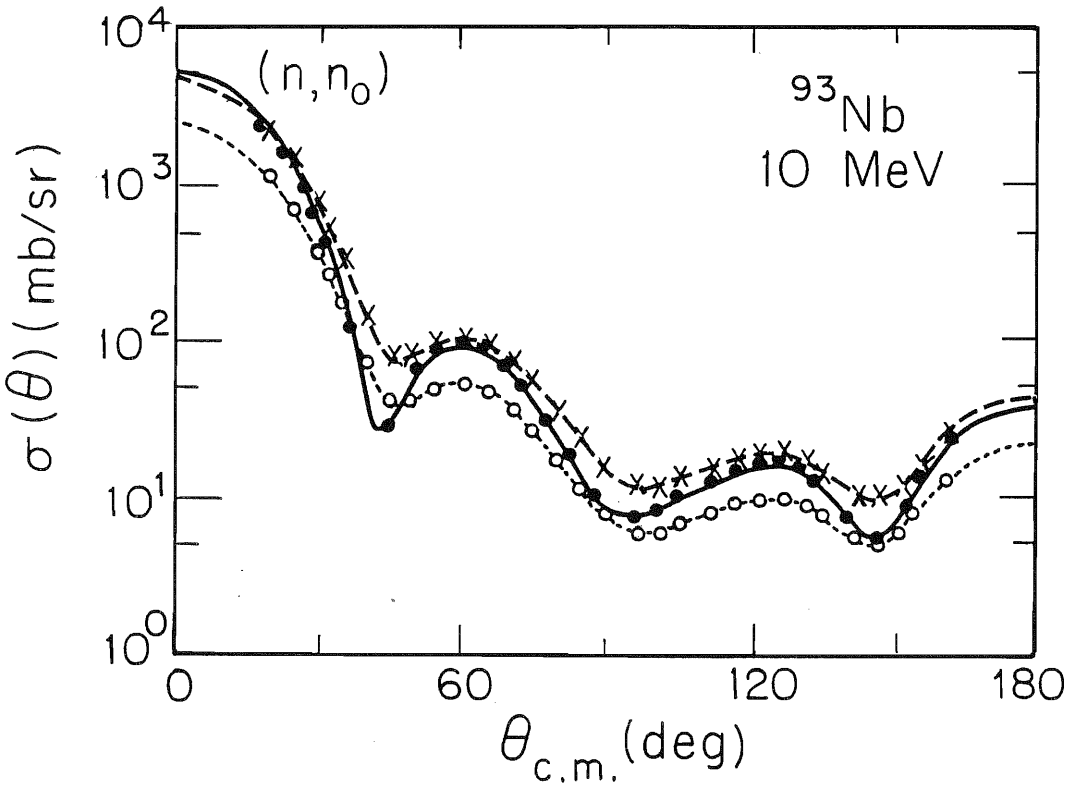

Figure 4.4. Multiple scattering corrections for $\sigma(\theta)$ data for neutron elastic scattering from ^{93}Nb at 10 MeV. The open circles are the uncorrected data, the crosses are the data corrected only for attenuation using the disc approximation (Kinney 1970), and the solid circles are the final data as corrected using EFFIGY15. All lines are Legendre polynomial fits to the data.

correction for second, third, and higher order scatterings and for the finite size or geometry of the scattering sample is to deepen the values in the vicinity of the $\sigma(\theta)$ minima.

4.2.4 Presentation of Final Data

The corrected $\sigma(\theta_{c.m.})$ data for all of the samples are tabulated in appendix A. The tabulations also include the normalized lab data (i.e., before corrections for finite geometry, efficiency, attenuation, and multiple scattering effects), the coefficients derived from Legendre polynomial fits to the data, and various other useful parameters associated with the data. The coefficients and equation A.1 can be used to reproduce the fits.

The listed relative uncertainties for the data include the uncertainty of the yields and the calculated uncertainties for the $M_S(\theta_{lab})$ factors. The uncertainty for each yield is calculated from the statistical uncertainty of the peak in the difference spectrum plus the additional uncertainties from the subtraction process for the in and out spectra, the background subtraction process, and the estimates of contaminant tails, which were obtained from the timing monitor line shapes (where applicable). Guss 1982a and Howell 1984 document the procedures for the calculation of uncertainties for the $\sigma(\theta)$ data.

The normalization uncertainties are tabulated by combining in quadrature the uncertainties for n_S (given in table 2-1), n_H (given in table D-1), $PCF(\theta_H)$ (given in table D-2), the relative efficiency (a maximum of 2.5% is used for all energies) and $Y_H(\theta_H)$ (1.2% to 2.8%). We note that the uncertainty in the $\sigma_H(\theta_H)$ factor of equation 4.2 drops out because this

factor exactly cancels with part of the $PCF(\theta_H)$ factor (see appendix D). However, the uncertainty for the $PCF(\theta_H)$ factor still includes an uncertainty associated with the $\sigma_H(\theta_H)$ values.

The corrected $\sigma(\theta_{c.m.})$ data for the elastic scattering of 17 MeV neutrons from ^{54}Fe and for the inelastic scattering of 17 MeV neutrons to the first excited state (Q = 1.41 MeV) of ^{54}Fe are shown in figure 4.5. Legendre polynomial fits to both of the ^{54}Fe distributions are also shown. The relative uncertainties in these data range from 2.2% to 6.5% for the elastic scattering data and from 6.1% to 33.7% for the inelastic scattering data.

The $\sigma(\theta_{c.m.})$ data at 17 MeV for ^{58}Ni for neutron elastic scattering and inelastic scattering to the first excited state (Q = -1.45 MeV) are shown in figure 4.6. Legendre polynomial fits are also shown. The relative uncertainties in these data range from 2.2% to 6.3% for the elastic scattering data and from 6.9% to 54.5% for the inelastic scattering data.

The corrected $\sigma(\theta_{c.m.})$ data for the elastic scattering of neutrons from ^{93}Nb at 8, 10, 12, 14, and 17 MeV are shown in figure 4.7 together with Legendre polynomial fits to the data. The relative uncertainties for these data range as follows: for 8, 10, and 12 MeV, generally from about 3% to 6%, but reaching a maximum of 8% in the first minimum of the distribution and for 14 17 MeV, generally from about 4% to 8.%, but reaching a maximum of around 13% in the first minimum of the distribution. Note that the ^{93}Nb data include a weak contribution from inelastic scattering to the first excited state (Q = -0.03 MeV, $J^{\pi} = 9/2^{+}$), which cause the minima of the $\sigma(\theta)$ distributions to be higher than they should. However, in all possible technological applications of this data, the combined $\sigma(\theta)$ for scattering to

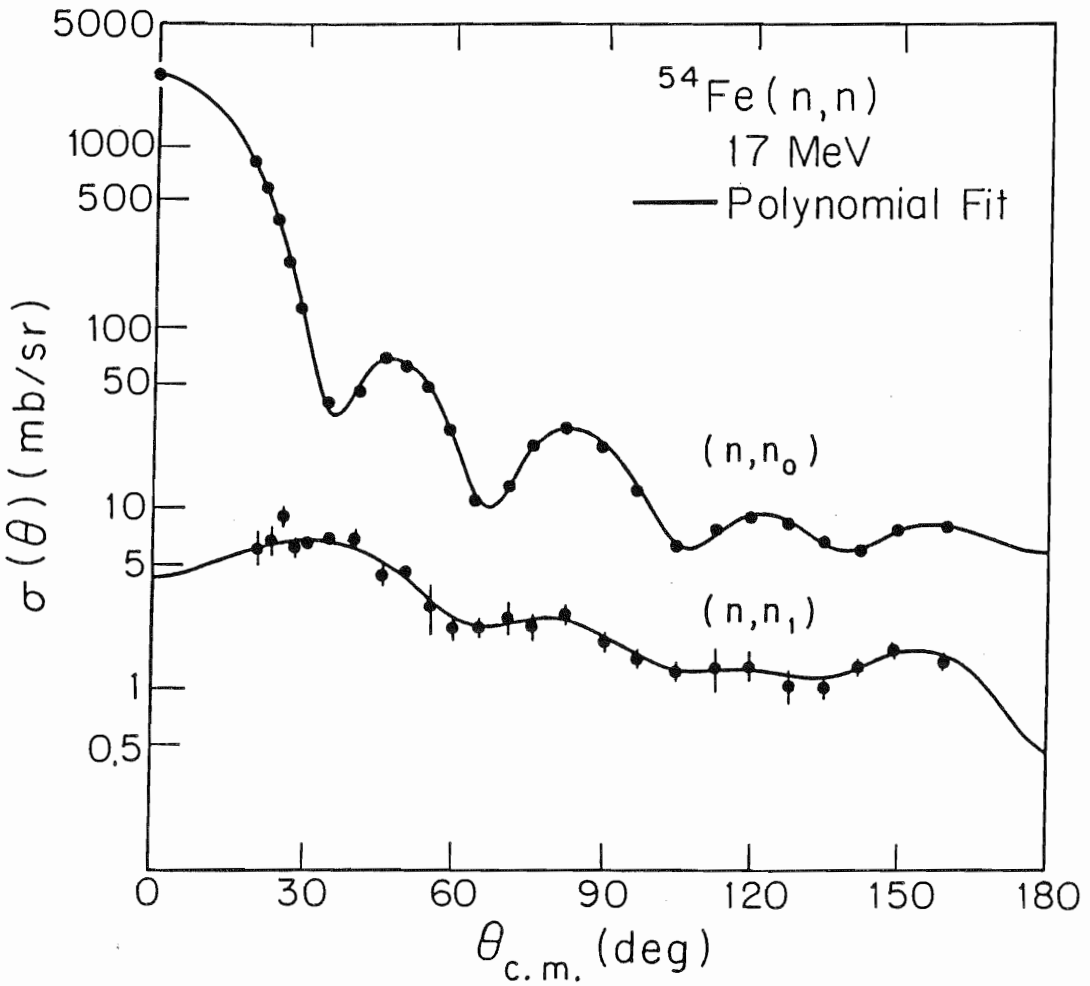

Figure 4.5. The $\sigma(\theta)$ data for the elastic scattering and inelastic scattering (to the first 2^+ state) of 17 MeV neutrons from ^{54}Fe. The curves are Legendre polynomial fits to the data. The point at 0^o for the elastic data is the calculated Wick's limit (Wick 1949).

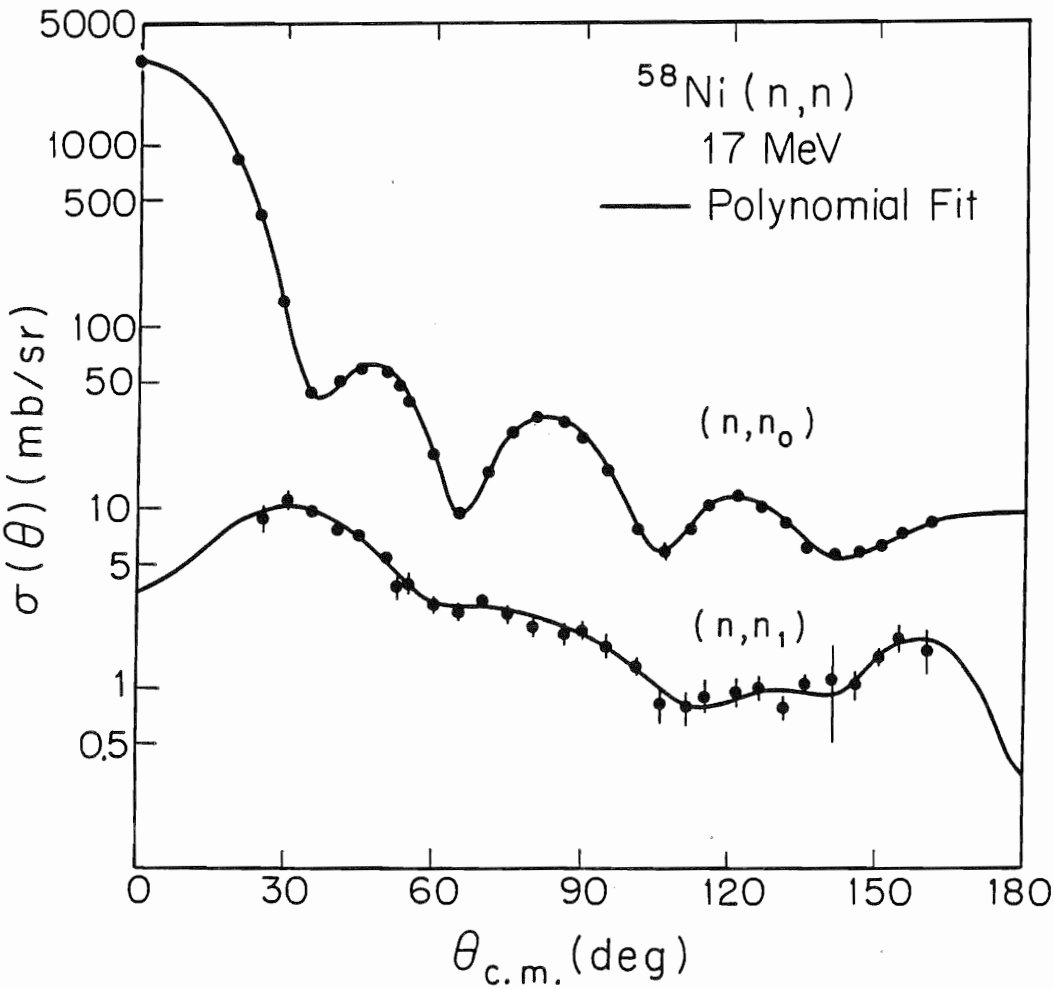

Figure 4.6. The $\sigma(\theta)$ data for the elastic scattering and inelastic scattering (to the first 2^+ state) of 17 MeV neutrons from ^{58}Ni. The curves are Legendre polynomial fits to the data. The point at 0^o for the elastic data is the calculated Wick's limit (Wick 1949).

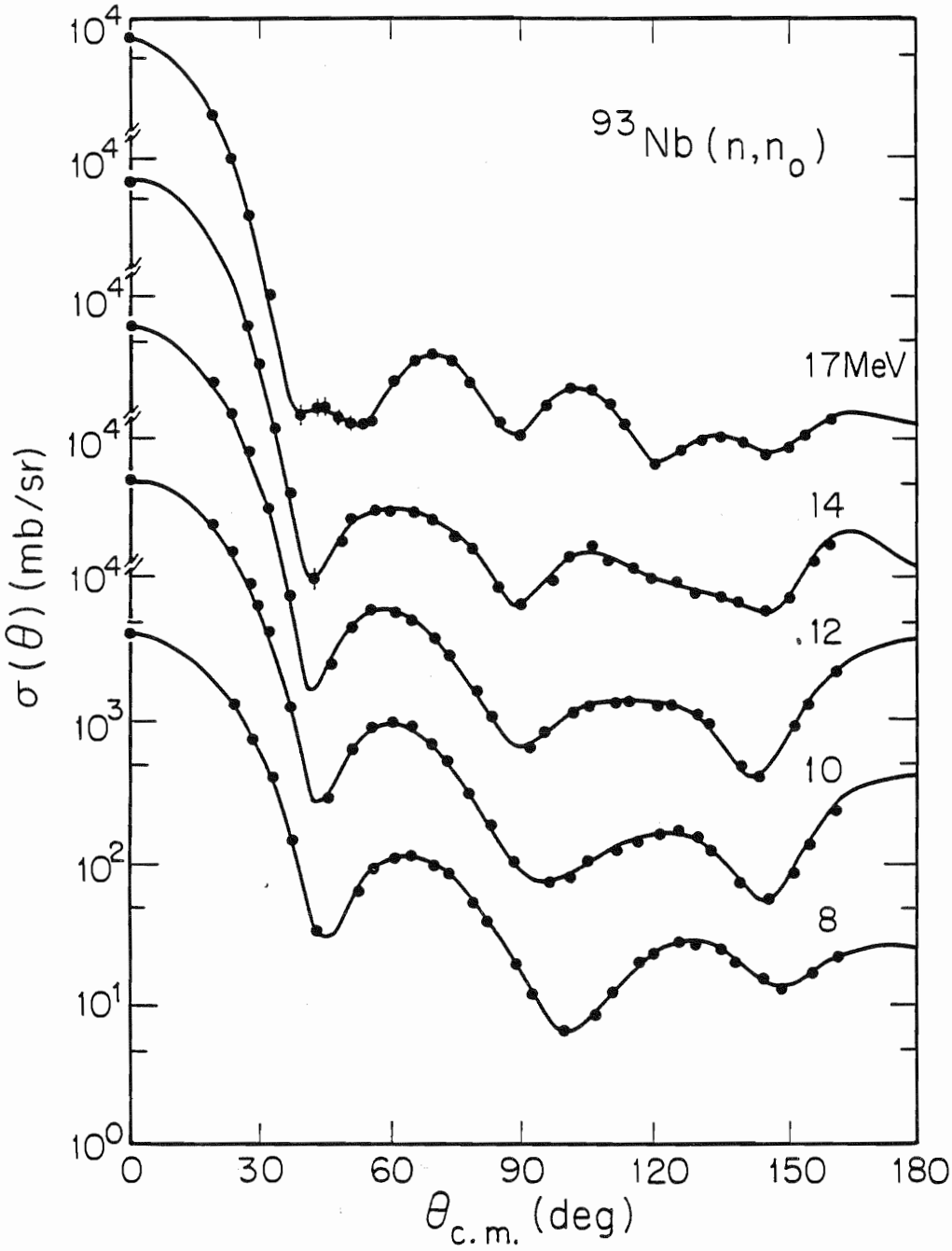

Figure 4.7. The $\sigma(\theta)$ data for the elastic scattering of 8, 10, 12, 14, and 17 MeV neutrons from ^{93}Nb. The curves are Legendre polynomial fits to the data. The points at 0^o are the calculated Wick's limits (Wick 1949).

this state and for elastic scattering would need to be known.

4.3 Analyzing Power Measurements

4.3.1 Data Stripping and Reduction

As with the $\sigma(\theta)$ data, in analyzing the $A_y(\theta)$ data, difference spectra for the right and left detectors must be calculated. However, these spectra must be calculated for both spin-up and spin-down measurements. The out spectra must be scaled relative to the in spectra, but here the ratio of the BCI-IN to BCI-OUT is used to scale out spectra. Various illustrative examples of difference spectra from $A_y(\theta)$ measurements are shown in figures 4.8 and 4.9.

After the calculation of the difference spectra for an angle, the stripping of the spectra initially proceeds in a manner similar to that for the $\sigma(\theta)$ data. As in the $\sigma(\theta)$ measurements, a smooth residual background remains in the spectra in the vicinity of the peaks of interest. The source of this background is not understood, but within statistical uncertainties, it is usually seen to have the same level in the spin-up and spin-down measurements. Therefore, a background is selected in both the spin-up and spin-down difference spectra, under the constraint that the level is the same for each spin orientation. Also, the same windows are used to calculate the yields of the peaks for both spin-up and spin-down spectra. For the $A_y(\theta)$ case, it is permissible to choose narrow windows to optimize the signal-to-noise ratio, that is, the ratio of the yield to the noise due to the background and the tails of neighboring peaks. In fact, several windows of different widths are used to investigate the variation of the calculated $A_y(\theta)$ across the peak. This investigation is especially

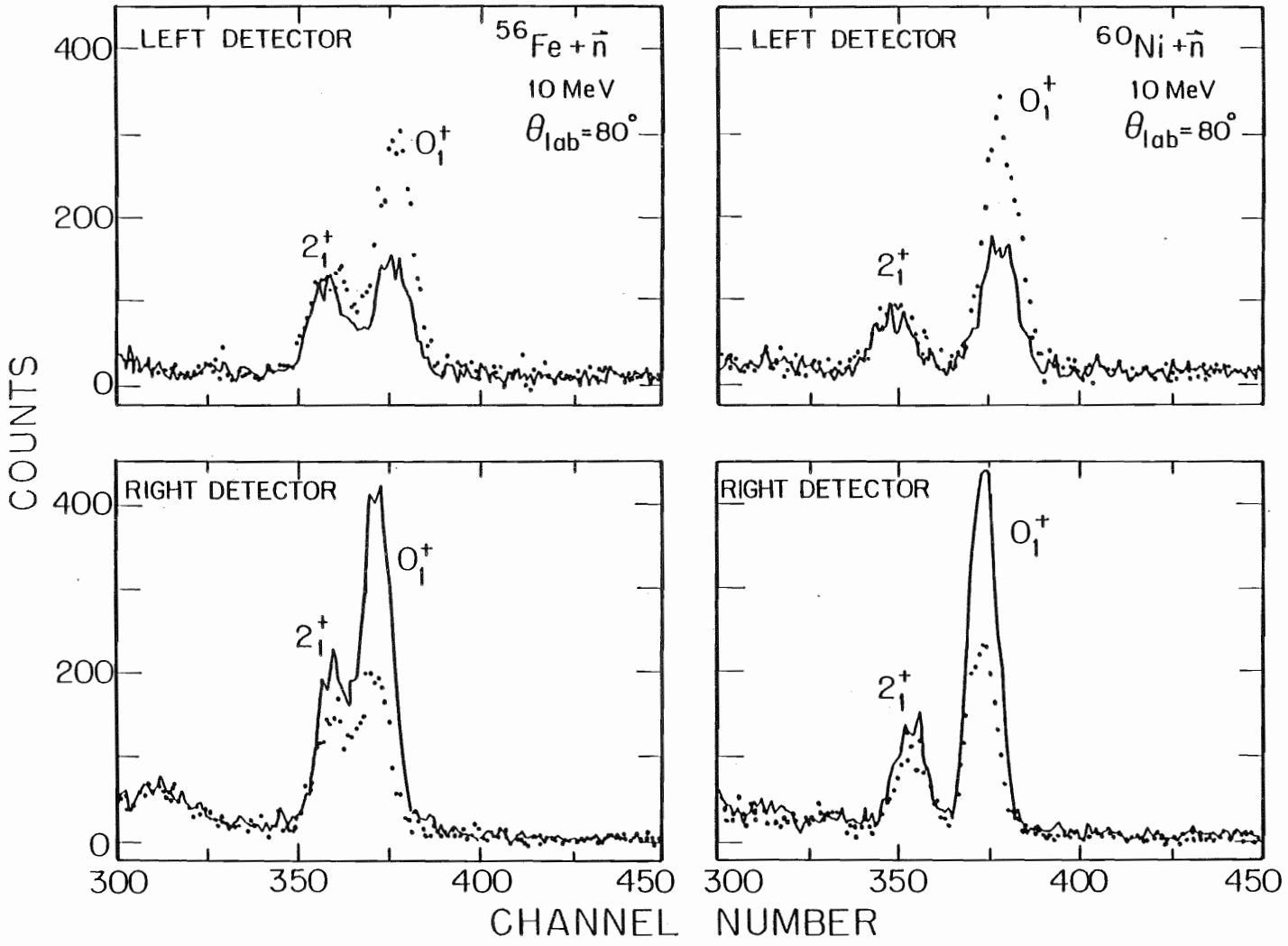

Figure 4.8. Difference spectra for $^{56}Fe+\vec{n}$ and $^{60}Ni+\vec{n}$ at 10 MeV. The dotted line is for spin-up, and the solid line is for spin-down.

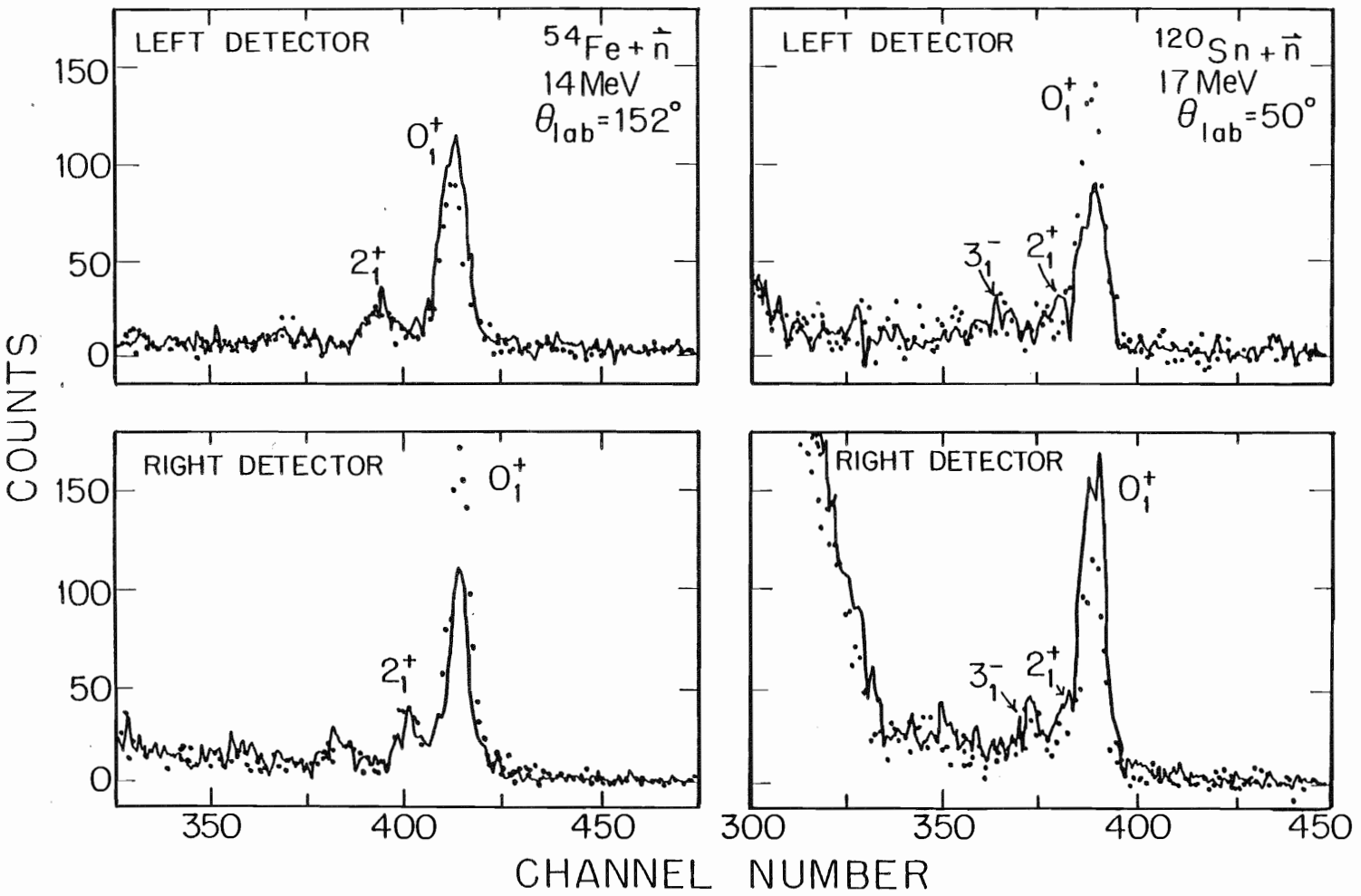

Figure 4.9. Difference spectra for $^{54}Fe+\vec{n}$ at 14 MeV and $^{120}Sn+\vec{n}$ at 17 MeV. The dotted line is for spin-up, and the solid line is for spin-down.

important where states in the spectra are not well resolved, and where they exhibit appreciably different magnitudes of $A_y(\theta)$. Results of these studies permitted us to obtain the best determination of $A_y(\theta)$ in complicated cases.

In extremely difficult cases (primarily $A_y(\theta)$ data for the $^{54,56}Fe$ and $^{58,60}Ni$ for inelastic scattering), the line shape of the timing monitor was used to subtract off contributions due to the tailing effect from the elastic peak. As seen from figure 4.10, the tails to the left of the peak are much more pronounced than they are in the $\sigma(\theta)$ measurements, especially in the region between channels 450 and 465. This region is the location of the inelastic scattering peaks for $^{54,56}Fe$ and $^{58,60}Ni$ for which measurements are reported in this work.

There will be four yields for each state of interest: the spin-up and spin-down yields from the spectra of the left detector, Y_{LU} and Y_{LD}, respectively, and the spin-up and spin-down yields from the spectra of the right detector, Y_{RU} and Y_{RD}, respectively. These four yields are combined to obtain the quantity α as follows:

$$\alpha = \left[\frac{Y_{LU}}{Y_{LD}} \times \frac{Y_{RD}}{Y_{RU}} \right]^{\frac{1}{2}} . \qquad (4.3)$$

The $A_y(\theta)$ values are then calculated from α using the formula:

$$A_y(\theta) = \frac{1}{p_n} \times \frac{\alpha - 1}{\alpha + 1} , \qquad (4.4)$$

where p_n is the polarization of the neutron beam, which is calculated from the deuteron beam quench ratio measurements and the polarization transfer of the $^2H(\vec{d},\vec{n})^3He$ reaction. The calculation of the polarization transfer is done using the formula given by Ohlsen and Keaton (Ohlsen 1973) with the

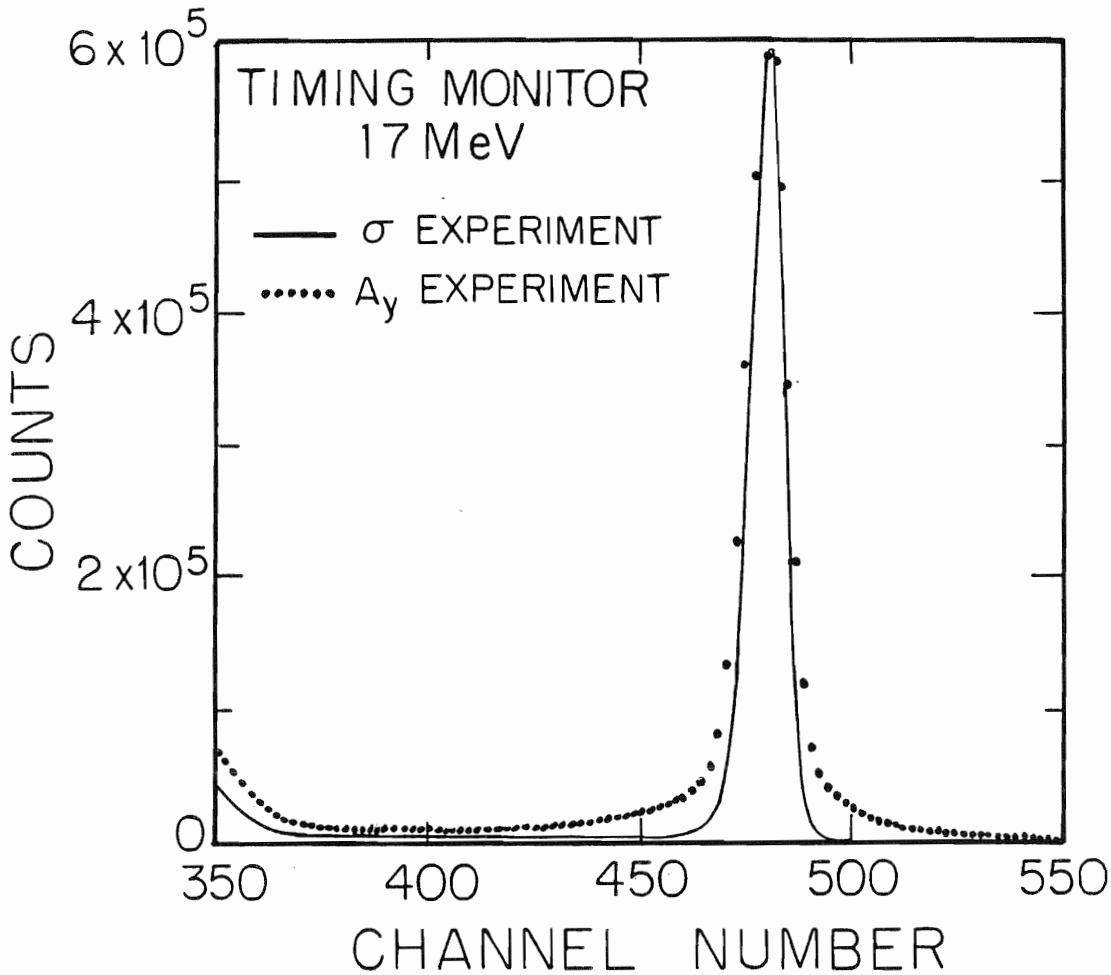

Figure 4.10. Comparison of spectra from the timing monitor for $\sigma(\theta)$ and $A_y(\theta)$ measurements at 17 MeV.

values measured by Lisowski (Lisowski 1975). For some of the data where the $\sigma(\theta)$ are particularly low, it is necessary to take a conservative method for evaluating the effect of the background. In this case, upper and lower limits were selected, and yields were obtained for "high" and "low" background levels (see Guss 1982a). Values for $A_y(\theta)$ were calculated for both situations and an average was calculated. Appropriate estimates of the uncertainties were assigned in these cases.

4.3.2 Multiple Scattering, Finite Geometry, and Attenuation Corrections

The $A_y(\theta)$ data must be corrected for attenuation, finite geometry, and multiple scattering effects after the values are calculated from equation 4.4. This is done using the Monte Carlo code JANE (version 1982) of Woye and Tornow (Woye 1980) together with the data manipulation code JANECOR of Byrd (Byrd 1983). The procedure for correcting the data is much more complicated than calculating the multiplicative correction factors for the $\sigma(\theta)$ data. The procedure, together with the theory behind the calculation, is documented by Guss (Guss 1982a), Howell (Howell 1984) and the user's manual for JANE of Honoré and Byrd (Honoré 1983).

The difference between the uncorrected and corrected $A_y(\theta)$ data at 10 MeV for ^{93}Nb is shown in figure 4.11. The effect of multiple scattering decreases the measured $A_y(\theta)$, since the $A_y(\theta)$ after second scatterings have small magnitudes and after third scatterings they are essentially zero in magnitude. As discussed below, the magnitudes of the corrected and uncorrected data are given in appendix B for all of the data.

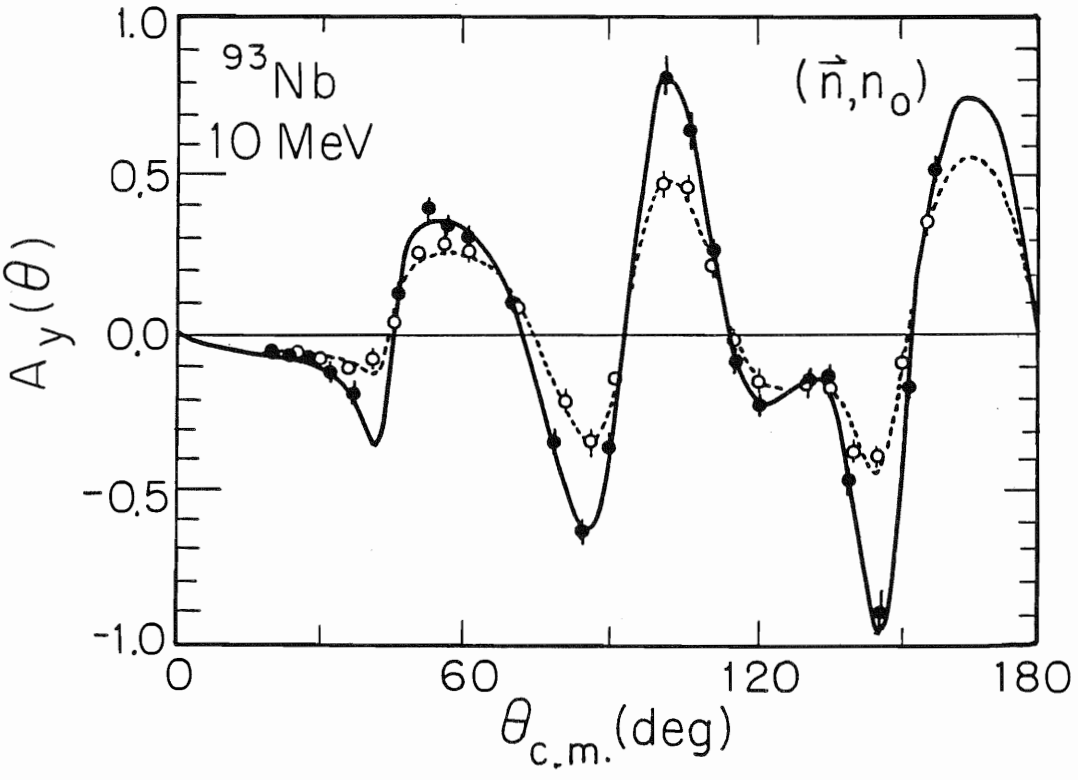

Figure 4.11. Multiple scattering corrections for $A_y(\theta)$ data for the elastic scattering of 10 MeV neutrons from ^{93}Nb. The open circles are the uncorrected data, and the solid circles are the final data as corrected using JANE. All lines are fits derived from associated Legendre polynomial fits to the product $A_y(\theta) \times \sigma(\theta)$.

4.3.3 Presentation of Final Data

The final corrected $A_y(\theta_{c.m.})$ data for all of the samples are tabulated in appendix B. Note, there is no lab-to-c.m. conversion for $A_y(\theta)$ values; however, there is one for the angles associated with the $A_y(\theta)$ values. The tabulations of appendix B also include the uncorrected data. The coefficients derived from associated Legendre polynomial fits to the product $A_y(\theta) \times \sigma(\theta)$, which can be used to reproduce the fits to the data (see equation B.1), are also tabulated in appendix B for those data sets which have enough data points to make a physically meaningful fit. Various other useful parameters are also given in the tabulations of appendix B. Note the $\sigma(\theta)$ used in the fits to the data for ^{93}Nb at all energies and for ^{54}Fe, ^{58}Ni, and ^{120}Sn at 17MeV are from the appendixes of the present work; those used for the ^{54,56}Fe data at 10 and 14 MeV are from Floyd 1983, and those for the ^{58,60}Ni data at 10 and 14 MeV are from Guss 1985. The relative uncertainties in the $A_y(\theta)$ data include the statistical uncertainty of the yields, the uncertainty in the deuteron beam polarization, and the additional uncertainties from the attenuation, finite geometry and multiple scattering corrections. An overall normalization uncertainty of about $\pm 3.0\%$ exists. It is due to uncertainties propagated through the calculations of the neutron beam polarization using the Lisowski polarization transfer measurements (Lisowski 1975).

The $A_y(\theta)$ values (including all corrections) for the ^{54,56}Fe isotopes are shown in figures 4.12 and 4.13. The neutron elastic and inelastic scattering $A_y(\theta)$ data for ^{54}Fe at 10 and 14 MeV are shown in figure 4.12. Several high quality $A_y(\theta)$ data points for the elastic and inelastic

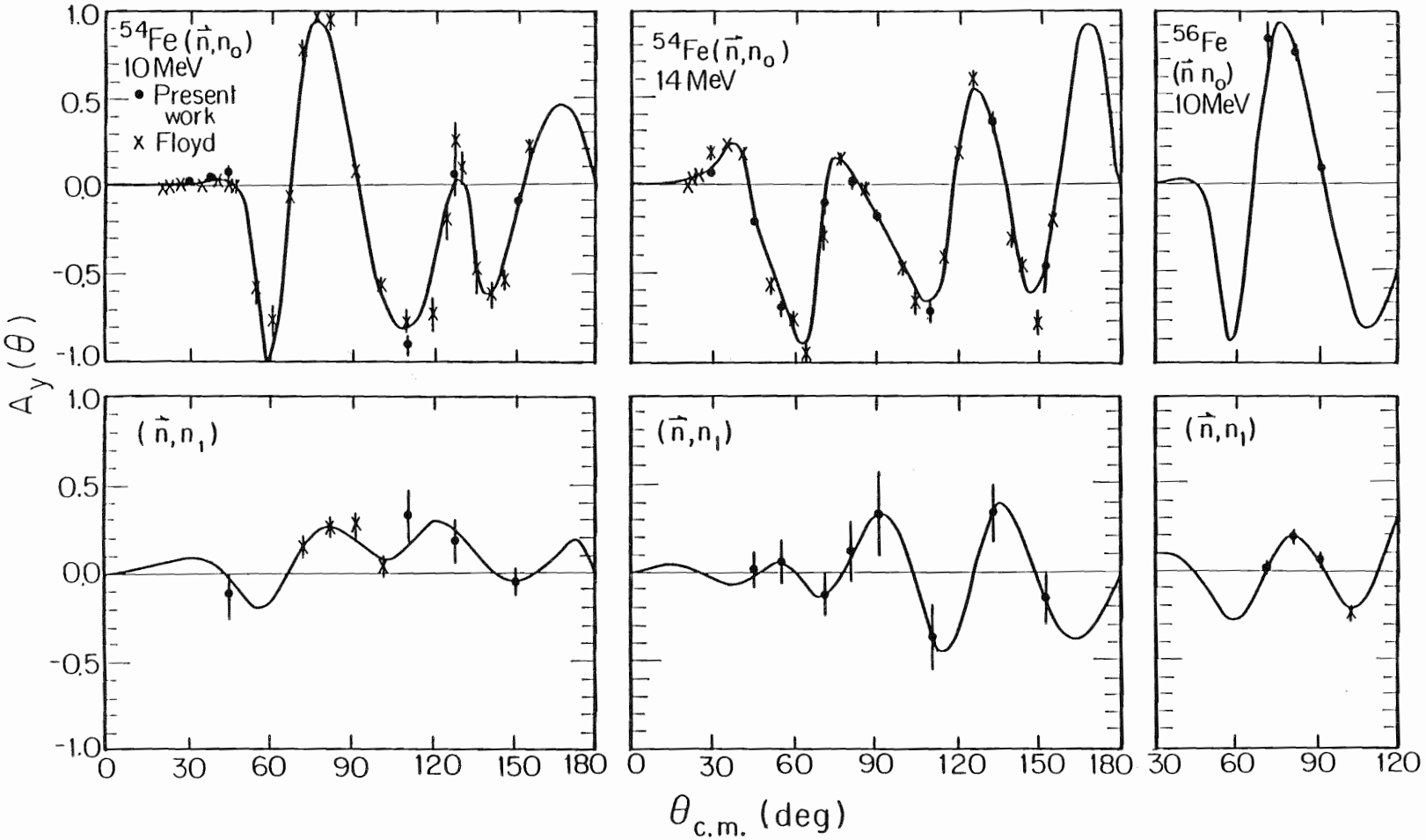

Figure 4.12. The $A_y(\theta)$ data for the elastic scattering and inelastic scattering (to the first 2^+ state) of 10 MeV neutrons from ^{54,56}Fe and 14 MeV neutrons from ^{54}Fe. The Floyd data are from Floyd 1983. The curves are fits derived from associated Legendre polynomial fits to the product $A_y(\theta) \times \sigma(\theta)$.

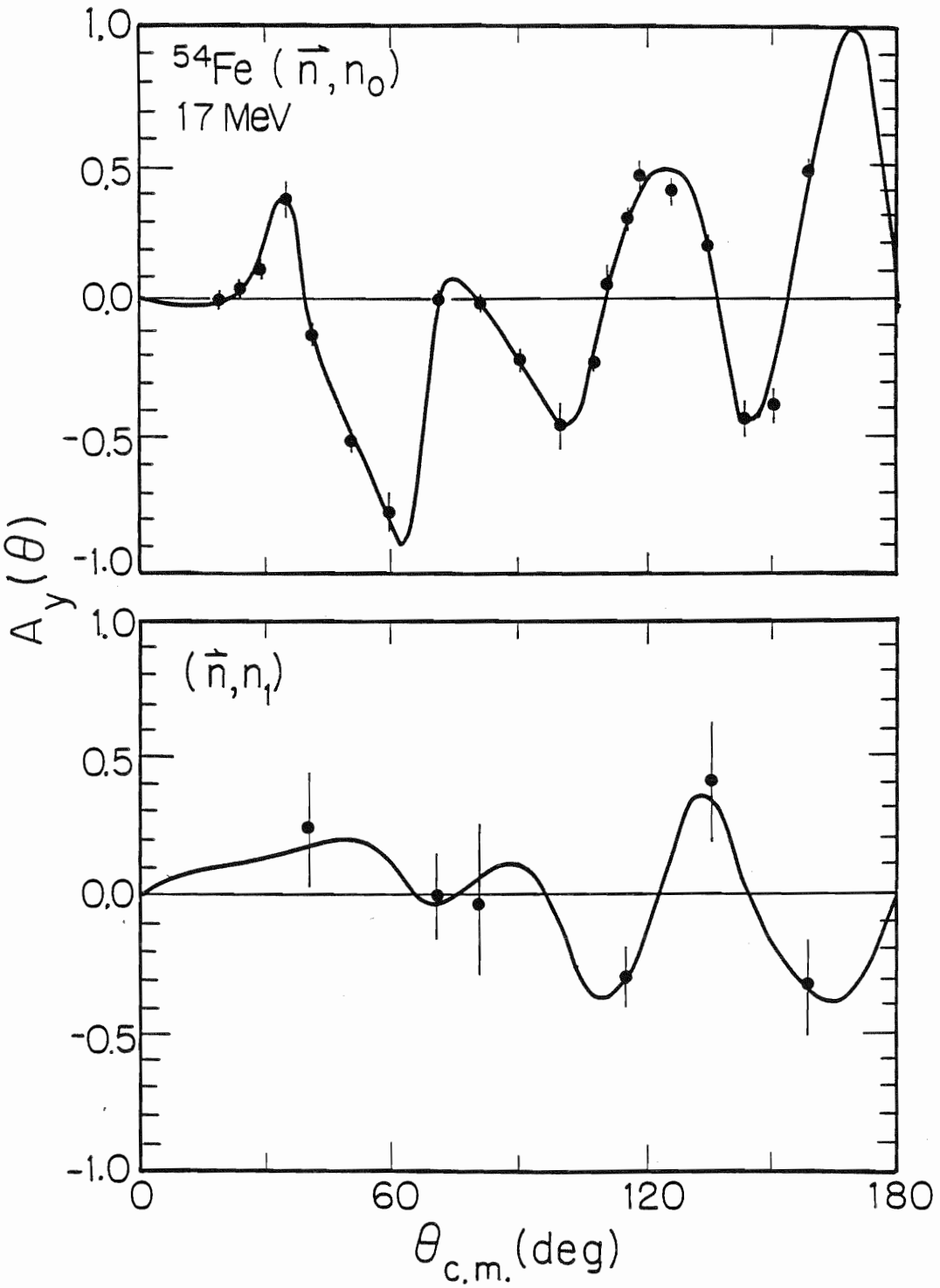

Figure 4.13. The $A_y(\theta)$ data for the elastic scattering and inelastic scattering (to the first 2^+ state) of 17 MeV neutrons from ^{54}Fe. The curves are fits derived from associated Legendre polynomial fits to the product $A_y(\theta) \times \sigma(\theta)$.

scattering of 10 MeV neutrons from ^{56}Fe are also shown in figure 4.12. The $A_y(\theta)$ data for the elastic and inelastic scattering of 17 MeV neutrons from ^{54}Fe are shown in figure 4.13. The parameters for the fits to the $A_y(\theta)$ distributions having only a few points are not given in appendix B. The elastic scattering data for ^{54}Fe have relative uncertainties ranging from $\pm$0.01 to $\pm$0.10; the inelastic scattering data for ^{54}Fe have relative uncertainties ranging from $\pm$0.08 to $\pm$0.29. The range of relative uncertainties for the elastic ^{56}Fe data is $\pm$0.01 to $\pm$0.05; the relative uncertainties for the inelastic ^{56}Fe data are all about $\pm$0.04. For the $A_y(\theta)$ data for ^{54}Fe at 10 and 14 MeV, there is good agreement between the data of the present work and those from Floyd 1983.

The final corrected $A_y(\theta)$ data for the ^{58,60}Ni isotopes are shown in figures 4.14 and 4.15. The neutron elastic and inelastic scattering $A_y(\theta)$ data for ^{58}Ni at 10 and 14 MeV are shown in figure 4.14. Several high quality $A_y(\theta)$ data points for the elastic and inelastic scattering of 10 MeV neutrons from ^{60}Ni are also shown in figure 4.14. The $A_y(\theta)$ data for the elastic and inelastic scattering of 17 MeV neutrons from ^{58}Ni are shown in figure 4.15. The parameters for the fits to the $A_y(\theta)$ distributions having only a few points are not given in appendix B. The elastic scattering data for ^{58}Ni have relative uncertainties ranging from $\pm$0.01 to $\pm$0.09; the inelastic scattering data for ^{58}Ni have relative uncertainties ranging from $\pm$0.08 to $\pm$0.35. The ranges of relative uncertainties for the elastic and inelastic ^{60}Ni data are $\pm$0.01 to $\pm$0.05 and $\pm$0.04 to $\pm$0.05, respectively. For the $A_y(\theta)$ data for ^{58}Ni at 10 and 14 MeV, there is good agreement between the data of the present work and those from Guss 1985.

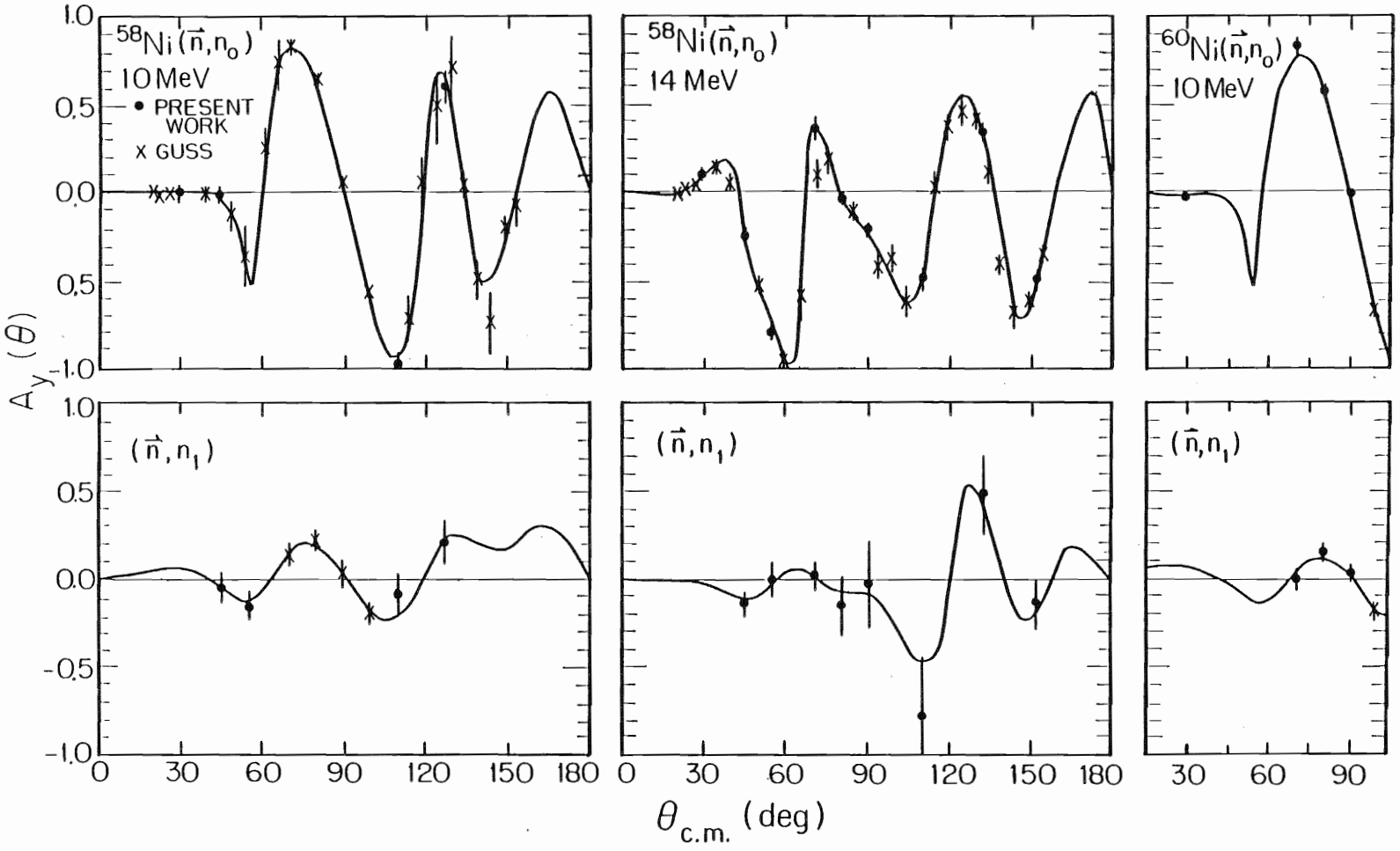

Figure 4.14. The $A_y(\theta)$ data for the elastic scattering and inelastic scattering (to the first 2^+ state) of 10 MeV neutrons from ^{58,60}Ni and 14 MeV neutrons from ^{58}Ni. The Guss data are from Guss 1985. The curves are fits derived from associated Legendre polynomial fits to the product $A_y(\theta) \times \sigma(\theta)$.

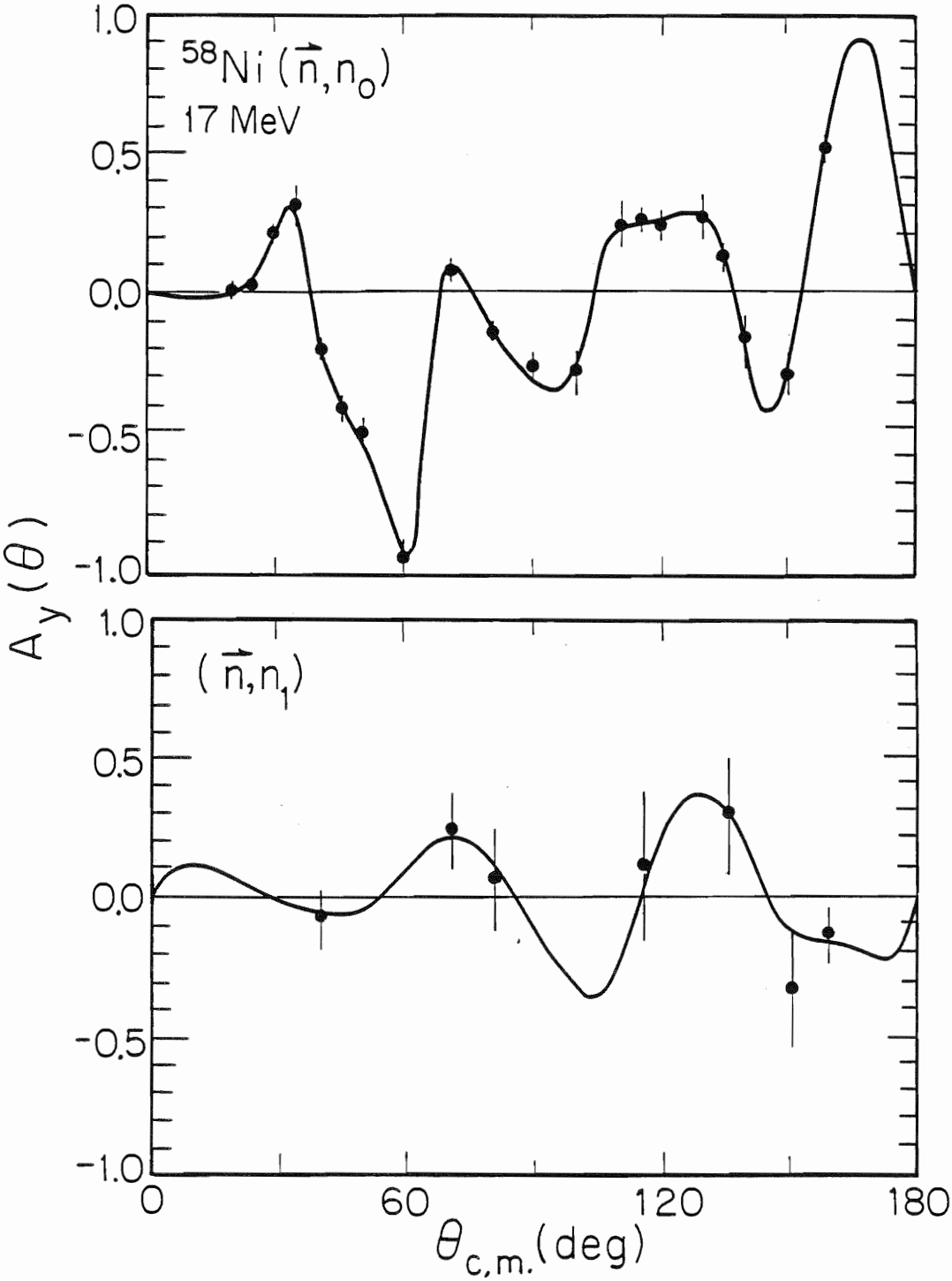

Figure 4.15. The $A_y(\theta)$ data for the elastic scattering and inelastic scattering (to the first 2^+ state) of 17 MeV neutrons from ^{58}Ni. The curves are fits derived from associated Legendre polynomial fits to the product $A_y(\theta) \times \sigma(\theta)$.

The corrected $A_y(\theta_{c.m.})$ data for the elastic scattering of neutrons from ^{93}Nb at 10 and 14 MeV are shown in figure 4.16 together with fits derived from Associated Legendre polynomial fits to the product $A_y(\theta) \times \sigma(\theta)$. The relative uncertainties for these data range from ± 0.01 to ± 0.10. Note, the data for ^{93}Nb also include the weak contribution from inelastic scattering to the first excited state of ^{93}Nb (Q = -0.03 MeV, $J^{\pi} = 9/2^{+}$).

The final $A_y(\theta_{c.m.})$ data for the elastic scattering of neutrons from ^{120}Sn at 17 MeV are shown in figure 4.17 together with a fit derived from an associated Legendre polynomial fit to the product $A_y(\theta) \times \sigma(\theta)$. The relative uncertainties for these data range from ± 0.02 to ± 0.12.

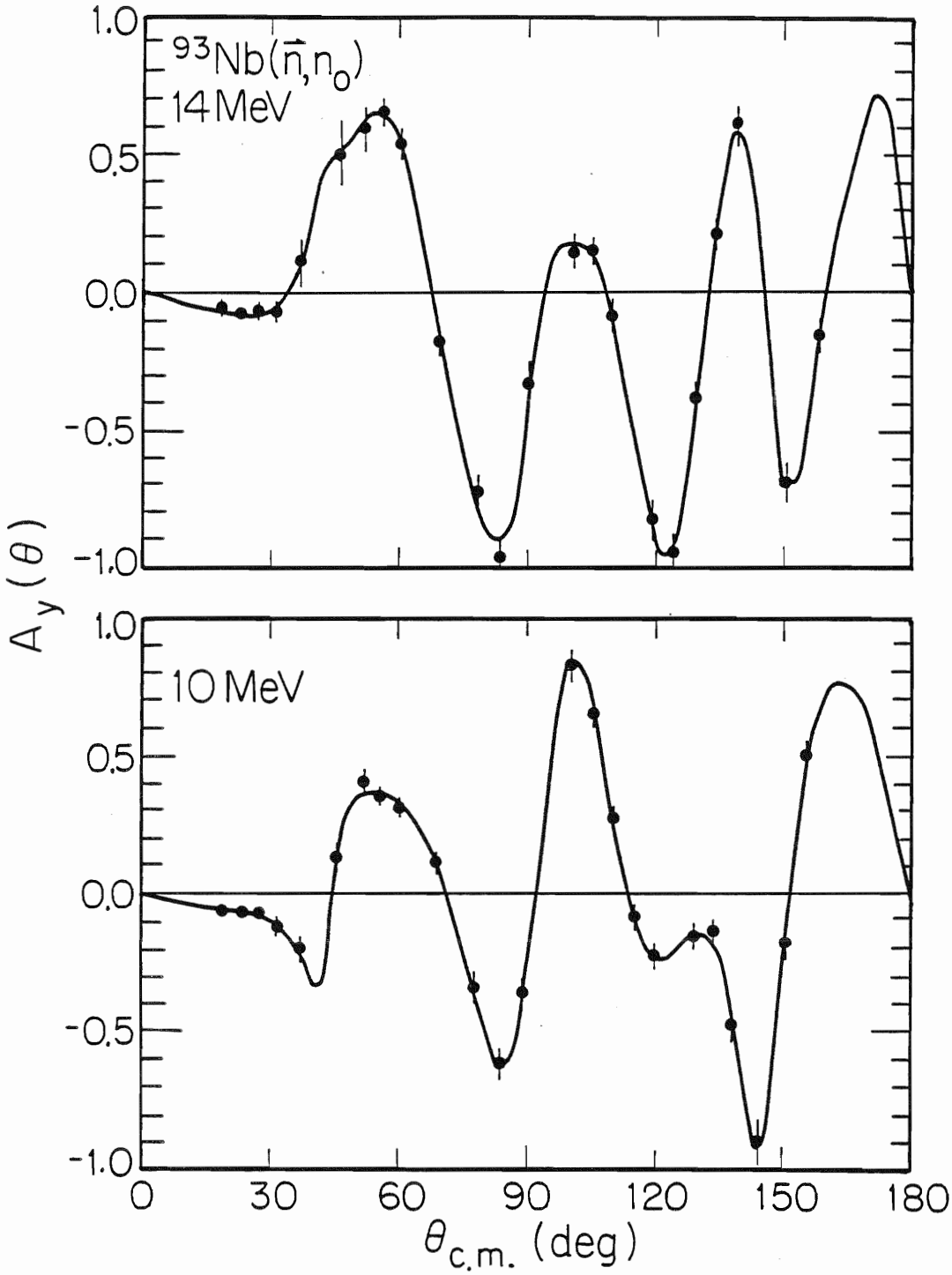

Figure 4.16. The $A_y(\theta)$ data for the elastic scattering of 10 and 14 MeV neutrons from ^{93}Nb. The curves are fits derived from associated Legendre polynomial fits to the product $A_y(\theta) \times \sigma(\theta)$.

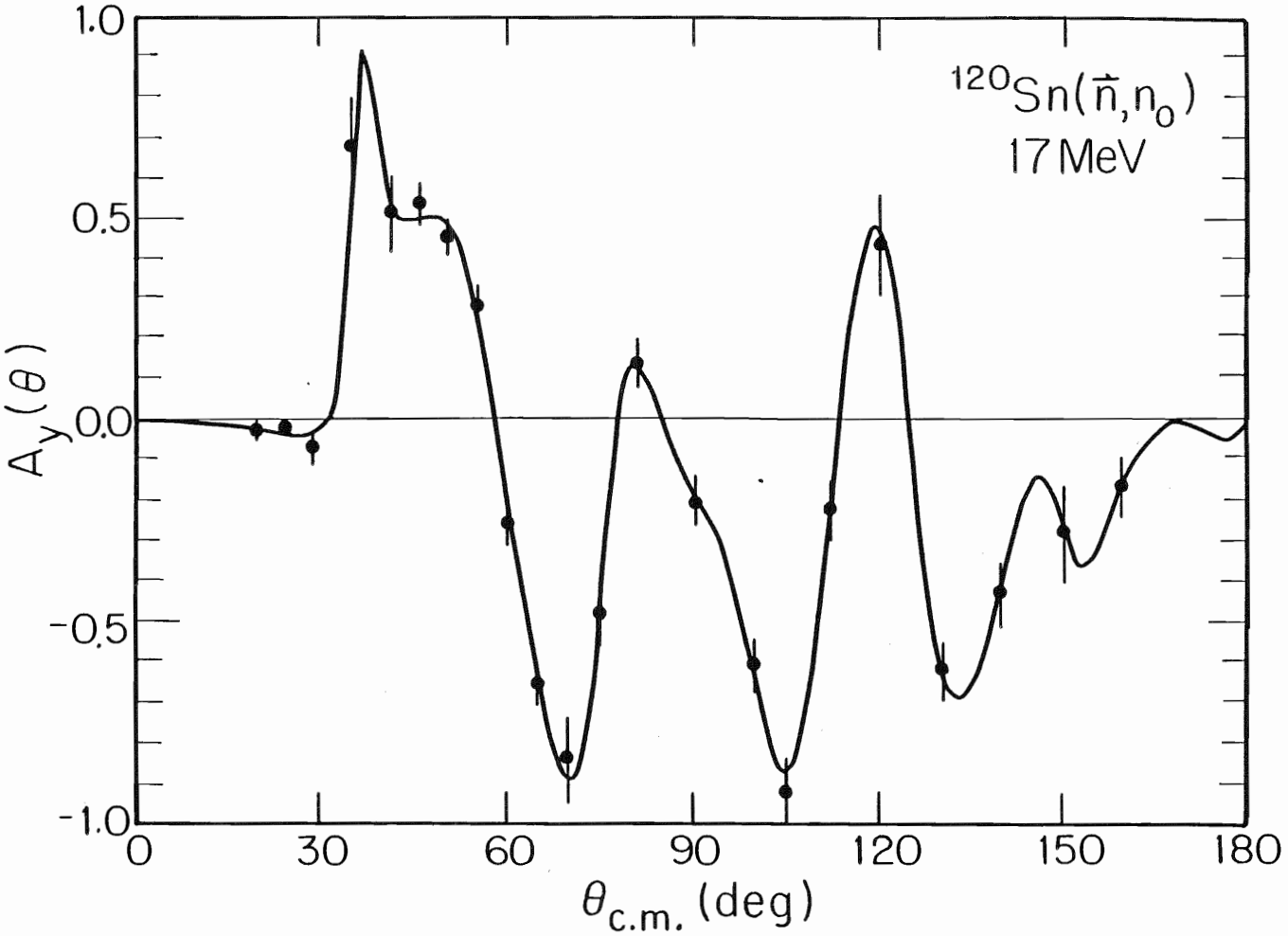

Figure 4.17. The $A_y(\theta)$ data for the elastic scattering of 17 MeV neutrons from ^{120}Sn. The curve is a fit derived from an associated Legendre polynomial fit to the product $A_y(\theta) \times \sigma(\theta)$.

CHAPTER 5

SMALL ANGLE CROSS SECTION DATA FOR ^{93}Nb AT 10 MeV

5.1 Introduction

Accurate measurements of neutron differential cross sections at far forward angles -- angles smaller than 15^{o} -- are difficult to make with typical time-of-flight spectrometer facilities, such as the one at TUNL. These measurements are difficult to make because in this angular range it is hard to shield detectors from the direct flux of neutrons from the neutron source, which at TUNL is the $^{2}H(d,n)^{3}He$ reaction at the gas cell. In order to measure $\sigma(\theta)$ data in this angular range, Bucher, Hollandsworth, and Lamoreaux designed and built a special "small-angle" scattering collimator (Bucher 1973). This apparatus has been obtained by TUNL and was used to make $\sigma(\theta)$ section measurements for the elastic scattering of neutrons from ^{93}Nb at 10 MeV. The measurements are for nine angles ranging from 1.8^{o} to 16.0^{o}.

Absolute normalizations of the data for ^{93}Nb were obtained for each angle by calculating the ratios of "standard" $\sigma(\theta)$ values for natural Pb to new measurements. The standard $\sigma(\theta)$ values were derived from the measured $\sigma(\theta)$ values for Pb of Bucher and Hollandsworth (Bucher 1975a). The new measurements for Pb were made in the same experiments as our measurements for ^{93}Nb.

5.2 Experimental Apparatus

The small-angle scattering apparatus and the theory of its construction are described in great detail in Bucher 1973. However, modifications have

been made to the apparatus since this article was published. Therefore, a brief description of the device and its use at TUNL will be given to document these changes.

The apparatus (see figures 5.1 and 5.2) consists of a hollow metal cylinder 159.2 cm long and about 41 cm in diameter through which nine metal-lined channels have been built. The space in the cylinder not taken up by the channels is filled with paraffin oil to shield the detector assembly. One channel coincides with the axis of the cylinder and is 1.11 cm in diameter. The other channels are located symmetrically around the axis and are divided into two groups, the large and small ports (see figure 5.2). The large ports are not parallel to the axis of the cylinder as in Bucher 1973, but they are inclined by 0.171^{o} toward the axis (i.e., the large ports are closer together at the exit face than they are at the entrance face). The small-port crossover point is not 2.8 m before the entrance face as stated in Bucher 1973, but at 3.60 m (i.e., the small ports are inclined 0.714^{o} away from the cylinder axis). There is a space of a few centimeters behind the main cylinder that is followed by a second cylinder, which is composed mostly of polyethylene. The detector assembly is attached to the second cylinder. The polyethylene cylinder has a center channel and four outer channels that lead to five NE-213 liquid scintillator filled housings, which are all coupled to the same photomultiplier tube by a lucite light pipe. The channels are aligned with the set of ports in use by rotating the cylinder. Scattering samples are large discs mounted so that the center of the sample is 11 cm from the entrance face.

The apparatus is aligned so that its axis coincides with the 0^{o} axis of the neutron source. The scattering angles are determined from the distance

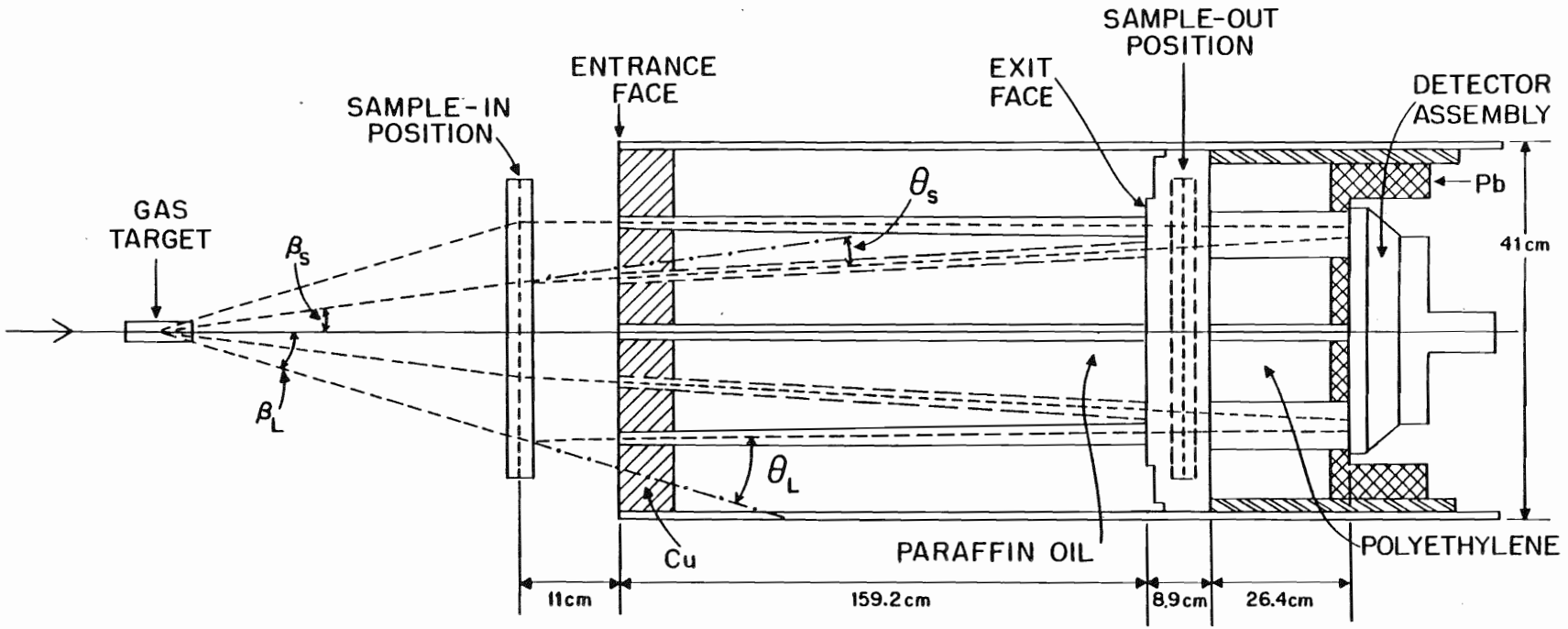

Figure 5.1. Longitudinal view of the small-angle scattering collimator.

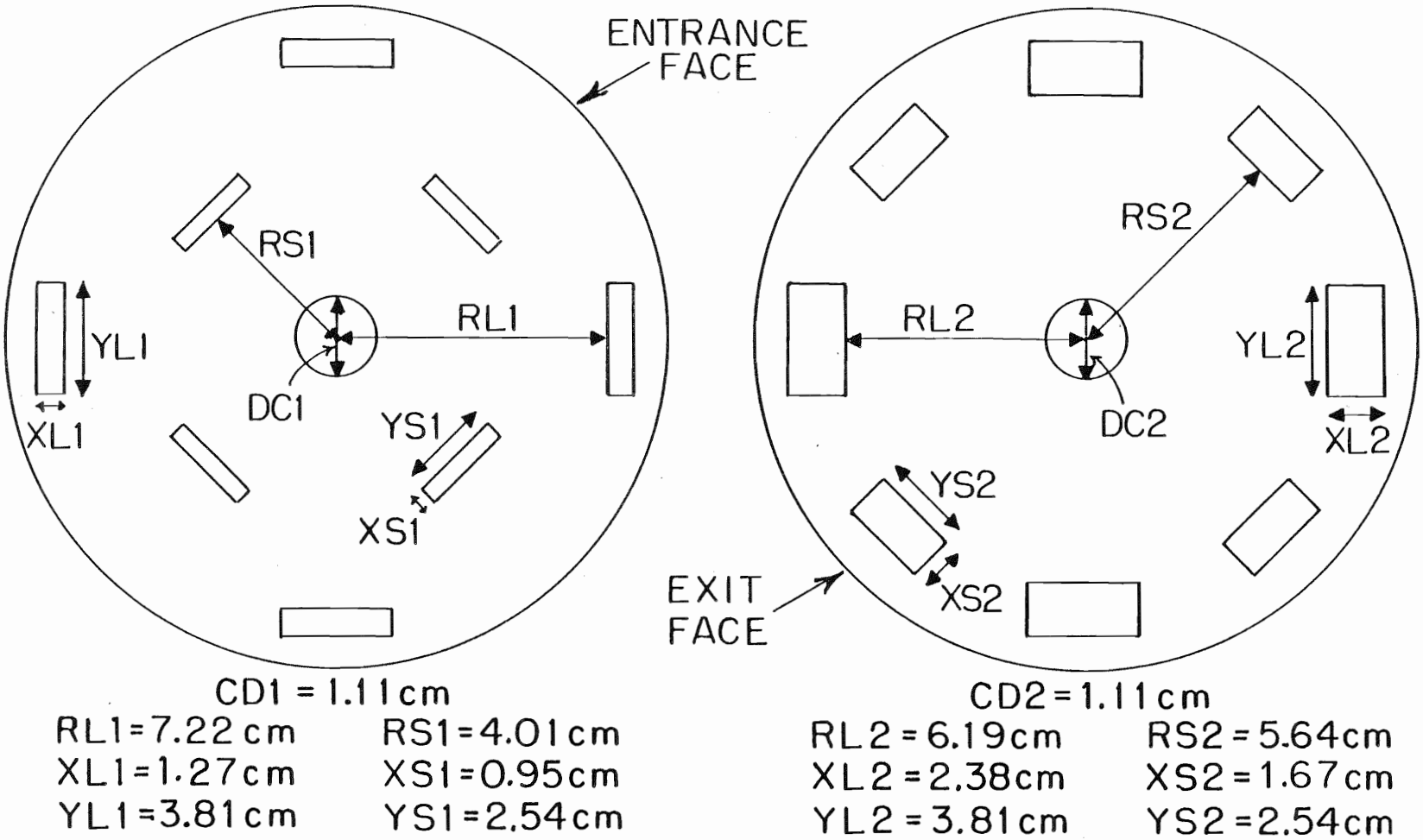

Figure 5.2. Views of the entrance and exit faces of the small-angle scattering collimator.

between the center of the neutron source and the center of the sample and the angles of inclination of the ports. Both sample-in and sample-out measurements are made for first one and then the other set of ports. The sample-out measurements are made by putting the sample in the space between the two cylinders in order that the neutrons in both sample-in and sample-out measurements have the same attenuation. The set of ports not in use and the center port are completely plugged with polyethylene strips.

The measurements carried out at 10 MeV for ^{93}Nb at TUNL were done with the apparatus set up in the neutron time-of-flight target room. The ^{2}H(d,n)^{3}He reaction was used as the neutron source reaction with gas cell C pressurized with 7.9 bars of deuterium. Boxes of paraffin were used as extra shielding and were stacked around the sides of the apparatus, especially the detector assembly, in order to reduce the background in the time-of-flight spectra due to room-scattered neutrons. The neutron flux monitor detector in the time-of-flight target room was removed from its shield and placed on a stand so that it viewed the direct neutron flux from the gas cell -- this was necessary since the extra shielding prevented it from being used in its normal position. The right-detector electronics were used for the detector assembly of the apparatus. Both 1×Cs and PSD biases were set for the detectors. The data taking code used was the normal time-of-flight $\sigma(\theta)$ code. A list of the distances from the end of the gas cell to the entrance face of the collimator and the corresponding lab angles for both the large and small ports is given in table 5-1. In table 5-2, values for various physical parameters and their uncertainties are listed for both the Nb and Pb scattering samples.

TABLE 5-1

Distances and Corresponding Angles for the Small and Large Ports of the Small-Angle Scattering Collimator

	Small Ports						Large Ports					
D (cm)	β_{lab} (deg.)	$\Delta\beta_{lab}$ (deg.)	θ_{lab} (deg.)	$\Delta\theta_{lab}$ (deg.)	PL	ΔPL	β_{lab} (deg.)	$\Delta\beta_{lab}$ (deg.)	θ_{lab} (deg.)	$\Delta\theta_{lab}$ (deg.)	PL	ΔPL
107.4	2.54	0.31	1.83	0.74	1.001	0.001	4.60	0.44	4.77	1.04	1.002	0.001
72.1	3.97	0.52	3.25	0.96	1.001	0.001	7.17	0.75	7.35	1.34	1.004	0.001
57.7	5.14	0.73	4.43	1.16	1.002	0.001	9.28	1.04	9.45	1.64	1.007	0.002
45.8	6.81	1.04	6.10	1.47	1.004	0.001	12.24	1.49	12.41	2.09	1.012	0.003
37.5[a)]	8.80	1.46	8.09	1.89	1.006	0.002	15.69	2.09	15.86	2.70	1.019	0.006

D = The distance from the end of the gas cell to the entrance face of the collimator. Note that L, the distance from the center of the gas cell to the center of the sample, is determined from the formula, L = D + 0.5 × (3.162 cm) − 11 cm.

β_{lab} = The angle at which the neutrons come out of the gas cell.

$\Delta\beta_{lab}$ = The maximum (±) angular spread for β_{lab}.

θ_{lab} = The scattering angle for the neutrons.

$\Delta\theta_{lab}$ = The maximum (±) angular spread for θ_{lab}.

PL = A dimensionless factor used to determine the path length of a neutron in the scattering sample. The path length is simply the thickness of the sample times this factor.

ΔPL = The maximum (±) spread in PL.

a) Note that measurements were made only using the large ports at this distance.

TABLE 5-2

Small-Angle Scattering Sample Parameters

Parameter	Nb	Pb
mass (kg)	5.75 ± 1.09%	9.75 ± 0.65%
diameter (cm)	26.04 ± 0.16%	25.72 ± 0.31%
thickness (cm)	1.275 ± 0.20%	1.643 ± 0.37%
volume (cm^3)	679. ± 0.38%	854. ± 0.72%
number of nuclei ($\times 10^{25}$ nuclei)	3.73 ± 1.09%	2.83 ± 0.65%
density of nuclei ($\times 10^{22}$ nuclei/cm^3)	5.49 ± 1.15%	3.32 ± 0.97%

5.3 Data Reduction, Normalization, and Corrections

The reduction of the time-of-flight spectra to monitor-normalized yields was done in the same manner discussed in Chapter 4 for the normal $\sigma(\theta)$ data. The conversion of the yields to corrected data was accomplished using the following equation, derived from equations 4.1 and 4.2:

$$\sigma_{Nb}(\theta_{c.m.}) = F_{norm} \times \frac{M_{Nb}(\theta_{c.m.})}{M_{Pb}(\theta_{c.m.})} \times \frac{Y_{Nb}(\theta_{c.m.})}{Y_{Pb}(\theta_{c.m.})} \times \sigma_{Pb}(\theta_{c.m.}) , \qquad (5.1)$$

where,

$$F_{norm} = \frac{n_{Pb}}{n_{Nb}} \times \frac{\varepsilon_{Pb}}{\varepsilon_{Nb}} \times \frac{T_{Pb}}{T_{Nb}} . \qquad (5.2)$$

The quantity n_{Pb}/n_{Nb} is the ratio of the numbers of nuclei in the Pb and Nb samples and is equal to 0.779. The quantity $\varepsilon_{Pb}/\varepsilon_{Nb}$ is the ratio of the relative efficiencies of the detector at the energies of neutrons scattered from Pb and Nb and is equal to 1.00, since at the angles of interest the maximum difference in the energies of neutrons scattered from Pb and Nb is only 0.05%. The quantity T_{Pb}/T_{Nb} is the ratio of the transmissions of the Pb and Nb samples and is equal to 1.02 for all nine angles. Note that this quantity is really a non-constant, angle-dependent value. However, it is included in the constant normalization since the values at each angle were all found to be within 0.05% of 1.02. Therefore, F_{norm} is equal to 0.795 and has a corresponding normalization percent uncertainty of ±2.63%.

The factor $M_{Nb}(\theta_{c.m.})/M_{Pb}(\theta_{c.m.})$ in equation 5.1 is used to correct the yields for Nb and Pb for multiple scattering and finite geometry effects, as well as "in" scattering of neutrons by channel walls of the collimator. This factor cannot be determined without the use of a Monte Carlo code. The code MUSE (Beverly 1972) was used by Bucher et al. (Bucher 1973, 1975a, and

1975b) to make these corrections. However, this code is not currently running at TUNL, nor can the code EFFIGY15 be easily modified to correct these data. Therefore, multiple scattering and finite geometry corrections cannot be made at this time. However, from looking at the results of Bucher et al., it appears that the correction factors for Nb and Pb should cancel and that $M_{Nb}(\theta_{c.m.})/M_{Pb}(\theta_{c.m.})$ equal to 1.00 should be within a maximum of ±5.0% of the actual ratio. Note that T_{Pb}/T_{Nb} equals 1.02 and that quantity is related to $M_{Nb}(\theta_{c.m.})/M_{Pb}(\theta_{c.m.})$. Therefore,

$$\sigma_{Nb}(\theta_{c.m.}) = 0.795 \times \frac{Y_{Nb}(\theta_{c.m.})}{Y_{Pb}(\theta_{c.m.})} \times \sigma_{Pb}(\theta_{c.m.}) \ . \qquad (5.3)$$

The relative uncertainty for $\sigma_{Nb}(\theta_{c.m.})$ is the sum in quadrature of the statistical uncertainties for both $Y_{Nb}(\theta_{c.m.})$ and $Y_{Pb}(\theta_{c.m.})$, the estimated uncertainty for the $M_{Nb}(\theta_{c.m.})/M_{Pb}(\theta_{c.m.})$ ratio (5.0%), and the uncertainty for the $\sigma_{Pb}(\theta_{c.m.})$ values. The final values and relative uncertainties for $\sigma_{Nb}(\theta_{c.m.})$ are given in table 5-3. This table also contains the $\sigma(\theta)$ values for Pb that were used to make the absolute normalizations for the ^{93}Nb data. The nine data points of this chapter are shown in figure 5.3 plotted with the 10 MeV $\sigma(\theta)$ data for ^{93}Nb from the normal time-of-flight experiment.

TABLE 5-3

^{93}Nb Small-Angle Neutron Elastic Scattering Cross Sections at 10 MeV

$\theta_{c.m.}$ (deg.)	$\sigma_{Nb}(\theta_{c.m.})$ (mb/sr)	$\Delta\sigma_{Nb}$ (mb/sr)	$\sigma_{Pb}(\theta_{c.m.})$ (mb/sr)	$\Delta\sigma_{Pb}$ (mb/sr)
1.9	5690	330	8010	176
3.3	5760	313	7800	158
4.5	5610	308	7560	156
4.8	5700	320	7480	153
6.2	5500	301	7010	144
7.4	5330	297	6640	138
9.5	5580	306	5700	121
12.5	4280	236	4370	98
16.0	3510	198	2960	72

The normalization uncertainty of the data for ^{93}Nb is $\pm$ 2.63%. The values for natural Pb are those used to make the absolute normalizations for the ^{93}Nb data, and were derived from the measured values of Bucher and Hollandsworth (Bucher 1975a). The Pb values are from linear interpolation between values taken from their fits to their 9.5 and 11 MeV data.

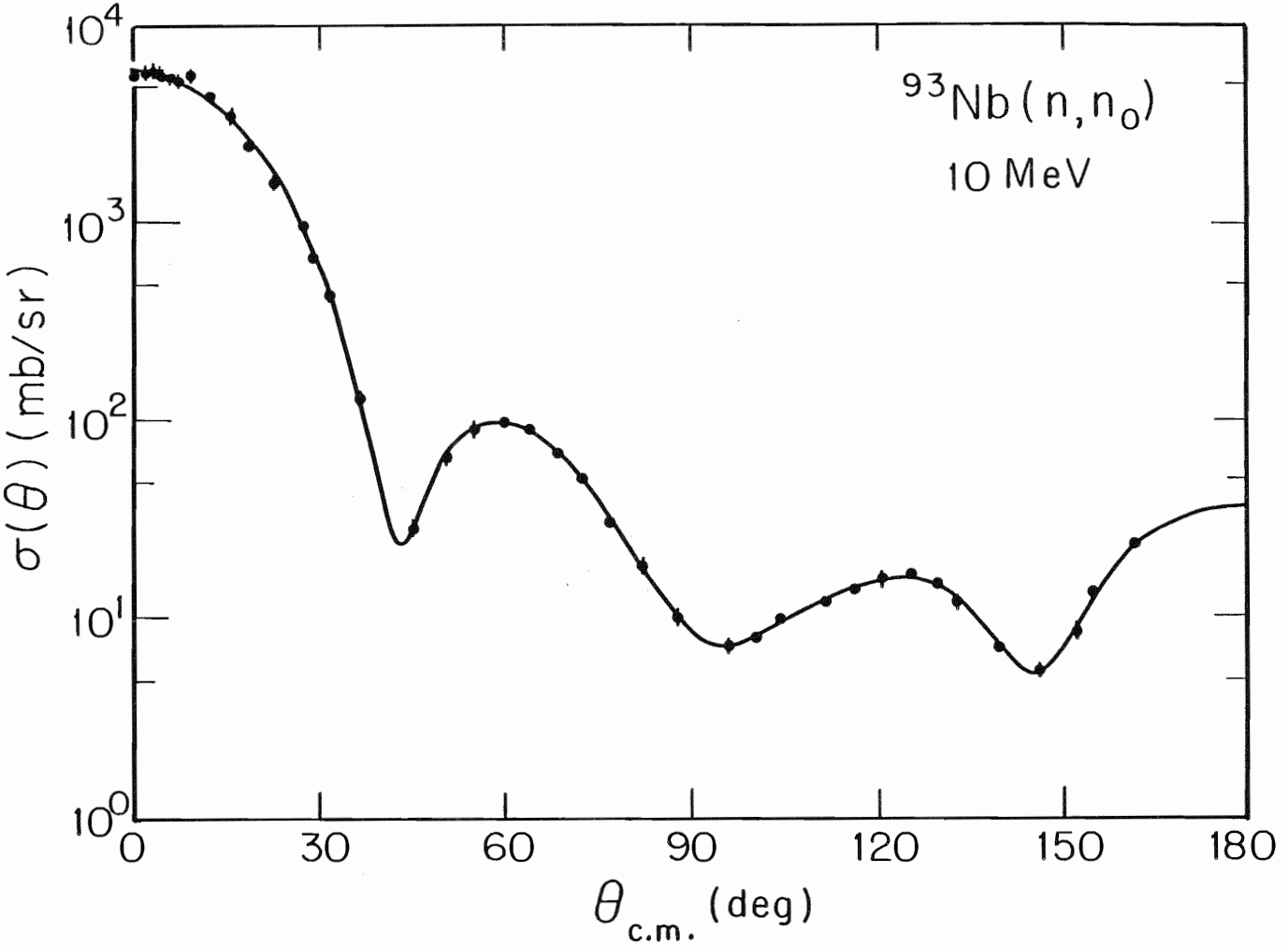

Figure 5.3. Complete cross section data set for ^{93}Nb at 10 MeV. The data between 0° and 16° are from the small-angle scattering measurements; the other data are those of chapter 4 from a normal cross section measurement.

CHAPTER 6

SPHERICAL OPTICAL MODEL CALCULATIONS FOR ^{93}Nb

6.1 Introduction

Spherical optical model (SOM) calculations for neutron elastic scattering from ^{93}Nb in the 7- to 20-MeV energy range are dealt with in this chapter. There are many excellent references on the theory of the SOM; the text of Hodgson (Hodgson 1971) has proven to be extremely valuable for background material in the present work. The SOM is a phenomenological model of the nucleon-nucleus interaction, and was first proposed in 1947 by Serber (Serber 1947). In this model, the scattering and absorption of nucleons by a nucleus is described mathematically using a complex potential in the Schrödinger equation for the scattering system. The name "optical model" comes from the similarity of this treatment to the use of a complex index of refraction to describe the scattering and absorption of light by a cloudy crystal ball.

The complex potential of the SOM is represented in the following way:

$$U(r) = V(r) + iW(r) \ . \tag{6.1}$$

The phenomenological potential is usually written using the conventional Woods-Saxon and derivative Woods-Saxon form factors. The Woods-Saxon form factor is written as

$$f(r,R_i,a_i) = \{1 + \exp[(r - R_i)/a_i]\}^{-1} \ , \tag{6.2}$$

where the nuclear radius $R_i = r_i A^{1/3}$. The radius parameter r_i and the diffuseness a_i are parameters, which are usually adjusted in empirical

studies to give optimum descriptions of the data. The real (refractive) part of the potential V(r) is represented by

$$V(r) = -V_R f(r, R_R, a_R) \ , \tag{6.3}$$

where V_R is the potential well strength. The imaginary (absorptive) part of the potential W(r) is usually taken to be the sum of two parts, a surface absorption term $W_D(r)$ and a volume absorption term $W_V(r)$. The volume term is written as

$$W_V(r) = -W_V f(r, R_V, a_V) \ , \tag{6.4}$$

where W_V is the potential well strength. The surface term is represented by

$$W_D(r) = 4W_D a_D \frac{df}{dr}(r, R_D, a_D) \ , \tag{6.5}$$

where W_D is the potential well strength.

An additional term dependent on the spin-orbit interaction is known to exist in the potential for the nuclear interaction. This term is also required in order to produce polarization phenomena in nucleon-nucleus scattering. The spin-orbit potential, which is added directly to the potential of equation 6.1, is also complex, and is written as

$$U_{so}(r) = V_{so}(r) + iW_{so}(r) \ , \tag{6.6}$$

where $V_{so}(r)$ is the strength of the real part of the potential and $W_{so}(r)$ is the strength of the imaginary part. The conventional Thomas form for the spin-orbit potential is written

$$U_{so}(r) = \left[\frac{\hbar}{m_\pi c}\right]^2 \left[V_{so}\frac{df}{dr}(r, R_{Vso}, a_{Vso}) + iW_{so}\frac{df}{dr}(r, R_{Wso}, a_{Wso})\right]\frac{1}{r}\vec{\sigma}\cdot\vec{l} \ . \tag{6.7}$$

Based on the above definitions, the entire SOM potential is

$$U(r) = -V_R f(r,R_R,a_R) - iW_V f(r,R_V,a_V) + i4W_D a_D \frac{df}{dr}(r,R_D,a_D) +$$

$$\left[\frac{\hbar}{m_\pi c}\right]^2 \left[V_{so}\frac{df}{dr}(r,R_{Vso},a_{Vso}) + iW_{so}\frac{df}{dr}(r,R_{Wso},a_{Wso})\right]\frac{1}{r}\vec{\sigma}\cdot\vec{l} \quad . \qquad (6.8)$$

This is the form employed in the SOM calculations for the present work. The calculations of the present work were made using a modified form of the SOM search code GENOA, obtained from F.G. Perey of Oak Ridge National Laboratory (ORNL). The main modification to GENOA made at TUNL is the inclusion of the calculation of the Mott-Schwinger interaction between the magnetic moment of an incident neutron and the Coulomb field of the nucleus; this modification was made by C.E. Floyd (Floyd 1981). This interaction has significant effects on calculations for $A_y(\theta)$ at forward angles between 0^o and 30^o, but negligible effects on calculations for $\sigma(\theta)$, except for the angular region close to 0^o.

Niobium, as stated earlier in this work, is well-suited to experimental study, since there is only one naturally occurring isotope. Lagrange and Lejeune (Lagrange 1982) have recently emphasized that ^{93}Nb is a good nucleus to study in the framework of the SOM, since it can be considered to have a spherical shape and it has insignificant compound nucleus contributions to elastic scattering cross sections above 7 MeV. They also note that it is important to study this nucleus, since it is a candidate for use in the construction of fusion reactors (as a component of superconducting alloys).

The main data base for the calculations of this chapter consists of the cross section and analyzing power data for ^{93}Nb measured between 8 and 17 MeV and included in this work. Also included in the data base, are the $\sigma(\theta)$ data for neutron elastic scattering at 7 MeV of Etemad (Etemad 1973)

and at 11 MeV of Ferrer et al. (Ferrer 1977), as well as the recently measured $\sigma(\Theta)$ data of Hansen et al. (Hansen 1985) at 14.6 MeV. References to the data of Etemad, Ferrer et al., and Hansen et al. will be by labels indicating the laboratories where the measurements were made: AE (Aktiebolaget Atomenergi, Studsvik, Sweden), OU (Ohio University), and LLNL (Lawrence Livermore National Laboratory), respectively. The total cross section (σ_T) data from 2.5 to 15 MeV of Foster and Glasgow (Foster 1971) and from 15 to 20 MeV from ENDF/B-V are included as well.

The old 8 MeV data of Holmqvist and Wiedling (Holmqvist 1971) were not used in the calculations, since our new data should supersede their older data. A comparison with the present 8 MeV data is shown in figure 6.1. As can be seen from the figure there are noticeable differences between the two data sets. These differences range from about 1% to 47%, with the larger differences occurring near the minima of the angular distribution.

6.2 Spherical Optical Model Calculations from Existing Parameter Sets

Predictions using several existing SOM parameter sets have been made for comparison to the ^{93}Nb data. First, are the set A parameters of the global analysis of Rapaport, Kulkarni, and Finlay (Rapaport 1979), covering an energy range from 7 to 26 MeV and based on neutron scattering data for ^{40}Ca, ^{90}Zr, ^{92}Mo, ^{116,124}Sn, and ^{208}Pb. Second, are the phenomenological parameters from the ^{93}Nb analysis over the 10-keV to 50-MeV range by Lagrange and Lejeune. These parameters were derived from a data base that included the following: the (n,n) data at 7 MeV of Etemad, at 8 MeV of Holmqvist and Wiedling, and at 11 MeV of Ferrer et al. ; the total cross sections of Foster and Glasgow from 2.5 to 15 MeV; the (p,p) data at

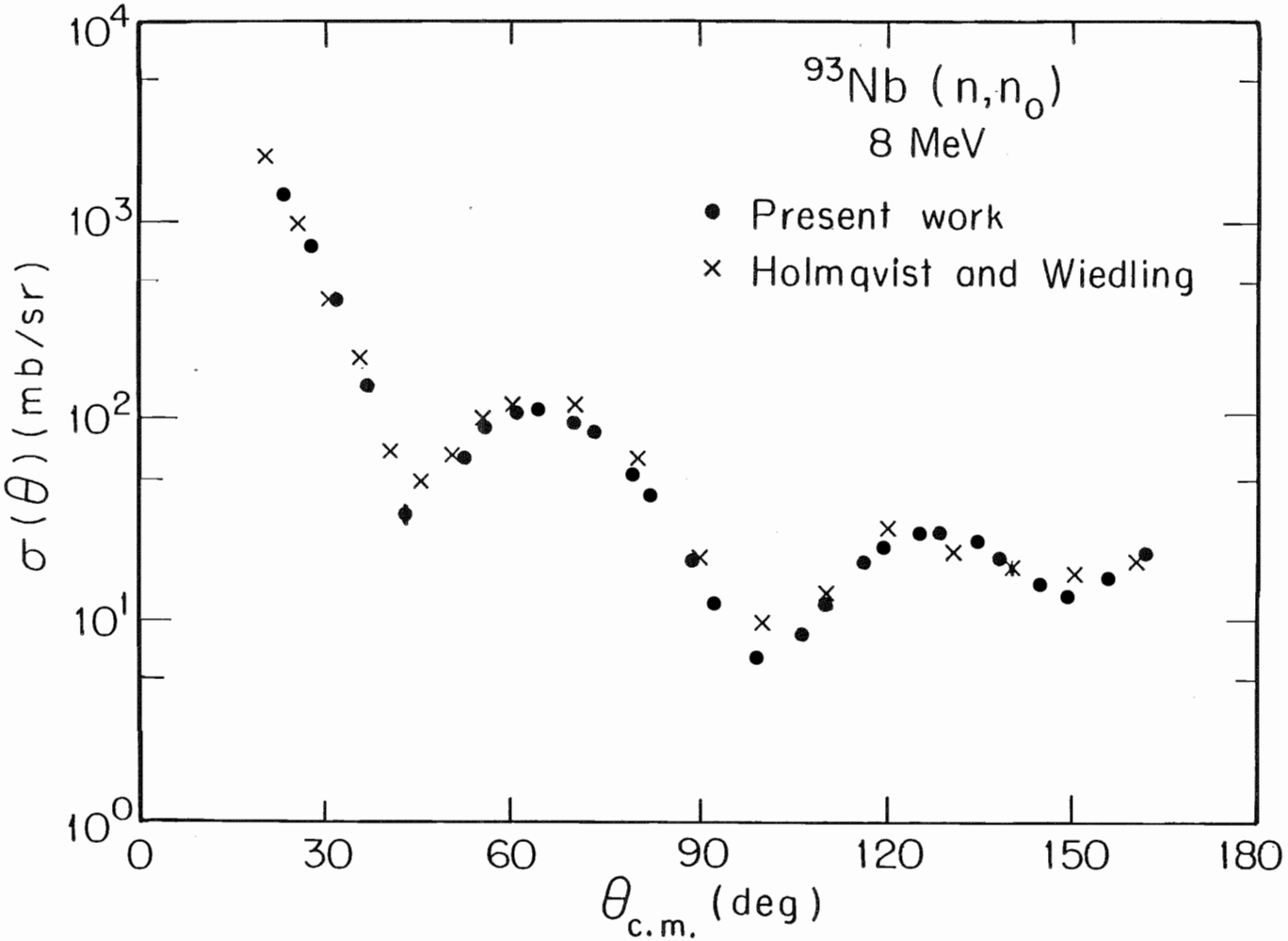

Figure 6.1. Comparison of the 8 MeV σ(θ) data for ^{93}Nb of the present work to those of Holmqvist and Wiedling (Holmqvist 1971).

22.2 MeV of Fulmer (Fulmer 1962); the (p,n) data at 18.7 MeV of Wong et al. (Wong 1972) and at 49.4 MeV of Batty et al. (Batty 1968); and finally, the $(\vec{p},p)$ data at 10.5 and 14.5 MeV of Rosen et al. (Rosen 1965). Third, are the global parameters of Walter and Guss (Walter 1985) for the 10- to 80-MeV range, based on both $\sigma(\theta)$ and $A_y(\theta)$ data for proton and neutron scattering from nuclei with A > 53. The Walter and Guss data base included our present $\sigma(\theta)$ data at 10, 14, and 17 MeV and our $A_y(\theta)$ data at 10 and 14 MeV for ^{93}Nb, although these data sets were given reduced weight in their searches. The parameters for these three models: Rapaport, Kulkarni, and Finlay set A (RKF-A); Lagrange and Lejeune (LL); and Walter and Guss (WG), are given in table 6-1.

The $\sigma(\theta)$ data for ^{93}Nb are compared in figure 6.2 with the calculations performed using the above parameters. As can be seen from this figure, the WG parameters provide the best representations of the data. Except for the angular ranges between 100° and 140° at 11 MeV and between 35° and 55° at 17 MeV, the predictions made from the WG parameters describe the structure in the distributions extremely well, considering that this model is highly constrained by the global data base employed in its derivation. In fact, in the ^{93}Nb model developed below for the present work, it also was not possible to describe the data at 17 MeV in the 35° to 55° angular range. The predictions of the other two parameter sets are fair at the lower energies but become worse with increasing energy, underestimating $\sigma(\theta)$ at the backward angles, an effect that indicates an absorptive potential that is too strong.

The analyzing power data are shown in figure 6.3 with the calculations from the same three parameter sets. The RKF-A parameters give a good

TABLE 6-1

SOM Parameters for ^{93}Nb from Existing Models

Parameter	LL	RKF-A	WG
V_R(MeV)	49.1-0.26E	51.51-0.31E	50.61-0.300E
r_R(fm)	1.24	1.198	1.219
a_R(fm)	0.62	0.663	0.688
W_V(MeV)	0.0, E≤11 MeV 0.16E-1.76, E≥11 MeV	0.0, E≤15 MeV 0.38E-4.3, E≥15 MeV	0.0, E≤6.3 MeV 0.153E-0.963, E≥6.3 MeV
r_V(fm)	1.24	1.295	1.420
a_V(fm)	0.62	0.590	0.509
W_D(MeV)	3.40+0.41E, E≤11 MeV 9.67-0.16E, E≥11 MeV	2.77+0.40E, E≤15 MeV 12.77-0.39E, E≥15 MeV	7.53, E≤9.9 MeV 9.083-0.157E, E≥9.9 MeV
r_D(fm)	1.26	1.295	1.282
a_D(fm)	0.58	0.590	0.512
V_{so}(MeV)	7.71	6.2	6.004-0.015E
r_{Vso}(fm)	1.12	1.01	1.103
a_{Vso}(fm)	0.47	0.75	0.560
W_{so}(MeV)			0.791-0.018E
r_{Wso}(fm)			1.364
a_{Wso}(fm)			0.632

The LL parameters are those of Lagrange and Lejeune (Lagrange 1982); the RKF-A parameters are the set A parameters of Rapaport, Kulkarni, and Finlay (Rapaport 1979); and the WG parameters are those of Walter and Guss (Walter 1985). Note that in the WG parameters, W_D is given only for $E \geq 9.9$ MeV; for the WG predictions at energies below 9.9 MeV, W_D has been set to a constant value of 7.53 MeV, its value at E = 9.9 MeV.

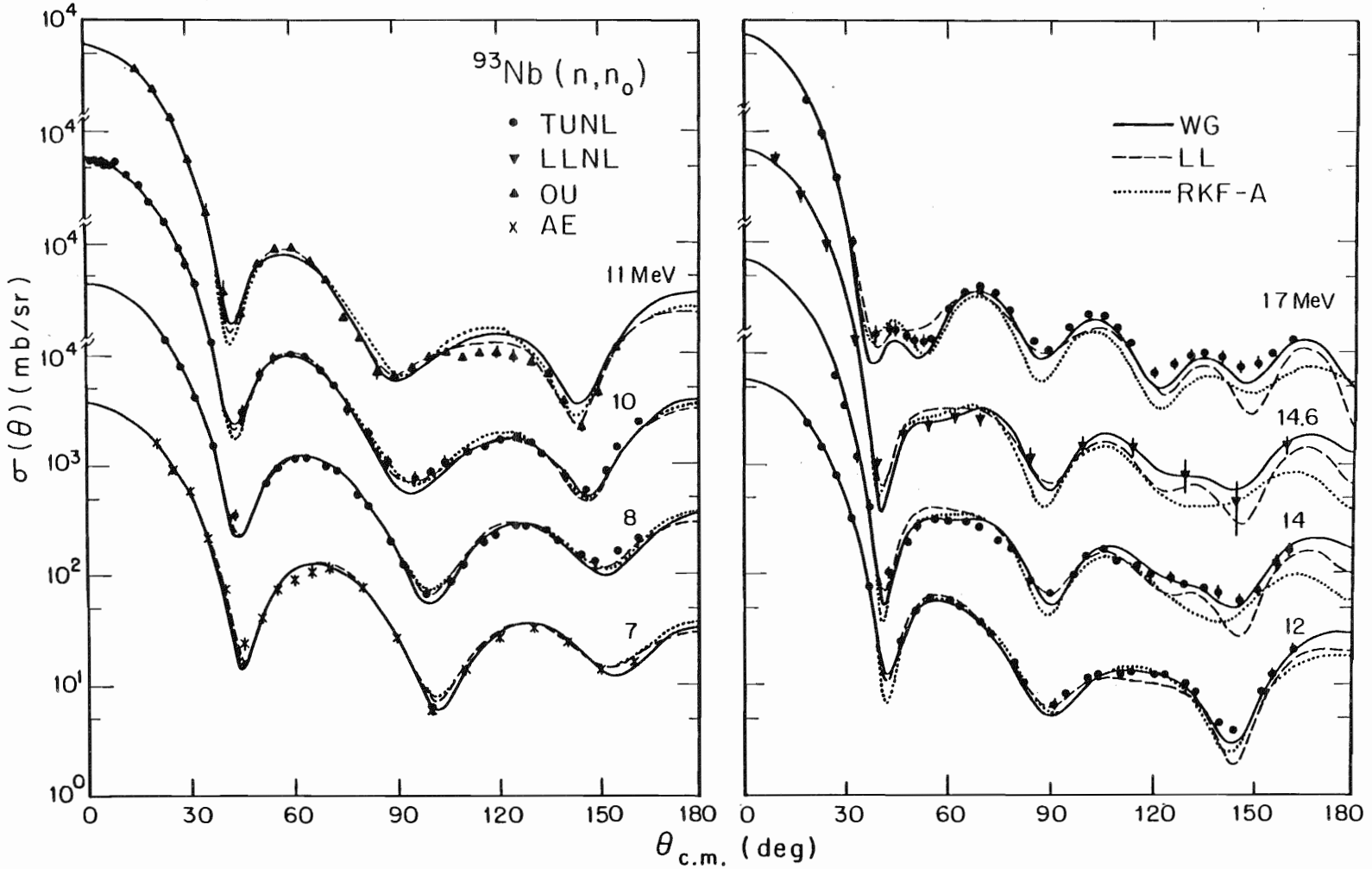

Figure 6.2. Comparison of the σ(θ) data for ^{93}Nb to the SOM parameter predictions of WG (Walter 1985), LL (Lagrange 1982), and RKF-A (Rapaport 1979). The TUNL data are those of the present work, the LLNL data are from Hansen 1985, the OU data are from Ferrer 1977, and the AE data are from Etemad 1973.

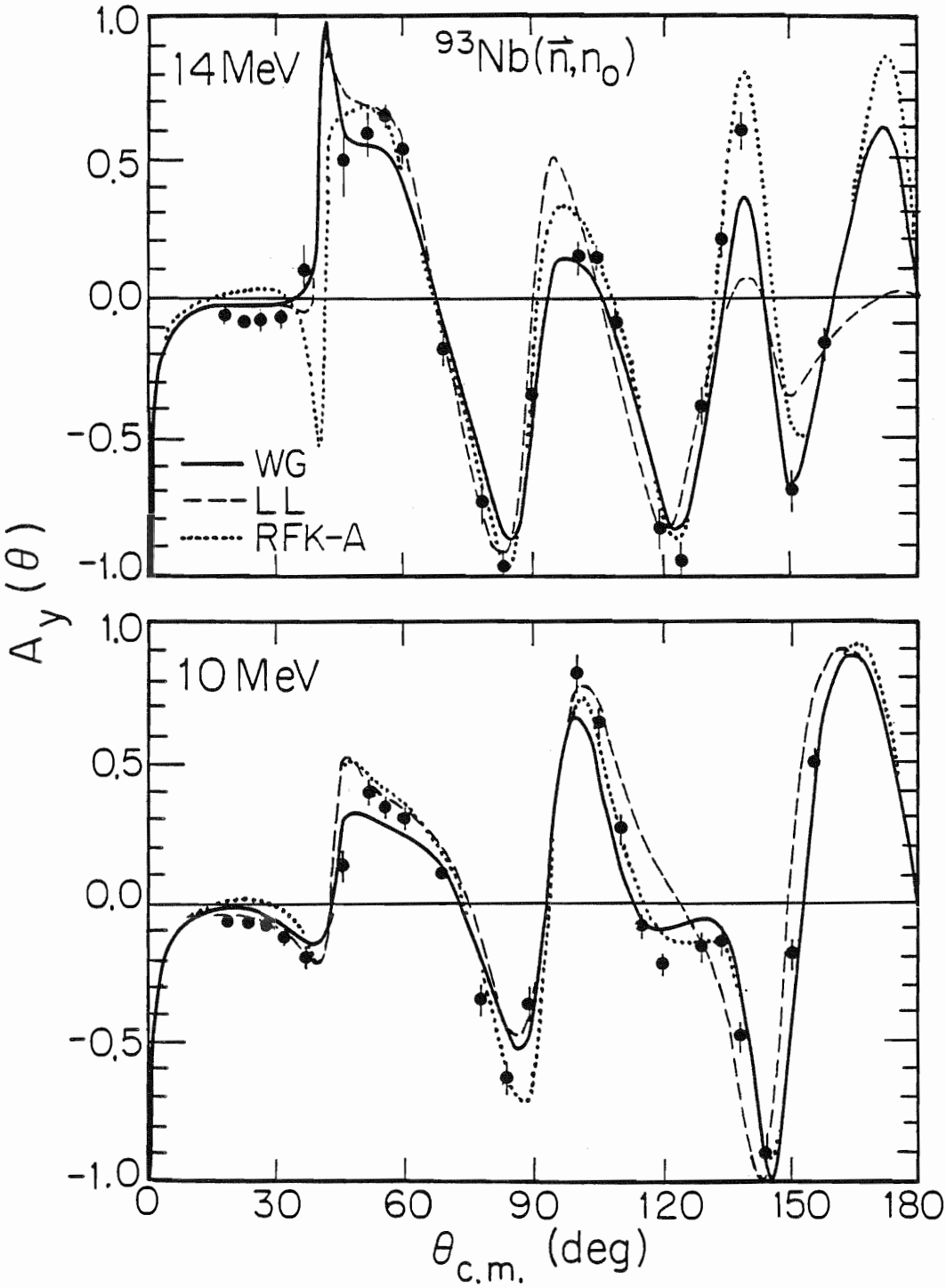

Figure 6.3. Comparison of the $A_y(\theta)$ data for ^{93}Nb of the present work to the SOM predictions from calculations using the WG (Walter 1985), LL (Lagrange 1982), and RKF-A (Rapaport 1979) parameters.

representation of these data. This is somewhat surprising since the data base of the RKF analysis did not include analyzing power data. Instead, these authors employed directly the spin-orbit parameters that Becchetti and Greenlees derived mainly from proton-nucleon scattering in an early global analysis (Becchetti 1969). The WG parameters, which were derived using $A_y(\theta)$ data for many nuclei, also give reasonable predictions for the $A_y(\theta)$ data (see figure 6.3), which are somewhat superior to those of the RKF-A parameters, particularly at 14 MeV and at forward angles. The calculations using the LL parameters clearly have problems at 14 MeV for angles greater than 130^o and at 10 MeV for angles between 110^o and 135^o.

6.3 Spherical Optical Model Parameter Searches

Three sets of SOM parameters for the ^{93}Nb data have been derived in the present work in searches using the code GENOA. These three parameters sets are given in table 6-2 and are designated as PW-A, PW-B, and PW-C. The SOM calculations for the $\sigma(\theta)$ data, using the three sets of parameters, are shown in figure 6.4, while those for the $A_y(\theta)$ data are shown in figure 6.5. The strengths of the potentials in these three sets of parameters were all constrained to have linear energy dependencies. Note that in all three parameter sets, W_V is set equal to 0.0 MeV below a specified energy. Because the data base was too limited at low energies, it was also decided to constrain W_D to a constant value below some other specified energy.

The first set of parameters (PW-A) were derived using the WG parameters as the starting point in the GENOA searches. Comparable $\sigma(\theta)$ and $A_y(\theta)$ predictions were obtained using the RKF-A and the LL parameters as starting points in the searches. The searches were performed in a way that gave

TABLE 6-2

SOM Search Parameters for ^{93}Nb

Parameter	PW-A	PW-B	PW-C
V_R(MeV)	50.41-0.293E	49.74-0.271E	50.41-0.297E
r_R(fm)	1.224	1.227	1.225
a_R(fm)	0.686	0.696	0.685
W_V(MeV)	0.0, E<6.18 MeV 0.184E-1.137, E>6.18 MeV	0.0, E<6.45 MeV 0.188E-1.212, E>6.45 MeV	0.0, E<6.53 MeV 0.182E-1.188, E>6.53 MeV
r_V(fm)	1.295	1.346	1.345
a_V(fm)	0.657	0.520	0.636
W_D(MeV)	7.295, E<11.08 MeV 10.24-0.266E, E>11.08 MeV	7.132, E<11.18 MeV 10.50-0.301E, E>11.18 MeV	7.303, E<11.08 MeV 10.25-0.266E, E>11.08 MeV
r_D(fm)	1.284	1.291	1.286
a_D(fm)	0.521	0.524	0.522
V_{so}(MeV)	7.024-0.051E	7.351-0.097E	6.740-0.015E
r_{Vso}(fm)	1.131	1.110	1.133
a_{Vso}(fm)	0.511	0.504	0.511
W_{so}(MeV)	1.092-0.035E		0.954-0.018E
r_{Wso}(fm)	1.261		1.267
a_{Wso}(fm)	0.511		0.511

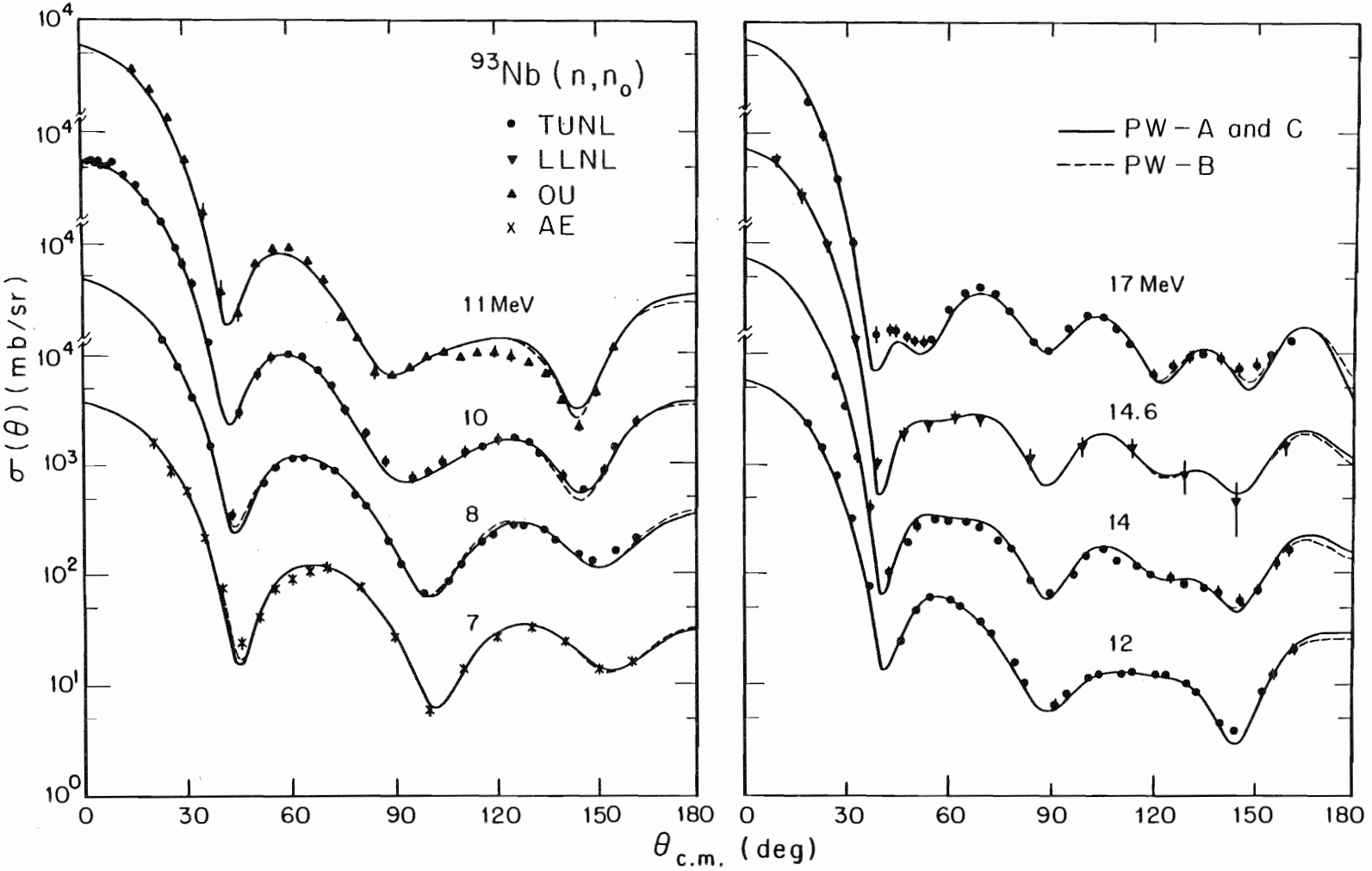

Figure 6.4. Comparison of the σ(θ) data for ^{93}Nb to the predictions calculated from the PW-A, PW-B, and PW-C SOM parameters of the present work. The TUNL data are those of the present work, the LLNL data are from Hansen 1985, the OU data are from Ferrer 1977, and the AE data are from Etemad 1973.

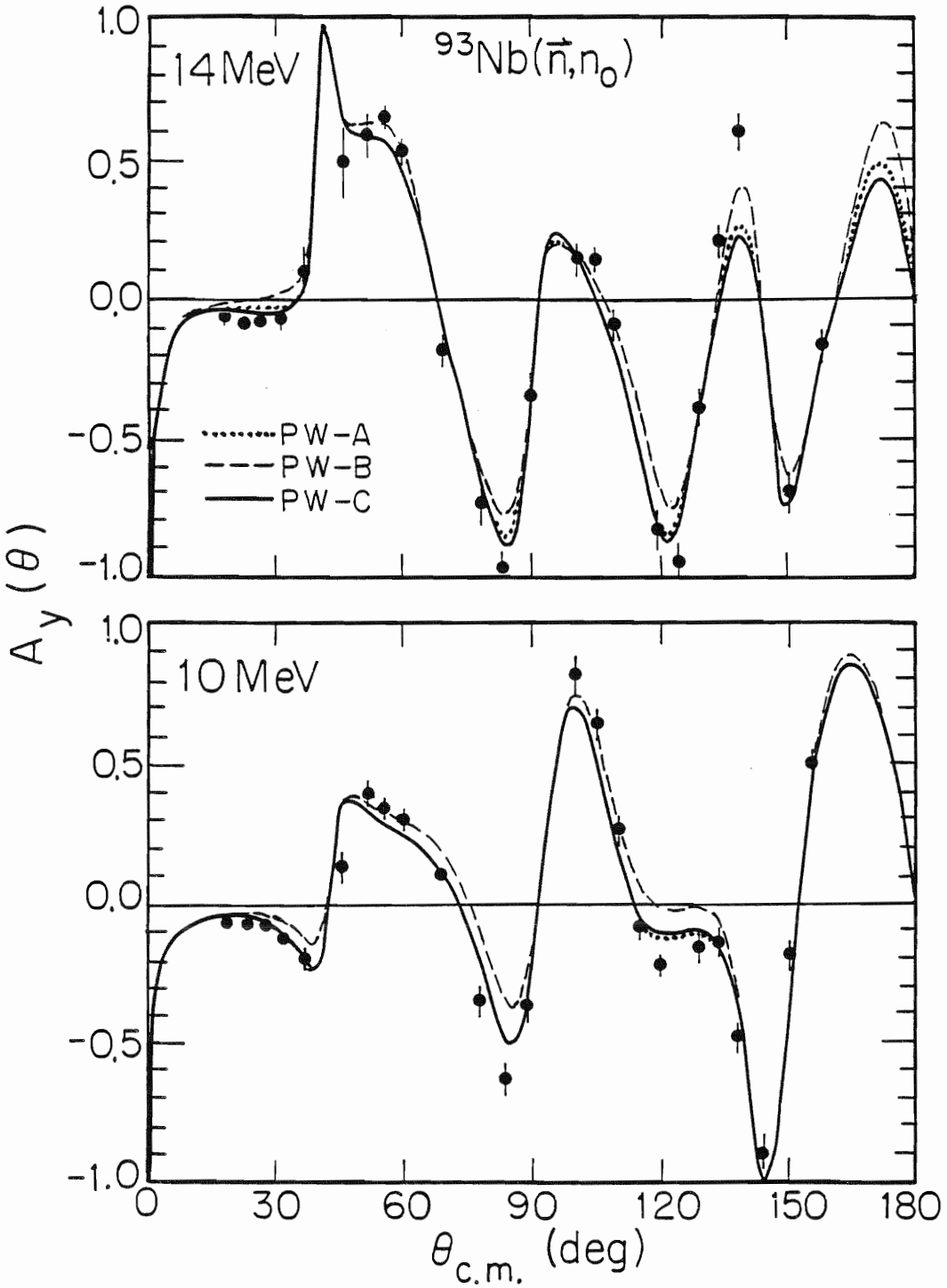

Figure 6.5. Comparison of the $A_y(\theta)$ data for ^{93}Nb to the predictions calculated from the PW-A, PW-B, and PW-C SOM parameters of the present work.

optimum values for all of the parameters. However, these searches indicated the need for unrealistically large energy dependencies for V_{so} and W_{so}, so restrictions were placed on the spin-orbit parameters. (These dependencies were on the order of a 1 MeV change in V_{so} and a 0.5 MeV change in W_{so} over a 10 MeV change in the neutron energy. The magnitudes of these dependencies are clearly outside of the realm of physically acceptable values.) Also, a_{Wso} was constrained to be equal to a_{Vso}, since the optimum value determined from searching was unreasonably small, i.e., less than 0.25 fm. Comparisons of figures 6.2 and 6.4, and of figures 6.3 and 6.5 show that the PW-A parameters give significantly improved results over those of the WG parameters, especially for the $\sigma(\theta)$ data and the $A_y(\theta)$ data at 10 MeV.

The PW-A parameter set includes an imaginary spin-orbit term, a term that until recently (Delaroche 1983, Floyd 1983, Walter 1985, Honoré 1986a, and Honoré 1986b) has been left out of SOM calculations for neutron-nucleus scattering, since such a term was felt to be unnecessary at energies below 50 MeV in both neutron- and proton-nucleus scattering. Therefore, it was decided to explore a parameter set in which this term is absent. From this exploration came the PW-B parameters, derived from the PW-A parameters by keeping W_{so} fixed at 0.0 and searching to optimize the remaining parameters. As can be seen in figure 6.4, there are only small differences between the $\sigma(\theta)$ calculations from the PW-A and PW-B parameters. The differences between the $A_y(\theta)$ calculations from the PW-A and PW-B parameters are much more pronounced, as can be seen in figure 6.5. The calculations with the PW-A parameters are clearly preferred over those with the PW-B parameters, when the values of χ^2 for the $A_y(\theta)$ cases are considered.

To explore the sensitivity to W_{so} further, predictions were made using the PW-A parameters, but with W_{so} set to 0.0. In figure 6.6, these predictions are compared to those made with the normal PW-A parameters. Again, a clear preference is seen for the parameter set with the nonzero W_{so}, when the values of χ^2 are considered, in agreement with an increasing number of findings at TUNL (Delaroche 1983, Floyd 1983, Walter 1985, Honoré 1986a, and Honoré 1986b). Note that for ^{93}Nb, unlike the nuclei studied in the immediately preceding references, there is very little sensitivity in the $A_y(\theta)$ calculations at forward angles to the inclusion of a Wso of about 1 MeV.

The linear energy dependencies of -0.051E for V_{so} and -0.035E for W_{so} obtained for the PW-A parameters are still larger than are desirable, if, as with the Walter and Guss parameters, the potential strengths are to connect at 80 MeV to those obtained by Schwandt et al. (Schwandt 1982) for proton-nucleus scattering. Therefore, the energy dependencies were fixed at -0.015E for V_{so} and -0.018E for W_{so}, the values derived in the global search of Walter and Guss, covering the 10- to 80-MeV energy range. New searches were made to obtain optimum values for the other parameters. The searches indicated that a_{Wso} still needed to be constrained to equal a_{Vso}, as with the PW-A parameters. This series of searches led to the PW-C parameters. The calculations made for $\sigma(\theta)$ using the PW-C parameters are essentially the same as those made with the PW-A parameters, as is indicated in figure 6.4. It can be seen in figure 6.5 that only small differences exist between the $A_y(\theta)$ calculations made using the PW-C and PW-A parameters. The total cross sections calculated from the PW-C parameters are plotted in figure 6.7 with some of the σ_T data of Smith et al. (Smith 1984) (1.0 to 4.5 MeV), Foster

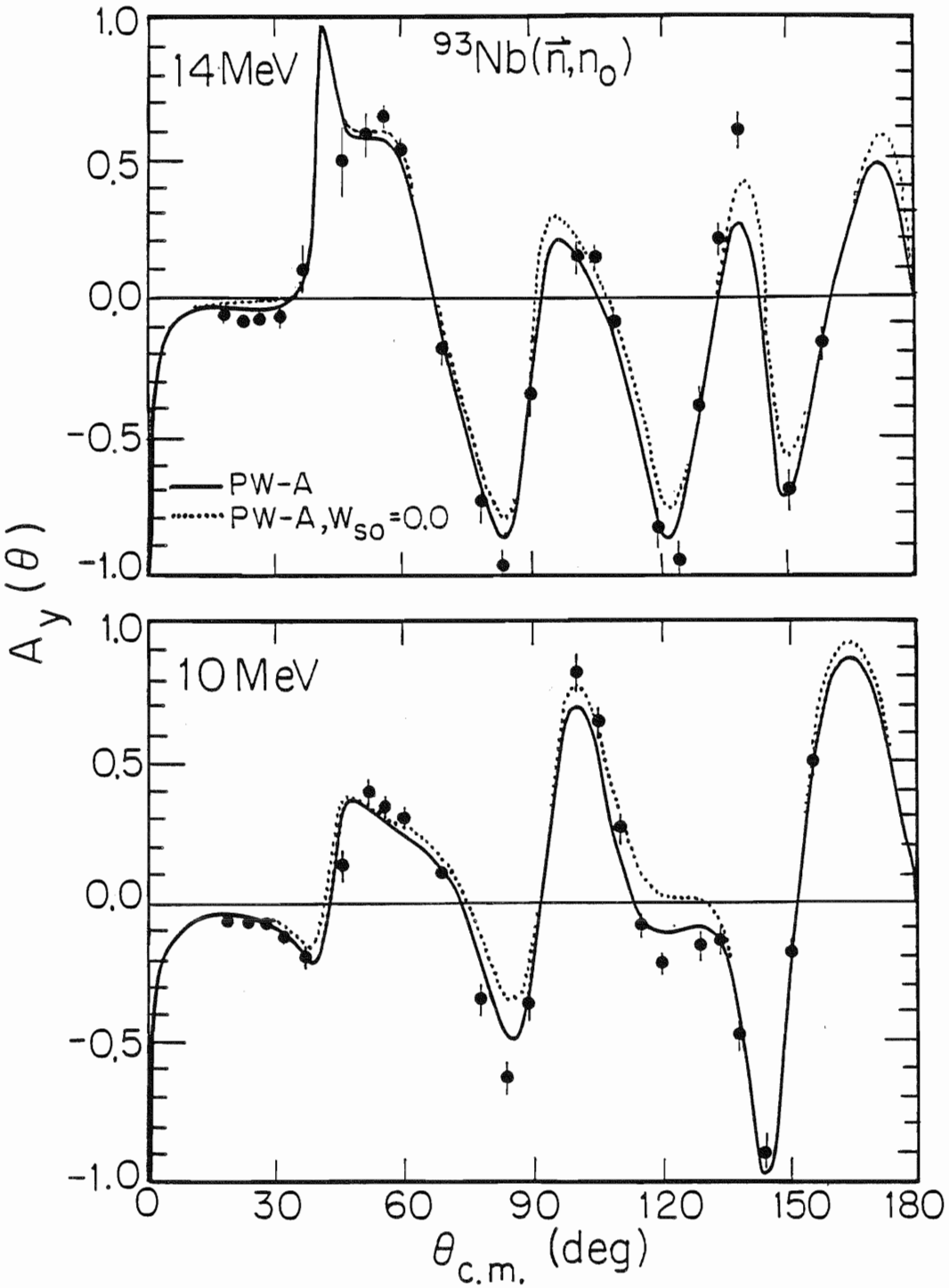

Figure 6.6. Comparison of the $A_y(\theta)$ data for ^{93}Nb of the present work to the SOM predictions from calculations using the PW-A parameters and the PW-A parameters with W_{so} set to 0.0 MeV.

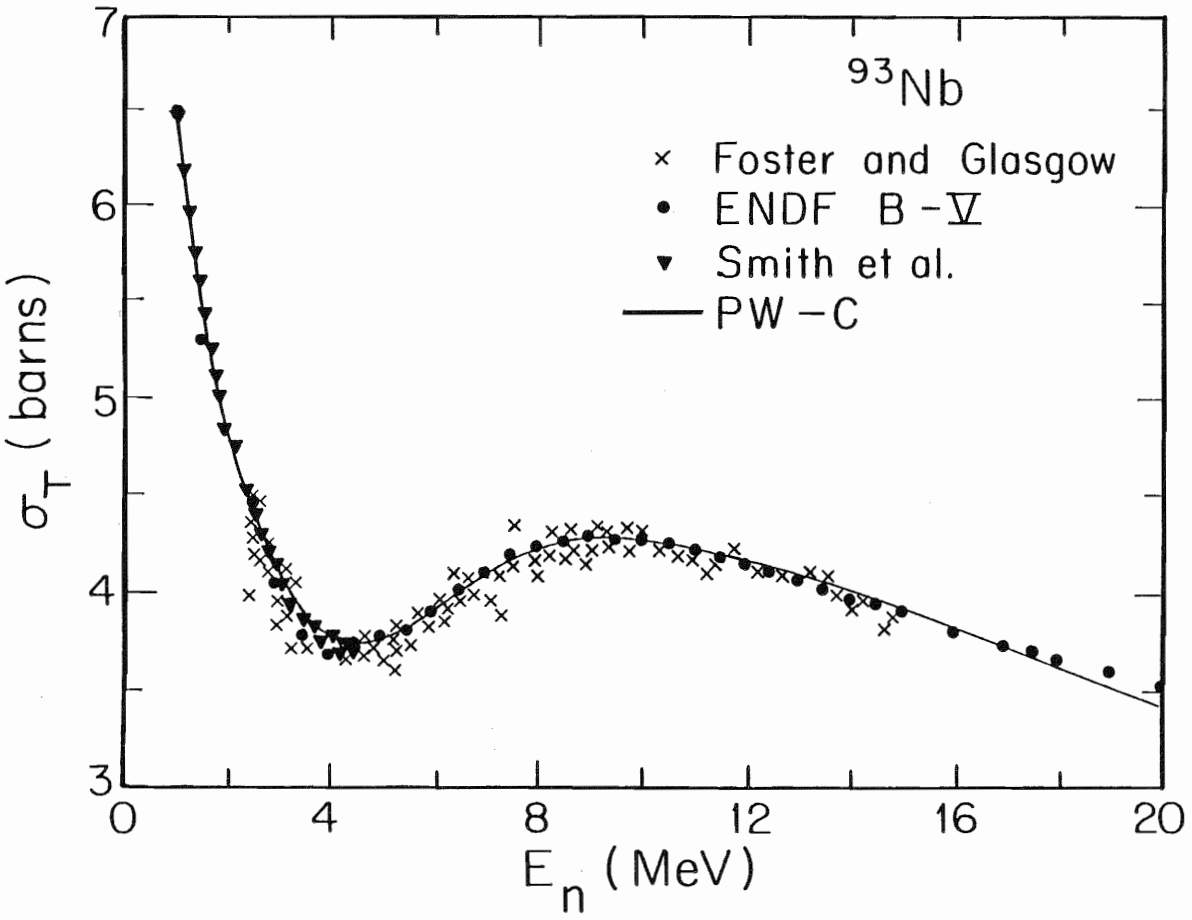

Figure 6.7. Comparison of σ_T data for ^{93}Nb to predictions calculated from the PW-C SOM parameters. The Foster and Glasgow data are from Foster 1971; those of Smith et al. are from Smith 1984.

and Glasgow (Foster 1971) (2.5 to 15 MeV), and ENDF/B-V (1 to 20 MeV). As can be seen from this figure, there is excellent agreement between the data and the calculated values in the 7- to 20-MeV range, and the agreement is good in the 1- to 7-MeV range, even though data below 7 MeV were not considered in the GENOA searches and W_D is held constant to its value at an incident neutron energy of 11.08 MeV. The linear energy dependencies for V_R, W_V, and W_D from the PW-C parameters are plotted in figure 6.8.

6.4 Conclusions

The PW-C parameters constitute the final parameter set derived in this work for ^{93}Nb. In the 7- to 20-MeV range, these parameters should give accurate predictions of $\sigma(\theta)$ and reasonable predictions of $A_y(\theta)$ for use in applied work. However, there are some discrepancies between the predictions calculated from the PW-C parameters and the $\sigma(\theta)$ data at 11 and 17 MeV and the $A_y(\theta)$ data at 10 and 14 MeV. The discrepancies at 11 MeV for $\sigma(\theta)$ might indicate a problem with the OU data at 11 MeV, since similar discrepancies exist between these data and predictions calculated from the LL parameters, which were derived using these data, and predictions calculated from the RKF-A parameters. The discrepancies at 17 MeV for $\sigma(\theta)$ are more intriguing. These discrepancies might be resolved if data were obtained in the 20- to 30-MeV range, so that the energy dependencies of the potential well strengths at energies above 14 MeV could be further explored. Such data would also indicate whether or not there is a problem with our 17 MeV data.

Reasons for differences between the SOM predictions and the $A_y(\theta)$ data are difficult to state. The trouble may be with the SOM: using a different

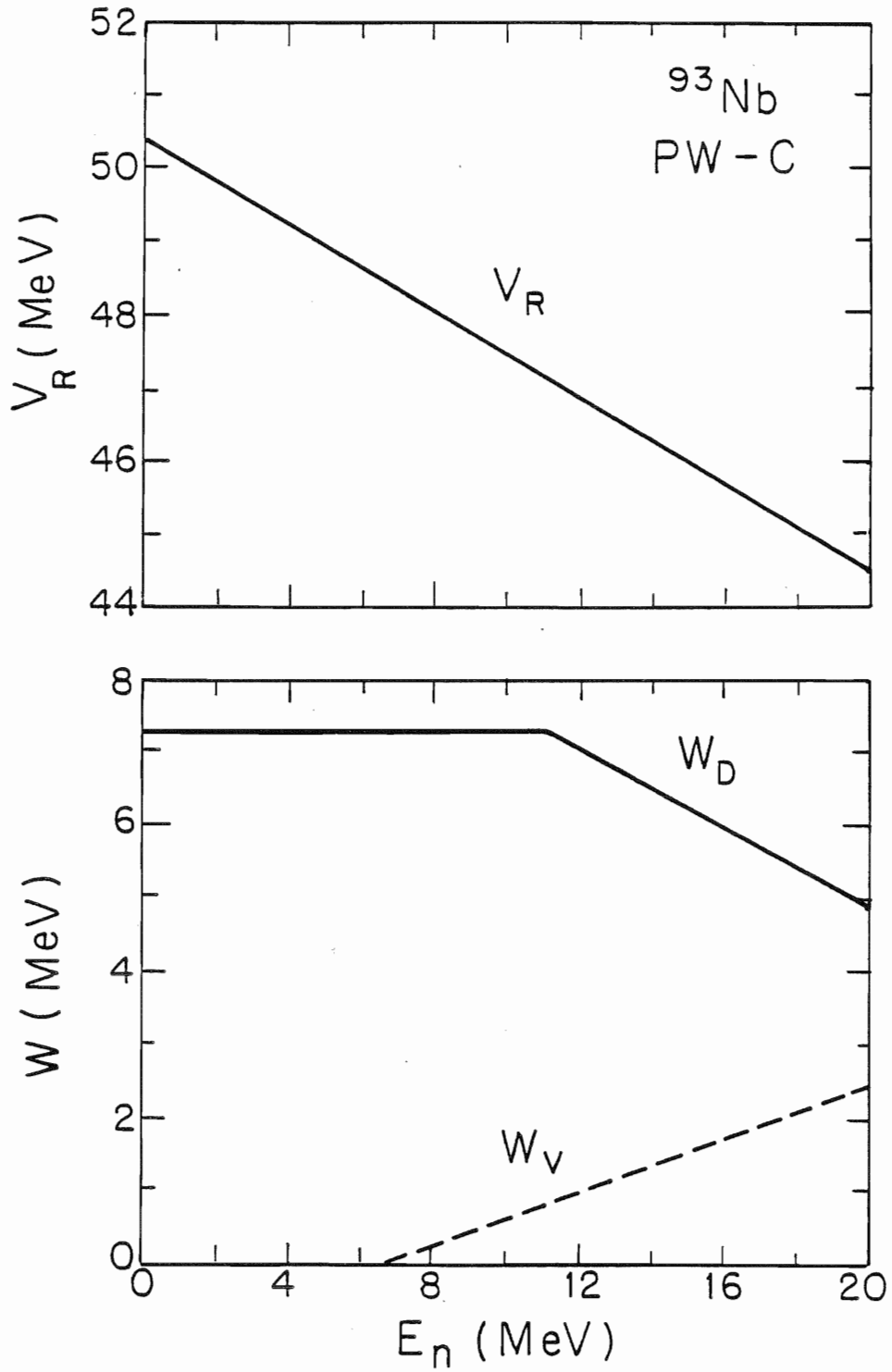

Figure 6.8. Plots of the energy dependencies of V_R, W_D, and W_V from the PW-C SOM parameters of the present work.

form factor might improve the predictions, as might using a different nuclear model. Coupled-channel calculations might be explored, but such calculations would require inelastic scattering data for the nucleus; these would be extremely difficult to obtain since there are over thirty states with excitation energies less than 2 MeV (Browne 1978), some of which are shown in figure 1.1. It is possible that the differences between the predictions and the $A_y(\theta)$ data are due to problems with the data, but we believe the error bars attached to the data truly represent the uncertainties in the measurements. Measurements of $A_y(\theta)$ at other laboratories are not likely to occur for some time. However, in the future, tests are planned with L.F. Hansen and F.S. Dietrich of LLNL to see if the microscopic model of Jeukenne, Lejeune, and Mahaux (JLM) (Jeukenne 1977) is capable of describing these data better than our SOM. Hansen et al. (Hansen 1985) obtained a good description for their $\sigma(\theta)$ data at 14.6 MeV using the JLM model, but they did not have $A_y(\theta)$ data for a more stringent test of this model. Consequently, they did not report any $A_y(\theta)$ predictions to which the present data might be compared.

Finally, as was stated in chapter 4, the data presented in the present work for ^{93}Nb contain any existing contributions from inelastic scattering to the first excited state (Q=-30. keV) of this nucleus, since this state is much too close to the ground state to be resolved. The J^{π} of the ground and first excited states of ^{93}Nb are $9/2^+$ and $1/2^-$, respectively. Therefore, partly due to the parity change and large angular momentum change required, we feel that the contributions from scattering to this state are probably very small and well within the uncertainties given for our data. Also, we ran a few test cases of coupled-channel calculations to explore the strength

of this inelastic state. The results of these calculations indicated that the largest $\sigma(\theta)$ for inelastic scattering to the first excited state could be as large as 0.5 mb/sr at 10 MeV. Of course, for these calculations we had to make several assumptions that may or may not be valid, due to the lack of experimental information. Experimental information concerning inelastic scattering to this state will not be forthcoming in the foreseeable future due to the extremely fine resolution needed. If the contributions for scattering to this state are larger than we believe, then the primary effects would be seen in the minima of the cross sections and for the larger magnitude $A_y(\theta)$ data. The true minima for elastic scattering would be deeper than indicated by our data, and the magnitudes of the larger magnitude $A_y(\theta)$ data would actually be larger.

CHAPTER 7

COUPLED-CHANNEL CALCULATIONS FOR $^{54,56}Fe$, $^{58,60}Ni$, AND ^{120}Sn

7.1 Introduction

Spherical optical model calculations can only describe nucleon-nucleus elastic scattering, and in principle should work well only for nuclei that are nearly spherical in shape. Such nuclei occur in the vicinity of the magic numbers; that is, nuclei that have closed shells of proton or neutrons. To describe both elastic and inelastic scattering and to describe scattering from nuclei that are non-spherical, coupled-channel (CC) calculations are used. These calculations use deformed optical potentials.

Coupled-channel calculations use a set of coupled Schrödinger equations to describe scattering for both elastic and inelastic channels or final states for the scattering system of a projectile and target nucleus. These equations are solved simultaneously. In principle, all of the excited states for the nucleus should be coupled in the calculations. However, this is not possible when there are many excited states, making the time needed for calculations too great. Also, information necessary for the calculations may not be available for all of the excited states. Therefore, only a few states are considered in actual calculations, and a complex optical potential is used to account for the effects of inelastic scattering to states that are not explicitly included in the coupled equations. The general theory of coupled-channel calculations is rather involved and for the most part will be omitted from the present work. The references for these types of calculations that have been of great importance to the present calculations are the papers of Raynal (Raynal 1972), Tamura (Tamura

1965), and Delaroche et al. (Delaroche 1976), and the texts of Satchler (Satchler 1980 and 1983) and Hodgson (Hodgson 1971).

There are two main categories of coupled-channel calculations: one for the vibrational model and one for the rotational model. These models describe the two simplest types of collective motion undergone by nucleons in a nucleus when excited by a projectile that scatters inelastically, depositing some of its energy into the nucleus. The ground states of vibrational nuclei are close to spherical in shape and may be said to undergo a collective motion wherein the nucleons vibrate about a spherical equilibrium shape. The ground states of rotational nuclei are deformed from a spherical shape, being either oblate or prolate in shape, and undergo a collective motion in which the nucleons rotate about an axis of symmetry. Most of the calculations contained in this work are based on the vibrational model; those for ^{56}Fe are the only ones based on the rotational model.

The deformed optical potential for neutron scattering is written as

$$U(r) = -V_R f(r,R_R,a_R) - iW_V f(r,R_V,a_V) + i4W_D a_D \frac{df}{dr}(r,R_D,a_D)$$
$$- 2i\lambda_\pi^2 V_{so} \vec{\nabla} f(r,R_{Vso},a_{Vso}) \times \vec{\nabla} \cdot \vec{s} - 2i\lambda_\pi^2 W_{so} \vec{\nabla} f(r,R_{Wso},a_{Wso}) \times \vec{\nabla} \cdot \vec{s} \quad , \quad (7.1)$$

where the strengths of the real potential, the volume absorption, the surface absorption, and the real spin-orbit potential are V_R, W_V, W_D, V_{so}, and W_{so}, respectively. The potential for proton scattering has an additional Coulomb-potential term. As in the SOM potential of the previous chapter, the form factor to be used here is of the Woods-Saxon type,

$$f(r,R_i,a_i) = \{1 + \exp[(r - R_i)/a_i]\}^{-1} \quad , \quad (7.2)$$

but for these calculations we now have

$$R_i = r_i A^{1/3}\left[1 + \sum_{\lambda\mu} \alpha_{\lambda\mu} Y_\lambda^\mu(\theta,\phi)\right] , \qquad (7.3)$$

for vibrational nuclei, where the $Y_\lambda^\mu(\theta,\phi)$ are spherical harmonics. The diffuseness a_i and radius parameter r_i are treated as adjustable parameters in attempts to describe data, as in SOM calculations. The first term of equation 7.3 is simply the nuclear radius of the SOM calculations used in equation 6.2. The second term introduces the vibrational deformations undergone by a nucleus excited to a state with angular momentum λ. In the CC calculations, single phonons of angular momentum λ, projection μ, and parity $(-1)^\lambda$ are either created or annihilated through the quantum operators $\alpha_{\lambda\mu}$, which are called multipole deformation parameters. The deformation parameters β_λ are related to the $\alpha_{\lambda\mu}$ operators in the manner defined by Tamura. The deformations lengths δ_i are defined to be equal to $\beta_i R_i$. Normally, the deformation lengths for all of the potentials are constrained to be equal to the central potential deformation length δ_C. However, for ^{54}Fe, as seen by Guss et al. (Guss 1982b) and to be shown in sections 7.3 and 7.4, the spin-orbit deformation length δ_{SO} is found to be nearly twice δ_C.

For rotational nuclei that are axially symmetric, instead of equation 7.3, we have

$$R_i = r_i A^{1/3}\left[1 + \sum_{\lambda} \beta_\lambda Y_\lambda^0(\theta,\phi)\right] , \qquad (7.4)$$

where β_λ is the permanent deformation of the nucleus. The remaining parameters are the same as those of equation 7.3.

The coupled-channel calculations contained in this work have been carried out using the code ECIS79 of Raynal (Raynal 1979). (Note that for all the CC calculations with ECIS79 in the present work relativistic

kinematics were used above 30 MeV.) These calculations consumed an extensive amount of time due to the requisite method of searching for an optimum parameter set. The code can calculate for only one energy at a time and requires several minutes to run. Searches are performed for one parameter at a time by varying the parameter and then deciding which value of the parameter is best by qualitatively comparing calculated and experimental values of $\sigma(\Theta)$, $A_y(\Theta)$, and σ_T over the appropriate energy range for the parameter. To obtain a very refined parameter set using this method requires many weeks of work, especially since the optimum value found for one parameter may no longer be optimum after optimizing other parameters. This is vastly different from the SOM code GENOA, which searches simultaneously for optimum values of as many parameters as desired by minimizing χ^2 for the data over a broad energy range.

7.2 Calculations for ^{58}Ni

Guss et al. (Guss 1985) have performed a comprehensive CC analysis for ^{58,60}Ni. Their calculations are based on the vibrational model and include couplings to the ground states (0^+) and first excited state (2^+) of ^{58,60}Ni. Note that throughout this section for ^{58}Ni references to inelastic scattering will mean scattering to the first 2^+ excited state. To account for the apparent differences in the structure of the two nuclei, the reorientation matrix elements of the 2^+ states $M_{22}^{(2)}$ were considered in the CC calculations. The $M_{22}^{(2)}$ values are calculated from the measured quadrupole moments $Q(2^+)$ and transition probabilities $B(E2:0^+\rightarrow 2^+)$ using the following equation, which is in the ECIS79 convention (Guss 1982a):

$$M_{22}^{(2)} = (-1)\frac{\langle 2^+||\mathcal{M}(E2)||2^+\rangle}{\langle 2^+||\mathcal{M}(E2)||0^+\rangle} \quad . \tag{7.5}$$

From de Boer and Eichler (de Boer 1968), we have

$$\langle 2^+||\mathcal{M}(E2)||2^+\rangle = 1.32Q(2^+) \tag{7.6}$$

and

$$\langle 2^+||\mathcal{M}(E2)||0^+\rangle = [B(E2:0^+\rightarrow 2^+)]^{1/2} \quad . \tag{7.7}$$

The $M_{22}^{(2)}$ values used in the Guss analysis are +1.16 and 0.0 e·b for ^{58}Ni and ^{60}Ni, respectively. The analysis of Guss was based on the SPRT method (Delaroche 1976), in which the CC calculations are first constrained to reproduce the s- and p-wave (if available) strength functions S_0 and S_1, the potential scattering length R', and the σ_T data.

The analysis of Guss et al. was based on a large set of $\sigma(\theta)$ and $A_y(\theta)$ data for the elastic and inelastic (to the first 2^+ excited state) scattering of neutrons from ^{58,60}Ni. Specifically, the data base for elastic and inelastic scattering included $\sigma(\theta)$ data at 8, 10, 12, and 14 MeV for ^{58,60}Ni and $A_y(\theta)$ data at 10 and 14 MeV for ^{58}Ni (Guss 1985). Four of the $A_y(\theta)$ measurements at 10 MeV for elastic and inelastic scattering from ^{58}Ni are of extremely high accuracy (i.e., they have uncertainties on the order of ± 0.02 for the elastic data and of ± 0.05 for the inelastic data). In addition, the $A_y(\theta)$ data at 10 MeV included one high accuracy data point for both elastic and inelastic scattering from ^{60}Ni. The $\sigma(\theta)$ data at 24 MeV of Yamanouti et al. (Yamanouti 1980), measured at Ohio University, were also used in the analysis, as were the σ_T data for nickel of Garber and Kinsey (Garber 1976) from 100 keV to 30 MeV and of the Larson et al. (Larson 1980) from 4 to 80 MeV. The analysis of Guss used s-wave strength-function

and scattering-length values determined by Mughabghab and Garber (Mughabghab 1973) in the SPRT procedure. A large number of data for the elastic scattering and inelastic scattering (to the first 2^+ state) of protons from $^{58,60}Ni$ in the energy range from 18 to 25 MeV was also considered in the analysis of Guss.

Guss et al. found that the elastic scattering $\sigma(\theta)$ data could be fairly well represented by the CC calculations, even if one ignored a contribution from compound nucleus (CN) formation. However, the 8 MeV inelastic scattering $\sigma(\theta)$ data indicated a need for a CN contribution of about 2 mb/sr, the same magnitude as that calculated for the nearby nucleus ^{54}Fe by Sheldon (Sheldon 1981). At 10 MeV, Sheldon calculates that the CN contribution would amount to only about 0.5 mb/sr.

The parameters (step 3) from the analysis of Guss et al. for $^{58,60}Ni$ are given in table 7-1. The real potential used by Guss contains a linear energy dependence up to 20 MeV, where the energy dependence becomes a natural-logarithmic dependence. The volume absorptive term is zero below 11 MeV; above 11 MeV it increases linearly with energy. The geometry parameters for the volume absorption and the real potential are constrained to be the same in the analysis of Guss. Below 12 MeV, the surface absorptive term varies as the square root of the energy; above 12 MeV it decreases linearly with energy. Both the real and imaginary surface potentials have the usual term for an isospin dependence, which is proportional to ε, where ε is equal to $(N - Z)/A$. The real spin-orbit potential term has a small energy dependence, which is a linearly decreasing function with increasing energy, and as stated above, δ_{SO} has a value of $1.0\delta_C$. No imaginary spin-orbit potential is used in the analysis of Guss et

TABLE 7-1

Coupled-Channel Parameters for $^{58,60}Ni$

Guss et al. (Guss 1985)			
$V_R = 57.75 - 21.75\varepsilon - 0.46E$			$0 \leq E \leq 20$ MeV
$V_R = 76.12 - 21.75\varepsilon - 9.2(\ln E)$			$20 \leq E \leq 80$ MeV
$W_V = 0.0$			$0 \leq E \leq 11$ MeV
$W_V = 0.1(E - 11)$			$11 \leq E \leq 80$ MeV
$W_D = 4.04 - 15.54\varepsilon - 1.1E^{1/2}$			$0 \leq E \leq 12$ MeV
$W_D = 7.73 - 15.54\varepsilon - 0.1(E - 12)$			$12 \leq E \leq 80$ MeV
$V_{so} = 6.50 - 0.035E$		$W_{so} = 0.0$	$0 \leq E \leq 80$ MeV
$r_R = r_V = 1.165$	$r_D = 1.261$	$r_{Vso} = 1.017$	
$a_R = a_V = 0.656$	$a_D = 0.593$	$a_{Vso} = 0.600$	
$\beta_2(^{58}Ni) = 0.19$		$\beta_2(^{60}Ni) = 0.21$	
Present Work			
$W_V = 8.00\{1 + \exp[-(E-50.0)/10.0]\}^{-1}$			$0 \leq E \leq 80$ MeV
$W_D(^{58}Ni) = 0.0640(E - \varepsilon_F)^2 \exp[-0.0670(E - \varepsilon_F)]$			$0 \leq E \leq 12$ MeV
$W_D(^{60}Ni) = 0.0624(E - \varepsilon_F)^2 \exp[-0.0681(E - \varepsilon_F)]$			$0 \leq E \leq 12$ MeV
$\varepsilon_F(^{58}Ni) = -10.6$ MeV		$\varepsilon_F(^{60}Ni) = -9.63$ MeV	
$W_D = 7.727 - 15.54\varepsilon - 0.082(E - 12)$			$12 \leq E \leq 80$ MeV
$V_{so} = 6.20 - 0.015E$		$W_{so} = 0.0$	$0 \leq E \leq 80$ MeV
$r_D = 1.290$		$a_D = 0.580$	

The units for the potential well strengths are MeV and for the geometry parameters are fm. The term ε is equivalent to $(N - Z)/A$. The Fermi energy ε_F is the average Fermi energy for neutrons for the nucleus. Except for W_V, W_D, r_D, and a_D, the parameters of the present work are the same as those of Guss.

al.

The parameters of the present analysis are also given in table 7-1 and were derived using the neutron data base employed by Guss, plus the data of the present work. Since some calculations for ^{60}Ni will also be presented, values are included in the table 7-1 for this nucleus. Except for W_D at energies lower than 12 MeV, as will be clear from the discussion given below for W_D, the isospin dependencies used by Guss have been preserved.

The present CC calculations for ^{58}Ni are intended to introduce two main advances beyond the analysis of Guss et al. The first is the use of a new formulation of W_D, so that at energies near the Fermi-energy ε_F we have

$$W \propto (E - \varepsilon_F)^2 \ , \tag{7.8}$$

as required by Mahaux and Ngo (Mahaux 1982) in their extensive paper, in which they apply dispersion theory to scattering from ^{40}Ca and ^{208}Pb. This relationship comes from the discussion by Jeukenne et al. (Jeukenne 1976) of the dispersion theory of the optical potential, in which they relate the Fermi gas model, as applied to nuclear matter theory, to the work of Luttinger (Luttinger 1961). In the dispersion theory, the real and imaginary parts of the optical potential are related through an equation known as the dispersion relation.

The energy-dependent form for W_D tried in our work is

$$W_D = c_1(E - \varepsilon_F)^2 \exp[d_1(E - \varepsilon_F)] \ , \tag{7.9}$$

where c_1 and d_1 are adjustable parameters to be determined from searches on the data. This is the same form adopted by Honoré et al. (Honoré 1986b) in their work on ^{40}Ca. As formulated in equation 7.9, W_D satisfies the

relation of equation 7.8 for energies near ε_F. The values of the Fermi energy ε_F of the nuclei used throughout this work are the average of the ε_F^+ and ε_F^- values for neutrons, calculated as prescribed by Mahaux and Ngo. In equation 7.9 at ε_F, W_D is 0.0, and for energies above ε_F, W_D increases with with increasing energy, reaching a maximum value at $E_{max}=\varepsilon_F-2/d_1$. Above E_{max}, W_D decreases with increasing energy, asymptotically approaching zero as E approaches infinity. However, in our calculations carried out for ^{58}Ni, although values of c_1 and d_1 were found such that fair results are obtained over the entire energy range of the CC calculations (10 keV to 80 MeV), better agreement with the data is obtained if a linearly decreasing energy dependence is adopted above 12 MeV, which is about 7.5 MeV below E_{max}. A value of 12 MeV is the same as that at which Guss changed from a square root of energy dependence to a W_D that decreases linearly with increasing energy. At 12 MeV, W_D is a continuous function of energy. However, the slope of W_D is discontinuous.

The second goal of the CC analysis for ^{58}Ni is to adjust W_D and W_V to obtain better agreement between the volume integrals for the imaginary potential calculated using the CC parameters and those calculated using information from the SOM work of Jeukenne, Lejeune, and Mahaux (JLM) (Jeukenne 1977). The JLM predictions indicate that at energies above 100 MeV the volume integral of the imaginary potential should approach a nearly constant value. However, with the energy dependencies of the Guss analysis the volume integral increases too rapidly after 84 MeV, where W_D becomes zero. This occurs because W_V is linearly increasing above this energy, having the same slope as at lower energies. In the present work, the potential strength W_V was made to roll off at high energies by using the

convenient form,

$$W_V = c_2\{1 + \exp[(e_2 - E)/d_2]\}^{-1} \quad . \tag{7.10}$$

This has a form similar to the shape of a Fermi form factor, but no physical implications should be read into this form. The quantities c_2, d_2, and e_2 are determined from searches on the data. Note that these parameters were also chosen so that W_V approaches a constant value at an energy around 100 MeV. In addition, the slope of W_D has been decreased so that it now becomes zero at 100 MeV instead of 84 MeV. The value of W_D at 12 MeV has a magnitude close to that used by Guss et al. Note that W_V should be formulated so that it also satisfies the relation of equation 7.8. However, since W_V is negligible below 0.0 MeV, this form has not been adopted for this work.

The final parameters for W_D and W_V are given in table 7-1. While making the changes to W_D and W_V, it was of course desirable to preserve the quality of agreement between the $\sigma(\theta)$ and $A_y(\theta)$ data and the predictions as obtained by Guss et al. To this end, r_D and a_D were shifted from the values used by Guss et al. Also, the slope of the linear energy dependence of V_{so} has been decreased from that used by Guss et al., so that near 80 MeV V_{so} is comparable to the V_{so} obtained by Schwandt et al. (Schwandt 1982) in their analysis for proton-nucleus scattering. With the exception of the corrected $M_{22}^{(2)}$ value for ^{58}Ni, which will be discussed below, it was possible to retain all of the rest of the parameters used by Guss and still maintain a good quality of agreement between the neutron observables and the calculations.

Finally, before displaying the results of the calculations, we mention one feature regarding the inclusion of an imaginary spin-orbit term. Calculations were performed to see if a nonzero W_{so} improved the description of the $A_y(\theta)$ data at 10, 14, and 17 MeV. These calculations indicate that the optimum strength of W_{so} must be between -0.25 and 0.0 MeV. A positive W_{so}, as found for other nuclei in this energy range (Delaroche 1983, Floyd 1983, Walter 1985, Honoré 1986a, and Honoré 1986b), would worsen the agreement between the 14 and 17 MeV calculations and data. For the calculations presented in this section, W_{so} has been set to zero, also the value used by Guss et al.

The $\sigma(\theta)$ data for neutron elastic scattering from ^{58}Ni are shown in the left half of figure 7.1 with the predictions from the CC parameters of the present analysis. The predictions from the analysis of Guss are not shown; there are only small differences between the two sets of predictions. That is, for the energy range in figure 7.1, the predictions from Guss's parameters produce slightly better agreement in the 30° to 60° range, the present predictions produce improved agreement in the 130° to 160° range.

The $\sigma(\theta)$ data for neutron inelastic scattering to the first 2^+ excited state of ^{58}Ni are compared to predictions from the CC parameters of the present analysis in the right half of figure 7.1. Again, the predictions from Guss's parameters are not shown due to the small differences between the two sets of predictions in this energy range. Except in the vicinity of 125° at 12, 14, and 17 MeV, the predictions from both sets of parameters are in quite good agreement with the data. No parameterization was found in the present work or in the work of Guss et al. that eliminates the disagreement between the data and predictions in the region near 125°. This curious

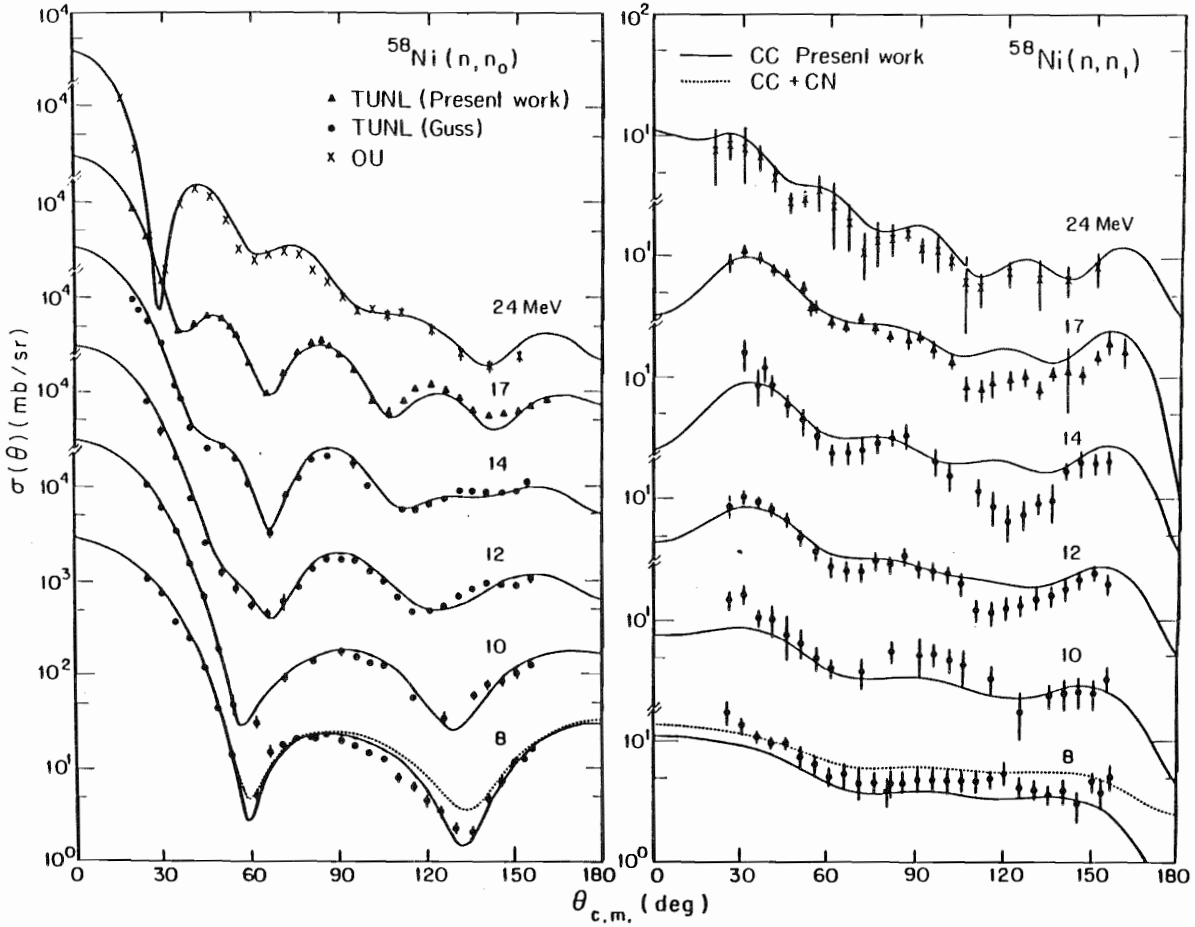

Figure 7.1. Comparison of neutron elastic and inelastic scattering σ(θ) data for ^{58}Ni to CC calculations. For the first excited state, Q and J^{π} are -1.45 MeV and 2^{+}, respectively. The TUNL data of Guss are from Guss 1985; the OU data are from Yamanouti 1980. The CC calculations were made using the present work parameters from table 7-1. The CN contribution is about 2 mb/sr and is the same as that calculated for ^{54}Fe by Sheldon (Sheldon 1981).

observation might signify some unusual feature in the structure of the Ni isotopes, or possibly some weakness in our CC approach. It should be explored further.

Dotted curves representing the addition of a CN contribution of 2 mb/sr to the CC calculations for elastic and inelastic scattering at 8 MeV are also shown in figure 7.1. This magnitude is comparable to the CN contributions calculated by Sheldon for ^{54}Fe at this energy. For inelastic scattering, it is apparent that instead of 2 mb/sr, a CN contribution of only 1 mb/sr would give better agreement between the data and calculation. A CN contribution of 1 mb/sr would also be better for the elastic scattering case.

The $A_y(\theta)$ data for neutron elastic scattering and inelastic scattering to the first 2^+ state for ^{58}Ni are compared in figure 7.2 to predictions based on the new CC parameters. The present calculations are in slightly better agreement with the elastic scattering $A_y(\theta)$ data at 10 and 17 MeV between 110^o and 150^o than are those of Guss et al. This improvement is primarily due to the changes in r_D and a_D mentioned above. However, for inelastic scattering, the predictions for $A_y(\theta)$ with the present parameters give slightly worse agreement with the data than do those of Guss et al. This is especially true at 10 MeV in the region between 70^o and 100^o where the high accuracy data were obtained. The reason for this poorer agreement for the inelastic scattering case is not our new potential parameterization, but lies primarily with the value of the $M_{22}^{(2)}$ reorientation matrix element. The present analysis uses the value $M_{22}^{(2)} = 0.75$, which was calculated from equations 7.5, 7.6, and 7.7 using the $Q(2^+)$ and $B(E2:0^+\rightarrow 2^+)$ values of -0.15 ± 0.08 e·b and 0.070 ± 0.002 $e^2\cdot b^2$ from Christy and and Häusser (Christy

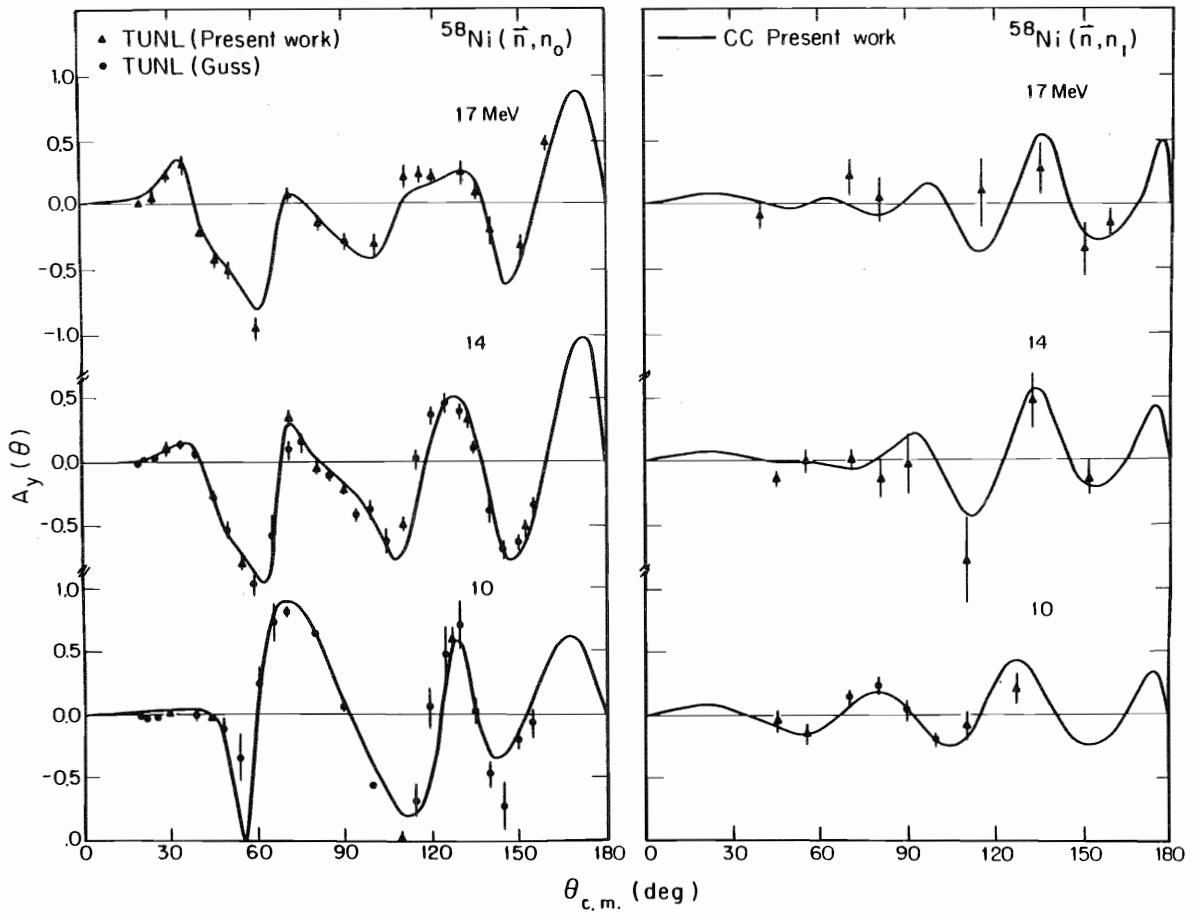

Figure 7.2. Comparison of neutron elastic and inelastic scattering $A_y(\theta)$ data for ^{58}Ni to CC calculations. For the first excited state, Q and J^π are -1.45 MeV and 2^+, respectively. The TUNL data of Guss are from Guss 1985. The CC calculations were made using the present work parameters from table 7-1.

1973). The value of $M_{22}^{(2)} = 1.16$ was used in the analysis of Guss et al., and this larger value is inconsistent with the tabulated $Q(2^+)$ and $B(E2:0^+ \rightarrow 2^+)$ values.

The σ_T calculated from the CC parameters are compared in figure 7.3 to the data of Larson et al. (Larson 1980) from 4 to 80 MeV and to some values from ENDF/B-V for elemental Ni. The uncertainties for Larson et al. data are about 2% at 4 MeV and increase to 4% by 80 MeV. In general, above 10 MeV, the agreement between the calculated and measured σ_T is very good and is slightly better than that for the calculations made using parameters of Guss et al. In the region between 5 and 8 MeV there is a systematic discrepancy between the data and the curve, which we can not explain. For comparison, the difference between the curve and the data in figure 7.3 is about 2% in the region from 30 to 40 MeV.

Recently, Perey et al. (Perey 1983) reported a new value for the s-wave strength function S_0 for ^{60}Ni, and Winters et al. published a paper (Winters 1985) in which new values for the p-wave strength function S_1 and scattering length R' are reported. The new value for S_0 for ^{60}Ni reported by Perey et al. and the old value reported by Mughabghab and Garber are in agreement. The value of R' for ^{60}Ni at a mean energy of 225 keV reported by Winters et al. is significantly different from that reported by Mughabghab and Garber and has a much smaller uncertainty.

The analysis of Guss is criticized in the Winters et al., for two main reasons. The first is that the total cross sections obtained using the Guss parameters for ^{60}Ni in the energy range from 100 keV to 2 MeV are too large. The second is that the Guss parameters give a value for R' at 10 keV that is consistent with the Mughabghab and Garber value, but not the Winters

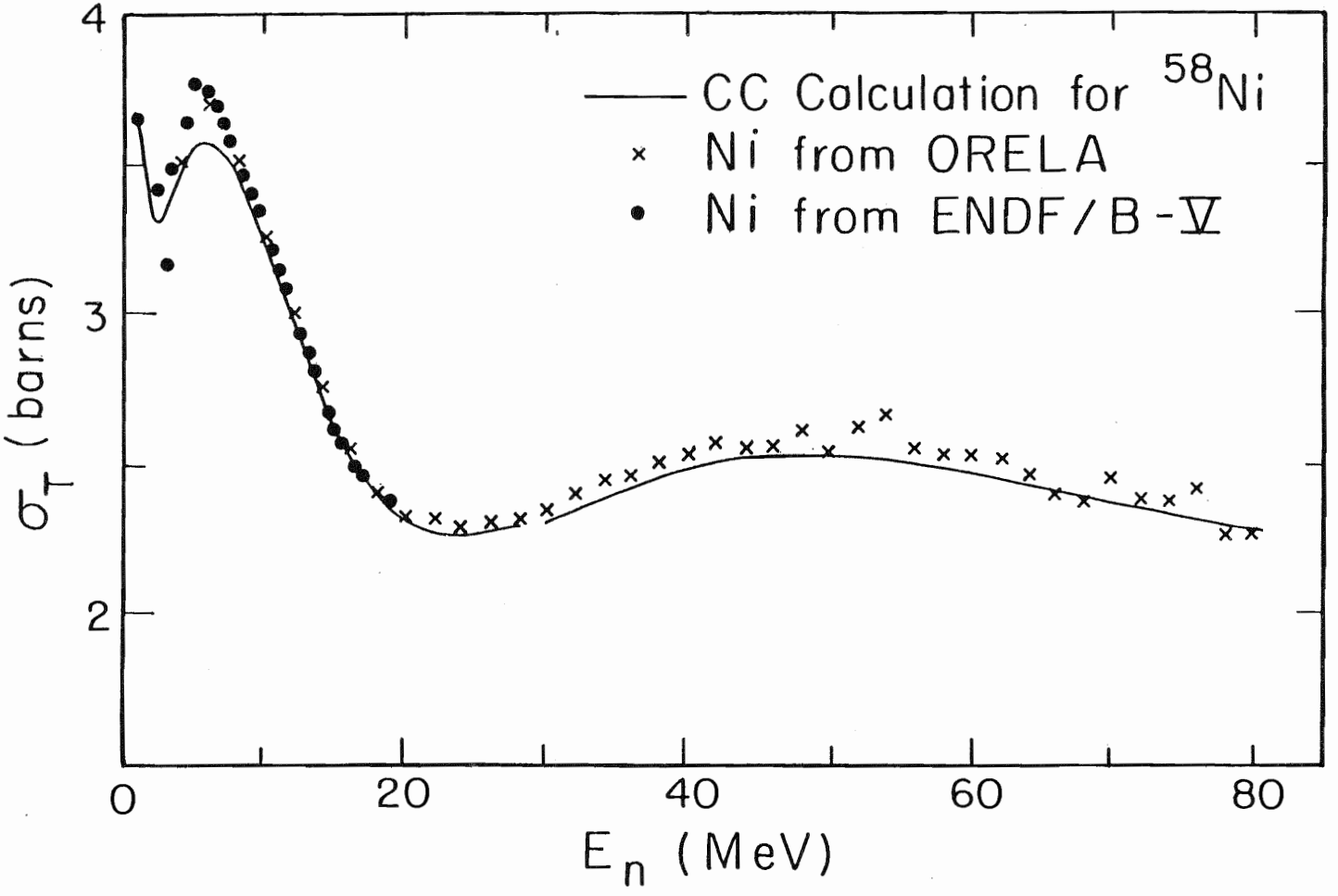

Figure 7.3. Comparison of σ_T data for elemental Ni to CC calculations for ^{58}Ni. The parameters of the present work from table 7-1 were used to make the calculations. The ORELA data are from Larson 1980. The break in the curve is due to the use of relativistic kinematics for $E_n \geq 30$ MeV.

value for a mean energy of 225 keV. The first criticism has not been resolved with the present analysis, but it might be resolved if an analysis similar to that of Honoré et al. for ^{40}Ca, in which dispersion relations are used, was carried out for the nickel isotopes.

In regard to their second criticism, the values of the s-wave strength function S_0 and the scattering length R′ for $^{58,60}Ni$ and the p-wave strength function S_1 for ^{60}Ni at 10 keV, 100 keV, and 225 keV calculated using the CC parameters of the present work and of Guss et al. are given in table 7-2. Also given are the experimentally determined S_0 and R′ for $^{58,60}Ni$ of Mughabghab and Garber, S_0 for ^{60}Ni from Perey et al. (Perey 1983), and R′ and S_1 for ^{60}Ni from Winters et al. (Winters 1985). The S_0 and R′ values for $^{58,60}Ni$ calculated at 10 keV using the CC parameters of the present work and of Guss et al. overlap with the values of Perey et al. and of Mughabghab and Garber. As can be seen, the calculations of R′ for ^{60}Ni at 225 keV using the parameters of Guss et al. and of the present work are in close agreement with Winters et al. The values of S_1 calculated at 100 keV using the parameters of the present work and of Guss et al. are a factor of two higher than the value given by Winters. However, this is not surprising given the limited energy range (0 to 200 KeV) of the resolvable resonance structure in the data of Perey et al. from which Winters determined his value for S_1. Note that it is difficult to assign uncertainties to the calculated values of S_0 and R′ since they are dependent on more than one of the CC parameters.

Finally, in figures 7.4 and 7.5, the energy dependencies and volume integrals for the real and imaginary potentials are plotted for ^{58}Ni. The plots were made using the parameters of the present work from table 7-1.

TABLE 7-2

Strength Functions and Scattering Lengths for $^{58,60}Ni$

	^{58}Ni		^{60}Ni		
	S_0	R′	S_0	S_1 [a]	R′
Experimental Determinations:					
Mughabghab and Garber	3.1±0.8	7.5±0.5	2.4±0.6		6.7±0.3
Perey et al.			2.2±0.6		
Winters et al.				3.0±0.5	5.5±0.03
CC Calculations at 10 keV:					
Present Work	2.46	6.72	1.90	6.04	6.82
Guss et al. (Step 3)	2.79	6.57	1.96	6.09	6.81
CC Calculations at 100 keV:					
Present Work	2.09	5.95	1.67	6.24	6.14
Guss et al. (Step 3)	2.32	5.77	1.76	6.65	6.09
CC Calculations at 225 keV:					
Present Work	1.87	5.34	1.53	6.43	5.56
Guss et al. (Step 3)	2.05	5.17	1.62	7.05	5.50

The units for the s- and p-wave strength functions S_0 and S_1 are 10^{-4} and 10^{-5}, respectively; those of the scattering lengths R′ are fm.

a) See the text for an explanation of the disagreement between the calculated and experimentally determined S_1 for ^{60}Ni.

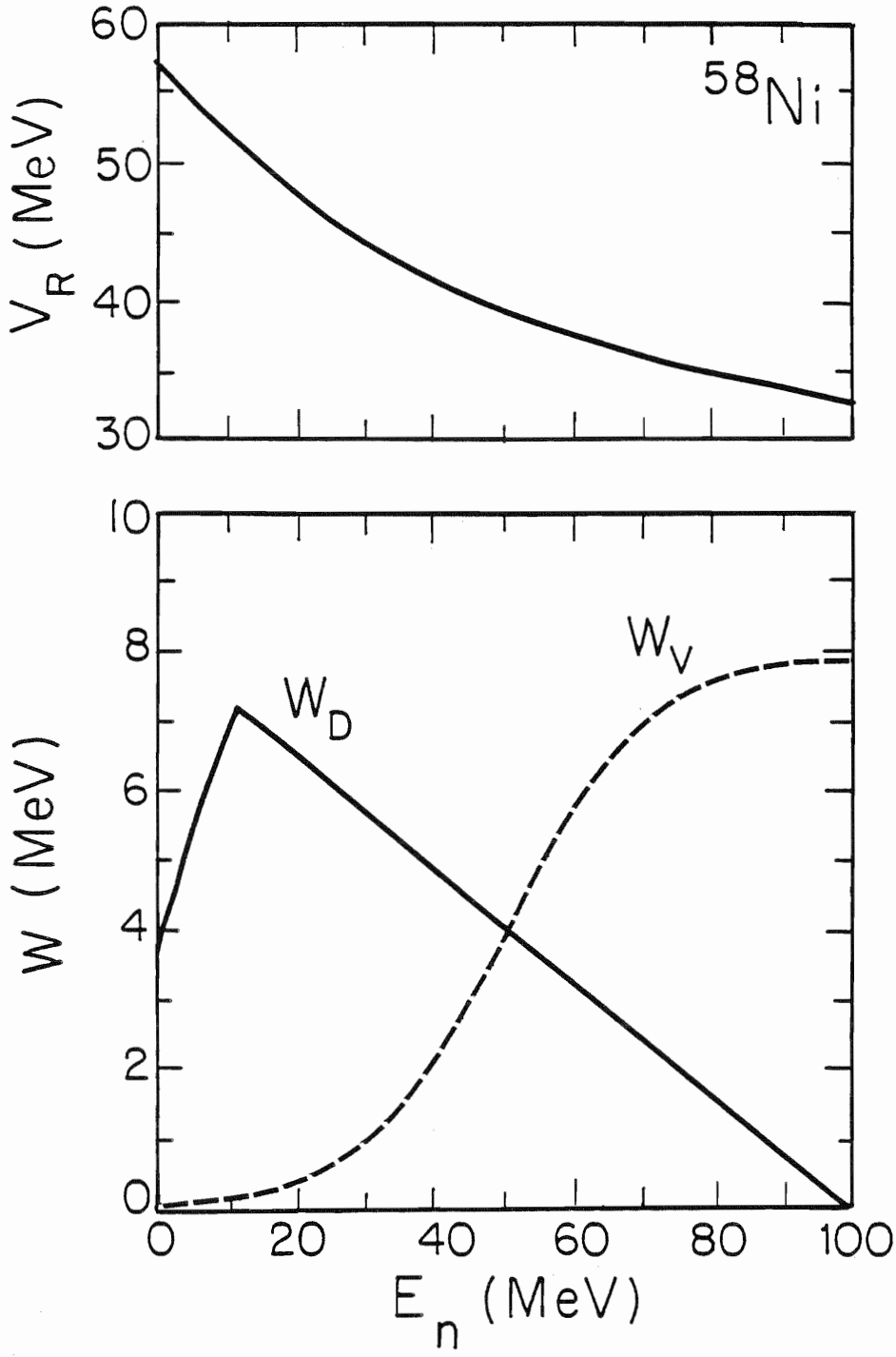

Figure 7.4. Plots of V_R, W_D, and W_V for ^{58}Ni. These plots demonstrate the energy dependencies of these potential strengths from the CC parameters of the present work given in table 7-1.

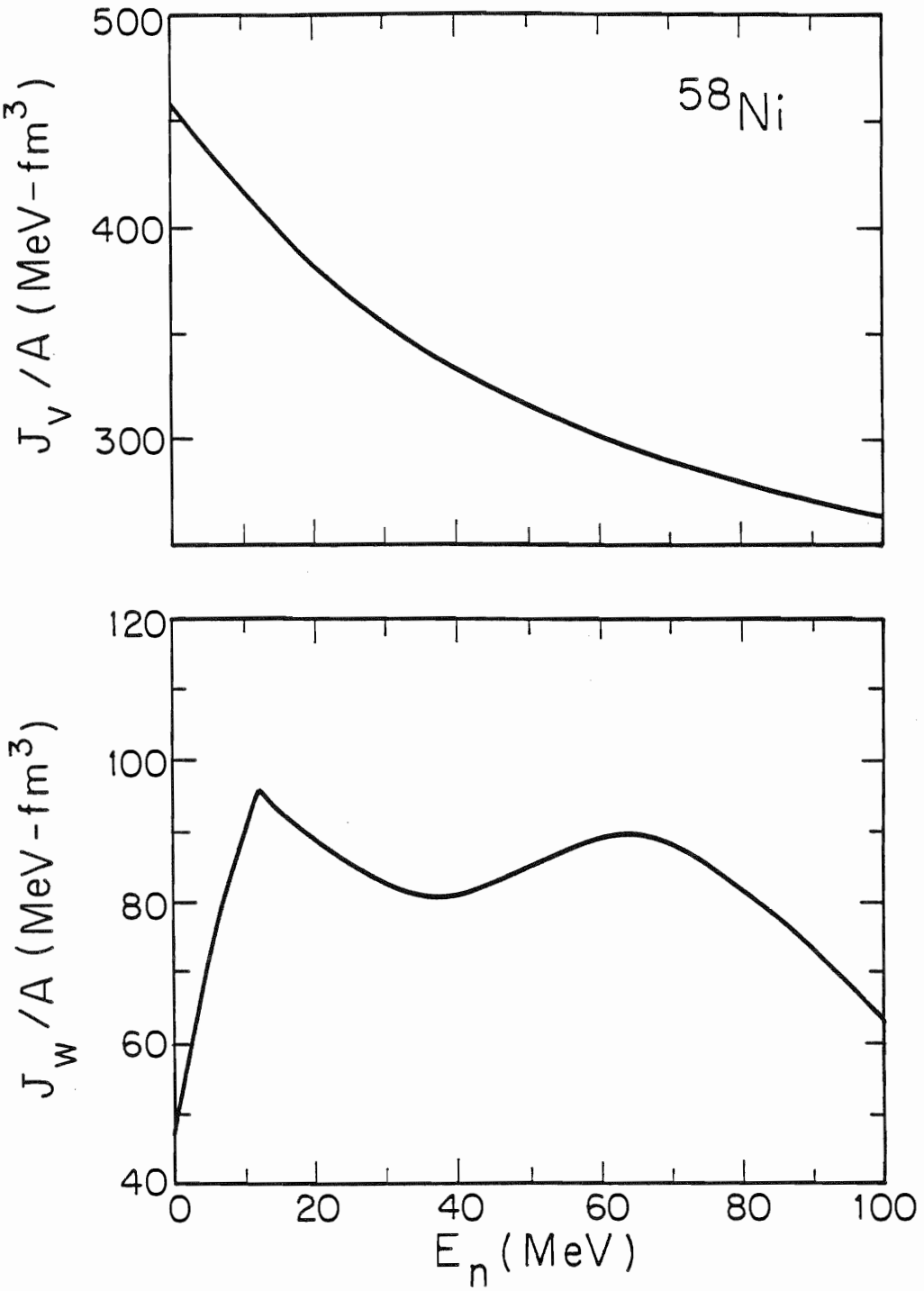

Figure 7.5. Plots of the volume integrals for the real and imaginary potentials for ^{58}Ni. The values were calculated using the CC parameters of the present work from table 7-1.

Plots are not given for the spin-orbit potential.

7.3 Calculations for ^{54}Fe

The intent of the present analysis for ^{54}Fe is to increase the energy range of the previous CC analyses for ^{54,56}Fe of Delaroche et al. (Delaroche 1982) and Floyd et al. (Floyd 1983). The Delaroche-Floyd analyses were restricted to the 100-keV to 14-MeV range. Thus, it was not necessary to use a W_V term, and it was possible to use a simple energy-dependent form of W_D that increases as the square root of the incident energy. In their analyses, the ground state (0^+) and first excited state (2^+) are coupled using the vibrational model for ^{54}Fe and the rotational model for ^{56}Fe. For simplicity in discussion, our references below to inelastic scattering data or calculations for ^{54,56}Fe will mean scattering to this excited state, unless specified otherwise. The analysis of Delaroche was based mainly on the $\sigma(\theta)$ data of El-Kadi et al. (El-Kadi 1982) for the elastic and inelastic scattering of neutrons from ^{54,56}Fe at 8, 10, 12, and 14 MeV. In a continuation of the work of Delaroche, Floyd et al. (Floyd 1983) extended the analysis by including their new $A_y(\theta)$ data for the elastic scattering of 10 and 14 MeV neutrons from ^{54}Fe. The Floyd analysis also included four high quality $A_y(\theta)$ data at 70°, 80°, 90°, and 100° for the inelastic scattering of 10 MeV neutrons to the first excited state of ^{54}Fe.

The availability of recently reported $\sigma(\theta)$ and σ_T data and our $\sigma(\theta)$ and $A_y(\theta)$ data makes it possible to increase the range of the CC analysis to 80 MeV. The new $\sigma(\theta)$ data are those at 17 MeV of the present work and at 11, 20, 22, 24, and 26 MeV of Mellema (Mellema 1983a) for neutron elastic and inelastic scattering from ^{54}Fe. The new $A_y(\theta)$ data are those of the

present work for the elastic and inelastic scattering of 10, 14, and 17 MeV neutrons from ^{54}Fe. The new σ_T data are those from 4 to 80 MeV for elemental Fe of Larson (Larson 1980).

The present analysis, instead of using the parameters from the analysis of Floyd, uses the $^{58,60}Ni$ parameters from section 7.2 of the present work, properly modified for $^{54,56}Fe$. This choice was made since the $^{58,60}Ni$ parameters already cover the energy range desired and since the neutron interaction with iron and nickel nuclei is similar. The CC parameters derived in the present analysis are given in table 7-3, together with those from the analyses of Delaroche and Floyd. The geometry parameters are identical to those obtained in section 7.2 for the nickel isotopes. The isospin dependencies of the Delaroche-Floyd analyses have been preserved for V_R and W_D above 12 MeV. As with nickel, calculations were performed to see if a nonzero W_{so} was needed. The results for these calculations were the same as those for nickel, and bracketed W_{so} between -0.25 and 0.0 MeV. The value of 0.0 was used for the calculations presented in this section.

The $\sigma(\Theta)$ elastic scattering data are shown in figure 7.6 together with predictions calculated from the present-work parameters. There are only minor differences between predictions using the Floyd et al. parameters and predictions using the present work parameters in the 8 to 14 MeV region. Comparisons above 14 MeV are are not justified, since the parameters of the Delaroche-Floyd analyses have energy dependencies that restrict calculations to energies of 14 MeV or below. The overall agreement between the calculations and the data is good, although at most energies there is a definite problem with the calculations for angles greater than 120^o. When the CN contributions of 2 mb/sr calculated by Sheldon are added to our

TABLE 7-3

Coupled-Channel Parameters for $^{54,56}Fe$

Delaroche et al. (Delaroche 1982)			Floyd et al. (Floyd 1983)	
$V_R = 58.50 - 20.35\varepsilon - 0.52E$		$0 \leq E \leq 14$ MeV	$V_{so} = 5.30$	$0 \leq E \leq 14$ MeV
$W_V = 0.0$		$0 \leq E \leq 14$ MeV	$r_{Vso} = 1.040$	
$W_D = 4.10 - 14.54\varepsilon + 1.1E^{1/2}$		$0 \leq E \leq 14$ MeV	$a_{Vso} = 0.464$	
$V_{so} = 6.108$	$W_{so} = 0.0$	$0 \leq E \leq 14$ MeV	$W_{so} = +0.5$	$0 \leq E \leq 14$ MeV
$r_R = 1.165$	$r_D = 1.261$	$r_{Vso} = 1.017$	$r_{Wso} = 1.071$	
$a_R = 0.656$	$a_D = 0.593$	$a_{Vso} = 0.600$	$a_{Wso} = 0.464$	
$\beta_2(^{54}Fe) = 0.20$		$\beta_2(^{56}Fe) = 0.24$		

Present Work

$V_R = 57.89 - 20.35\varepsilon - 0.46E$		$0 \leq E \leq 20$ MeV
$V_R = 76.25 - 20.35\varepsilon - 9.2(\ln E)$		$20 \leq E \leq 80$ MeV
$W_V = 8.40\{1 + \exp[-(E-50.0)/10.0]\}^{-1}$		$0 \leq E \leq 80$ MeV
$W_D(^{54}Fe) = 0.0780(E - \varepsilon_F)^2 \exp[-0.0750(E - \varepsilon_F)]$		$0 \leq E \leq 12$ MeV
$W_D(^{56}Fe) = 0.0677(E - \varepsilon_F)^2 \exp[-0.0704(E - \varepsilon_F)]$		$0 \leq E \leq 12$ MeV
$\varepsilon_F(^{54}Fe) = -11.3$ MeV	$\varepsilon_F(^{56}Fe) = -9.42$ MeV	
$W_D = 7.919 - 14.54\varepsilon - 0.082(E - 12)$		$12 \leq E \leq 80$ MeV
$V_{so} = 6.20 - 0.015E$	$W_{so} = 0.0$	$0 \leq E \leq 80$ MeV
$r_V = 1.165$	$r_D = 1.290$	
$a_V = 0.656$	$a_D = 0.580$	
$\beta_2(^{54}Fe) = 0.20$	$\beta_2(^{56}Fe) = 0.24$	

The units for the potential well strengths are MeV and for the geometry parameters are fm. The term ε is equivlent to $(N - Z)/A$. The Fermi energy ε_F is the average Fermi energy for neutrons. Except for the spin-orbit parameters, the parameters of Floyd are the same as the parameters of Delaroche. The present work retains the values for r_R, a_R, r_{Vso}, and a_{Vso} from the Delaroche analysis.

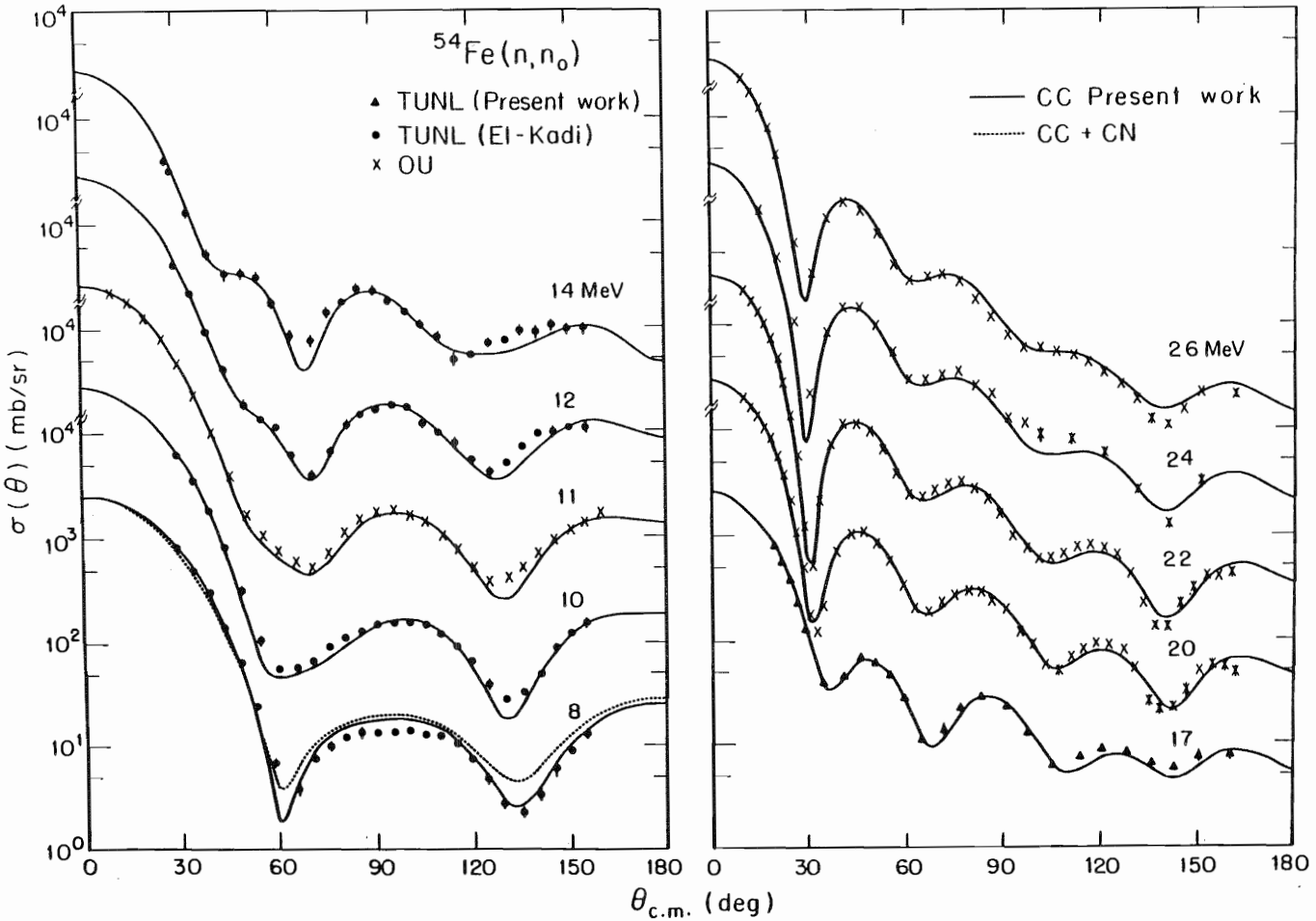

Figure 7.6. Comparison of σ(θ) data for the elastic scattering of neutrons from ^{54}Fe to CC calculations. The TUNL data of El-Kadi are from El-Kadi 1982; the OU data are from Mellema 1983a. The CC calculations were made using the present work parameters from table 7-3. The CN contribution is about 2 mb/sr and was calculated by Sheldon (Sheldon 1981).

calculation at 8 MeV, then there is a large difference between the prediction and the data. From the systematic agreement of the calculations to the data as a function of energy, we must conclude that 2 mb/sr is an overestimate of the CN contribution. The disagreement between the calculations above 17 MeV and data at backward angles is similar to that seen by Mellema (Mellema 1983a) in his CC calculations (which are almost identical to his SOM calculations) and by Mellema et al. (Mellema 1983b) in their JLM microscopic optical model calculations for ^{54}Fe. Clearly, the data at backward angles for energies above 17 MeV are difficult to describe exactly with conventional models.

The inelastic-scattering data and the predictions from calculations using the CC parameters of the present work are shown in figure 7.7. As can be seen in figure 7.7, the inclusion of the CN contributions calculated by Sheldon improves the agreement between the calculation and the data at 8 MeV. There is a trade-off at 10 and 11 MeV in the agreement for calculations made using the parameters of the present work and of Floyd. That is, the calculations from the parameters of the present work produce better agreement with the data forward of 115^{o} at these energies, but the reverse is true for angles greater than 115^{o}. At 8 MeV (if the CN contribution is included) and at 12 MeV, the calculations of Floyd give slightly better agreement with the data than do the present ones. At 14 MeV, there are no significant differences between the two calculations.

The $A_y(\theta)$ data for ^{54}Fe and the CC predictions of the present work are shown in figure 7.8. For the elastic scattering data at 10 MeV, both the predictions of the present work and of Floyd give good agreement with the data at angles forward of 110^{o}, but both give poor agreement for angles

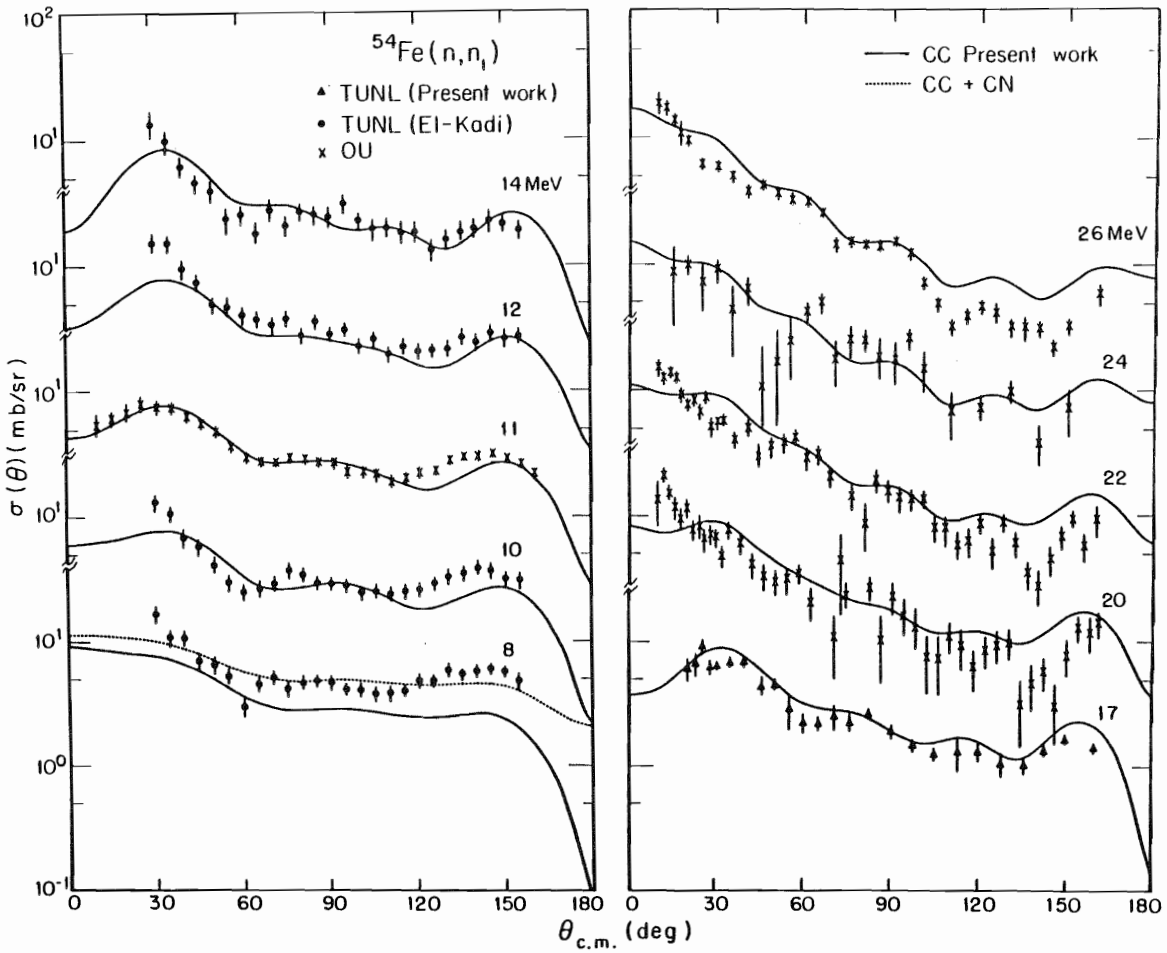

Figure 7.7. Comparison of $\sigma(\theta)$ data for the inelastic scattering of neutrons to the first 2^+ excited state (Q=-1.41 MeV) of ^{54}Fe to CC calculations. The TUNL data of El-Kadi are from El-Kadi 1982; the OU data are from Mellema 1983a. The CC calculations were made using the present work parameters from table 7-3. The CN contribution is about 2 mb/sr and was calculated by Sheldon (Sheldon 1981).

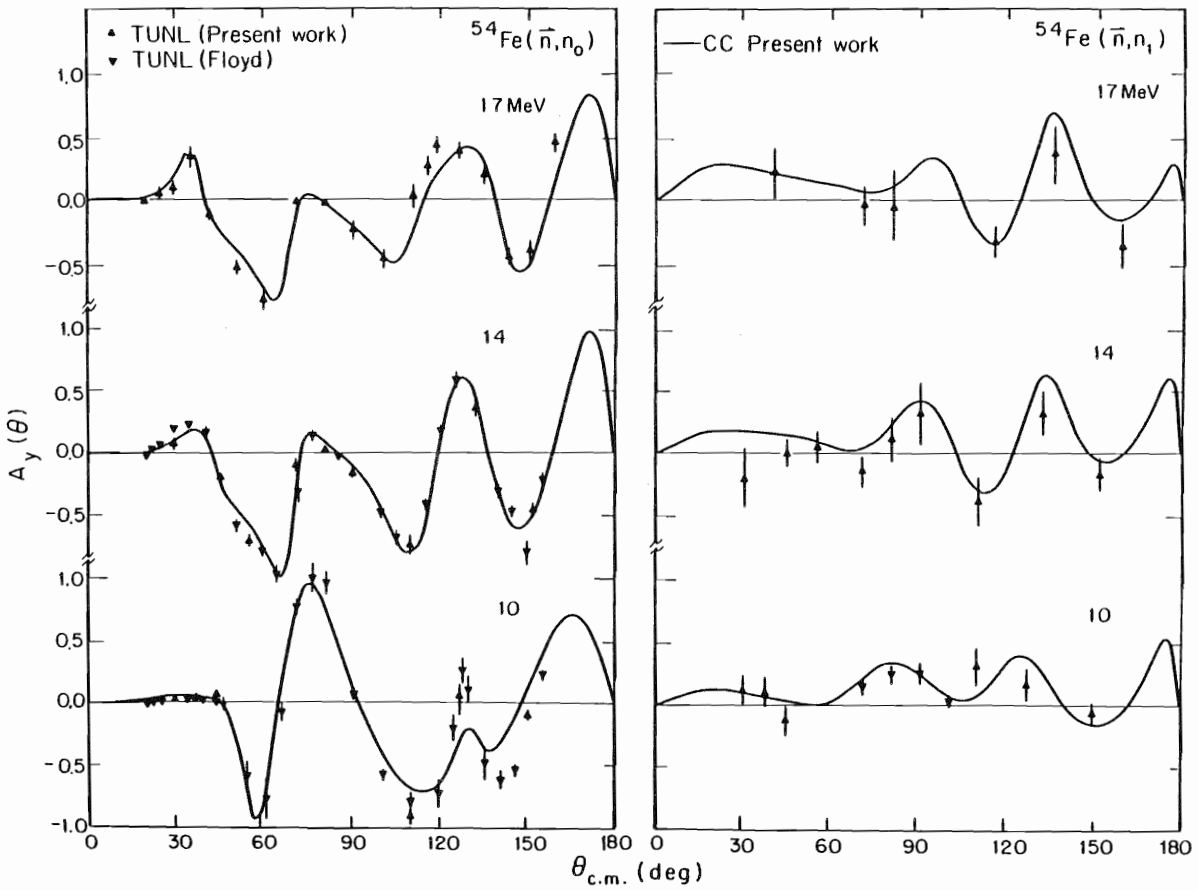

Figure 7.8. Comparison of neutron elastic and inelastic scattering $A_y(\theta)$ data for ^{54}Fe to CC calculations. For the first excited state, Q and J^π are -1.41 MeV and 2^+, respectively. The TUNL data of Floyd are from Floyd 1983. The CC calculations were made using the present work parameters from table 7-3.

greater than 110°. Both sets of predictions for elastic scattering at 14 MeV are very reasonable. For inelastic scattering, the quality of agreement between the data and both sets of predictions is comparable and quite good.

The σ_T data of Larson et al. and some values from ENDF/B-V are shown in figure 7.9 with a solid line representing the σ_T calculated using the parameters of the present work. The uncertainties for Larson et al. data are about 2% at 4 MeV and increase to 4% by 80 MeV. The agreement between the calculated curve and the data is excellent above 10 MeV. Between 5 and 8 MeV, a systematic discrepancy between the data and the prediction exists for Fe, similar to that seen for Ni (figure 7.3).

The s-wave strength functions and the scattering lengths calculated at 100 keV for ^{54,56}Fe using the parameters of the present work are tabulated in table 7-4 with the values of Mughabghab and Garber. Note, the calculations for ^{56}Fe were made using the rotational model and included a reorientation matrix element $M_{22}^{(2)} = 0.78$. This value was calculated using the values for $Q(2^+)$ and $B(E2:0^+\rightarrow 2^+)$ of -0.19 ± 0.08 e·b and 0.1022 ± 0.0055 $e^2\cdot b^2$ from LeVine et al. (LeVine 1981). At this energy, the parameters of the present work and those of Delaroche et al. and Floyd et al. predict approximately the same values for S_0 and R'; therefore, the quality of agreement with the values of Mughabghab and Garber is about the same (see table 7-4). Except for S_0 for ^{54}Fe, the calculated values are in good agreement with the empirical ones. As observed by Delaroche et al., the discrepancy for S_0 is probably due to the influence of large nonstatistical effects (which have been seen in (n,γ) measurements (Allen 1977) for ^{54}Fe) on the individual resonance parameters.

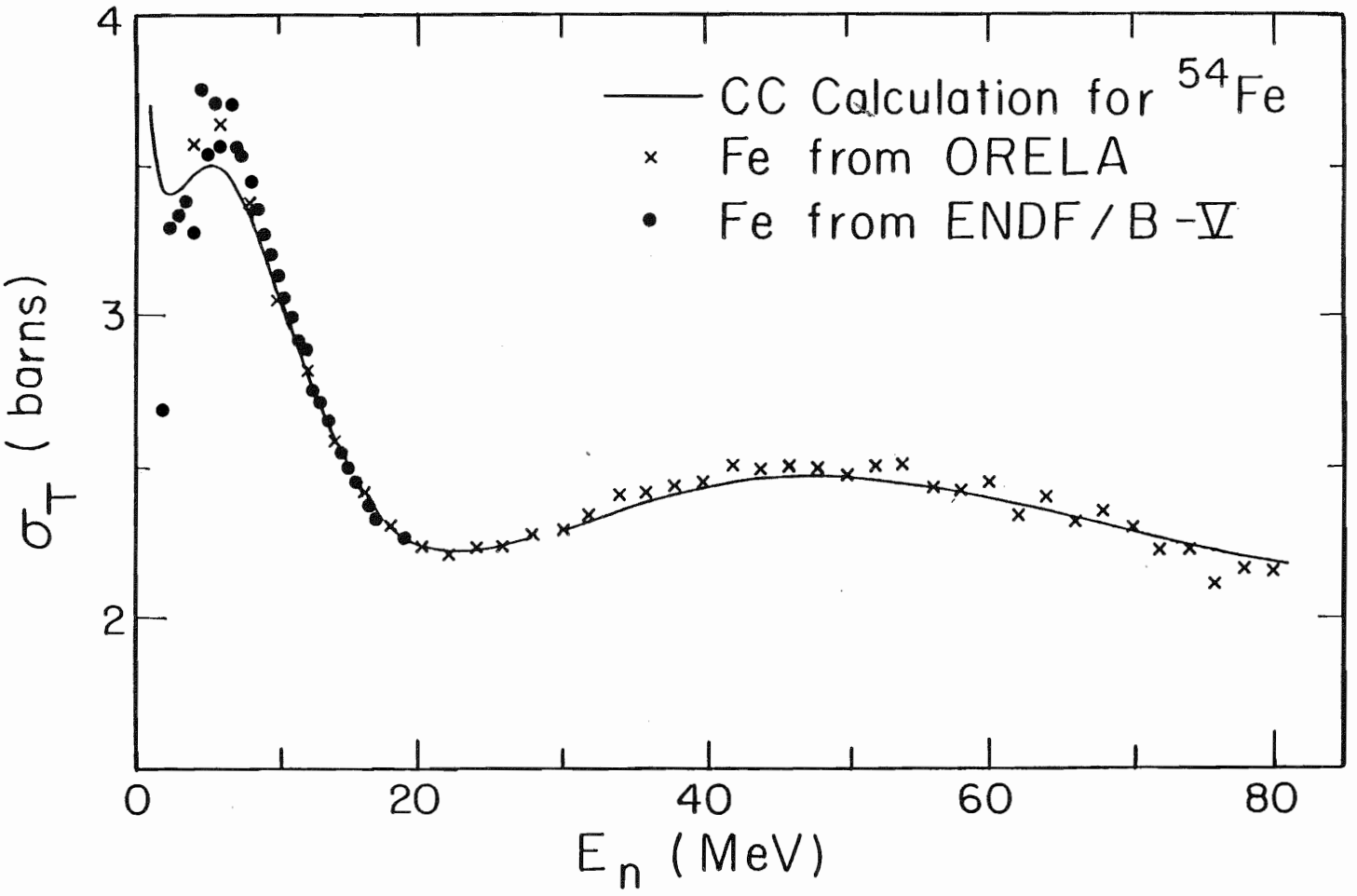

Figure 7.9. Comparison of σ_T data for elemental Fe to CC calculations for ^{54}Fe. The parameters of the present work from table 7-3 were used to make the calculations. The ORELA data are from Larson 1980. The break in the curve is due to the use of relativistic kinematics for $E_n \geq 30$ MeV.

TABLE 7-4

S-Wave Strength Functions and Scattering Lengths for $^{54,56}Fe$

	^{54}Fe		^{56}Fe	
	S_0 [a)]	R′	S_0	R′
Experimental Determinations:				
Mughabghab and Garber	5.6±1.7	5.6±0.6	1.6±0.5	6.1±0.7
CC Calculations at 100 keV:				
Present Work Parameters	2.64	6.22	1.95	5.49
Delaroche et al.	2.31	6.30	2.04	5.38
Floyd et al.	2.30	6.33	1.93	5.41

The units for the s-wave strength functions S_0 are 10^{-4}; those of the scattering lengths R′ are fm.

a) See the text for an explanation of the disagreement between the calculated and experimentally determined S_0 for ^{54}Fe.

Finally, in figures 7.10 and 7.11, the energy dependencies and volume integrals for the real and imaginary potentials are plotted for ^{54}Fe. The plots were made using the parameters of the present work from table 7-3. Plots are not given for the spin-orbit potential.

7.4 Spin-Orbit Deformation Lengths for ^{54,56}Fe and ^{58,60}Ni

One of the purposes in obtaining the inelastic $A_y(\theta)$ data for ^{54,56}Fe and ^{58,60}Ni was to explore further the relationships established by Guss et al. (Guss 1982b) between the deformation lengths δ_{SO} and δ_C of the spin-orbit and central potentials for these isotopes. They found that at 10 MeV, $\delta_{SO} = 1.0\delta_C$ for ^{56}Fe and ^{58,60}Ni, but $\delta_{SO} = 2.0\delta_C$ for ^{54}Fe. These findings were based on only four data points each for ^{54}Fe and ^{58}Ni and one data point each for ^{56}Fe and ^{60}Ni. Therefore, new data were acquired at 10 MeV for ^{54,56}Fe and ^{58,60}Ni to examine their findings more completely, and at 14 and 17 MeV for ^{54}Fe and ^{58}Ni to explore the energy dependence of the spin-orbit deformation lengths.

The $A_y(\theta)$ data for inelastic scattering for ^{54}Fe at 10, 14, and 17 MeV are shown in figure 7.12 with predictions from the coupled-channel parameters of section 7.3, with δ_{SO} equal to 0.0, 1.0, and 2.0 times δ_C. It appears that at 10 MeV the optimum value of δ_{SO} is about $1.7\delta_C$, consistent with $2.0\delta_C$ as found by Guss et al. and as used in section 7.3. The corresponding figure for ^{58}Ni is figure 7.13, in which the data are shown with the predictions from the parameters of section 7.2, again with δ_{SO} equal to 0.0, 1.0, and 2.0 times δ_C. As can be seen, the optimum value of δ_{SO} at 10 MeV is about $1.0\delta_C$, also consistent with Guss et al. Finally, in figure 7.14, comparisons are shown for ^{56}Fe using the section 7.3 parameters

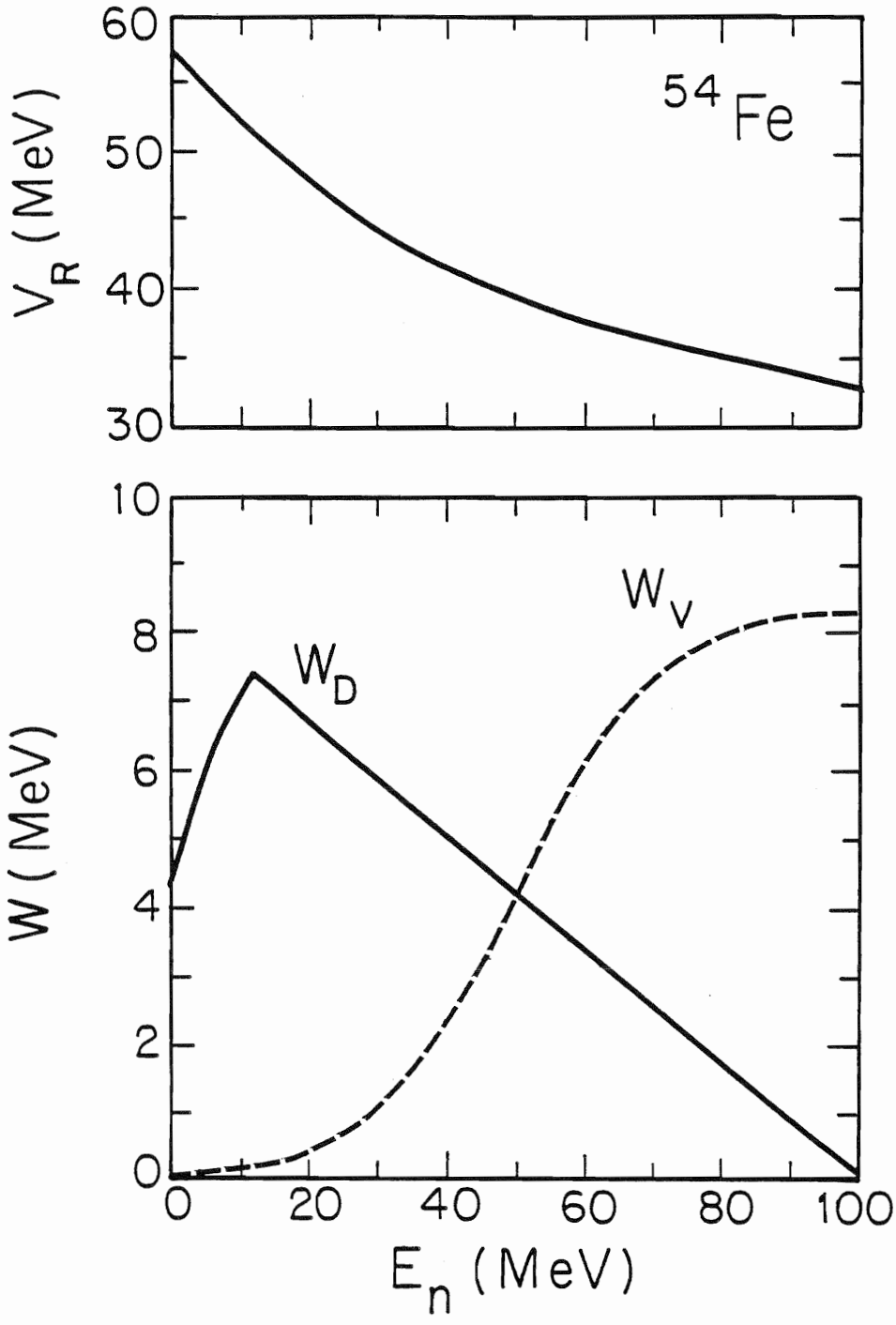

Figure 7.10. Plots of V_R, W_D, and W_V for ^{54}Fe. These plots demonstrate the energy dependencies of these potential strengths from the CC parameters of the present work given in table 7-3.

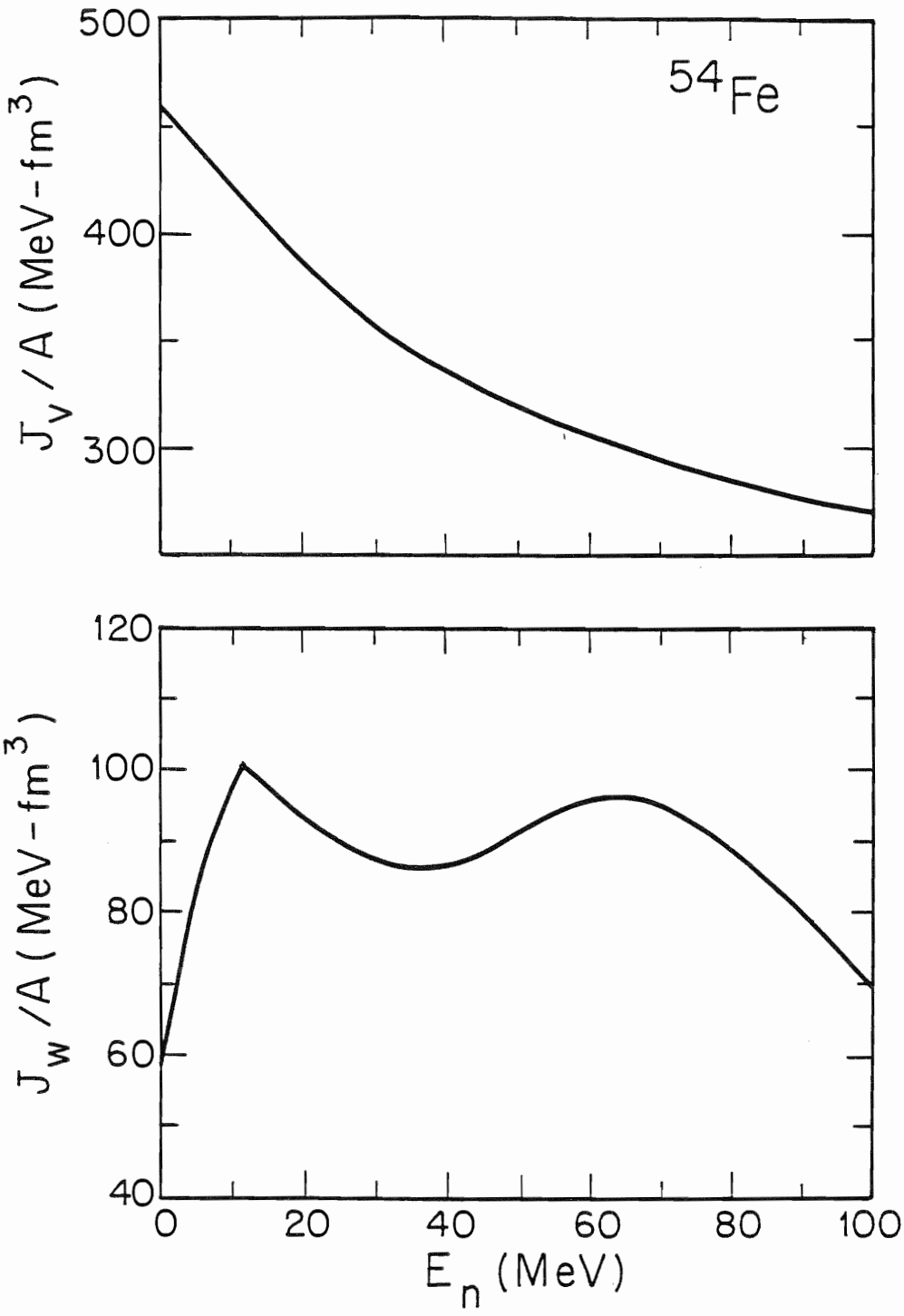

Figure 7.11. Plots of the volume integrals for the real and imaginary potentials for ^{54}Fe. The values were calculated using the CC parameters of the present work from table 7-3.

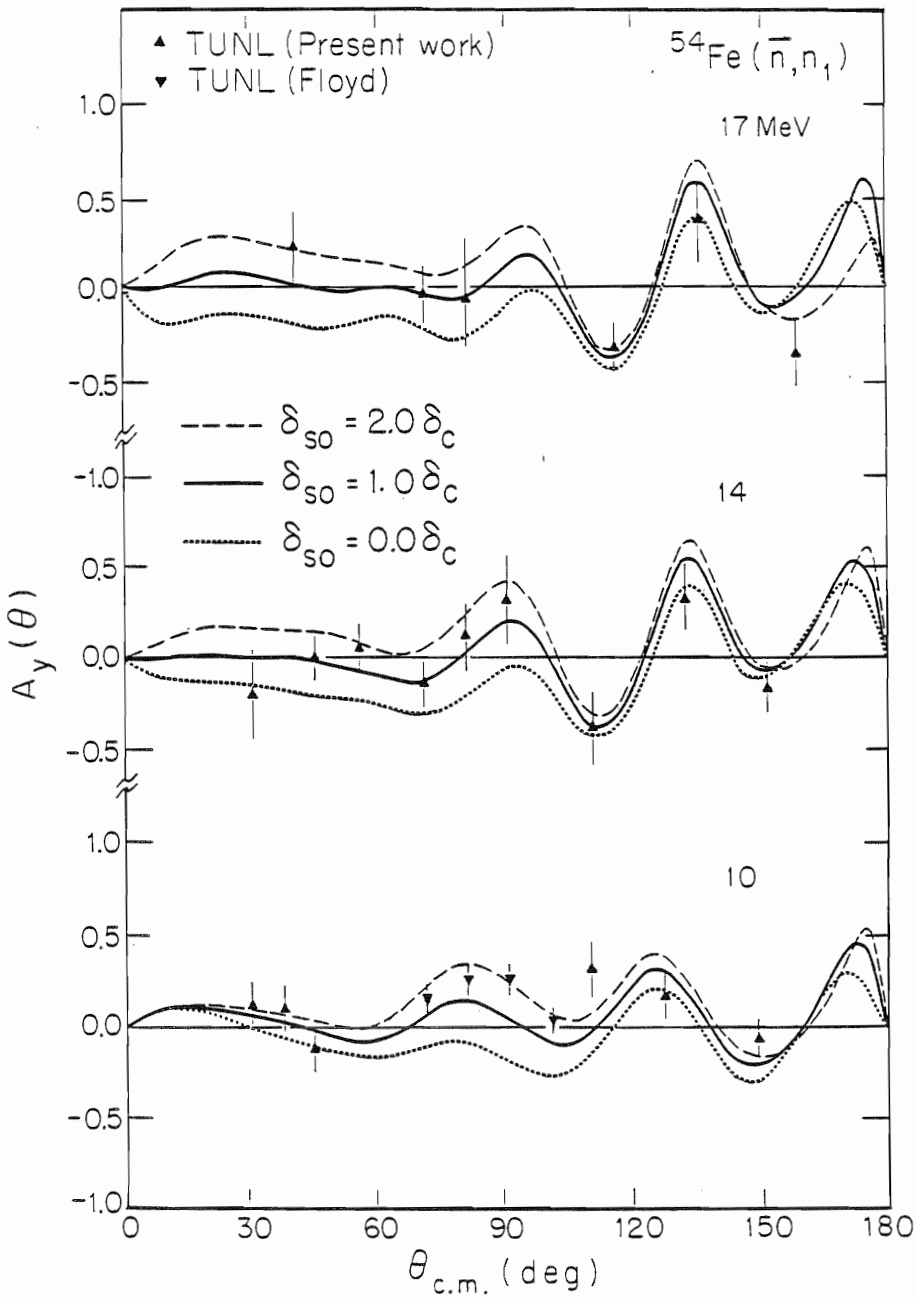

Figure 7.12. Comparison of the $A_y(\Theta)$ data for the inelastic scattering of neutrons to the first 2^+ excited state (Q=-1.41 MeV) of ^{54}Fe to CC calculations for δ_{SO} equal to 0.0, 1.0, and $2.0\delta_C$. The parameters used are those from the present work given in table 7-3. The TUNL data of Floyd are from Floyd 1983.

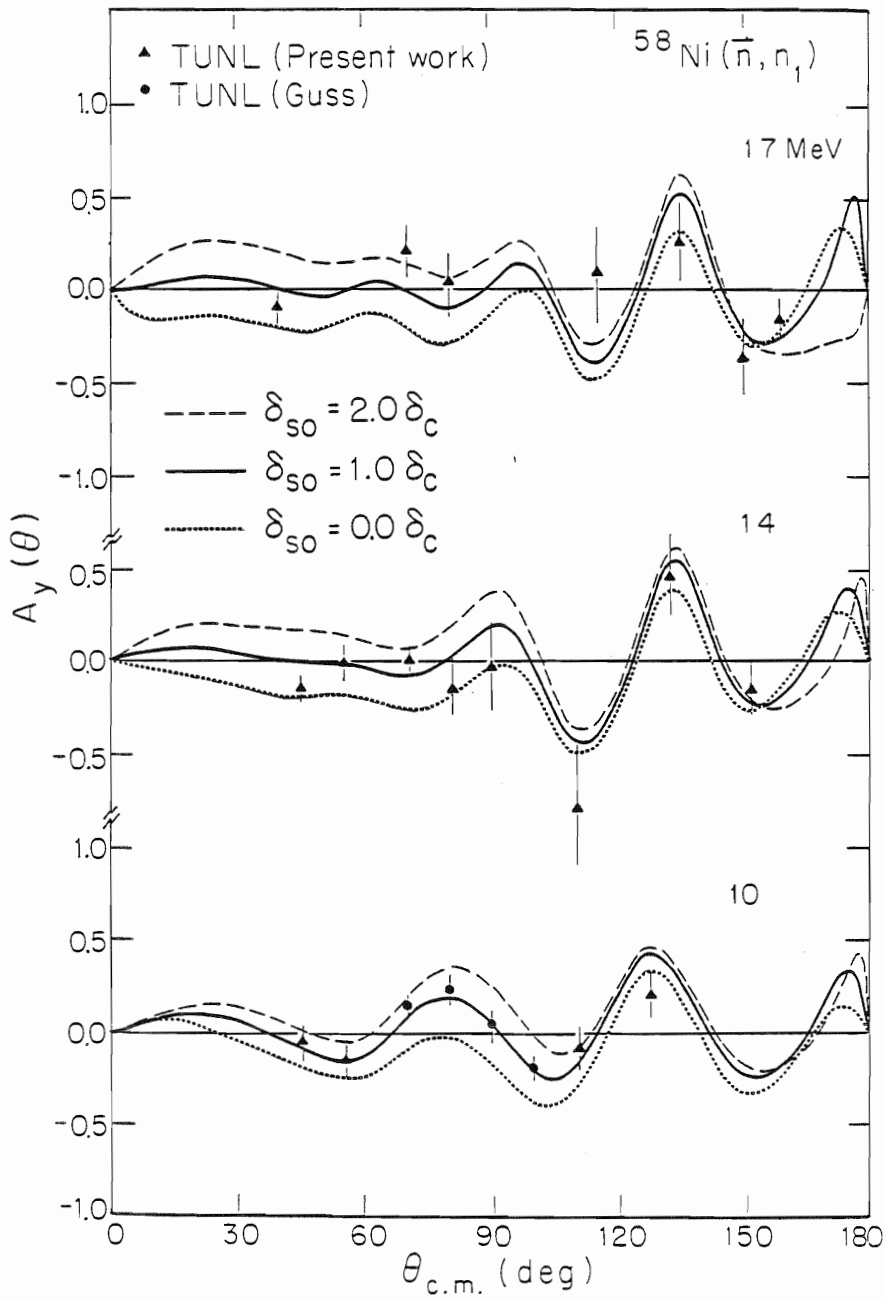

Figure 7.13. Comparison of the $A_y(\theta)$ data for the inelastic scattering of neutrons to the first 2^+ excited state (Q=-1.45 MeV) of ^{58}Ni to CC calculations for δ_{SO} equal to 0.0, 1.0, and $2.0\delta_C$. The parameters used are those from the present work given in table 7-1. The TUNL data of Guss are from Guss 1982b.

and for ^{60}Ni using the section 7.2 parameters. The additional ^{56}Fe and ^{60}Ni data support the conclusion of Guss et al. for these isotopes that δ_{SO} is about $1.0\delta_C$ at 10 MeV.

Regrettably, the new data at 14 and 17 MeV for ^{54}Fe and ^{58}Ni are not of sufficient statistical accuracy to determine accurately the energy dependence of the relationship between δ_{SO} and δ_C. High-quality data as shown in figure 7.14 for 10 MeV take 12 to 14 hours of accelerator time per point, and it was decided that we could not expend this amount of time at 14 and 17 MeV to obtain data of similar quality. Nevertheless, the data appear to suggest that δ_{SO} for ^{54}Fe decreases as the energy increases, perhaps to a value of 1.0 to 1.2 times δ_C around 14 to 17 MeV. For ^{58}Ni, δ_{SO} might drop to a value below $1.0\delta_C$. In both cases, a few more data points with error bars that are half the values of those that we report at 14 and 17 MeV would be very useful.

7.5 Calculations for ^{120}Sn

The $A_y(\theta)$ data for the elastic scattering of 17 MeV neutrons from ^{120}Sn are shown in figure 7.15 with predictions calculated from the preliminary CC parameters for ^{116,120}Sn of Guss et al. (Guss 1986). The parameters were derived using the extensive neutron data set of Guss (Guss 1982a) for neutron elastic scattering from ^{116,120}Sn and inelastic scattering to the first 2^+ and 3^- states of ^{116,120}Sn in the 10- to 17-MeV range. The Guss analysis was performed by coupling the ground state (0^+), first excited state (2^+), and second excited state (3^-) in the vibrational model. The agreement between the calculation and data is good at the forward angles, but poor at the backward angles. A similar problem was seen by Guss et al.

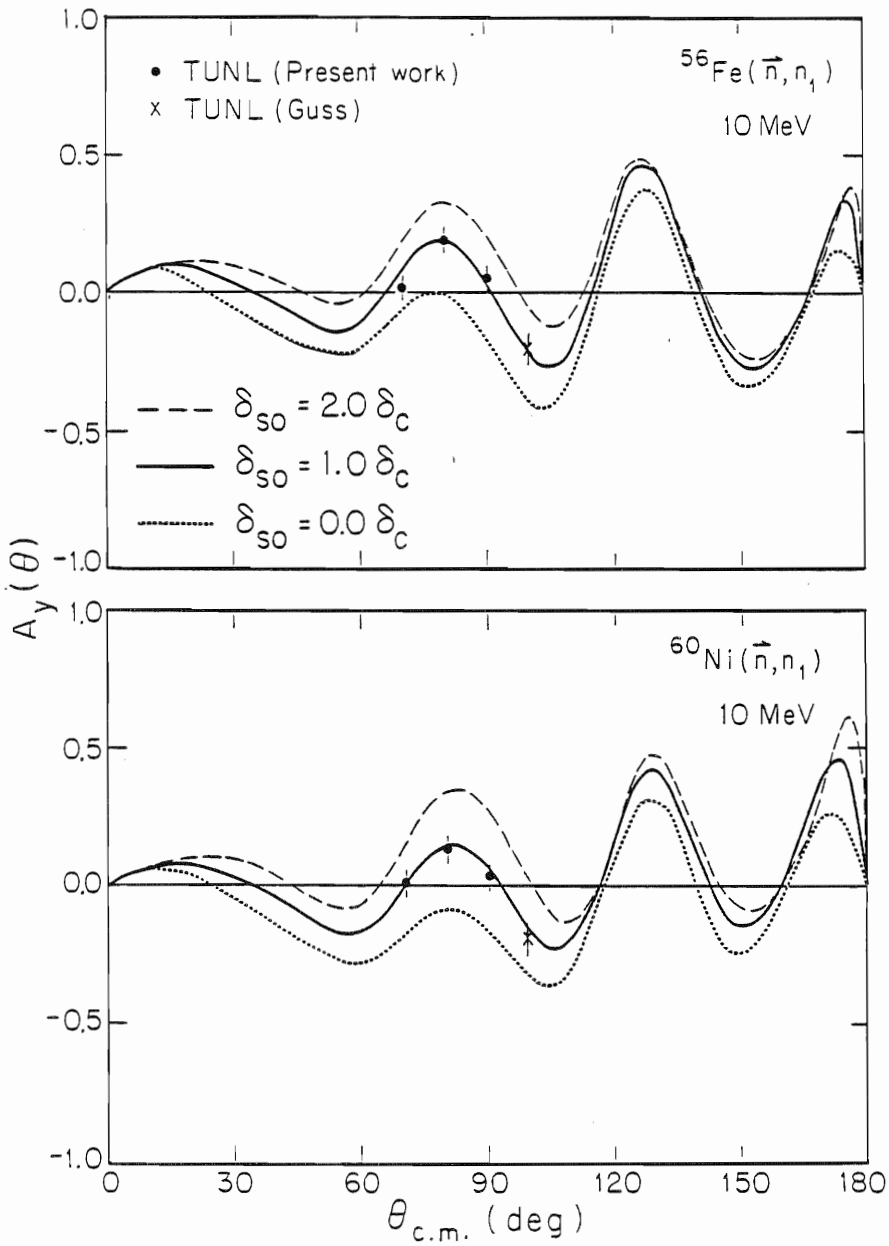

Figure 7.14. Comparison of the $A_y(\theta)$ data for the inelastic scattering of neutrons to the first 2^+ excited states of ^{56}Fe (Q=-0.85 MeV) and ^{60}Ni (Q=-1.33 MeV) to CC calculations for δ_{SO} equal to 0.0, 1.0, and $2.0\delta_C$. The parameters used are those from the present work given in tables 7-1 and 7-3. The TUNL data of Guss are from Guss 1982b.

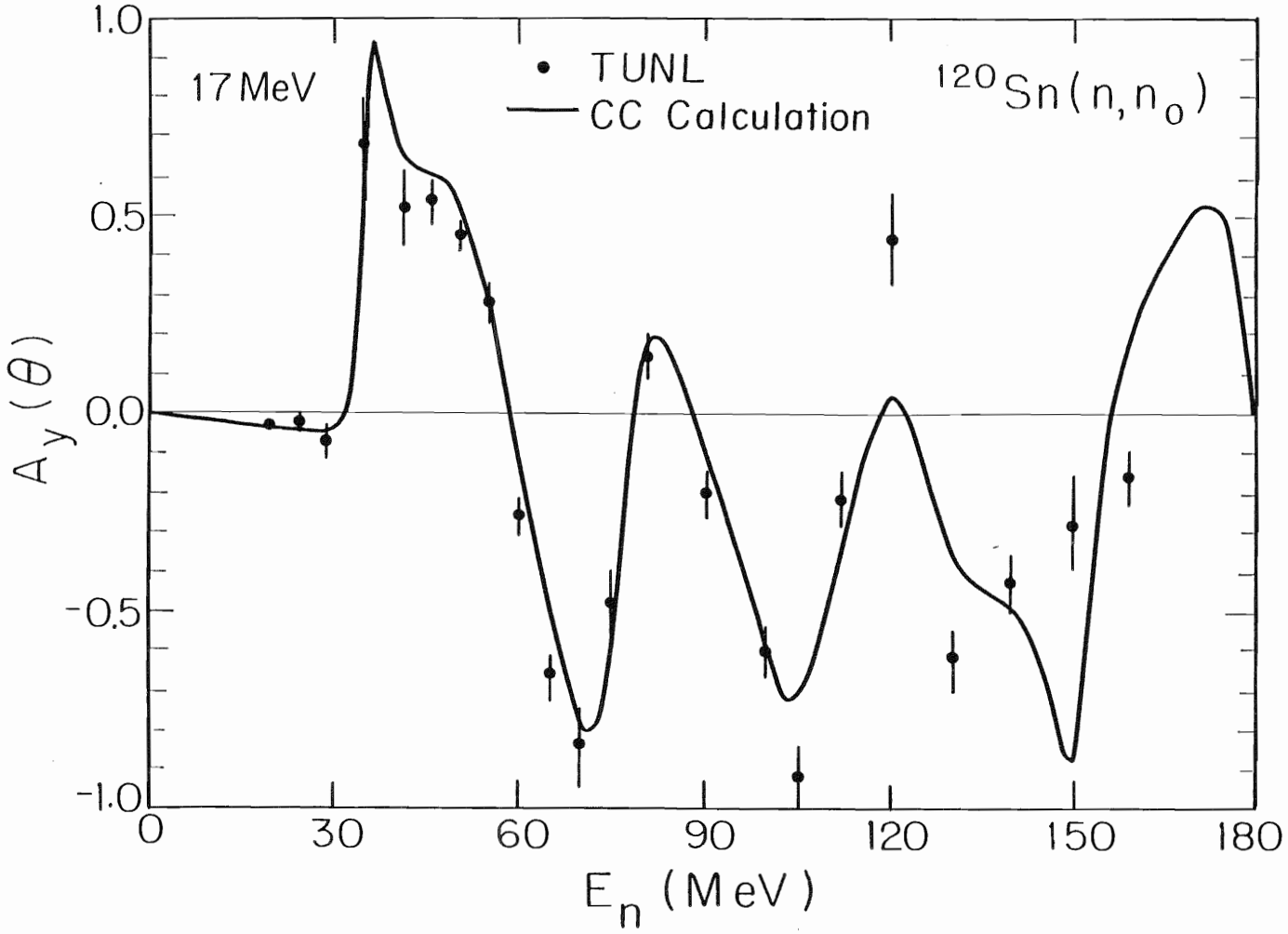

Figure 7.15. Comparison of the $A_y(\theta)$ data for the elastic scattering of neutrons from ^{120}Sn at 17 MeV to CC calculations. The CC calculations were made using the parameters of Guss et al. (Guss 1986).

for their 14 MeV $A_y(\theta)$ data and CC calculations, although at 10 MeV they obtained excellent agreement between their $A_y(\theta)$ data and CC calculations.

Perhaps it will be profitable to explore these difficulties in additional CC analyses. But, for the present time, no new CC calculations for ^{120}Sn are reported here; such work was not performed mainly because of time constraints, but there is also only a small quantity of new data that was not included in the analysis of Guss et al.

7.6 Conclusions

The CC calculations for ^{54}Fe and ^{58}Ni, have done quite well in explaining the neutron scattering observables, and useful nuclear structure information has been obtained. Nevertheless, some questions still persist and, further explorations with CC calculations are indicated. For example, the backward-angle discrepancies between the calculation and data might be resolved by using dispersion relations and coupling to giant isoscalar resonances as has been done for ^{40}Ca by Honoré et al. (Honoré 1986b). Such an analysis might also resolve the problem raised by Winters et al. of the σ_T for ^{60}Ni for incident neutron energies below 2 MeV. Additional analyses for $^{58,60}Ni$ could be greatly enhanced if more $\sigma(\theta)$ data at energies above 17 MeV were obtained, as was done for $^{54,56}Fe$ by Mellema. Unfortunately, such measurements are presently outside the energy range convenient at TUNL.

The relationship between δ_{SO} and δ_C cannot be futher explored without more high accuracy $A_y(\theta)$ data for inelastic scattering. Such data are not likely to be forthcomimg for several years. New data of this type will require several experimental improvements, such as better time-of-flight resolution and more intense polarized beams. Both of these improvements are

currently being initiated at TUNL, and high accuracy data should be easily obtained when the proposed atomic-beam polarized ion source comes online in 1989. This source will have a beam intensity of about twenty times that of the present source -- a great advantage for inelastic scattering measurements.

Further CC studies of ^{116,120}Sn similar to the work presented for ^{54,56}Fe and ^{58,60}Ni and to that of Honoré et al. for ^{40}Ca should also be performed in the future, but preferably after additional data are available at energies above 17 MeV. Good quality $A_y(\theta)$ data for neutron scattering in the 20- to 30-MeV range would be extremely useful for understanding the CC calculations for any of the nuclei studied in this thesis, or for that matter any other nuclei as well. Such measurements are possible at TUNL with the $^{3}\vec{H}(\vec{d},\vec{n})^{4}$He polarization transfer reaction, but the lower neutron flux will make such experiments time consuming. Only measurements for elastic scattering at forward angles are probably justifiable now.

APPENDIX A

DIFFERENTIAL CROSS SECTION TABULATIONS

The $\sigma(\Theta)$ data measured for this work are tabulated in this appendix. Coefficients calculated for Legendre polynomial fits to the data and various parameters associated with the fits and experiments are included in the tabulations. The fits are compared with the data in chapter 4 (figures 4.5, 4.6, and 4.7). The following equation was used to fit the data:

$$\sigma(\Theta,E) = \sum_{\ell=0} A_\ell(E) P_\ell(\cos\Theta)$$

$$= (\sigma_{int}/4\pi)\left[a_0 + \sum_{\ell=1} (2\ell+1) a_\ell(E) P_\ell(\cos\Theta)\right] . \qquad (A.1)$$

The parameters of the fits and the symbols used in the tables are:

ℓ-Value = order of the Legendre polynomial in the expansion.

A_ℓ = ℓ^{th} coefficient $A_\ell(E)$ of the Legendre polynomial expansion.

ΔA_ℓ = absolute uncertainty in the coefficient $A_\ell(E)$.

σ_{int} = integrated differential cross section over the 4π solid angle. The values quoted in the tables are obtained by integrating the fits to the cross section data over 4π.

a_ℓ = reduced expansion coefficients in ENDF/B-V form, defined to be:

$$a_0 = 1$$

$$a_\ell = A_\ell/A_0(2\ell+1).$$

Δa_ℓ = the absolute uncertainty in the reduced coefficient a_ℓ.

θ_{lab} = experimental laboratory angle.

$\sigma(\theta_{lab})$ = normalized differential cross section as measured in the laboratory, before corrections for multiple scattering, finite geometry, attenuation, and detector efficiency.

$\Delta\sigma_{lab}$ = absolute error in the uncorrected cross sections. This does not include the uncertainties due to data normalization.

$\theta_{c.m.}$ = reaction angle given in the center-of-mass.

$\sigma(\theta_{c.m.})$ = corrected differential cross section in the center-of-mass.

$\Delta\sigma_{c.m.}$ = absolute error in the corrected cross sections. This does not include uncertainties due to data normalization.

%Dev. = percentage deviation of the calculated cross section from the experimental value.

χ^2 = the χ^2 per point for the calculation at that angle.

F-Test = integral probability $P_F(F,\gamma_1,\gamma_2) = \int_F^\infty P_f(f,\gamma_1,\gamma_2)df$, in which γ_1 and γ_2 are the respective degrees of freedom.

F-Value = $F_\chi = \frac{\chi^2_{n-1}-\chi^2_n}{\chi^2_n}(N-n-1)$.

Here N is the number of data points, and n is the number of terms in the fit.

The σ_T values for ^{54}Fe and ^{58}Ni at 17 MeV are the averages of the σ_T at 16 and 18 MeV of Larson et al. (Larson 1980) for elemental Fe and Ni. The σ_T values for ^{93}Nb are from ENDF/B-V. The calculated Wick's limits and accompanying uncertainties are based on the σ_T values used. The zero degree cross sections are calculated from the fits to the data.

^{54}Fe NEUTRON ELASTIC SCATTERING CROSS SECTIONS

Neutron Energy ± Energy Spread	16.929 ± 0.150	MeV
Excitation Energy (J^{π})	0.000	MeV (0^+)
Total Cross Section	2.354 ± 0.165	barns
Integrated Cross Section	0.970 ± 0.011	barns
Calculated Wick's Limit	2814.18 ± 394.0	mb/sr
Zero Degree Cross Section	2530.52 ± 14.98	mb/sr
Normalization Uncertainty	4.54	%
Chi-square/degree-of-freedom	2.456	

ℓ-Value	A_ℓ	ΔA_ℓ	a_ℓ	Δa_ℓ	F-Value	F-Test
0	77.15	0.856	1.00000	0.00000	26.000	0.467
1	184.44	2.447	0.79687	0.01057	12.053	0.468
2	256.29	3.871	0.66438	0.01003	4.391	0.469
3	304.34	4.848	0.56353	0.00898	1.411	0.469
4	331.92	5.592	0.47802	0.00805	1.757	0.470
5	327.99	5.771	0.38648	0.00680	1.703	0.471
6	300.21	5.793	0.29932	0.00578	1.107	0.472
7	266.03	5.285	0.22987	0.00457	0.004	0.473
8	223.44	4.788	0.17036	0.00365	2.820	0.474
9	155.03	3.815	0.10576	0.00260	38.526	0.475
10	73.69	3.131	0.04548	0.00193	93.190	0.476
11	24.49	2.081	0.01380	0.00117	53.060	0.478
12	5.50	1.173	0.00285	0.00061	8.345	0.479

Uncorrected			Corrected			Calculation		
θ_{lab}	$\sigma(\theta_{lab})$	$\Delta\sigma_{lab}$	$\theta_{c.m.}$	$\sigma(\theta_{c.m.})$	$\Delta\sigma_{c.m.}$	$\sigma(\theta_{c.m.})$	%Dev.	χ^2
20.0	524.64	5.84	19.6	830.35	18.34	795.84	4.2	3.54
22.5	359.33	4.80	21.9	581.31	13.21	574.43	1.2	0.27
25.0	244.28	2.63	24.2	394.75	9.56	389.20	1.4	0.34
27.5	150.03	1.95	26.6	237.15	6.15	245.18	-3.4	1.70
30.0	87.31	1.07	29.0	129.56	3.58	139.86	-8.0	8.26
34.8	39.90	0.79	34.7	39.37	1.22	36.84	6.4	4.26
39.8	35.94	0.57	40.9	45.51	1.24	47.17	-3.6	1.80
45.3	49.17	1.06	46.2	69.34	1.91	67.37	2.8	1.05
50.3	42.56	0.64	50.7	61.71	1.45	65.06	-5.4	5.32
55.3	33.01	0.71	55.3	48.85	1.26	46.91	4.0	2.36
59.8	19.61	0.50	59.5	28.34	0.93	27.24	3.9	1.39
64.8	10.67	0.31	64.9	11.38	0.48	11.73	-3.1	0.54
70.3	11.02	0.50	71.7	13.81	0.84	14.01	-1.4	0.05
75.3	15.74	0.22	76.6	22.65	0.54	22.43	1.0	0.16
82.3	20.01	0.37	83.1	28.61	0.67	28.67	-0.2	0.01
90.3	16.28	0.28	90.7	22.97	0.56	22.93	0.2	0.00
97.3	9.72	0.25	97.4	13.00	0.45	13.02	-0.2	0.00
104.8	5.63	0.17	105.3	6.43	0.28	6.47	-0.7	0.03
112.8	5.95	0.30	113.7	7.88	0.51	7.44	5.5	0.74
119.8	6.71	0.12	120.5	9.25	0.22	9.31	-0.6	0.07
127.8	6.22	0.18	128.2	8.52	0.30	8.64	-1.4	0.16
135.3	5.15	0.14	135.5	6.74	0.23	6.55	2.7	0.64
142.3	4.68	0.13	142.7	5.93	0.22	6.09	-2.8	0.59
149.8	5.57	0.22	150.2	7.64	0.37	7.39	3.2	0.46
160.3	6.04	0.27	160.2	7.96	0.44	8.05	-1.2	0.04

^{54}Fe NEUTRON INELASTIC SCATTERING CROSS SECTIONS

Neutron Energy ± Energy Spread	16.929 ± 0.150	MeV
Excitation Energy ($J\pi$)	1.408	MeV (2^+)
Integrated Cross Section	0.032 ± 0.001	barns
Zero Degree Cross Section	4.33 ± 1.05	mb/sr
Normalization Uncertainty	4.54	%
Chi-square/degree-of-freedom	1.045	

ℓ-Value	A_ℓ	ΔA_ℓ	a_ℓ	Δa_ℓ	F-Value	F-Test
0	2.530	0.081	1.00000	0.00000	26.000	0.467
1	2.463	0.189	0.32446	0.02485	26.367	0.468
2	1.671	0.276	0.13207	0.02182	57.976	0.469
3	0.402	0.350	0.02270	0.01974	6.704	0.469
4	-0.114	0.391	-0.00500	0.01717	3.159	0.470
5	-0.759	0.412	-0.02726	0.01480	2.423	0.471
6	-1.498	0.409	-0.04555	0.01242	8.449	0.472
7	-0.804	0.400	-0.02119	0.01053	2.769	0.473
8	-0.185	0.370	-0.00431	0.00860	6.846	0.474
9	0.629	0.260	0.01309	0.00541	5.596	0.475

Uncorrected			Corrected			Calculation		
θ_{lab}	$\sigma(\theta_{lab})$	$\Delta\sigma_{lab}$	$\theta_{c.m.}$	$\sigma(\theta_{c.m.})$	$\Delta\sigma_{c.m.}$	$\sigma(\theta_{c.m.})$	%Dev.	χ^2
20.0	4.18	0.82	20.8	6.03	1.22	6.14	-1.7	0.01
22.5	4.50	0.92	23.3	6.62	1.36	6.41	3.2	0.02
25.0	6.27	0.71	25.7	9.23	1.05	6.63	28.1	6.13
27.5	4.18	0.50	28.2	6.18	0.74	6.78	-9.8	0.67
30.0	4.30	0.27	30.7	6.39	0.40	6.84	-7.1	1.32
34.8	4.59	0.27	35.3	6.81	0.41	6.67	2.0	0.11
39.8	4.72	0.48	40.3	6.88	0.73	6.08	11.6	1.18
45.3	3.14	0.40	45.7	4.34	0.63	5.05	-16.2	1.23
50.3	3.01	0.26	50.6	4.45	0.40	4.00	10.0	1.26
55.3	2.12	0.63	55.7	2.89	0.97	3.07	-6.2	0.03
59.8	1.74	0.21	60.3	2.22	0.33	2.49	-12.5	0.69
64.8	1.79	0.15	65.6	2.22	0.24	2.23	-0.3	0.00
70.3	1.91	0.33	71.2	2.51	0.52	2.27	9.4	0.20
75.3	1.73	0.21	76.2	2.25	0.35	2.40	-6.8	0.19
82.3	1.87	0.14	83.0	2.63	0.23	2.40	8.7	1.02
90.3	1.33	0.13	90.8	1.89	0.20	2.02	-6.4	0.36
97.3	1.18	0.09	97.9	1.49	0.15	1.54	-3.2	0.10
104.8	1.02	0.08	105.6	1.27	0.14	1.24	2.5	0.06
112.8	1.10	0.24	113.5	1.33	0.40	1.22	8.1	0.07
119.8	1.05	0.12	120.3	1.33	0.20	1.24	6.5	0.18
127.8	0.91	0.13	128.2	1.06	0.22	1.17	-10.6	0.25
135.3	0.84	0.10	135.9	1.03	0.15	1.13	-9.9	0.44
142.3	1.05	0.08	142.9	1.35	0.13	1.29	4.1	0.18
149.8	1.24	0.08	150.1	1.65	0.13	1.55	6.0	0.56
160.3	1.03	0.08	160.0	1.43	0.13	1.55	-8.4	0.90

^{58}Ni NEUTRON ELASTIC SCATTERING CROSS SECTIONS

Neutron Energy ± Energy Spread	16.934 ± 0.150 MeV
Excitation Energy (J^{π})	0.000 MeV (0^+)
Total Cross Section	2.493 ± 0.175 barns
Integrated Cross Section	1.077 ± 0.017 barns
Calculated Wick's Limit	3161.27 ± 442.6 mb/sr
Zero Degree Cross Section	2929.71 ± 24.67 mb/sr
Normalization Uncertainty	4.44 %
Chi-square/degree-of-freedom	0.628

ℓ-Value	A_ℓ	ΔA_ℓ	a_ℓ	Δa_ℓ	F-Value	F-Test
0	85.68	1.362	1.00000	0.00000	31.000	0.465
1	208.01	3.992	0.80925	0.01553	15.862	0.466
2	293.33	6.216	0.68471	0.01451	3.834	0.466
3	353.27	8.025	0.58902	0.01338	1.960	0.466
4	386.76	9.064	0.50155	0.01175	4.453	0.466
5	379.76	9.629	0.40294	0.01022	3.368	0.467
6	343.71	9.403	0.30858	0.00844	0.533	0.468
7	296.05	8.936	0.23036	0.00695	2.821	0.469
8	252.23	7.743	0.17317	0.00532	0.067	0.469
9	183.57	6.524	0.11277	0.00401	34.302	0.470
10	95.44	4.862	0.05305	0.00270	104.385	0.471
11	36.85	3.560	0.01870	0.00181	80.615	0.472
12	12.43	2.098	0.00580	0.00098	53.004	0.473
13	2.61	1.166	0.00113	0.00050	6.764	0.474

Uncorrected			Corrected			Calculation		
θ_{lab}	$\sigma(\theta_{lab})$	$\Delta\sigma_{lab}$	$\theta_{c.m.}$	$\sigma(\theta_{c.m.})$	$\Delta\sigma_{c.m.}$	$\sigma(\theta_{c.m.})$	%Dev.	χ^2
20.0	580.27	13.32	19.9	839.57	20.70	860.00	-2.4	0.97
25.0	279.07	5.58	24.7	415.01	9.64	403.05	2.9	1.54
30.0	99.24	2.26	29.5	140.24	4.10	142.96	-1.9	0.44
35.0	42.62	1.16	35.1	43.57	1.70	43.48	0.2	0.00
40.0	40.82	1.00	40.9	50.75	1.64	49.48	2.5	0.60
44.4	44.91	0.90	45.2	60.39	1.43	61.90	-2.5	1.11
50.0	40.99	0.82	50.5	56.94	1.28	57.00	-0.1	0.00
52.5	34.51	0.69	52.8	48.52	1.09	48.24	0.6	0.07
54.4	28.79	0.58	54.6	40.52	0.93	40.24	0.7	0.09
59.4	14.98	0.38	59.4	19.90	0.63	19.85	0.2	0.01
64.4	9.04	0.26	65.1	9.35	0.37	9.44	-0.9	0.05
69.4	11.78	0.26	70.8	15.43	0.42	15.49	-0.4	0.02
74.4	18.62	0.39	75.6	25.94	0.61	25.54	1.5	0.42
79.4	22.85	0.46	80.3	32.07	0.70	32.07	0.0	0.00
85.6	21.80	0.52	86.3	30.37	0.80	30.53	-0.5	0.04
89.4	17.87	0.35	89.9	24.67	0.56	25.06	-1.6	0.51
94.4	12.04	0.34	94.7	16.34	0.55	16.07	1.7	0.24
100.6	6.28	0.17	101.0	7.70	0.28	7.59	1.4	0.15
105.6	5.01	0.29	106.4	5.80	0.43	5.95	-2.6	0.13
110.6	5.92	0.23	111.6	7.76	0.36	8.11	-4.5	0.95
114.4	7.63	0.23	115.3	10.41	0.36	10.09	3.0	0.78
120.6	8.47	0.31	121.2	11.63	0.48	11.48	1.3	0.10
125.6	7.58	0.27	126.0	10.31	0.41	10.41	-1.0	0.06
130.6	6.30	0.25	130.9	8.31	0.38	8.22	1.0	0.05
135.0	4.90	0.17	135.3	6.23	0.25	6.40	-2.8	0.46
140.6	4.41	0.21	140.9	5.56	0.32	5.32	4.4	0.60
145.6	4.49	0.24	145.9	5.69	0.36	5.56	2.4	0.14
150.6	4.77	0.22	150.9	6.16	0.33	6.40	-3.9	0.51
154.4	5.44	0.18	154.6	7.11	0.28	7.13	-0.3	0.01
160.6	6.30	0.24	160.6	8.28	0.35	8.14	1.7	0.16

^{58}Ni NEUTRON INELASTIC SCATTERING CROSS SECTIONS

Neutron Energy ± Energy Spread	16.934 ± 0.150 MeV
Excitation Energy (J^{π})	1.454 MeV (2^+)
Integrated Cross Section	0.037 ± 0.002 barns
Zero Degree Cross Section	3.48 ± 1.83 mb/sr
Normalization Uncertainty	4.44 %
Chi-square/degree-of-freedom	0.685

ℓ-Value	A_ℓ	ΔA_ℓ	a_ℓ	Δa_ℓ	F-Value	F-Test
0	2.929	0.120	1.00000	0.00000	31.000	0.465
1	3.663	0.322	0.41689	0.03669	41.416	0.466
2	2.650	0.482	0.18098	0.03294	65.351	0.466
3	0.324	0.590	0.01581	0.02877	3.920	0.466
4	-0.366	0.653	-0.01389	0.02476	16.344	0.466
5	-1.561	0.669	-0.04846	0.02078	7.079	0.467
6	-2.463	0.656	-0.06469	0.01722	1.490	0.468
7	-1.764	0.628	-0.04015	0.01430	10.747	0.469
8	-0.909	0.574	-0.01827	0.01152	13.628	0.469
9	0.305	0.549	0.00549	0.00987	0.010	0.470
10	0.063	0.437	0.00103	0.00710	1.539	0.471
11	0.608	0.359	0.00903	0.00533	4.189	0.472

Uncorrected			Corrected			Calculation		
θ_{lab}	$\sigma(\theta_{lab})$	$\Delta\sigma_{lab}$	$\theta_{c.m.}$	$\sigma(\theta_{c.m.})$	$\Delta\sigma_{c.m.}$	$\sigma(\theta_{c.m.})$	%Dev.	χ^2
20.0	0.00	0.00	20.7	9.91	6.46	8.27	16.5	0.06
25.0	6.27	1.03	25.6	8.89	1.49	9.63	-8.3	0.25
30.0	7.78	0.77	30.6	11.12	1.14	10.21	8.2	0.64
35.0	6.68	0.45	35.6	9.61	0.66	9.75	-1.5	0.04
40.0	5.49	0.51	40.6	7.82	0.73	8.38	-7.1	0.59
44.4	5.14	0.37	44.9	7.02	0.54	6.81	3.0	0.15
50.0	3.81	0.31	50.4	5.38	0.44	4.88	9.4	1.31
52.5	2.71	0.36	53.0	3.73	0.52	4.19	-12.3	0.78
54.4	2.81	0.30	54.9	3.75	0.43	3.76	-0.2	0.00
59.4	2.27	0.20	60.1	2.91	0.28	3.07	-5.3	0.29
64.4	2.08	0.21	65.2	2.67	0.31	2.84	-6.5	0.32
69.4	2.26	0.14	70.2	3.08	0.21	2.79	9.6	1.96
74.4	1.97	0.18	75.1	2.61	0.27	2.69	-3.2	0.10
79.4	1.74	0.18	80.2	2.19	0.27	2.49	-13.7	1.28
85.6	1.54	0.24	86.4	2.05	0.35	2.17	-6.0	0.12
89.4	1.48	0.15	90.2	2.12	0.22	1.96	7.6	0.53
94.4	1.24	0.18	95.1	1.74	0.27	1.68	3.9	0.06
100.6	1.01	0.11	101.1	1.34	0.16	1.30	2.9	0.06
105.6	0.64	0.13	106.2	0.83	0.19	1.01	-21.6	0.87
110.6	0.65	0.12	111.4	0.80	0.17	0.82	-3.0	0.02
114.4	0.73	0.15	115.2	0.91	0.23	0.79	13.2	0.27
120.6	0.73	0.12	121.3	0.97	0.18	0.87	9.5	0.26
125.6	0.79	0.11	126.2	1.01	0.17	0.95	5.7	0.12
130.6	0.65	0.08	131.2	0.80	0.12	0.96	-20.0	1.81
135.0	0.87	0.09	135.6	1.07	0.14	0.92	13.8	1.17
140.6	0.92	0.40	141.1	1.13	0.61	0.94	16.8	0.09
145.6	0.82	0.13	146.0	1.07	0.19	1.14	-6.5	0.13
150.6	1.14	0.14	151.0	1.50	0.22	1.49	0.4	0.00
154.4	1.43	0.26	154.7	1.91	0.40	1.75	8.6	0.17
160.6	1.21	0.33	160.5	1.66	0.50	1.89	-13.7	0.20

^{93}Nb NEUTRON ELASTIC SCATTERING CROSS SECTIONS

Neutron Energy ± Energy Spread	7.952 ± 0.095 MeV
Excitation Energy (J^{π})	0.000 MeV ($9/2^{+}$)
Total Cross Section	4.250 ± 0.213 barns
Integrated Cross Section	2.208 ± 0.043 barns
Calculated Wick's Limit	4342.28 ± 434.2 mb/sr
Zero Degree Cross Section	4185.21 ± 51.85 mb/sr
Normalization Uncertainty	3.39 %
Chi-square/degree-of-freedom	0.625

ℓ-Value	A_ℓ	ΔA_ℓ	a_ℓ	Δa_ℓ	F-Value	F-Test
0	175.67	3.452	1.00000	0.00000	28.000	0.466
1	416.68	10.016	0.79064	0.01901	0.258	0.466
2	566.57	15.370	0.64504	0.01750	14.158	0.467
3	629.16	19.373	0.51164	0.01575	3.665	0.468
4	656.15	21.167	0.41502	0.01339	5.778	0.469
5	639.50	21.528	0.33094	0.01114	1.026	0.469
6	517.99	19.810	0.22682	0.00867	24.381	0.470
7	315.93	17.640	0.11990	0.00669	16.826	0.471
8	167.50	14.058	0.05609	0.00471	86.585	0.472
9	69.27	10.427	0.02075	0.00312	164.857	0.473
10	21.15	5.889	0.00573	0.00160	1.197	0.474
11	9.63	2.849	0.00238	0.00071	15.719	0.475

Uncorrected			Corrected			Calculation		
θ_{lab}	$\sigma(\theta_{lab})$	$\Delta\sigma_{lab}$	$\theta_{c.m.}$	$\sigma(\theta_{c.m.})$	$\Delta\sigma_{c.m.}$	$\sigma(\theta_{c.m.})$	%Dev.	χ^2
25.0	625.91	12.52	23.6	1328.24	37.64	1321.36	0.5	0.03
30.0	338.71	6.77	27.9	765.12	22.87	780.00	-1.9	0.42
35.0	167.40	3.35	32.2	398.12	14.90	398.42	-0.1	0.00
40.0	73.56	1.47	37.0	146.77	7.87	147.18	-0.3	0.00
44.3	42.84	0.86	43.1	34.07	2.67	33.09	2.9	0.13
50.8	40.06	0.80	52.6	65.91	2.66	68.74	-4.3	1.13
54.3	51.49	1.03	55.7	92.52	3.04	90.04	2.7	0.67
60.8	62.02	1.24	61.2	111.71	3.13	112.11	-0.4	0.02
64.3	64.29	1.29	64.2	115.48	3.07	113.80	1.5	0.30
70.8	54.08	1.08	70.1	97.17	2.64	99.20	-2.1	0.59
74.3	48.75	0.98	73.3	87.50	2.37	84.93	2.9	1.18
80.8	29.94	0.60	79.3	53.22	1.49	55.23	-3.8	1.83
84.3	24.22	0.48	82.6	42.06	1.38	40.59	3.5	1.14
90.8	12.55	0.25	88.9	19.60	0.68	19.75	-0.8	0.05
94.3	9.23	0.20	92.6	12.39	0.53	12.34	0.4	0.01
100.0	6.68	0.13	99.7	6.61	0.27	6.58	0.3	0.01
105.8	6.78	0.15	106.9	8.58	0.48	8.79	-2.4	0.19
109.3	8.40	0.19	110.6	12.32	0.57	12.14	1.5	0.11
115.8	12.02	0.30	116.8	19.74	0.78	19.47	1.4	0.12
119.3	13.73	0.28	120.0	22.89	0.68	23.16	-1.2	0.15
125.8	16.55	0.35	125.9	27.98	0.82	27.57	1.4	0.24
129.3	16.19	0.37	129.0	27.36	0.86	27.84	-1.8	0.32
135.8	14.87	0.36	135.0	24.79	0.82	24.17	2.5	0.57
139.3	12.39	0.28	138.3	20.08	0.68	20.64	-2.8	0.67
145.8	10.51	0.31	145.1	14.90	0.69	14.40	3.4	0.53
149.3	9.52	0.22	149.0	13.07	0.52	13.22	-1.2	0.08
155.8	10.63	0.22	156.0	16.36	0.57	16.37	-0.1	0.00
162.0	12.89	0.26	162.0	21.23	0.64	21.21	0.1	0.00

^{93}Nb NEUTRON ELASTIC SCATTERING CROSS SECTIONS

Neutron Energy ± Energy Spread	9.941 ± 0.071 MeV
Excitation Energy (J^{π})	0.000 MeV ($9/2^{+}$)
Total Cross Section	4.280 ± 0.214 barns
Integrated Cross Section	2.456 ± 0.035 barns
Calculated Wick's Limit	5505.30 ± 550.5 mb/sr
Zero Degree Cross Section	5408.95 ± 43.50 mb/sr
Normalization Uncertainty	3.74 %
Chi-square/degree-of-freedom	0.765

ℓ-Value	A_ℓ	ΔA_ℓ	a_ℓ	Δa_ℓ	F-Value	F-Test
0	195.42	2.779	1.00000	0.00000	30.000	0.466
1	497.20	8.011	0.84810	0.01366	0.869	0.466
2	703.67	12.252	0.72018	0.01254	5.383	0.466
3	797.04	15.508	0.58267	0.01134	5.211	0.466
4	831.29	17.256	0.47266	0.00981	0.134	0.467
5	787.02	18.055	0.36613	0.00840	2.408	0.468
6	677.37	17.276	0.26664	0.00680	13.079	0.469
7	466.68	15.680	0.15921	0.00535	11.619	0.469
8	274.83	12.410	0.08273	0.00374	64.795	0.470
9	124.75	8.873	0.03360	0.00239	107.685	0.471
10	41.37	4.859	0.01008	0.00118	26.382	0.472
11	12.30	2.220	0.00274	0.00049	36.717	0.473

Uncorrected			Corrected			Calculation		
θ_{lab}	$\sigma(\theta_{lab})$	$\Delta\sigma_{lab}$	$\theta_{c.m.}$	$\sigma(\theta_{c.m.})$	$\Delta\sigma_{c.m.}$	$\sigma(\theta_{c.m.})$	%Dev.	χ^2
20.0	1118.47	22.37	18.9	2422.71	63.57	2486.58	-2.6	1.01
25.0	719.25	14.39	23.2	1615.60	41.52	1609.58	0.4	0.02
30.0	388.39	7.77	27.5	947.57	29.98	911.44	3.8	1.45
32.0	275.42	5.51	29.2	675.97	27.23	695.48	-2.9	0.51
35.0	177.78	3.56	31.8	439.82	23.28	432.90	1.6	0.09
40.0	72.54	1.45	36.9	128.56	9.33	130.69	-1.7	0.05
45.0	41.24	0.82	45.3	29.55	2.64	29.44	0.4	0.00
49.0	41.94	0.84	50.8	65.97	5.68	66.49	-0.8	0.01
54.0	50.25	2.02	55.0	91.07	7.19	91.78	-0.8	0.01
60.0	53.45	1.07	59.9	99.40	3.41	100.27	-0.9	0.07
65.0	48.90	0.98	64.2	92.38	2.77	90.26	2.3	0.58
70.0	37.49	0.75	68.8	69.91	2.17	70.19	-0.4	0.02
74.0	28.39	0.57	72.5	52.19	1.80	52.33	-0.3	0.01
79.0	18.13	0.36	77.2	31.59	1.27	32.64	-3.3	0.69
84.0	12.25	0.24	82.2	19.14	1.06	18.37	4.0	0.53
89.0	8.09	0.25	87.7	10.43	0.72	10.21	2.1	0.09
96.0	6.11	0.12	95.9	7.45	0.29	7.51	-0.8	0.04
100.0	6.05	0.12	100.4	8.16	0.32	8.35	-2.3	0.35
104.0	6.94	0.14	104.5	10.14	0.39	9.69	4.4	1.31
111.0	7.99	0.22	111.4	12.64	0.52	12.57	0.6	0.02
116.0	8.69	0.17	116.3	14.25	0.43	14.69	-3.1	1.06
121.0	9.68	0.24	121.0	16.26	0.60	16.22	0.2	0.00
126.0	9.94	0.19	125.6	16.92	0.53	16.39	3.1	0.97
131.0	9.04	0.23	130.1	15.37	0.61	14.75	4.1	1.03
134.0	7.44	0.15	132.8	12.47	0.40	12.95	-3.8	1.41
141.0	5.45	0.18	139.7	7.43	0.45	7.44	-0.1	0.00
146.0	5.08	0.11	146.0	5.53	0.28	5.38	2.7	0.28
151.0	5.83	0.19	152.1	8.70	0.49	9.43	-8.3	2.16
154.0	8.08	0.16	155.1	13.85	0.43	13.48	2.7	0.72
161.0	12.88	0.26	161.4	23.62	0.82	23.76	-0.6	0.03

^{93}Nb NEUTRON ELASTIC SCATTERING CROSS SECTIONS

Neutron Energy ± Energy Spread	11.928 ± 0.057 MeV
Excitation Energy (J^{π})	0.000 MeV ($9/2^{+}$)
Total Cross Section	4.165 ± 0.208 barns
Integrated Cross Section	2.285 ± 0.039 barns
Calculated Wick's Limit	6255.49 ± 625.5 mb/sr
Zero Degree Cross Section	5915.21 ± 48.62 mb/sr
Normalization Uncertainty	3.27 %
Chi-square/degree-of-freedom	0.425

ℓ-Value	A_ℓ	ΔA_ℓ	a_ℓ	Δa_ℓ	F-Value	F-Test
0	181.85	3.138	1.00000	0.00000	29.000	0.466
1	475.55	9.029	0.87167	0.01655	4.893	0.466
2	697.79	14.124	0.76742	0.01553	3.358	0.466
3	820.01	17.656	0.64417	0.01387	2.046	0.467
4	870.52	19.769	0.53189	0.01208	2.335	0.468
5	830.06	19.824	0.41495	0.00991	2.826	0.469
6	737.28	18.780	0.31187	0.00794	8.433	0.469
7	555.18	16.182	0.20353	0.00593	7.131	0.470
8	372.24	13.555	0.12041	0.00438	24.798	0.471
9	214.80	10.138	0.06217	0.00293	22.365	0.472
10	106.48	7.384	0.02788	0.00193	20.782	0.473
11	44.45	4.185	0.01063	0.00100	156.126	0.474
12	9.02	2.087	0.00198	0.00046	34.138	0.475

Uncorrected			Corrected			Calculation		
θ_{lab}	$\sigma(\theta_{lab})$	$\Delta\sigma_{lab}$	$\theta_{c.m.}$	$\sigma(\theta_{c.m.})$	$\Delta\sigma_{c.m.}$	$\sigma(\theta_{c.m.})$	%Dev.	χ^2
20.0	1102.06	22.04	18.8	2440.05	70.20	2441.97	-0.1	0.00
25.0	647.94	12.96	23.0	1487.46	49.09	1495.87	-0.6	0.03
30.0	321.85	6.44	27.3	807.81	27.27	789.01	2.3	0.48
35.0	123.00	2.46	31.5	325.12	10.50	340.48	-4.7	2.14
40.0	49.78	1.00	36.8	79.27	3.91	75.73	4.5	0.82
45.0	28.32	0.57	46.0	25.22	1.57	25.69	-1.9	0.09
49.0	28.57	0.57	50.8	47.82	2.07	48.55	-1.5	0.12
54.0	33.80	0.75	54.7	61.94	2.79	59.17	4.5	0.99
61.0	31.20	0.62	60.7	57.98	2.58	57.84	0.2	0.00
64.0	28.05	0.58	63.4	52.08	2.41	52.87	-1.5	0.11
71.0	20.74	0.41	69.9	37.95	1.56	37.48	1.2	0.09
74.0	16.48	0.33	72.7	29.92	1.19	30.58	-2.2	0.31
81.0	9.74	0.19	79.4	16.09	0.57	15.90	1.1	0.10
84.0	7.51	0.15	82.6	10.89	0.42	10.91	-0.2	0.00
91.0	5.41	0.11	91.2	6.66	0.37	6.81	-2.3	0.17
94.0	5.87	0.12	94.7	8.53	0.46	8.22	3.6	0.45
101.0	6.78	0.14	101.5	11.58	0.52	11.83	-2.2	0.23
104.0	7.46	0.15	104.3	12.84	0.54	12.74	0.8	0.03
111.0	7.80	0.16	111.1	13.21	0.58	13.34	-1.0	0.05
114.0	8.09	0.16	114.0	13.59	0.55	13.30	2.1	0.28
121.0	7.55	0.15	120.8	12.89	0.52	13.15	-2.0	0.25
124.0	7.53	0.15	123.7	12.93	0.50	12.85	0.6	0.03
131.0	6.18	0.12	130.0	10.61	0.45	10.66	-0.4	0.01
134.0	5.46	0.13	132.7	9.15	0.37	9.05	1.2	0.08
141.0	3.74	0.07	140.0	4.66	0.22	4.71	-1.0	0.04
144.0	3.66	0.08	143.9	3.93	0.22	3.91	0.7	0.02
151.0	5.45	0.11	152.4	9.11	0.39	9.12	-0.1	0.00
154.0	7.02	0.14	155.3	12.72	0.50	12.72	0.0	0.00
161.0	11.73	0.23	161.5	21.56	0.76	21.55	0.0	0.00

^{93}Nb NEUTRON ELASTIC SCATTERING CROSS SECTIONS

Neutron Energy ± Energy Spread	13.915 ± 0.047 MeV
Excitation Energy (J^{π})	0.000 MeV ($9/2^{+}$)
Total Cross Section	3.980 ± 0.199 barns
Integrated Cross Section	2.262 ± 0.114 barns
Calculated Wick's Limit	6663.66 ± 666.4 mb/sr
Zero Degree Cross Section	7511.42 ± 163.1 mb/sr
Normalization Uncertainty	3.24 %
Chi-square/degree-of-freedom	1.256

ℓ-Value	A_ℓ	ΔA_ℓ	a_ℓ	Δa_ℓ	F-Value	F-Test
0	180.01	9.056	1.00000	0.00000	29.000	0.466
1	481.61	26.581	0.89185	0.04922	6.018	0.466
2	728.09	41.410	0.80896	0.04601	2.805	0.466
3	892.26	53.490	0.70812	0.04245	0.172	0.467
4	978.42	60.388	0.60395	0.03728	0.000	0.468
5	969.46	64.075	0.48961	0.03236	6.390	0.469
6	897.67	62.080	0.38361	0.02653	3.969	0.469
7	749.74	58.237	0.27767	0.02157	11.212	0.470
8	576.73	49.879	0.18847	0.01630	20.362	0.471
9	417.41	42.057	0.12205	0.01230	1.552	0.472
10	283.34	31.661	0.07496	0.00838	14.251	0.473
11	177.31	24.113	0.04283	0.00582	46.417	0.474
12	93.83	15.517	0.02085	0.00345	8.229	0.475
13	52.37	10.612	0.01078	0.00218	2.923	0.476
14	23.72	5.131	0.00454	0.00098	7.262	0.478
15	9.44	2.972	0.00169	0.00053	8.797	0.479

Uncorrected			Corrected			Calculation		
θ_{lab}	$\sigma(\theta_{lab})$	$\Delta\sigma_{lab}$	$\theta_{c.m.}$	$\sigma(\theta_{c.m.})$	$\Delta\sigma_{c.m.}$	$\sigma(\theta_{c.m.})$	%Dev.	χ^2
30.0	247.96	4.96	26.9	632.89	31.33	616.74	2.6	0.27
33.0	133.08	2.66	29.5	346.54	18.41	345.44	0.3	0.00
37.0	54.98	1.32	33.2	119.75	8.51	128.07	-6.9	0.95
40.0	32.06	0.64	36.9	41.32	4.21	38.31	7.3	0.51
43.0	18.84	0.42	42.2	10.44	1.31	10.54	-0.9	0.01
47.0	15.95	0.35	48.5	19.75	1.24	20.54	-4.0	0.41
49.5	17.82	0.39	50.9	27.46	1.70	25.31	7.8	1.59
55.5	18.85	0.38	56.1	31.22	1.66	31.41	-0.6	0.01
59.5	18.47	0.49	59.6	30.93	1.63	32.21	-4.1	0.61
65.5	17.86	0.45	65.3	30.05	1.19	29.64	1.4	0.12
69.5	16.18	0.46	69.1	27.38	1.19	26.78	2.2	0.26
75.5	11.87	0.37	74.6	20.47	1.02	21.39	-4.5	0.81
79.5	10.08	0.28	78.3	17.22	0.82	16.83	2.3	0.23
85.5	6.49	0.19	84.5	8.83	0.47	8.96	-1.5	0.08
89.5	5.89	0.17	89.7	6.69	0.38	6.49	3.1	0.29
95.5	6.32	0.19	96.7	10.14	0.53	10.85	-7.0	1.77
99.5	8.45	0.25	100.3	14.55	0.73	13.89	4.5	0.82
105.5	9.78	0.26	105.6	16.87	0.76	15.53	7.9	3.08
109.5	8.07	0.23	109.2	13.57	0.62	14.61	-7.7	2.87
115.5	7.66	0.18	115.0	12.07	0.47	11.84	1.9	0.23
119.5	6.69	0.20	119.1	10.18	0.51	10.32	-1.4	0.08
125.5	6.37	0.24	125.2	9.53	0.65	9.04	5.1	0.56
129.5	5.47	0.16	129.2	8.22	0.46	8.46	-3.0	0.28
135.5	5.08	0.16	135.0	7.61	0.43	7.58	0.4	0.01
139.5	4.74	0.14	139.0	6.90	0.53	6.85	0.7	0.01
145.5	4.57	0.14	145.4	5.96	0.47	5.93	0.4	0.00
150.0	5.26	0.13	150.6	7.19	0.56	7.30	-1.5	0.04
155.5	7.59	0.24	156.4	13.02	0.75	12.85	1.3	0.05
159.5	9.58	0.30	160.0	17.30	0.85	17.39	-0.5	0.01

^{93}Nb NEUTRON ELASTIC SCATTERING CROSS SECTIONS

Neutron Energy ± Energy Spread	16.910 ± 0.150 MeV
Excitation Energy (J^{π})	0.000 MeV ($9/2^{+}$)
Total Cross Section	3.744 ± 0.187 barns
Integrated Cross Section	1.949 ± 0.072 barns
Calculated Wick's Limit	7166.04 ± 716.6 mb/sr
Zero Degree Cross Section	6711.13 ± 111.2 mb/sr
Normalization Uncertainty	4.19 %
Chi-square/degree-of-freedom	0.334

ℓ-Value	A_ℓ	ΔA_ℓ	a_ℓ	Δa_ℓ	F-Value	F-Test
0	155.09	5.755	1.00000	0.00000	32.000	0.464
1	405.79	17.018	0.87219	0.03658	7.862	0.465
2	610.49	26.490	0.78728	0.03416	0.084	0.466
3	763.78	34.719	0.70355	0.03198	2.578	0.466
4	855.27	39.369	0.61275	0.02821	0.300	0.466
5	860.65	42.660	0.50450	0.02501	0.152	0.466
6	802.78	41.759	0.39818	0.02071	4.661	0.467
7	686.30	40.444	0.29502	0.01739	11.860	0.468
8	539.83	35.239	0.20475	0.01337	5.637	0.469
9	405.17	30.986	0.13750	0.01052	1.960	0.469
10	296.30	23.782	0.09098	0.00730	2.994	0.470
11	187.23	19.000	0.05249	0.00533	65.906	0.471
12	87.91	12.368	0.02267	0.00319	37.646	0.472
13	38.21	9.096	0.00912	0.00217	38.055	0.473
14	13.78	4.599	0.00306	0.00102	27.889	0.474
15	2.55	3.032	0.00053	0.00063	1.513	0.475

Uncorrected			Corrected			Calculation		
θ_{lab}	$\sigma(\theta_{lab})$	$\Delta\sigma_{lab}$	$\theta_{c.m.}$	$\sigma(\theta_{c.m.})$	$\Delta\sigma_{c.m.}$	$\sigma(\theta_{c.m.})$	%Dev.	χ^2
20.0	993.77	32.72	18.6	1969.64	113.41	2027.54	-2.9	0.26
25.0	475.84	17.51	22.9	981.53	70.75	1011.26	-3.0	0.18
30.0	171.32	5.14	27.3	383.75	18.97	394.23	-2.7	0.30
35.0	56.52	1.70	32.1	104.87	6.73	99.69	4.9	0.59
40.0	21.35	0.88	38.8	14.89	2.39	15.71	-5.6	0.12
43.0	16.46	0.49	42.9	16.32	1.80	16.34	-0.1	0.00
44.4	15.03	0.71	44.4	16.67	2.19	16.46	1.3	0.01
48.0	12.06	0.36	48.0	14.14	0.86	14.31	-1.2	0.04
50.0	11.95	0.48	50.1	13.10	1.25	12.55	4.2	0.19
52.5	11.87	0.41	53.1	12.71	1.09	11.94	6.0	0.50
54.4	11.06	0.37	55.4	13.19	0.83	13.91	-5.5	0.75
59.0	15.86	0.56	60.3	25.04	1.24	24.59	1.8	0.13
64.4	21.50	0.64	65.2	36.06	1.46	36.04	0.0	0.00
69.0	23.87	0.72	69.1	39.80	1.65	39.73	0.2	0.00
74.4	21.53	0.65	73.9	35.61	1.56	35.05	1.6	0.13
79.0	15.60	0.47	78.1	24.96	1.10	25.63	-2.7	0.37
85.6	10.48	0.42	85.1	12.71	0.83	12.23	3.8	0.34
89.0	9.20	0.32	89.3	10.74	0.66	10.99	-2.3	0.14
94.4	11.16	0.33	95.3	17.06	0.83	16.87	1.1	0.05
100.6	13.56	0.43	101.0	22.35	1.16	22.48	-0.6	0.01
105.6	13.23	0.40	105.4	21.82	0.97	22.05	-1.1	0.06
110.6	10.79	0.32	109.8	17.46	0.72	17.36	0.6	0.02
114.4	8.24	0.25	113.4	12.52	0.54	12.40	1.0	0.05
120.6	5.47	0.26	120.3	6.53	0.47	6.77	-3.7	0.27
125.6	5.85	0.25	126.0	8.01	0.50	7.70	3.8	0.37
130.6	6.30	0.29	130.9	9.56	0.61	9.65	-0.9	0.02
135.0	6.46	0.19	134.9	9.99	0.44	10.14	-1.5	0.12
140.6	6.34	0.30	140.2	9.21	0.62	8.92	3.2	0.22
145.6	5.59	0.24	145.4	7.47	0.47	7.53	-0.8	0.01
150.6	5.92	0.34	150.8	8.08	0.72	8.13	-0.6	0.00
154.4	6.91	0.21	154.7	10.01	0.51	9.99	0.3	0.00
160.6	8.65	0.28	160.6	13.19	0.63	13.20	-0.1	0.00

APPENDIX B

ANALYZING POWER TABULATIONS

Tabulations of the $A_y(\theta)$ data measured for this work are presented in this appendix. Coefficients derived from Associated Legendre polynomial fits to $A_y(\theta,E) \times \sigma(\theta,E)$ are also tabulated, as are various parameters associated with the data and fits. Note that fits are tabulated only for the data sets which comprised reasonably complete angular distributions. The $\sigma(\theta)$ used in calculating the fits are determined from Legendre polynomial fits to $\sigma(\theta)$ data. The fits for $\sigma(\theta)$ used for the ^{54}Fe, ^{58}Ni, and ^{93}Nb data are those given in appendix A; that for the ^{120}Sn data is from appendix C. The fits were calculated using the following equation:

$$A_y(\theta,E) \times \sigma(\theta,E) = \sum_{\ell=1} B_\ell(E) P_\ell^1(\cos\theta) \quad . \tag{B.1}$$

The parameters of the fits and the symbols used in the tables are:

ℓ-Value = order of the associated Legendre polynomial in the expansion.

B_ℓ = ℓ^{th} coefficient $B_\ell(E)$ of the associated Legendre polynomial expansion.

ΔB_ℓ = absolute uncertainty in the coefficient $B_\ell(E)$.

Ratio = $B_\ell(E)/B_1(E)$.

θ_{lab} = experimental laboratory angle.

$A_y(\theta_{lab})$ = vector analyzing power measured in the laboratory, before

corrections for multiple scattering and finite geometry.

ΔA_{ylab} = absolute error in the uncorrected analyzing power. This does not include uncertainty due to calibration error.

$\theta_{c.m.}$ = reaction angle given in the center-of-mass.

$A_y(\theta_{c.m.})$ = corrected analyzing power at the center-of-mass angle.

$\Delta A_{yc.m.}$ = absolute error in the corrected analyzing powers. This does not include uncertainty due to calibration error.

Dev. = absolute deviation of the calculated A_y from the experimental value.

χ^2 = χ^2 per point for the calculation at that angle.

F-Test = integral probability $P_F(F,\gamma_1,\gamma_2) = \int_F^\infty P_f(f,\gamma_1,\gamma_2)df$, in which γ_1 and γ_2 are the respective degrees of freedom.

F-Value = $F_\chi = \frac{\chi^2_{n-1}-\chi^2_n}{\chi^2_n}(N-n-1)$.

Here N is the number of data points, and n the number of terms in the fit.

^{54}Fe NEUTRON ELASTIC SCATTERING ANALYZING POWERS

Neutron Energy ± Energy Spread 9.941 ± 0.277 MeV
Excitation Energy (J^{π}) 0.000 MeV (0^+)

Normalization ± Calibration Error 1.00 ± 0.030

Uncorrected			Corrected		
θ_{lab}	$A_y(\theta_{lab})$	$\Delta A_{y\,lab}$	$\theta_{c.m.}$	$A_y(\theta_{c.m.})$	$\Delta A_{y\,c.m.}$
30.0	0.024	0.005	29.8	0.024	0.006
37.5	0.044	0.006	36.9	0.050	0.008
45.0	0.045	0.010	44.3	0.078	0.021
110.0	-0.796	0.038	110.0	-0.898	0.052
127.0	-0.094	0.071	126.8	0.062	0.102
150.0	-0.079	0.029	150.4	-0.085	0.033

^{54}Fe NEUTRON INELASTIC SCATTERING ANALYZING POWERS

Neutron Energy ± Energy Spread 9.941 ± 0.277 MeV
Excitation Energy (J^{π}) 1.408 MeV (2^+)

Normalization ± Calibration Error 1.00 ± 0.030

Uncorrected			Corrected		
θ_{lab}	$A_y(\theta_{lab})$	$\Delta A_{y\,lab}$	$\theta_{c.m.}$	$A_y(\theta_{c.m.})$	$\Delta A_{y\,c.m.}$
45.0	-0.073	0.083	45.1	-0.107	0.114
110.0	0.286	0.116	110.4	0.325	0.141
127.0	0.153	0.092	127.4	0.182	0.117
150.0	-0.030	0.065	149.8	-0.045	0.075

^{54}Fe NEUTRON ELASTIC SCATTERING ANALYZING POWERS

Neutron Energy ± Energy Spread 13.937 ± 0.186 MeV
Excitation Energy (J^{π}) 0.000 MeV (0^+)

Normalization ± Calibration Error 1.00 ± 0.030

Uncorrected			Corrected		
θ_{lab}	$A_y(\theta_{lab})$	$\Delta A_{y\,lab}$	$\theta_{c.m.}$	$A_y(\theta_{c.m.})$	$\Delta A_{y\,c.m.}$
30.0	0.078	0.015	29.4	0.081	0.016
45.0	-0.144	0.014	45.4	-0.197	0.019
55.0	-0.581	0.016	55.0	-0.689	0.035
70.0	-0.182	0.040	71.0	-0.096	0.055
80.0	0.013	0.023	80.9	0.029	0.026
90.0	-0.159	0.025	90.4	-0.164	0.027
110.0	-0.578	0.044	110.1	-0.711	0.065
132.0	0.281	0.046	132.5	0.360	0.055
152.0	-0.343	0.037	151.9	-0.447	0.045

^{54}Fe NEUTRON INELASTIC SCATTERING ANALYZING POWERS

Neutron Energy ± Energy Spread 13.937 ± 0.186 MeV
Excitation Energy (J^{π}) 1.408 MeV (2^+)

Normalization ± Calibration Error 1.00 ± 0.030

Uncorrected			Corrected		
θ_{lab}	$A_y(\theta_{lab})$	$\Delta A_{y\,lab}$	$\theta_{c.m.}$	$A_y(\theta_{c.m.})$	$\Delta A_{y\,c.m.}$
45.0	0.007	0.089	45.1	0.006	0.104
55.0	0.025	0.085	55.3	0.058	0.112
70.0	-0.092	0.094	70.7	-0.127	0.109
80.0	0.109	0.149	80.6	0.121	0.171
90.0	0.277	0.207	90.5	0.327	0.237
110.0	-0.288	0.152	110.4	-0.363	0.183
132.0	0.265	0.136	132.4	0.332	0.163
152.0	-0.120	0.109	152.0	-0.146	0.127

^{54}Fe NEUTRON ELASTIC SCATTERING ANALYZING POWERS

Neutron Energy ± Energy Spread 16.930 ± 0.150 MeV
Excitation Energy (J^{π}) 0.000 MeV (0^+)

Normalization ± Calibration Error 1.00 ± 0.030
Chi-square/degree-of-freedom 1.604

ℓ-Value	B_ℓ	ΔB_ℓ	Ratio	F-Value	F-Test
1	-4.9527	0.4038	1.0000	19.000	0.473
2	-4.3760	0.4397	0.8836	3.104	0.474
3	-0.6577	0.4416	0.1328	0.018	0.475
4	1.1042	0.4146	-0.2229	0.395	0.476
5	1.5524	0.4132	-0.3134	0.786	0.478
6	1.3042	0.3900	-0.2633	0.392	0.479
7	-0.3158	0.3587	0.0638	58.379	0.480
8	-3.1904	0.3260	0.6442	4.590	0.484
9	-2.3516	0.2667	0.4748	0.006	0.486
10	-1.5976	0.1925	0.3226	26.632	0.490
11	-0.4061	0.1040	0.0820	8.060	0.494

Uncorrected			Corrected			Calculation		
θ_{lab}	$A_y(\theta_{lab})$	$\Delta A_{y\,lab}$	$\theta_{c.m.}$	$A_y(\theta_{c.m.})$	$\Delta A_{y\,c.m.}$	$A_y(\theta_{c.m.})$	Dev.	χ^2
20.0	0.006	0.020	19.7	0.004	0.021	-0.016	0.019	0.84
25.0	0.049	0.025	24.4	0.042	0.027	0.018	0.024	0.79
30.0	0.112	0.025	29.1	0.106	0.028	0.131	-0.025	0.78
35.0	0.179	0.045	35.2	0.363	0.057	0.381	-0.018	0.10
40.0	-0.084	0.014	41.2	-0.131	0.016	-0.137	0.007	0.18
50.0	-0.485	0.035	50.5	-0.514	0.038	-0.467	-0.047	1.49
60.0	-0.696	0.060	59.8	-0.779	0.069	-0.816	0.037	0.29
70.0	-0.128	0.022	71.2	-0.003	0.026	-0.001	-0.002	0.01
80.0	-0.020	0.018	80.8	-0.009	0.020	-0.011	0.002	0.01
90.0	-0.218	0.045	90.4	-0.226	0.049	-0.220	-0.006	0.01
100.0	-0.386	0.070	100.3	-0.460	0.083	-0.448	-0.012	0.02
110.0	0.012	0.065	110.9	0.052	0.078	0.034	0.018	0.06
115.0	0.234	0.034	115.7	0.286	0.039	0.297	-0.011	0.08
118.0	0.378	0.050	118.8	0.447	0.057	0.396	0.052	0.81
126.0	0.368	0.050	126.4	0.397	0.055	0.480	-0.083	2.28
135.0	0.149	0.039	135.1	0.194	0.046	0.148	0.046	0.98
143.0	-0.319	0.060	143.4	-0.435	0.072	-0.433	-0.002	0.00
150.0	-0.299	0.055	150.3	-0.389	0.061	-0.267	-0.122	3.96
159.0	0.428	0.032	158.7	0.464	0.039	0.396	0.068	3.14

^{54}Fe NEUTRON INELASTIC SCATTERING ANALYZING POWERS

Neutron Energy ± Energy Spread 16.930 ± 0.150 MeV
Excitation Energy (J^π) 1.408 MeV (2^+)

Normalization ± Calibration Error 1.00 ± 0.030

Uncorrected			Corrected		
θ_{lab}	$A_y(\theta_{lab})$	$\Delta A_{y\,lab}$	$\theta_{c.m.}$	$A_y(\theta_{c.m.})$	$\Delta A_{y\,c.m.}$
40.0	0.173	0.181	40.5	0.235	0.209
70.0	-0.001	0.128	70.7	-0.011	0.150
80.0	-0.030	0.246	80.6	-0.031	0.285
115.0	-0.247	0.097	115.4	-0.298	0.114
135.0	0.294	0.160	135.4	0.404	0.211
159.0	-0.283	0.145	158.6	-0.333	0.166

^{56}Fe NEUTRON ELASTIC SCATTERING ANALYZING POWERS

Neutron Energy ± Energy Spread 9.933 ± 0.277 MeV
Excitation Energy (J^π) 0.000 MeV (0^+)

Normalization ± Calibration Error 1.00 ± 0.030

Uncorrected			Corrected		
θ_{lab}	$A_y(\theta_{lab})$	$\Delta A_{y\,lab}$	$\theta_{c.m.}$	$A_y(\theta_{c.m.})$	$\Delta A_{y\,c.m.}$
70.0	0.564	0.042	70.8	0.831	0.096
80.0	0.612	0.021	80.7	0.753	0.039
90.0	0.077	0.014	90.5	0.099	0.017

^{56}Fe NEUTRON INELASTIC SCATTERING ANALYZING POWERS

Neutron Energy ± Energy Spread 9.933 ± 0.277 MeV
Excitation Energy (J^π) 0.847 MeV (2^+)

Normalization ± Calibration Error 1.00 ± 0.030

Uncorrected			Corrected		
θ_{lab}	$A_y(\theta_{lab})$	$\Delta A_{y\,lab}$	$\theta_{c.m.}$	$A_y(\theta_{c.m.})$	$\Delta A_{y\,c.m.}$
70.0	0.013	0.032	70.5	0.017	0.040
80.0	0.159	0.035	80.4	0.192	0.044
90.0	0.041	0.032	90.3	0.054	0.039

^{58}Ni NEUTRON ELASTIC SCATTERING ANALYZING POWERS

Neutron Energy ± Energy Spread 9.906 ± 0.277 MeV
Excitation Energy (J^{π}) 0.000 MeV (0^+)

Normalization ± Calibration Error 1.00 ± 0.030

Uncorrected			Corrected		
θ_{lab}	$A_y(\theta_{lab})$	$\Delta A_{y\,lab}$	$\theta_{c.m.}$	$A_y(\theta_{c.m.})$	$\Delta A_{y\,c.m.}$
30.0	0.005	0.005	30.0	0.004	0.006
45.0	-0.019	0.011	44.5	-0.016	0.017
110.0	-0.843	0.046	110.2	-0.988	0.066
127.0	0.402	0.058	127.5	0.604	0.089

^{58}Ni NEUTRON INELASTIC SCATTERING ANALYZING POWERS

Neutron Energy ± Energy Spread 9.906 ± 0.277 MeV
Excitation Energy (J^{π}) 1.454 MeV (2^+)

Normalization ± Calibration Error 1.00 ± 0.030

Uncorrected			Corrected		
θ_{lab}	$A_y(\theta_{lab})$	$\Delta A_{y\,lab}$	$\theta_{c.m.}$	$A_y(\theta_{c.m.})$	$\Delta A_{y\,c.m.}$
45.0	-0.039	0.070	45.4	-0.045	0.081
55.0	-0.114	0.064	55.5	-0.147	0.077
110.0	-0.074	0.097	110.4	-0.082	0.112
127.0	0.175	0.109	127.3	0.208	0.127

^{58}Ni NEUTRON ELASTIC SCATTERING ANALYZING POWERS

Neutron Energy ± Energy Spread 13.940 ± 0.186 MeV
Excitation Energy (J^{π}) 0.000 MeV (0^+)

Normalization ± Calibration Error 1.00 ± 0.030

Uncorrected			Corrected		
θ_{lab}	$A_y(\theta_{lab})$	$\Delta A_{y\,lab}$	$\theta_{c.m.}$	$A_y(\theta_{c.m.})$	$\Delta A_{y\,c.m.}$
30.0	0.086	0.026	29.8	0.089	0.028
45.0	-0.204	0.022	45.5	-0.256	0.027
55.0	-0.700	0.023	55.2	-0.804	0.037
70.0	0.177	0.034	71.5	0.353	0.053
80.0	-0.047	0.027	80.9	-0.051	0.029
90.0	-0.211	0.031	90.5	-0.218	0.033
110.0	-0.414	0.051	110.5	-0.493	0.064
132.0	0.285	0.042	132.4	0.333	0.047
152.0	-0.436	0.054	152.2	-0.508	0.061

^{58}Ni NEUTRON INELASTIC SCATTERING ANALYZING POWERS

Neutron Energy ± Energy Spread 13.940 ± 0.186 MeV
Excitation Energy (J^{π}) 1.454 MeV (2^+)

Normalization ± Calibration Error 1.00 ± 0.030

Uncorrected			Corrected		
θ_{lab}	$A_y(\theta_{lab})$	$\Delta A_{y\,lab}$	$\theta_{c.m.}$	$A_y(\theta_{c.m.})$	$\Delta A_{y\,c.m.}$
45.0	-0.141	0.064	45.3	-0.142	0.073
55.0	-0.015	0.080	55.4	0.001	0.100
70.0	0.014	0.066	70.9	0.015	0.074
80.0	-0.127	0.143	80.7	-0.143	0.158
90.0	-0.034	0.218	90.5	-0.025	0.243
110.0	-0.658	0.283	110.5	-0.781	0.348
132.0	0.375	0.182	132.7	0.471	0.220
152.0	-0.107	0.118	152.0	-0.140	0.133

^{58}Ni NEUTRON ELASTIC SCATTERING ANALYZING POWERS

Neutron Energy ± Energy Spread 16.934 ± 0.150 MeV
Excitation Energy (J^{π}) 0.000 MeV (0^+)

Normalization ± Calibration Error 1.00 ± 0.030
Chi-square/degree-of-freedom 0.348

f-Value	B_f	ΔB_f	Ratio	F-Value	F-Test
1	-4.5192	0.4106	1.0000	20.000	0.472
2	-3.5639	0.4409	0.7886	4.560	0.473
3	0.5036	0.4521	-0.1114	0.070	0.474
4	2.1865	0.4453	-0.4838	0.772	0.475
5	2.4509	0.4517	-0.5423	1.287	0.476
6	2.1280	0.4165	-0.4709	0.466	0.478
7	1.2213	0.3824	-0.2702	47.589	0.479
8	-1.9560	0.3492	0.4328	0.008	0.480
9	-2.2568	0.2896	0.4994	2.123	0.484
10	-1.8947	0.2169	0.4193	81.218	0.486
11	-0.3873	0.1240	0.0857	12.762	0.490

Uncorrected			Corrected			Calculation		
θ_{lab}	$A_y(\theta_{lab})$	$\Delta A_{y\,lab}$	$\theta_{c.m.}$	$A_y(\theta_{c.m.})$	$\Delta A_{y\,c.m.}$	$A_y(\theta_{c.m.})$	Dev.	χ^2
20.0	0.014	0.020	20.0	0.012	0.021	0.011	0.000	0.00
25.0	0.032	0.020	24.8	0.028	0.021	0.059	-0.032	2.26
30.0	0.201	0.025	29.5	0.219	0.028	0.185	0.034	1.52
35.0	0.195	0.056	35.2	0.315	0.066	0.306	0.008	0.02
40.0	-0.163	0.020	40.9	-0.213	0.023	-0.202	-0.011	0.24
45.0	-0.380	0.040	45.8	-0.415	0.044	-0.418	0.003	0.01
50.0	-0.471	0.044	50.4	-0.498	0.048	-0.557	0.060	1.51
60.0	-0.815	0.075	59.9	-0.963	0.090	-0.906	-0.056	0.39
70.0	0.016	0.030	71.3	0.082	0.034	0.075	0.008	0.05
80.0	-0.144	0.021	80.8	-0.147	0.022	-0.138	-0.008	0.14
90.0	-0.259	0.053	90.4	-0.273	0.057	-0.320	0.048	0.69
100.0	-0.253	0.070	100.3	-0.294	0.082	-0.267	-0.027	0.11
110.0	0.192	0.071	110.9	0.236	0.081	0.239	-0.003	0.00
115.0	0.234	0.035	115.8	0.249	0.038	0.238	0.011	0.08
120.0	0.229	0.047	120.5	0.237	0.051	0.249	-0.012	0.06
130.0	0.239	0.078	130.2	0.268	0.084	0.279	-0.012	0.02
135.0	0.092	0.042	135.1	0.121	0.046	0.126	-0.005	0.01
140.0	-0.145	0.081	140.2	-0.182	0.094	-0.230	0.048	0.26
150.0	-0.244	0.068	150.2	-0.302	0.077	-0.268	-0.034	0.19
158.9	0.464	0.043	158.9	0.505	0.048	0.494	0.012	0.06

^{58}Ni NEUTRON INELASTIC SCATTERING ANALYZING POWERS

Neutron Energy ± Energy Spread 16.934 ± 0.150 MeV
Excitation Energy (J^{π}) 1.454 MeV (2^+)

Normalization ± Calibration Error 1.00 ± 0.030

Uncorrected			Corrected		
θ_{lab}	$A_y(\theta_{lab})$	$\Delta A_{y\,lab}$	$\theta_{c.m.}$	$A_y(\theta_{c.m.})$	$\Delta A_{y\,c.m.}$
40.0	-0.070	0.092	40.4	-0.075	0.099
70.0	0.205	0.123	70.7	0.234	0.137
80.0	0.048	0.164	80.7	0.060	0.181
115.0	0.072	0.231	115.6	0.107	0.262
135.0	0.246	0.187	135.3	0.285	0.211
150.0	-0.296	0.183	150.3	-0.331	0.204
158.7	-0.132	0.089	158.8	-0.142	0.096

^{60}Ni NEUTRON ELASTIC SCATTERING ANALYZING POWERS

Neutron Energy ± Energy Spread 9.943 ± 0.277 MeV
Excitation Energy (J^{π}) 0.000 MeV (0^+)

Normalization ± Calibration Error 1.00 ± 0.030

Uncorrected			Corrected		
θ_{lab}	$A_y(\theta_{lab})$	$\Delta A_{y\,lab}$	$\theta_{c.m.}$	$A_y(\theta_{c.m.})$	$\Delta A_{y\,c.m.}$
30.0	-0.024	0.006	30.0	-0.026	0.007
70.0	0.685	0.021	70.8	0.802	0.046
80.0	0.479	0.019	80.7	0.543	0.028
90.0	-0.008	0.015	90.5	-0.017	0.019

^{60}Ni NEUTRON INELASTIC SCATTERING ANALYZING POWERS

Neutron Energy ± Energy Spread 9.943 ± 0.277 MeV
Excitation Energy (J^{π}) 1.332 MeV (2^+)

Normalization ± Calibration Error 1.00 ± 0.030

Uncorrected			Corrected		
θ_{lab}	$A_y(\theta_{lab})$	$\Delta A_{y\,lab}$	$\theta_{c.m.}$	$A_y(\theta_{c.m.})$	$\Delta A_{y\,c.m.}$
70.0	0.008	0.036	70.7	0.015	0.041
80.0	0.113	0.043	80.6	0.135	0.050
90.0	0.029	0.042	90.5	0.036	0.050

^{93}Nb NEUTRON ELASTIC SCATTERING ANALYZING POWERS

Neutron Energy ± Energy Spread 9.941 ± 0.277 MeV
Excitation Energy (J^{π}) 0.000 MeV ($9/2^{+}$)

Normalization ± Calibration Error 1.00 ± 0.030
Chi-square/degree-of-freedom 0.375

ℓ-Value	B_ℓ	ΔB_ℓ	Ratio	F-Value	F-Test
1	-1.2274	0.4715	1.0000	23.000	0.469
2	-4.2086	0.5797	3.4289	1.668	0.470
3	-7.9212	0.7199	6.4536	0.018	0.471
4	-11.4447	0.8039	9.3243	0.219	0.472
5	-11.1049	0.8999	9.0475	0.448	0.473
6	-10.8368	0.8663	8.8290	26.002	0.474
7	-3.7857	0.8580	3.0843	11.921	0.475
8	-2.3178	0.7306	1.8884	0.103	0.476
9	-1.5760	0.6701	1.2840	47.562	0.478
10	-3.4237	0.5084	2.7894	25.467	0.479
11	-1.8457	0.4184	1.5037	0.010	0.480
12	-1.2778	0.2509	1.0410	10.091	0.484
13	-0.5430	0.1640	0.4424	15.349	0.486

Uncorrected			Corrected			Calculation		
θ_{lab}	$A_y(\theta_{lab})$	$\Delta A_{y\,lab}$	$\theta_{c.m.}$	$A_y(\theta_{c.m.})$	$\Delta A_{y\,c.m.}$	$A_y(\theta_{c.m.})$	Dev.	χ^2
20.0	-0.060	0.010	19.3	-0.064	0.011	-0.062	-0.003	0.05
25.0	-0.070	0.010	23.6	-0.072	0.012	-0.070	-0.003	0.05
30.0	-0.076	0.005	27.6	-0.076	0.007	-0.080	0.004	0.37
35.0	-0.115	0.010	32.0	-0.126	0.015	-0.109	-0.016	1.14
40.0	-0.097	0.015	37.0	-0.195	0.029	-0.213	0.018	0.38
45.0	0.027	0.025	45.7	0.133	0.049	0.154	-0.021	0.18
50.0	0.244	0.015	51.9	0.395	0.029	0.365	0.030	1.09
55.0	0.279	0.020	55.8	0.342	0.027	0.358	-0.016	0.34
60.0	0.257	0.020	60.1	0.306	0.024	0.317	-0.011	0.21
70.0	0.081	0.015	68.9	0.108	0.019	0.103	0.006	0.09
80.0	-0.219	0.035	78.0	-0.343	0.051	-0.344	0.001	0.00
85.0	-0.356	0.030	83.9	-0.620	0.052	-0.598	-0.022	0.17
90.0	-0.156	0.035	89.1	-0.364	0.055	-0.382	0.018	0.10
100.0	0.465	0.040	100.4	0.823	0.060	0.838	-0.014	0.06
105.0	0.454	0.040	105.5	0.645	0.057	0.645	0.000	0.00
110.0	0.221	0.040	110.4	0.265	0.053	0.244	0.021	0.15
115.0	-0.027	0.025	115.3	-0.083	0.033	-0.081	-0.003	0.01
120.0	-0.146	0.030	120.1	-0.222	0.038	-0.214	-0.008	0.05
130.0	-0.157	0.035	129.5	-0.153	0.043	-0.146	-0.008	0.03
135.0	-0.175	0.030	134.1	-0.140	0.038	-0.177	0.038	1.00
140.0	-0.373	0.030	138.4	-0.472	0.046	-0.416	-0.056	1.46
145.0	-0.395	0.035	144.7	-0.894	0.074	-0.957	0.063	0.73
150.0	-0.100	0.030	150.6	-0.181	0.045	-0.162	-0.018	0.16
155.0	0.350	0.030	155.7	0.504	0.041	0.497	0.007	0.03

^{93}Nb NEUTRON ELASTIC SCATTERING ANALYZING POWERS

Neutron Energy ± Energy Spread 13.915 ± 0.155 MeV
Excitation Energy/(J^π) 0.000 MeV ($9/2^+$)

Normalization ± Calibration Error 1.00 ± 0.030
Chi-square/degree-of-freedom 0.447

ℓ-Value	B_ℓ	ΔB_ℓ	Ratio	F-Value	F-Test
1	-3.7352	0.5212	1.0000	22.000	0.470
2	-2.5552	0.6831	0.6841	0.352	0.471
3	-4.8893	0.8363	1.3090	3.551	0.472
4	-8.0088	0.9256	2.1442	1.587	0.473
5	-9.2815	0.9853	2.4849	0.009	0.474
6	-9.8062	0.9579	2.6254	0.433	0.475
7	-6.9927	0.9141	1.8721	35.111	0.476
8	-4.0446	0.7898	1.0828	2.412	0.478
9	-3.6762	0.6850	0.9842	5.926	0.479
10	-4.5239	0.5186	1.2112	10.974	0.480
11	-2.2498	0.4078	0.6023	0.660	0.484
12	-1.9622	0.2535	0.5253	108.388	0.486
13	-0.3380	0.1595	0.0905	8.941	0.490

Uncorrected			Corrected			Calculation		
θ_{lab}	$A_y(\theta_{lab})$	$\Delta A_{y\,lab}$	$\theta_{c.m.}$	$A_y(\theta_{c.m.})$	$\Delta A_{y\,c.m.}$	$A_y(\theta_{c.m.})$	Dev.	χ^2
20.0	-0.049	0.020	18.6	-0.055	0.022	-0.065	0.010	0.18
25.0	-0.067	0.010	22.9	-0.077	0.013	-0.074	-0.003	0.04
30.0	-0.056	0.015	26.7	-0.068	0.019	-0.074	0.005	0.08
35.0	-0.049	0.020	31.2	-0.066	0.032	-0.050	-0.016	0.25
40.0	0.047	0.035	36.8	0.110	0.082	0.083	0.027	0.11
45.0	0.239	0.035	46.0	0.502	0.111	0.515	-0.013	0.01
50.0	0.422	0.050	51.7	0.598	0.074	0.620	-0.022	0.09
55.0	0.494	0.030	55.8	0.659	0.040	0.644	0.015	0.13
60.0	0.392	0.040	60.1	0.535	0.050	0.539	-0.004	0.01
70.0	-0.129	0.040	69.4	-0.176	0.048	-0.158	-0.018	0.14
80.0	-0.517	0.050	78.7	-0.721	0.068	-0.785	0.064	0.89
85.0	-0.609	0.050	83.8	-0.961	0.074	-0.904	-0.057	0.60
90.0	-0.280	0.050	90.2	-0.329	0.072	-0.349	0.020	0.08
100.0	0.076	0.045	100.7	0.155	0.056	0.181	-0.027	0.23
105.0	0.072	0.040	105.0	0.154	0.050	0.120	0.035	0.48
110.0	-0.128	0.045	109.5	-0.083	0.056	-0.054	-0.028	0.25
120.0	-0.566	0.055	119.4	-0.818	0.071	-0.847	0.029	0.16
125.0	-0.626	0.050	124.5	-0.936	0.066	-0.893	-0.043	0.42
130.0	-0.275	0.045	129.4	-0.380	0.057	-0.421	0.041	0.52
135.0	0.057	0.040	134.2	0.219	0.052	0.247	-0.028	0.29
140.0	0.266	0.045	139.3	0.615	0.061	0.599	0.015	0.06
150.0	-0.306	0.045	150.4	-0.681	0.064	-0.678	-0.003	0.00
158.0	-0.082	0.040	158.4	-0.151	0.050	-0.152	0.001	0.00

^{120}Sn NEUTRON ELASTIC SCATTERING ANALYZING POWERS

Neutron Energy ± Energy Spread 16.916 ± 0.150 MeV
Excitation Energy (J^{π}) 0.000 MeV (0^+)

Normalization ± Calibration Error 1.00 ± 0.030
Chi-square/degree-of-freedom 0.682

f-Value	B_f	ΔB_f	Ratio	F-Value	F-Test
1	-3.2510	0.7068	1.0000	23.000	0.469
2	1.0423	1.0266	-0.3206	0.948	0.470
3	0.5894	1.3202	-0.1813	3.567	0.471
4	-1.3293	1.5202	0.4089	3.424	0.472
5	-3.6804	1.6343	1.1321	0.773	0.473
6	-4.6578	1.6814	1.4327	0.039	0.474
7	-4.4236	1.6559	1.3607	0.117	0.475
8	-3.5000	1.5536	1.0766	10.216	0.476
9	-0.6597	1.4016	0.2029	17.796	0.478
10	0.8957	1.2320	-0.2755	14.041	0.479
11	-0.5555	1.0283	0.1709	7.807	0.480
12	-1.0439	0.8223	0.3211	0.489	0.484
13	-0.4566	0.6153	0.1404	0.042	0.486
14	-0.3256	0.4291	0.1002	9.092	0.490
15	0.4001	0.2814	-0.1231	4.725	0.494
16	0.5002	0.1443	-0.1539	16.293	0.499

Uncorrected			Corrected			Calculation		
θ_{lab}	$A_y(\theta_{lab})$	$\Delta A_{y\,lab}$	$\theta_{c.m.}$	$A_y(\theta_{c.m.})$	$\Delta A_{y\,c.m.}$	$A_y(\theta_{c.m.})$	Dev.	χ^2
20.0	-0.028	0.015	19.7	-0.029	0.016	-0.028	-0.001	0.01
25.0	-0.020	0.020	24.3	-0.022	0.022	-0.037	0.015	0.44
30.0	-0.040	0.032	28.7	-0.074	0.039	-0.033	-0.041	1.08
35.0	0.300	0.045	34.7	0.679	0.115	0.601	0.078	0.46
40.0	0.427	0.070	41.2	0.515	0.097	0.535	-0.020	0.04
45.0	0.465	0.040	45.7	0.536	0.050	0.498	0.038	0.58
50.0	0.400	0.035	50.4	0.456	0.039	0.488	-0.032	0.66
55.0	0.245	0.050	55.2	0.282	0.056	0.228	0.054	0.93
60.0	-0.229	0.045	60.2	-0.259	0.049	-0.243	-0.016	0.11
65.0	-0.544	0.040	65.0	-0.657	0.050	-0.646	-0.010	0.04
70.0	-0.700	0.080	69.8	-0.837	0.096	-0.886	0.049	0.26
75.0	-0.375	0.058	75.0	-0.479	0.082	-0.463	-0.016	0.04
80.0	0.028	0.048	80.9	0.144	0.059	0.136	0.009	0.02
90.0	-0.195	0.050	90.4	-0.203	0.054	-0.189	-0.014	0.06
100.0	-0.555	0.055	99.9	-0.605	0.065	-0.637	0.032	0.25
105.0	-0.740	0.060	105.1	-0.923	0.081	-0.870	-0.053	0.42
112.0	-0.220	0.060	112.1	-0.220	0.067	-0.243	0.023	0.12
120.0	0.270	0.100	120.1	0.440	0.116	0.474	-0.034	0.09
130.0	-0.537	0.065	130.3	-0.618	0.072	-0.628	0.010	0.02
140.0	-0.400	0.065	139.6	-0.428	0.073	-0.422	-0.007	0.01
150.0	-0.255	0.100	149.9	-0.278	0.121	-0.283	0.005	0.00
159.0	-0.160	0.060	159.0	-0.163	0.068	-0.160	-0.003	0.00

APPENDIX C.

CORRECTIONS TO PREVIOUSLY REPORTED ^{116,120}Sn DATA

C.1 Introduction

Errors have been discovered in the calculations of corrections for the neutron scattering data contained in the Ph.D. dissertation of P.P. Guss (Guss 1982a) for the ^{116,120}Sn isotopes. The errors were in the calculations of the multiple scattering, finite geometry, and attenuation corrections for both the $\sigma(\theta)$ and the $A_y(\theta)$ data. The errors were due to the use of incorrect densities of nuclei for these samples in the Monte Carlo calculations made using the codes EFFIGY and JANE. The values used were 2.21×10^{22} and 2.26×10^{22} nuclei/cm^3 for ^{116}Sn and ^{120}Sn, respectively. The correct value is 3.69×10^{22} nuclei/cm^3 for both tin isotopes. This value was calculated for each isotope based on the physical parameters of the samples, and agrees very well with the value of 3.70×10^{22} nuclei/cm^3 given by Marion and Young (Marion 1968) for natural tin. The use of incorrect densities of nuclei (that were too small in the original data corrections) caused underestimates of the amount of multiple scattering and the resulting correction factors. Using the uncorrected experimental data that Guss previously used as input to EFFIGY and JANE, all of the multiple scattering, finite geometry, and attenuation corrections for the ^{116,120}Sn data were recalculated with the correct densities of nuclei for the samples.

C.2 Cross Section Tabulations

Tabulations of the uncorrected and newly corrected $\sigma(\theta)$ data for ^{116,120}Sn and of coefficients derived from Legendre polynomial fits to the data are contained in this section. The $\sigma(\theta)$ data are for the elastic scattering of neutrons from both isotopes and for the inelastic scattering of neutrons to the first 2^+ excited states (Q = -1.29 MeV for ^{116}Sn and Q = -1.17 MeV for ^{120}Sn) and first 3^- excited states (Q = -2.27 MeV for ^{116}Sn and Q = -2.40 MeV for ^{120}Sn). The incident neutron energies are 9.94 and 13.92 MeV for both isotopes and also 16.9 MeV for ^{120}Sn. Some of the inelastic scattering data for angles less than 40° that appeared in the dissertation of P.P. Guss have been deleted. This was done because reevaluation of the spectra from these measurements suggests that experimental problems (not understood at the present time) might be causing some sample correlated background, which is associated with the large elastic scattering yields at forward angles, to enter into the spectra in the region of the elastic scattering events. The elastic scattering data, the data for the 2^+ states, and the data for the 3^- states for both tin isotopes are shown in figures C.1, C.2, and C.3, respectively. The differences between the $\sigma(\theta)$ data from the old and new corrections are in the 0.0 to $\pm$20% range (with a few exceptions near the cross section minima). Generally, the new $\sigma(\theta)$ values near maxima increased, those near minima decreased, and those in between changed little. For inelastic scattering, most of the new $\sigma(\theta)$ values are larger than the old ones. The symbols and terms used in the tabulations are the same as those defined in appendix A. The σ_T values used are those of Garber and Kinsey (Garber 1976).

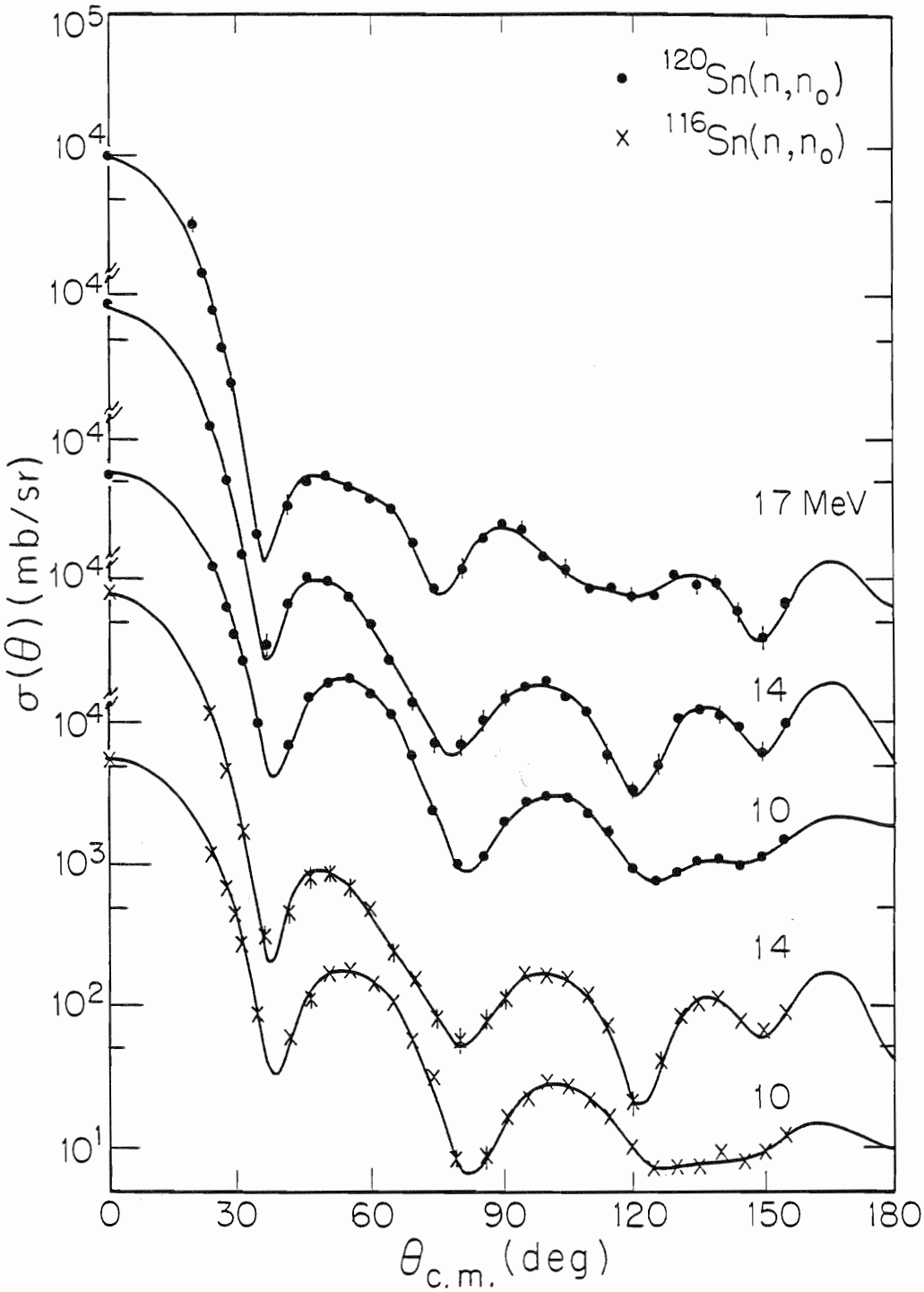

Figure C.1. The σ(θ) data for the elastic scattering of neutrons from ^{116,120}Sn. The curves are Legendre polynomial fits to the data.

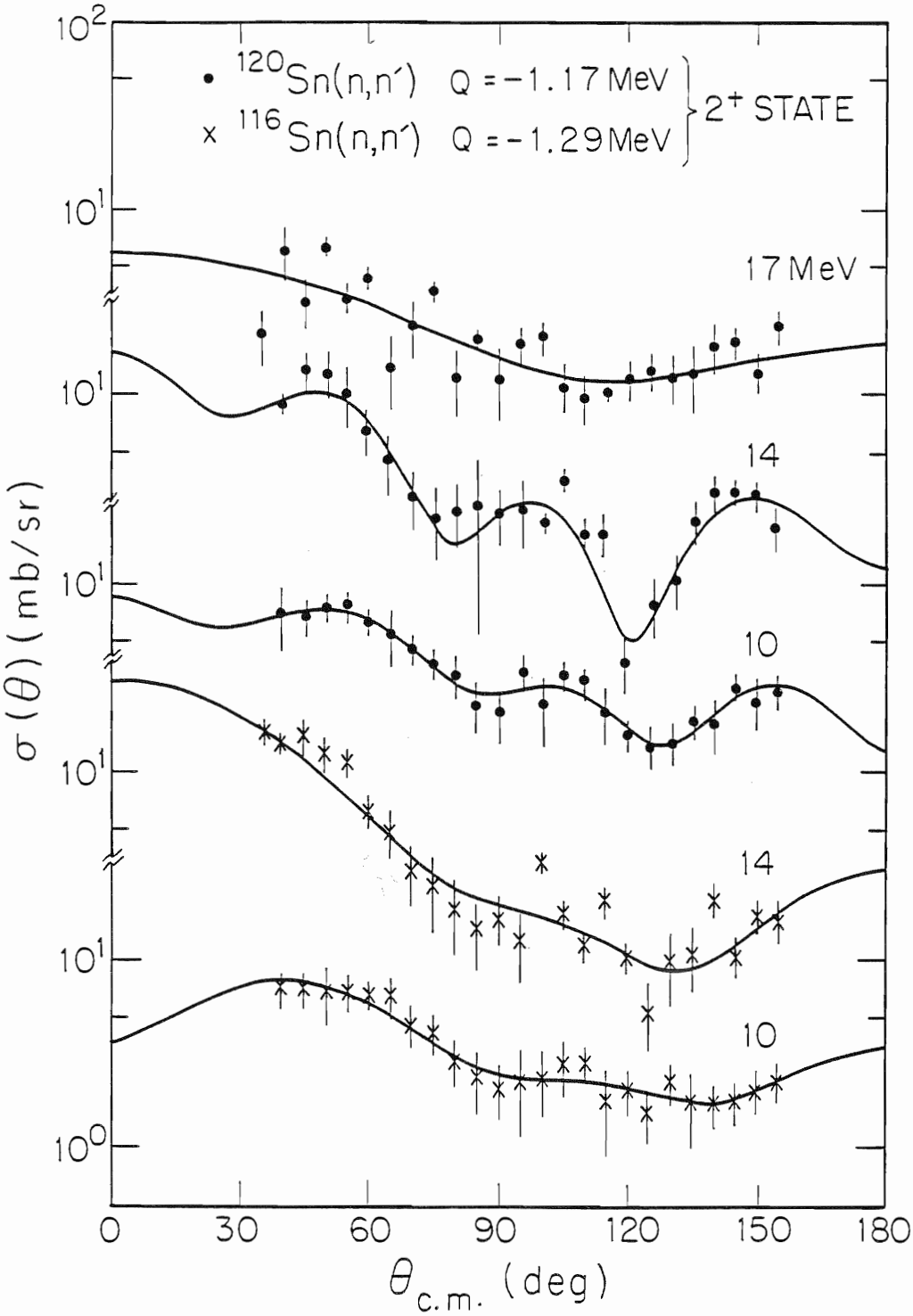

Figure C.2. The σ(θ) data for the inelastic scattering of neutrons to the first 2^+ excited states of ^{116,120}Sn. The curves are Legendre polynomial fits to the data.

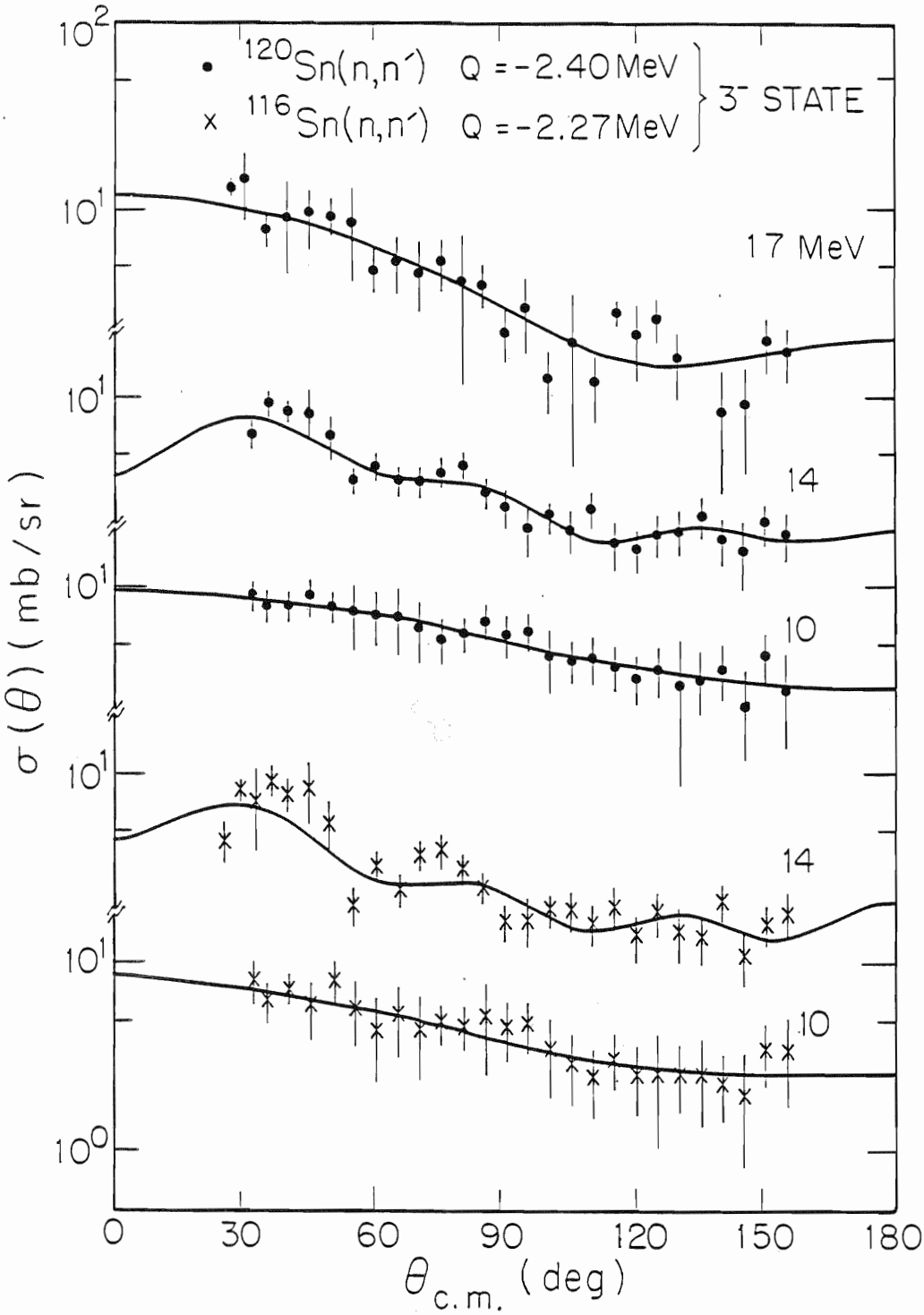

Figure C.3. The σ(Θ) data for the inelastic scattering of neutrons to the first 3^- excited states of ^{116,120}Sn. The curves are Legendre polynomial fits to the data.

^{116}Sn NEUTRON ELASTIC SCATTERING CROSS SECTIONS

Neutron Energy ± Energy Spread	9.945 ± 0.071 MeV
Excitation Energy (J^{π})	0.000 MeV (0^+)
Total Cross Section	4.240 ± 0.212 barns
Integrated Cross Section	2.239 ± 0.062 barns
Calculated Wick's Limit	5416.60 ± 541.7 mb/sr
Zero Degree Cross Section	5455.52 ± 71.56 mb/sr
Normalization Uncertainty	4.33 %
Chi-square/degree-of-freedom	1.633

f-Value	A_f	ΔA_f	a_f	Δa_f	F-Value	F-Test
0	178.18	4.970	1.00000	0.00000	30.000	0.466
1	442.39	14.468	0.82761	0.02707	5.411	0.466
2	603.21	22.124	0.67709	0.02483	4.599	0.466
3	686.86	27.777	0.55070	0.02227	5.284	0.466
4	731.07	29.862	0.45589	0.01862	3.111	0.467
5	740.89	29.932	0.37801	0.01527	5.301	0.468
6	723.50	27.103	0.31235	0.01170	8.304	0.469
7	612.88	23.563	0.22931	0.00882	2.911	0.469
8	407.16	17.940	0.13442	0.00592	43.287	0.470
9	211.76	12.877	0.06255	0.00380	26.733	0.471
10	89.44	7.064	0.02390	0.00189	23.987	0.472
11	28.18	3.378	0.00688	0.00082	41.477	0.473

Uncorrected			Corrected			Calculation		
θ_{lab}	$\sigma(\theta_{lab})$	$\Delta\sigma_{lab}$	$\theta_{c.m.}$	$\sigma(\theta_{c.m.})$	$\Delta\sigma_{c.m.}$	$\sigma(\theta_{c.m.})$	%Dev.	χ^2
24.0	726.16	24.03	23.5	1204.71	68.04	1151.80	4.4	0.60
28.0	373.75	15.64	27.1	663.90	47.54	611.46	7.9	1.22
30.0	254.50	14.26	28.9	451.95	41.71	415.29	8.1	0.77
32.0	153.21	7.54	30.7	268.93	22.75	262.20	2.5	0.09
35.0	68.62	2.03	33.9	89.85	4.44	95.45	-6.2	1.59
40.0	53.47	1.65	41.4	62.04	4.23	53.48	13.8	4.09
45.0	73.37	5.72	46.3	110.64	11.15	123.49	-11.6	1.33
50.0	111.18	1.78	50.7	166.58	4.52	170.60	-2.4	0.79
55.0	116.68	3.23	55.4	174.12	7.08	177.32	-1.8	0.20
60.0	95.56	2.12	60.1	143.12	5.25	146.79	-2.6	0.49
65.0	71.77	2.79	64.8	107.46	6.31	100.11	6.8	1.36
70.0	36.60	1.24	69.5	55.73	2.98	56.32	-1.0	0.04
75.0	21.22	0.89	74.1	31.46	2.16	25.67	18.4	7.19
80.0	7.91	0.39	79.5	8.08	0.64	8.86	-9.7	1.51
85.0	7.71	0.46	86.1	8.72	0.83	8.48	2.8	0.08
90.0	11.84	0.51	91.1	16.85	1.05	15.80	6.2	0.99
95.0	15.73	0.60	95.7	22.72	1.23	23.27	-2.4	0.20
100.0	20.02	0.88	100.4	28.88	1.64	27.85	3.6	0.40
105.0	18.68	0.59	105.1	26.78	1.21	27.45	-2.5	0.31
110.0	14.99	0.50	109.9	21.26	1.03	22.45	-5.6	1.36
115.0	11.72	0.49	114.7	16.36	0.98	15.56	4.9	0.68
120.0	7.73	0.34	119.6	10.17	0.64	9.74	4.2	0.45
125.0	5.64	0.30	124.9	6.92	0.50	7.03	-1.6	0.05
130.0	5.51	0.28	130.2	7.13	0.48	7.18	-0.7	0.01
135.0	5.39	0.27	135.2	7.35	0.50	7.89	-7.4	1.19
140.0	6.57	0.27	140.0	9.00	0.52	8.06	10.4	3.29
145.0	5.90	0.29	144.9	7.84	0.51	8.18	-4.3	0.43
150.0	6.77	0.38	150.0	9.12	0.68	9.41	-3.1	0.17
155.0	8.56	0.39	155.0	12.10	0.72	11.88	1.9	0.10

^{116}Sn NEUTRON INELASTIC SCATTERING CROSS SECTIONS

Neutron Energy ± Energy Spread	9.945 ± 0.071 MeV
Excitation Energy (J^{π})	1.293 MeV (2^+)
Integrated Cross Section	0.048 ± 0.003 barns
Zero Degree Cross Section	3.72 ± 1.95 mb/sr
Normalization Uncertainty	4.33 %
Chi-square/degree-of-freedom	0.250

ℓ-Value	A_ℓ	ΔA_ℓ	a_ℓ	Δa_ℓ	F-Value	F-Test
0	3.781	0.278	1.00000	0.00000	26.000	0.467
1	3.027	0.660	0.26690	0.05821	45.000	0.468
2	1.315	0.860	0.06957	0.04552	40.070	0.469
3	-1.327	1.005	-0.05013	0.03797	0.231	0.469
4	-1.551	0.901	-0.04557	0.02648	2.367	0.470
5	-1.525	0.842	-0.03665	0.02025	13.111	0.471

Uncorrected			Corrected			Calculation		
θ_{lab}	$\sigma(\theta_{lab})$	$\Delta\sigma_{lab}$	$\theta_{c.m.}$	$\sigma(\theta_{c.m.})$	$\Delta\sigma_{c.m.}$	$\sigma(\theta_{c.m.})$	%Dev.	χ^2
40.0	5.68	0.78	40.3	6.98	1.46	7.77	-11.4	0.30
45.0	5.79	0.80	45.4	7.08	1.50	7.67	-8.3	0.15
50.0	5.48	1.22	50.5	6.84	2.28	7.28	-6.5	0.04
55.0	5.31	0.79	55.5	6.78	1.56	6.69	1.3	0.00
60.0	4.99	0.46	60.4	6.49	0.99	5.95	8.3	0.30
65.0	4.99	0.87	65.3	6.47	1.77	5.18	20.1	0.54
70.0	3.47	0.57	70.2	4.54	1.18	4.41	2.7	0.01
75.0	3.18	0.51	75.1	4.14	1.06	3.74	9.7	0.14
80.0	2.32	0.40	80.1	2.95	0.82	3.19	-7.9	0.08
85.0	1.92	0.44	85.2	2.38	0.86	2.78	-17.0	0.22
90.0	1.70	0.37	90.4	2.10	0.71	2.53	-20.7	0.37
95.0	1.81	0.57	95.5	2.28	1.11	2.40	-5.1	0.01
100.0	1.87	0.48	100.5	2.43	0.95	2.34	3.5	0.01
105.0	2.16	0.45	105.4	2.88	0.94	2.31	19.8	0.37
110.0	2.14	0.30	110.3	2.88	0.64	2.27	21.0	0.89
115.0	1.35	0.43	115.1	1.81	0.88	2.21	-21.9	0.20
120.0	1.55	0.28	120.0	2.04	0.57	2.11	-3.1	0.01
125.0	1.22	0.25	125.0	1.58	0.50	1.99	-25.8	0.67
130.0	1.80	0.29	130.0	2.27	0.55	1.87	17.5	0.51
135.0	1.44	0.44	135.1	1.81	0.82	1.79	0.9	0.00
140.0	1.36	0.24	140.1	1.74	0.46	1.78	-2.3	0.01
145.0	1.38	0.25	145.0	1.80	0.48	1.86	-3.4	0.02
150.0	1.57	0.29	149.9	2.09	0.58	2.03	2.6	0.01
155.0	1.70	0.28	154.7	2.29	0.57	2.27	1.1	0.00

^{116}Sn NEUTRON INELASTIC SCATTERING CROSS SECTIONS

Neutron Energy ± Energy Spread	9.945 ± 0.071 MeV
Excitation Energy (J^{π})	2.266 MeV (3^-)
Integrated Cross Section	0.057 ± 0.004 barns
Zero Degree Cross Section	8.53 ± 1.01 mb/sr
Normalization Uncertainty	4.33 %
Chi-square/degree-of-freedom	0.179

ℓ-Value	A_ℓ	ΔA_ℓ	a_ℓ	Δa_ℓ	F-Value	F-Test
0	4.529	0.316	1.00000	0.00000	25.000	0.468
1	2.943	0.565	0.21662	0.04160	101.084	0.469
2	1.056	0.772	0.04663	0.03408	10.445	0.469

Uncorrected			Corrected			Calculation		
θ_{lab}	$\sigma(\theta_{lab})$	$\Delta\sigma_{lab}$	$\theta_{c.m.}$	$\sigma(\theta_{c.m.})$	$\Delta\sigma_{c.m.}$	$\sigma(\theta_{c.m.})$	%Dev.	χ^2
32.0	6.85	0.91	32.4	8.19	2.19	7.62	7.0	0.07
35.0	5.44	0.69	35.4	6.44	1.65	7.45	-15.7	0.38
40.0	6.43	0.64	40.4	7.50	1.55	7.16	4.6	0.05
45.0	5.29	1.01	45.4	6.12	2.24	6.85	-11.8	0.10
50.0	7.09	0.98	50.5	8.24	2.24	6.51	21.0	0.60
55.0	5.12	1.07	55.5	6.04	2.39	6.17	-2.2	0.00
60.0	3.63	0.95	60.6	4.50	2.17	5.83	-29.6	0.38
65.0	4.46	1.00	65.5	5.47	2.31	5.49	-0.4	0.00
70.0	3.87	1.02	70.5	4.59	2.26	5.16	-12.4	0.06
75.0	4.26	0.52	75.4	5.01	1.22	4.84	3.4	0.02
80.0	4.05	0.59	80.4	4.78	1.37	4.54	5.1	0.03
85.0	4.53	1.25	85.3	5.35	2.80	4.25	20.5	0.15
90.0	3.99	0.72	90.3	4.70	1.67	3.98	15.2	0.18
95.0	4.04	0.63	95.3	4.79	1.50	3.74	21.9	0.49
100.0	2.96	0.70	100.3	3.58	1.63	3.53	1.5	0.00
105.0	2.47	0.54	105.3	3.02	1.27	3.34	-10.6	0.06
110.0	2.06	0.43	110.3	2.54	1.03	3.17	-25.0	0.38
115.0	2.60	0.43	115.2	3.21	1.06	3.03	5.6	0.03
120.0	2.15	0.45	120.2	2.65	1.09	2.92	-10.2	0.06
125.0	2.17	0.69	125.1	2.70	1.67	2.83	-4.9	0.01
130.0	2.31	0.42	130.1	2.68	1.00	2.76	-3.2	0.01
135.0	2.31	0.56	135.1	2.71	1.31	2.71	0.1	0.00
140.0	1.99	0.38	140.0	2.42	0.93	2.68	-10.6	0.08
145.0	1.67	0.51	145.0	2.09	1.27	2.65	-27.0	0.20
150.0	2.84	0.50	149.9	3.56	1.28	2.64	25.8	0.51
155.0	2.84	0.72	154.8	3.57	1.79	2.63	26.1	0.27

^{116}Sn NEUTRON ELASTIC SCATTERING CROSS SECTIONS

Neutron Energy ± Energy Spread	13.925 ± 0.047 MeV
Excitation Energy (J^{π})	0.000 MeV (0^+)
Total Cross Section	4.540 ± 0.114 barns
Integrated Cross Section	2.325 ± 0.071 barns
Calculated Wick's Limit	8695.55 ± 434.8 mb/sr
Zero Degree Cross Section	7803.10 ± 94.82 mb/sr
Normalization Uncertainty	4.29 %
Chi-square/degree-of-freedom	1.786

ℓ-Value	A_ℓ	ΔA_ℓ	a_ℓ	Δa_ℓ	F-Value	F-Test
0	185.05	5.647	1.00000	0.00000	30.000	0.466
1	497.31	16.349	0.89581	0.02945	3.307	0.466
2	744.37	25.546	0.80450	0.02761	3.303	0.466
3	903.75	32.350	0.69769	0.02497	0.807	0.466
4	990.36	36.463	0.59465	0.02189	3.950	0.467
5	997.15	37.632	0.48987	0.01849	0.827	0.468
6	949.77	36.367	0.39481	0.01512	3.956	0.469
7	842.26	33.140	0.30343	0.01194	0.243	0.469
8	668.73	28.511	0.21258	0.00906	15.103	0.470
9	468.72	23.085	0.13331	0.00657	2.420	0.471
10	300.42	17.152	0.07731	0.00441	6.788	0.472
11	165.61	11.665	0.03891	0.00274	50.662	0.473
12	65.00	6.481	0.01405	0.00140	5.751	0.474
13	24.60	2.935	0.00492	0.00059	33.648	0.475

Uncorrected			Corrected			Calculation		
θ_{lab}	$\sigma(\theta_{lab})$	$\Delta\sigma_{lab}$	$\theta_{c.m.}$	$\sigma(\theta_{c.m.})$	$\Delta\sigma_{c.m.}$	$\sigma(\theta_{c.m.})$	%Dev.	χ^2
24.0	709.26	31.47	23.3	1160.65	73.72	1173.58	-1.1	0.03
28.0	259.50	11.72	26.9	451.09	29.56	530.17	-17.5	7.16
32.0	111.36	6.38	30.6	174.97	15.23	168.89	3.5	0.16
36.0	41.59	4.52	35.7	30.40	6.09	21.51	29.2	2.13
40.0	38.30	3.39	41.3	44.63	6.25	52.19	-16.9	1.46
45.0	57.62	3.82	45.9	82.27	6.83	84.94	-3.2	0.15
50.0	57.77	3.50	50.4	84.12	5.95	86.04	-2.3	0.10
55.0	45.99	4.44	54.9	67.61	7.52	66.41	1.8	0.03
60.0	33.42	1.87	59.7	48.24	3.19	43.39	10.0	2.31
65.0	17.11	1.52	64.6	23.24	2.54	26.31	-13.2	1.46
70.0	11.65	0.67	69.7	15.53	1.13	15.40	0.8	0.01
75.0	6.10	0.81	74.6	7.95	1.42	8.41	-5.8	0.10
80.0	5.14	0.73	80.1	5.49	1.11	5.09	7.2	0.13
85.0	5.87	0.48	86.0	7.59	0.81	7.45	1.9	0.03
90.0	7.59	0.63	90.9	10.93	1.09	11.85	-8.4	0.72
95.0	11.23	0.47	95.5	16.18	0.79	15.41	4.8	0.95
100.0	11.13	0.47	100.3	15.93	0.77	16.72	-4.9	1.03
105.0	10.42	0.48	105.0	15.08	0.80	15.19	-0.7	0.02
110.0	7.97	0.30	109.6	11.76	0.56	11.38	3.2	0.45
115.0	4.70	0.34	114.1	7.11	0.66	6.67	6.1	0.43
120.0	2.11	0.28	119.3	2.02	0.42	2.51	-24.5	1.39
125.0	2.85	0.25	126.3	3.98	0.49	3.75	5.8	0.23
130.0	5.47	0.33	130.8	8.47	0.60	7.78	8.1	1.30
135.0	6.99	0.33	135.2	10.44	0.57	10.93	-4.8	0.77
140.0	7.74	0.41	139.7	11.12	0.70	11.04	0.8	0.02
145.0	5.82	0.29	144.6	7.71	0.48	8.08	-4.8	0.59
150.0	5.26	0.33	149.9	6.64	0.52	5.97	10.1	1.65
155.0	6.24	0.33	155.0	8.53	0.56	8.86	-3.9	0.35

^{116}Sn NEUTRON INELASTIC SCATTERING CROSS SECTIONS

Neutron Energy ± Energy Spread	13.925 ± 0.047 MeV
Excitation Energy (J^{π})	1.293 MeV (2^+)
Integrated Cross Section	0.068 ± 0.004 barns
Zero Degree Cross Section	31.13 ± 1.64 mb/sr
Normalization Uncertainty	4.29 %
Chi-square/degree-of-freedom	1.730

ℓ-Value	A_ℓ	ΔA_ℓ	a_ℓ	Δa_ℓ	F-Value	F-Test
0	5.379	0.299	1.00000	0.00000	27.000	0.466
1	9.075	0.717	0.56237	0.04441	8.709	0.467
2	8.886	0.953	0.33037	0.03543	34.191	0.468
3	4.978	0.868	0.13220	0.02304	6.477	0.469
4	2.807	0.660	0.05798	0.01364	10.443	0.469

Uncorrected			Corrected			Calculation		
θ_{lab}	$\sigma(\theta_{lab})$	$\Delta\sigma_{lab}$	$\theta_{c.m.}$	$\sigma(\theta_{c.m.})$	$\Delta\sigma_{c.m.}$	$\sigma(\theta_{c.m.})$	%Dev.	χ^2
36.0	12.26	1.23	36.3	16.14	2.26	16.80	-4.1	0.08
40.0	10.68	0.88	40.2	13.94	1.60	14.55	-4.4	0.15
45.0	11.52	2.01	45.2	15.12	3.62	11.91	21.2	0.79
50.0	9.42	1.50	50.1	12.42	2.70	9.53	23.3	1.15
55.0	8.65	1.10	55.1	11.32	2.00	7.48	33.9	3.69
60.0	4.80	0.71	60.1	6.24	1.28	5.79	7.2	0.12
65.0	3.75	0.86	65.1	4.83	1.54	4.48	7.3	0.05
70.0	2.34	0.59	70.1	2.98	1.06	3.52	-18.0	0.26
75.0	1.99	0.65	75.1	2.51	1.16	2.85	-13.6	0.09
80.0	1.46	0.47	80.2	1.87	0.86	2.41	-28.9	0.40
85.0	1.11	0.31	85.3	1.45	0.57	2.15	-48.4	1.50
90.0	1.33	0.27	90.3	1.69	0.49	1.98	-17.1	0.34
95.0	0.99	0.29	95.3	1.26	0.54	1.86	-47.6	1.22
100.0	2.61	0.24	100.2	3.30	0.46	1.73	47.5	11.84
105.0	1.34	0.18	105.2	1.76	0.35	1.60	9.5	0.23
110.0	0.92	0.12	110.1	1.21	0.26	1.43	-18.7	0.77
115.0	1.62	0.19	115.0	2.07	0.39	1.26	39.1	4.26
120.0	0.83	0.10	120.0	1.05	0.21	1.10	-4.4	0.05
125.0	0.44	0.11	125.0	0.53	0.23	0.97	-82.0	3.67
130.0	0.81	0.21	130.0	1.01	0.42	0.90	10.1	0.06
135.0	0.87	0.21	135.1	1.08	0.42	0.92	14.7	0.14
140.0	1.64	0.24	140.2	2.10	0.48	1.04	50.4	4.78
145.0	0.81	0.14	145.2	1.07	0.28	1.25	-16.8	0.42
150.0	1.30	0.17	150.1	1.76	0.33	1.53	13.1	0.48
155.0	1.20	0.19	154.9	1.63	0.37	1.85	-13.9	0.36

^{116}Sn NEUTRON INELASTIC SCATTERING CROSS SECTIONS

Neutron Energy ± Energy Spread	13.925 ± 0.047 MeV
Excitation Energy (J^{π})	2.266 MeV (3^-)
Integrated Cross Section	0.035 ± 0.002 barns
Zero Degree Cross Section	4.54 ± 1.14 mb/sr
Normalization Uncertainty	4.29 %
Chi-square/degree-of-freedom	1.462

ℓ-Value	A_ℓ	ΔA_ℓ	a_ℓ	Δa_ℓ	F-Value	F-Test
0	2.817	0.129	1.00000	0.00000	33.000	0.463
1	2.318	0.259	0.27430	0.03068	25.725	0.464
2	1.520	0.329	0.10789	0.02333	10.700	0.465
3	0.579	0.383	0.02938	0.01945	2.212	0.466
4	0.106	0.467	0.00419	0.01844	1.188	0.466
5	-0.479	0.538	-0.01544	0.01735	0.121	0.466
6	-1.111	0.516	-0.03034	0.01409	0.516	0.466
7	-1.214	0.442	-0.02872	0.01045	5.166	0.467

Uncorrected			Corrected			Calculation		
θ_{lab}	$\sigma(\theta_{lab})$	$\Delta\sigma_{lab}$	$\theta_{c.m.}$	$\sigma(\theta_{c.m.})$	$\Delta\sigma_{c.m.}$	$\sigma(\theta_{c.m.})$	%Dev.	χ^2
24.0	3.37	0.39	25.4	4.50	1.11	7.00	-55.6	5.04
28.0	6.27	0.41	29.1	8.42	1.12	7.02	16.7	1.57
32.0	5.45	1.26	32.8	7.46	3.50	6.80	8.9	0.04
36.0	7.13	0.63	36.5	9.36	1.69	6.36	32.1	3.14
40.0	5.85	0.52	40.3	8.02	1.45	5.76	28.3	2.44
45.0	6.32	1.14	45.0	8.60	3.17	4.88	43.2	1.38
50.0	4.21	0.65	49.8	5.57	1.76	4.01	28.0	0.79
55.0	1.73	0.20	55.1	2.05	0.48	3.26	-58.8	6.45
60.0	2.81	0.28	60.6	3.30	0.63	2.79	15.2	0.64
65.0	1.96	0.23	65.8	2.50	0.56	2.65	-6.1	0.08
70.0	2.95	0.32	70.6	3.85	0.76	2.68	30.5	2.39
75.0	3.08	0.32	75.4	3.94	0.74	2.75	30.2	2.59
80.0	2.59	0.28	80.2	3.25	0.63	2.77	14.9	0.60
85.0	2.16	0.25	85.1	2.61	0.53	2.67	-2.2	0.01
90.0	1.46	0.20	90.1	1.68	0.41	2.44	-45.4	3.46
95.0	1.53	0.28	95.2	1.71	0.55	2.12	-24.0	0.55
100.0	1.68	0.20	100.3	1.94	0.40	1.81	6.5	0.10
105.0	1.60	0.22	105.3	1.94	0.48	1.60	17.4	0.49
110.0	1.32	0.19	110.2	1.66	0.42	1.51	9.1	0.13
115.0	1.65	0.24	115.2	2.06	0.52	1.54	25.0	0.96
120.0	1.12	0.19	120.1	1.42	0.42	1.65	-16.0	0.29
125.0	1.50	0.21	125.2	1.94	0.49	1.75	9.4	0.14
130.0	1.15	0.21	130.1	1.49	0.50	1.80	-20.7	0.39
135.0	1.09	0.19	135.0	1.40	0.44	1.76	-25.4	0.66
140.0	1.72	0.26	139.9	2.16	0.58	1.64	24.1	0.81
145.0	0.88	0.18	145.0	1.11	0.40	1.49	-34.5	0.90
150.0	1.30	0.18	150.0	1.64	0.40	1.38	15.8	0.42
155.0	1.45	0.24	154.9	1.86	0.54	1.37	26.2	0.80

^{120}Sn NEUTRON ELASTIC SCATTERING CROSS SECTIONS

Neutron Energy ± Energy Spread	9.943 ± 0.071 MeV
Excitation Energy (J^{π})	0.000 MeV (0^+)
Total Cross Section	4.240 ± 0.212 barns
Integrated Cross Section	2.386 ± 0.055 barns
Calculated Wick's Limit	5417.07 ± 541.7 mb/sr
Zero Degree Cross Section	5838.02 ± 62.99 mb/sr
Normalization Uncertainty	4.33 %
Chi-square/degree-of-freedom	0.899

ℓ-Value	A_ℓ	ΔA_ℓ	a_ℓ	Δa_ℓ	F-Value	F-Test
0	189.91	4.388	1.00000	0.00000	30.000	0.466
1	469.67	12.767	0.82437	0.02241	5.817	0.466
2	642.08	19.504	0.67620	0.02054	5.769	0.466
3	727.67	24.511	0.54738	0.01844	5.329	0.466
4	775.95	26.415	0.45399	0.01545	4.511	0.467
5	784.02	26.558	0.37531	0.01271	3.627	0.468
6	768.82	23.998	0.31141	0.00972	15.247	0.469
7	659.08	20.652	0.23137	0.00725	1.075	0.469
8	449.56	15.464	0.13925	0.00479	40.104	0.470
9	237.26	10.897	0.06575	0.00302	21.852	0.471
10	101.89	5.811	0.02555	0.00146	29.444	0.472
11	32.12	2.765	0.00735	0.00063	155.269	0.473

Uncorrected			Corrected			Calculation		
θ_{lab}	$\sigma(\theta_{lab})$	$\Delta\sigma_{lab}$	$\theta_{c.m.}$	$\sigma(\theta_{c.m.})$	$\Delta\sigma_{c.m.}$	$\sigma(\theta_{c.m.})$	%Dev.	χ^2
24.0	733.76	24.52	23.6	1196.56	57.10	1192.67	0.3	0.00
28.0	365.15	17.08	27.2	630.52	43.85	623.71	1.1	0.02
30.0	233.56	10.78	29.0	405.28	28.18	419.91	-3.6	0.27
32.0	154.66	6.95	30.8	261.84	18.01	262.90	-0.4	0.00
35.0	75.14	1.84	34.0	97.46	3.80	97.26	0.2	0.00
40.0	58.65	2.80	41.4	68.43	5.12	67.64	1.2	0.02
45.0	95.10	2.02	46.3	144.71	3.88	143.34	0.9	0.13
50.0	119.02	3.41	50.7	179.13	5.79	189.63	-5.9	3.30
55.0	130.69	2.91	55.3	196.38	5.11	191.15	2.7	1.05
60.0	101.35	2.10	60.0	152.80	3.98	154.40	-1.0	0.16
65.0	73.00	2.39	64.7	110.74	4.79	102.37	7.6	3.06
70.0	37.39	1.26	69.4	55.32	2.62	55.72	-0.7	0.02
75.0	16.92	0.71	74.2	23.05	1.36	24.38	-5.8	0.96
80.0	10.01	0.35	79.9	9.80	0.56	9.55	2.6	0.20
85.0	9.47	0.39	85.9	11.01	0.67	11.30	-2.6	0.18
90.0	14.25	0.47	90.9	19.54	0.82	18.98	2.9	0.47
95.0	18.41	0.54	95.6	26.10	0.92	26.31	-0.8	0.05
100.0	20.58	0.66	100.4	29.52	1.11	30.10	-1.9	0.27
105.0	19.91	0.49	105.1	28.64	0.83	28.63	0.0	0.00
110.0	15.49	0.47	109.8	22.28	0.79	22.75	-2.1	0.35
115.0	11.93	0.41	114.6	16.58	0.72	15.22	8.2	3.50
120.0	7.29	0.21	119.7	9.16	0.35	9.36	-2.3	0.36
125.0	6.19	0.23	125.1	7.48	0.38	7.51	-0.4	0.01
130.0	6.47	0.29	130.3	8.52	0.48	8.65	-1.6	0.08
135.0	7.32	0.24	135.1	10.02	0.42	9.85	1.7	0.17
140.0	7.66	0.32	139.8	10.36	0.53	9.99	3.6	0.48
145.0	7.25	0.26	144.8	9.41	0.44	9.78	-3.9	0.69
150.0	8.36	0.42	150.0	10.92	0.68	10.95	-0.2	0.00
155.0	10.38	0.35	155.0	14.32	0.59	14.10	1.5	0.14

^{120}Sn NEUTRON INELASTIC SCATTERING CROSS SECTIONS

Neutron Energy ± Energy Spread	9.943 ± 0.071 MeV
Excitation Energy (J^π)	1.171 MeV (2^+)
Integrated Cross Section	0.048 ± 0.003 barns
Zero Degree Cross Section	8.54 ± 2.04 mb/sr
Normalization Uncertainty	4.33 %
Chi-square/degree-of-freedom	0.329

ℓ-Value	A_ℓ	ΔA_ℓ	a_ℓ	Δa_ℓ	F-Value	F-Test
0	3.848	0.245	1.00000	0.00000	27.000	0.466
1	3.025	0.564	0.26204	0.04884	29.015	0.467
2	1.309	0.728	0.06804	0.03784	35.743	0.468
3	-1.060	0.750	-0.03934	0.02786	1.607	0.469
4	-0.880	0.772	-0.02540	0.02228	0.006	0.469
5	-0.538	0.880	-0.01271	0.02079	4.998	0.470
6	0.669	0.878	0.01338	0.01756	2.928	0.471
7	2.165	0.746	0.03751	0.01292	25.649	0.472

Uncorrected			Corrected			Calculation		
θ_{lab}	$\sigma(\theta_{lab})$	$\Delta\sigma_{lab}$	$\theta_{c.m.}$	$\sigma(\theta_{c.m.})$	$\Delta\sigma_{c.m.}$	$\sigma(\theta_{c.m.})$	%Dev.	χ^2
40.0	5.90	0.80	40.3	6.93	2.66	6.79	2.0	0.00
45.0	5.37	0.86	45.7	6.69	1.46	7.28	-8.8	0.16
50.0	5.74	0.71	50.6	7.55	1.27	7.43	1.5	0.01
55.0	5.89	0.80	55.4	7.79	1.45	7.18	7.8	0.18
60.0	4.80	0.45	60.2	6.29	0.82	6.53	-3.8	0.09
65.0	4.22	1.03	65.2	5.46	1.83	5.56	-1.9	0.00
70.0	3.53	0.45	70.2	4.55	0.81	4.50	1.1	0.00
75.0	2.88	0.42	75.1	3.78	0.78	3.58	5.4	0.07
80.0	2.55	0.39	80.1	3.31	0.72	2.95	11.1	0.26
85.0	1.88	0.42	85.2	2.30	0.72	2.65	-15.5	0.24
90.0	1.74	0.38	90.5	2.09	0.64	2.66	-27.7	0.81
95.0	2.71	0.43	95.6	3.44	0.77	2.81	18.3	0.66
100.0	1.72	0.48	100.4	2.27	0.90	2.91	-28.4	0.51
105.0	2.51	0.35	105.2	3.32	0.66	2.85	14.1	0.51
110.0	2.33	0.33	109.9	3.12	0.64	2.60	16.7	0.67
115.0	1.63	0.37	114.8	2.09	0.68	2.19	-5.2	0.03
120.0	1.32	0.17	119.9	1.59	0.30	1.75	-10.6	0.31
125.0	1.18	0.21	125.1	1.38	0.36	1.44	-4.6	0.03
130.0	1.21	0.21	130.3	1.44	0.37	1.41	2.1	0.01
135.0	1.52	0.22	135.3	1.89	0.42	1.65	12.8	0.34
140.0	1.41	0.32	140.2	1.82	0.61	2.07	-14.0	0.17
145.0	2.15	0.23	145.0	2.83	0.45	2.53	10.7	0.46
150.0	1.81	0.38	149.7	2.42	0.74	2.87	-18.6	0.37
155.0	2.03	0.30	154.4	2.70	0.57	2.99	-10.9	0.26

^{120}Sn NEUTRON INELASTIC SCATTERING CROSS SECTIONS

Neutron Energy ± Energy Spread	9.943 ± 0.071 MeV
Excitation Energy (J^{π})	2.400 MeV (3^-)
Integrated Cross Section	0.069 ± 0.004 barns
Zero Degree Cross Section	9.54 ± 0.91 mb/sr
Normalization Uncertainty	4.33 %
Chi-square/degree-of-freedom	0.168

ℓ-Value	A_ℓ	ΔA_ℓ	a_ℓ	Δa_ℓ	F-Value	F-Test
0	5.503	0.287	1.00000	0.00000	25.000	0.468
1	3.352	0.515	0.20304	0.03118	205.311	0.469
2	0.684	0.688	0.02484	0.02501	5.877	0.469

Uncorrected			Corrected			Calculation		
θ_{lab}	$\sigma(\theta_{lab})$	$\Delta\sigma_{lab}$	$\theta_{c.m.}$	$\sigma(\theta_{c.m.})$	$\Delta\sigma_{c.m.}$	$\sigma(\theta_{c.m.})$	%Dev.	χ^2
32.0	7.67	0.71	32.4	8.95	1.50	8.72	2.5	0.02
35.0	6.92	0.74	35.5	8.03	1.57	8.57	-6.8	0.12
40.0	6.65	0.68	40.6	7.86	1.49	8.30	-5.6	0.09
45.0	7.35	0.83	45.6	8.88	1.85	8.01	9.8	0.22
50.0	6.44	0.72	50.5	7.83	1.59	7.71	1.5	0.01
55.0	6.07	1.30	55.4	7.43	2.90	7.39	0.5	0.00
60.0	5.86	1.05	60.4	7.09	2.30	7.07	0.2	0.00
65.0	5.90	1.24	65.3	6.95	2.64	6.74	3.1	0.01
70.0	5.46	1.10	70.4	6.20	2.26	6.40	-3.2	0.01
75.0	4.60	0.69	75.5	5.30	1.42	6.07	-14.5	0.29
80.0	4.82	0.57	80.5	5.63	1.19	5.74	-2.0	0.01
85.0	5.54	0.68	85.4	6.47	1.40	5.44	16.0	0.55
90.0	4.72	0.67	90.3	5.50	1.39	5.14	6.5	0.07
95.0	4.91	0.58	95.3	5.70	1.22	4.86	14.6	0.47
100.0	3.67	0.71	100.2	4.28	1.50	4.60	-7.4	0.04
105.0	3.47	0.50	105.2	4.03	1.07	4.35	-8.1	0.09
110.0	3.58	0.54	110.2	4.11	1.16	4.13	-0.3	0.00
115.0	3.30	0.46	115.2	3.81	0.99	3.92	-3.0	0.01
120.0	2.80	0.44	120.2	3.29	0.96	3.74	-13.7	0.22
125.0	2.99	0.49	125.1	3.56	1.10	3.57	-0.5	0.00
130.0	2.49	0.94	130.1	2.97	2.09	3.43	-15.4	0.05
135.0	2.63	0.54	135.0	3.20	1.23	3.30	-3.3	0.01
140.0	2.94	0.48	139.9	3.58	1.09	3.20	10.7	0.12
145.0	1.91	0.50	144.9	2.33	1.15	3.11	-33.3	0.45
150.0	3.51	0.56	149.8	4.32	1.29	3.03	29.8	0.99
155.0	2.27	0.65	154.6	2.81	1.49	2.97	-5.7	0.01

^{120}Sn NEUTRON ELASTIC SCATTERING CROSS SECTIONS

Neutron Energy ± Energy Spread	13.923 ± 0.047 MeV
Excitation Energy (J^{π})	0.000 MeV (0^+)
Total Cross Section	4.540 ± 0.227 barns
Integrated Cross Section	2.365 ± 0.095 barns
Calculated Wick's Limit	8696.81 ± 869.7 mb/sr
Zero Degree Cross Section	7895.45 PM88126.45 mb/sr
Normalization Uncertainty	4.29 %
Chi-square/degree-of-freedom	0.870

ℓ-Value	A_ℓ	ΔA_ℓ	a_ℓ	Δa_ℓ	F-Value	F-Test
0	188.22	7.527	1.00000	0.00000	30.000	0.466
1	502.65	21.798	0.89018	0.03860	4.917	0.466
2	749.56	34.119	0.79647	0.03625	2.773	0.466
3	907.39	43.291	0.68870	0.03286	1.106	0.466
4	992.52	48.928	0.58591	0.02888	8.287	0.467
5	1000.12	50.617	0.48305	0.02445	0.917	0.468
6	957.18	48.925	0.39119	0.01999	7.889	0.469
7	856.62	44.415	0.30341	0.01573	0.186	0.469
8	688.61	37.867	0.21521	0.01183	16.861	0.470
9	483.13	30.075	0.13510	0.00841	2.589	0.471
10	307.96	21.859	0.07791	0.00553	4.638	0.472
11	170.36	14.456	0.03935	0.00334	59.590	0.473
12	66.57	7.802	0.01415	0.00166	5.509	0.474
13	24.56	3.365	0.00483	0.00066	51.353	0.475

Uncorrected			Corrected			Calculation		
θ_{lab}	$\sigma(\theta_{lab})$	$\Delta\sigma_{lab}$	$\theta_{c.m.}$	$\sigma(\theta_{c.m.})$	$\Delta\sigma_{c.m.}$	$\sigma(\theta_{c.m.})$	%Dev.	χ^2
24.0	707.92	31.67	23.3	1185.83	73.11	1156.54	2.5	0.16
28.0	277.64	15.80	26.8	500.86	37.96	522.54	-4.3	0.33
32.0	98.49	6.46	30.6	151.40	15.11	163.28	-7.8	0.62
36.0	45.25	5.07	36.3	32.95	6.46	27.11	17.7	0.82
40.0	48.94	2.49	41.3	66.20	4.69	67.34	-1.7	0.06
45.0	67.45	4.26	45.8	100.39	7.36	100.77	-0.4	0.00
50.0	64.24	3.79	50.3	95.12	6.28	99.54	-4.6	0.49
55.0	48.47	3.53	55.0	71.67	5.89	74.28	-3.7	0.20
60.0	33.71	1.75	59.7	49.53	3.10	46.08	7.0	1.24
65.0	18.42	1.01	64.6	26.02	1.76	26.08	-0.2	0.00
70.0	10.41	0.80	69.6	13.54	1.38	14.03	-3.6	0.12
75.0	6.05	0.54	75.0	6.94	0.86	7.15	-3.1	0.06
80.0	5.59	0.62	80.7	6.58	0.99	5.95	9.6	0.40
85.0	7.34	0.90	86.0	9.98	1.54	9.82	1.6	0.01
90.0	9.85	0.74	90.8	14.14	1.26	14.84	-5.0	0.31
95.0	11.95	0.74	95.5	17.25	1.23	18.09	-4.9	0.46
100.0	12.94	0.31	100.2	18.66	0.53	18.30	1.9	0.47
105.0	10.08	0.60	104.9	14.49	1.01	15.61	-7.7	1.23
110.0	8.09	0.39	109.6	11.57	0.68	11.07	4.3	0.52
115.0	4.31	0.38	114.4	5.71	0.68	6.20	-8.6	0.52
120.0	3.17	0.21	120.0	3.22	0.43	3.04	5.4	0.16
125.0	3.59	0.29	125.9	4.75	0.51	5.20	-9.4	0.76
130.0	6.83	0.32	130.7	10.22	0.56	9.51	7.0	1.63
135.0	8.02	0.47	135.2	11.83	0.82	12.37	-4.5	0.43
140.0	7.21	0.61	139.7	10.54	1.05	11.77	-11.7	1.38
145.0	6.58	0.38	144.4	8.89	0.65	8.41	5.4	0.53
150.0	5.02	0.40	149.9	5.91	0.60	6.03	-1.9	0.04
155.0	6.79	0.36	155.3	9.55	0.61	9.53	0.2	0.00

^{120}Sn NEUTRON INELASTIC SCATTERING CROSS SECTIONS

Neutron Energy ± Energy Spread	13.923 ± 0.047 MeV
Excitation Energy (J^{π})	1.171 MeV (2^{+})
Integrated Cross Section	0.051 ± 0.004 barns
Zero Degree Cross Section	17.08 ± 3.44 mb/sr
Normalization Uncertainty	4.29 %
Chi-square/degree-of-freedom	1.302

ℓ-Value	A_ℓ	ΔA_ℓ	a_ℓ	Δa_ℓ	F-Value	F-Test
0	4.063	0.335	1.00000	0.00000	28.000	0.466
1	4.763	0.837	0.39072	0.06869	6.523	0.466
2	3.490	1.188	0.17180	0.05846	25.822	0.467
3	-0.402	1.422	-0.01414	0.05000	1.354	0.468
4	-1.181	1.447	-0.03231	0.03957	3.032	0.469
5	-0.776	1.283	-0.01737	0.02870	1.518	0.469
6	0.501	1.323	0.00949	0.02504	16.444	0.470
7	4.334	1.221	0.07110	0.02004	2.550	0.471
8	2.291	0.789	0.03316	0.01142	6.479	0.472

Uncorrected			Corrected			Calculation		
θ_{lab}	$\sigma(\theta_{lab})$	$\Delta\sigma_{lab}$	$\theta_{c.m.}$	$\sigma(\theta_{c.m.})$	$\Delta\sigma_{c.m.}$	$\sigma(\theta_{c.m.})$	%Dev.	χ^2
40.0	8.31	0.69	40.4	9.06	1.14	9.56	-5.5	0.19
45.0	10.91	1.78	45.8	13.56	3.19	10.37	23.5	1.00
50.0	9.72	1.96	50.5	13.26	3.74	10.25	22.7	0.65
55.0	7.58	1.98	55.1	10.51	3.78	9.24	12.1	0.11
60.0	4.68	0.92	59.8	6.46	1.76	7.52	-16.4	0.36
65.0	3.56	0.87	64.7	4.56	1.58	5.36	-17.7	0.26
70.0	2.60	0.58	70.2	2.95	0.97	3.22	-8.9	0.07
75.0	1.78	0.49	75.6	2.26	0.92	1.96	13.1	0.10
80.0	1.82	0.44	80.3	2.44	0.88	1.63	33.3	0.85
85.0	2.02	1.10	85.1	2.60	2.06	1.86	28.5	0.13
90.0	1.99	0.45	90.3	2.36	0.76	2.37	-0.4	0.00
95.0	2.00	0.54	95.6	2.52	0.96	2.72	-8.3	0.05
100.0	1.53	0.14	100.5	2.07	0.29	2.64	-27.2	3.86
105.0	2.58	0.24	105.2	3.60	0.49	2.18	39.4	8.34
110.0	1.30	0.18	109.7	1.81	0.36	1.54	14.8	0.55
115.0	1.33	0.23	114.2	1.83	0.48	0.94	48.5	3.40
120.0	0.40	0.09	119.2	0.38	0.14	0.53	-39.6	1.11
125.0	0.72	0.15	126.2	0.78	0.30	0.68	12.1	0.10
130.0	0.72	0.15	131.1	1.06	0.34	1.22	-15.2	0.22
135.0	1.51	0.26	135.7	2.21	0.54	1.84	16.7	0.46
140.0	2.13	0.35	140.3	3.08	0.70	2.41	21.9	0.92
145.0	2.17	0.30	144.9	3.15	0.59	2.77	12.0	0.41
150.0	2.07	0.30	149.5	3.00	0.59	2.87	4.3	0.05
155.0	1.43	0.26	154.1	2.01	0.52	2.72	-35.3	1.84

^{120}Sn NEUTRON INELASTIC SCATTERING CROSS SECTIONS

Neutron Energy ± Energy Spread	13.923 ± 0.047 MeV
Excitation Energy (J^{π})	2.400 MeV (3^-)
Integrated Cross Section	0.043 ± 0.002 barns
Zero Degree Cross Section	3.87 ± 1.81 mb/sr
Normalization Uncertainty	4.29 %
Chi-square/degree-of-freedom	0.700

ℓ-Value	A_ℓ	ΔA_ℓ	a_ℓ	Δa_ℓ	F-Value	F-Test
0	3.426	0.180	1.00000	0.00000	28.000	0.466
1	2.810	0.430	0.27345	0.04188	50.683	0.466
2	1.356	0.616	0.07915	0.03597	22.286	0.467
3	-0.069	0.740	-0.00290	0.03088	0.807	0.468
4	-0.400	0.810	-0.01299	0.02627	0.653	0.469
5	-0.695	0.807	-0.01844	0.02142	1.223	0.469
6	-1.478	0.710	-0.03319	0.01594	1.670	0.470
7	-1.081	0.570	-0.02105	0.01110	5.138	0.471

Uncorrected			Corrected			Calculation		
θ_{lab}	$\sigma(\theta_{lab})$	$\Delta\sigma_{lab}$	$\theta_{c.m.}$	$\sigma(\theta_{c.m.})$	$\Delta\sigma_{c.m.}$	$\sigma(\theta_{c.m.})$	%Dev.	χ^2
32.0	4.79	0.43	32.4	6.40	1.13	7.81	-22.1	1.56
36.0	7.01	0.58	36.4	9.26	1.45	7.55	18.4	1.39
40.0	6.49	0.53	40.3	8.39	1.31	7.05	15.9	1.04
45.0	6.66	1.01	45.3	8.28	2.41	6.21	25.0	0.74
50.0	4.89	0.64	50.4	6.20	1.56	5.31	14.4	0.33
55.0	2.91	0.25	55.4	3.66	0.59	4.53	-23.9	2.22
60.0	3.43	0.29	60.4	4.32	0.67	3.99	7.6	0.24
65.0	2.91	0.31	65.4	3.65	0.69	3.70	-1.5	0.01
70.0	2.81	0.27	70.4	3.60	0.61	3.60	0.1	0.00
75.0	3.09	0.31	75.4	4.02	0.72	3.57	11.2	0.40
80.0	3.34	0.32	80.4	4.34	0.73	3.51	19.3	1.30
85.0	2.44	0.26	85.4	3.14	0.60	3.33	-6.1	0.10
90.0	2.11	0.26	90.3	2.68	0.59	3.04	-13.3	0.36
95.0	1.61	0.26	95.3	2.02	0.59	2.66	-31.2	1.15
100.0	1.86	0.19	100.2	2.34	0.44	2.27	3.3	0.03
105.0	1.56	0.21	105.2	1.95	0.49	1.94	0.5	0.00
110.0	2.08	0.25	110.2	2.56	0.57	1.75	31.6	1.99
115.0	1.36	0.19	115.2	1.69	0.45	1.70	-1.0	0.00
120.0	1.29	0.18	120.2	1.58	0.41	1.77	-12.1	0.22
125.0	1.47	0.20	125.2	1.85	0.46	1.88	-1.6	0.00
130.0	1.53	0.23	130.2	1.92	0.53	1.98	-3.4	0.02
135.0	1.79	0.24	135.2	2.33	0.57	2.02	13.2	0.29
140.0	1.34	0.21	140.1	1.75	0.50	1.99	-13.7	0.23
145.0	1.17	0.26	144.9	1.53	0.61	1.91	-24.5	0.38
150.0	1.69	0.22	149.8	2.15	0.51	1.81	15.8	0.45
155.0	1.46	0.23	154.6	1.86	0.54	1.74	6.2	0.05

^{120}Sn NEUTRON ELASTIC SCATTERING CROSS SECTIONS

Neutron Energy ± Energy Spread	16.905 ± 0.039 MeV
Excitation Energy (J^{π})	0.000 MeV (0^{+})
Total Cross Section	4.400 ± 0.110 barns
Integrated Cross Section	2.388 ± 0.066 barns
Calculated Wick's Limit	9918.27 ± 495.9 mb/sr
Zero Degree Cross Section	8935.60 ± 92.62 mb/sr
Normalization Uncertainty	8.69 %
Chi-square/degree-of-freedom	2.549

ℓ-Value	A_ℓ	ΔA_ℓ	a_ℓ	Δa_ℓ	F-Value	F-Test
0	190.00	5.271	1.00000	0.00000	32.000	0.464
1	512.33	15.345	0.89881	0.02692	17.849	0.465
2	774.13	23.880	0.81485	0.02514	2.960	0.466
3	965.54	30.473	0.72595	0.02291	0.812	0.466
4	1079.74	34.424	0.63141	0.02013	0.357	0.466
5	1105.90	36.033	0.52913	0.01724	1.853	0.466
6	1061.09	35.142	0.42958	0.01423	3.290	0.467
7	951.28	32.508	0.33378	0.01141	0.767	0.468
8	791.16	28.493	0.24494	0.00882	6.252	0.469
9	591.13	23.830	0.16374	0.00660	9.900	0.469
10	408.67	18.829	0.10242	0.00472	6.433	0.470
11	267.11	13.712	0.06112	0.00314	8.866	0.471
12	151.13	9.237	0.03182	0.00194	4.184	0.472
13	71.28	5.243	0.01389	0.00102	76.954	0.473
14	15.11	2.658	0.00274	0.00048	11.446	0.474

Uncorrected			Corrected			Calculation		
θ_{lab}	$\sigma(\theta_{lab})$	$\Delta\sigma_{lab}$	$\theta_{c.m.}$	$\sigma(\theta_{c.m.})$	$\Delta\sigma_{c.m.}$	$\sigma(\theta_{c.m.})$	%Dev.	χ^2
20.0	1873.22	128.97	19.6	3107.80	289.90	2137.10	31.2	11.21
22.5	843.74	43.60	21.8	1461.87	106.64	1445.29	1.1	0.02
25.0	476.43	24.28	24.0	824.09	63.67	912.99	-10.8	1.95
27.5	248.55	14.37	26.2	430.78	35.61	524.47	-21.7	6.92
30.0	141.71	6.64	28.4	244.92	17.12	266.36	-8.8	1.57
35.0	30.84	1.10	34.4	20.74	1.63	19.44	6.2	0.64
40.0	27.48	2.10	41.3	32.26	4.00	40.02	-24.1	3.77
45.0	35.74	1.68	45.7	48.93	2.88	53.40	-9.1	2.41
50.0	37.83	0.95	50.4	52.82	1.57	50.21	5.0	2.77
55.0	31.79	1.02	55.2	44.76	1.65	44.02	1.6	0.20
60.0	26.11	0.83	60.1	37.01	1.36	39.20	-5.9	2.61
65.0	21.65	1.23	64.9	31.28	2.11	30.27	3.2	0.23
70.0	12.77	0.65	69.6	18.23	1.18	17.62	3.3	0.27
75.0	7.76	0.42	74.9	8.59	0.65	8.47	1.4	0.03
80.0	9.14	0.69	81.1	11.80	1.17	12.60	-6.8	0.48
85.0	13.08	0.56	85.9	19.89	0.99	20.20	-1.6	0.10
90.0	15.97	0.95	90.4	24.31	1.62	22.94	5.6	0.72
95.0	15.06	1.19	94.9	22.45	2.03	20.01	10.9	1.45
100.0	10.18	0.41	99.7	14.07	0.69	14.51	-3.1	0.40
105.0	8.99	0.90	105.0	11.53	1.42	10.55	8.5	0.48
110.0	6.64	0.33	110.1	8.97	0.55	9.23	-2.9	0.22
115.0	6.19	0.21	115.0	8.51	0.36	8.34	1.9	0.21
120.0	5.64	0.36	120.1	7.37	0.57	7.49	-1.7	0.05
125.0	5.95	0.33	125.4	7.84	0.54	8.17	-4.2	0.38
130.0	7.43	0.32	130.3	10.54	0.54	10.05	4.7	0.84
135.0	6.52	0.72	134.9	9.14	1.23	10.79	-18.1	1.80
140.0	6.63	0.42	139.5	9.18	0.72	9.03	1.7	0.05
145.0	4.62	0.69	144.3	5.75	1.16	5.57	3.1	0.02
150.0	3.43	0.31	149.9	3.62	0.47	3.68	-1.7	0.02
155.0	5.00	0.33	155.4	6.61	0.56	6.56	0.8	0.01

^{120}Sn NEUTRON INELASTIC SCATTERING CROSS SECTIONS

Neutron Energy ± Energy Spread	16.905 ± 0.039 MeV
Excitation Energy (J^{π})	1.171 MeV (2^{+})
Integrated Cross Section	0.030 ± 0.001 barns
Zero Degree Cross Section	5.79 ± 0.35 mb/sr
Normalization Uncertainty	8.69 %
Chi-square/degree-of-freedom	2.562

ℓ-Value	A_ℓ	ΔA_ℓ	a_ℓ	Δa_ℓ	F-Value	F-Test
0	2.369	0.115	1.00000	0.00000	26.000	0.467
1	1.957	0.214	0.27536	0.03015	13.426	0.468
2	1.467	0.248	0.12386	0.02090	13.713	0.469

Uncorrected			Corrected			Calculation		
θ_{lab}	$\sigma(\theta_{lab})$	$\Delta\sigma_{lab}$	$\theta_{c.m.}$	$\sigma(\theta_{c.m.})$	$\Delta\sigma_{c.m.}$	$\sigma(\theta_{c.m.})$	%Dev.	χ^2
35.0	2.21	0.48	35.7	2.14	0.67	4.67	-118.4	14.11
40.0	4.18	0.94	41.1	5.95	1.81	4.36	26.7	0.77
45.0	2.08	0.49	45.7	3.15	1.02	4.08	-29.3	0.82
50.0	4.07	0.31	50.3	6.15	0.66	3.78	38.5	12.81
55.0	2.22	0.34	55.1	3.35	0.70	3.48	-3.9	0.04
60.0	2.96	0.33	60.1	4.22	0.67	3.16	25.1	2.53
65.0	1.00	0.31	65.2	1.43	0.61	2.84	-99.3	5.44
70.0	1.66	0.38	70.4	2.41	0.75	2.54	-5.4	0.03
75.0	2.22	0.18	75.3	3.63	0.44	2.27	37.3	9.41
80.0	0.80	0.24	80.2	1.27	0.53	2.03	-59.5	2.07
85.0	1.31	0.12	85.2	2.02	0.25	1.82	10.3	0.68
90.0	0.87	0.26	90.2	1.26	0.52	1.63	-29.1	0.50
95.0	1.21	0.22	95.3	1.91	0.48	1.47	23.0	0.84
100.0	1.33	0.16	100.2	2.11	0.37	1.36	35.6	4.02
105.0	0.73	0.15	105.1	1.14	0.34	1.28	-11.6	0.15
110.0	0.66	0.13	110.0	0.99	0.28	1.22	-23.9	0.72
115.0	0.75	0.05	115.1	1.06	0.10	1.20	-13.8	1.93
120.0	0.86	0.12	120.3	1.23	0.29	1.21	1.6	0.00
125.0	0.96	0.13	125.4	1.36	0.30	1.24	8.7	0.15
130.0	0.90	0.15	130.2	1.27	0.35	1.29	-1.1	0.00
135.0	0.90	0.21	135.1	1.32	0.51	1.35	-2.5	0.00
140.0	1.31	0.24	140.0	1.84	0.53	1.43	22.5	0.60
145.0	1.45	0.19	145.0	1.96	0.39	1.51	23.1	1.36
150.0	1.01	0.18	150.0	1.36	0.35	1.59	-16.7	0.42
155.0	1.71	0.24	154.9	2.35	0.48	1.67	28.9	1.96

^{120}Sn NEUTRON INELASTIC SCATTERING CROSS SECTIONS

Neutron Energy ± Energy Spread	16.905 ± 0.039 MeV
Excitation Energy (J^{π})	2.400 MeV (3^-)
Integrated Cross Section	0.054 ± 0.003 barns
Zero Degree Cross Section	11.91 ± 0.68 mb/sr
Normalization Uncertainty	8.69 %
Chi-square/degree-of-freedom	1.518

ℓ-Value	A_ℓ	ΔA_ℓ	a_ℓ	Δa_ℓ	F-Value	F-Test
0	4.317	0.249	1.00000	0.00000	25.000	0.468
1	4.941	0.464	0.38154	0.03585	25.138	0.469
2	2.650	0.433	0.12279	0.02006	24.680	0.469

Uncorrected			Corrected			Calculation		
θ_{lab}	$\sigma(\theta_{lab})$	$\Delta\sigma_{lab}$	$\theta_{c.m.}$	$\sigma(\theta_{c.m.})$	$\Delta\sigma_{c.m.}$	$\sigma(\theta_{c.m.})$	%Dev.	χ^2
27.5	10.13	0.55	27.7	13.03	1.35	10.48	19.6	3.59
30.0	11.19	2.22	30.2	14.32	5.36	10.23	28.6	0.58
35.0	6.12	0.62	35.4	7.81	1.46	9.66	-23.7	1.60
40.0	6.82	1.89	40.5	8.96	4.47	9.05	-1.0	0.00
45.0	7.02	1.35	45.4	9.53	3.26	8.42	11.7	0.12
50.0	6.63	0.89	50.3	9.18	2.16	7.77	15.4	0.43
55.0	6.10	1.71	55.3	8.50	4.21	7.10	16.5	0.11
60.0	3.44	0.54	60.2	4.83	1.34	6.43	-33.0	1.41
65.0	3.78	0.70	65.3	5.29	1.76	5.75	-8.7	0.07
70.0	3.26	0.81	70.4	4.55	2.02	5.10	-12.1	0.07
75.0	3.69	0.61	75.3	5.20	1.54	4.50	13.6	0.21
80.0	2.88	1.18	80.3	4.10	2.96	3.94	4.0	0.00
85.0	2.74	0.42	85.1	3.92	1.08	3.44	12.2	0.20
90.0	1.54	0.28	89.9	2.22	0.71	3.00	-35.2	1.19
95.0	2.07	0.49	94.8	2.92	1.27	2.61	10.7	0.06
100.0	0.99	0.18	100.0	1.25	0.44	2.25	-80.8	5.21
105.0	1.51	0.62	105.6	1.94	1.52	1.95	-0.7	0.00
110.0	0.84	0.16	110.7	1.20	0.46	1.74	-45.2	1.40
115.0	1.89	0.13	115.5	2.77	0.35	1.60	42.1	11.06
120.0	1.46	0.34	120.2	2.13	0.90	1.51	28.9	0.46
125.0	1.86	0.25	124.9	2.57	0.62	1.47	42.9	3.12
130.0	1.20	0.24	129.7	1.55	0.57	1.46	6.2	0.03
140.0	0.79	0.26	139.8	0.83	0.52	1.54	-85.6	1.83
145.0	0.80	0.23	145.3	0.90	0.50	1.62	-80.1	2.03
150.0	1.48	0.27	150.3	1.92	0.65	1.70	11.6	0.12
155.0	1.28	0.21	155.0	1.74	0.52	1.78	-2.0	0.00

C.3 Analyzing Power Tabulations

Tabulations of the uncorrected and corrected $A_y(\theta)$ data for $^{116,120}Sn$ and the coefficients derived from associated Legendre polynomial fits to the product $A_y(\theta) \times \sigma(\theta)$ are contained in this section. The $\sigma(\theta)$ used in this product were calculated from the Legendre polynomial coefficients listed in section C.2. The corrected $A_y(\theta)$ data and the fits are shown in figure C.4. The $A_y(\theta)$ data are for the elastic scattering of 10 and 14 MeV neutrons from both isotopes. The 14 MeV distribution for ^{116}Sn consists of data at only six angles. There are also $A_y(\theta)$ data at five angles for the inelastic scattering of 10 MeV neutrons to the 2^+ and 3^- states of ^{120}Sn. The differences between the new and old corrected $A_y(\theta)$ data for elastic scattering range from 0.00 to ± 0.21 in magnitude; as expected, the data points that had large magnitudes tended to increase after the new calculations, while those with small magnitudes changed little. The inelastic $A_y(\theta)$ data changed less than ± 0.02 in magnitude. Note that two new measurements, one at 70° and the other at 80°, are included in each of the $A_y(\theta)$ data sets for ^{120}Sn at 10 MeV. These new data were taken in the summer of 1982. The new elastic scattering data supersede the data in Guss 1982a and have much smaller uncertainties. The new inelastic scattering data supplement the existing inelastic data in Guss 1982a. The symbols and terms used in the tabulations are the same as those defined at the beginning of appendix B.

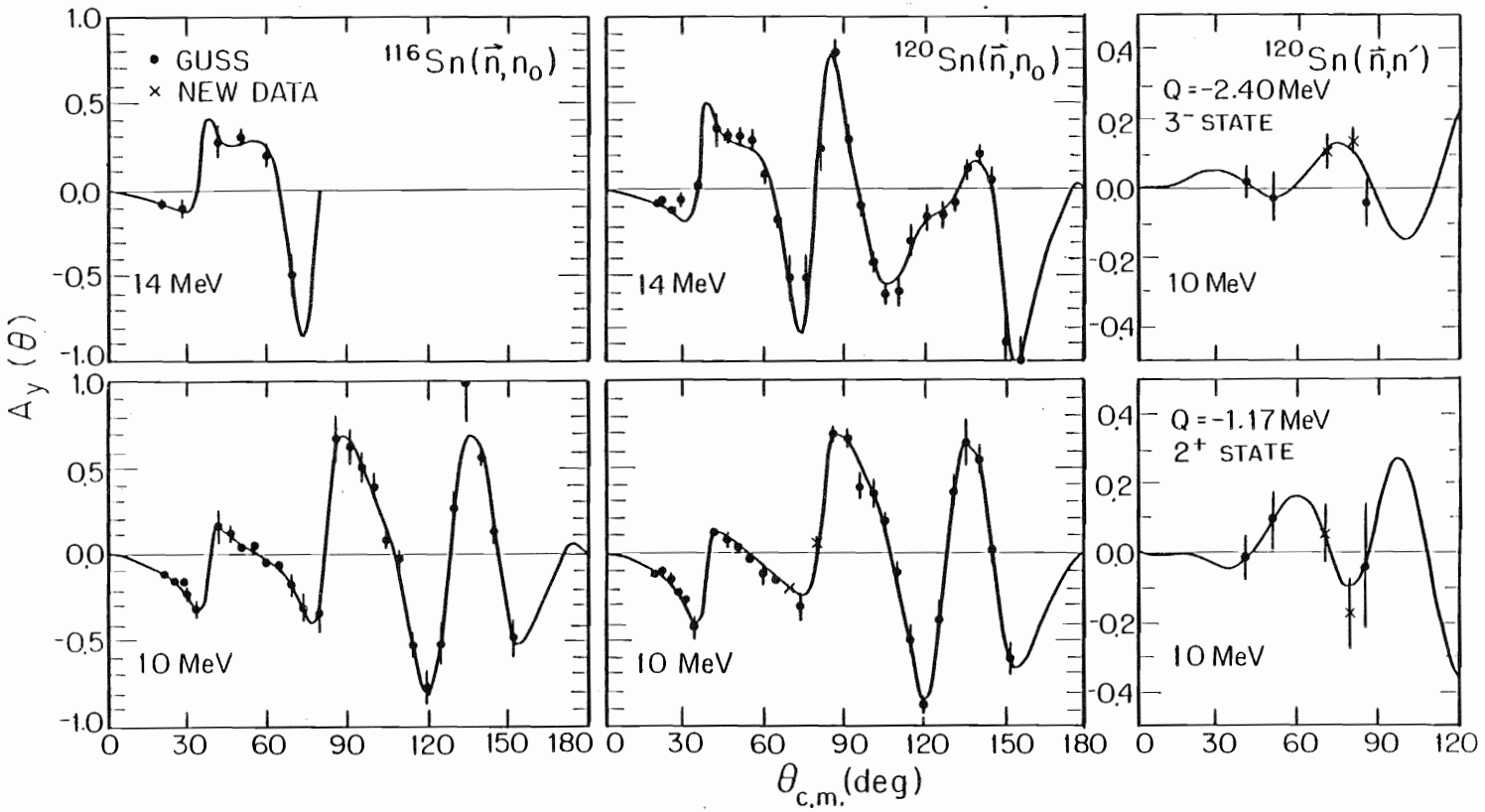

Figure C.4. The $A_y(\theta)$ data for the elastic scattering of neutrons from $^{116,120}Sn$ and for the inelastic scattering of neutrons to the first 2^+ and 3^- states of ^{120}Sn. The curves are derived from associated Legendre polynomial fits to the product $A_y(\theta) \times \sigma(\theta)$.

^{116}Sn NEUTRON ELASTIC SCATTERING ANALYZING POWERS

Neutron Energy ± Energy Spread: 9.907 ± 0.232 MeV
Excitation Energy (J^{π}): 0.000 MeV (0^+)

Normalization ± Calibration Error: 1.00 ± 0.030
Chi-square/degree-of-freedom: 0.391

f-Value	B_f	ΔB_f	Ratio	F-Value	F-Test
1	-3.6108	0.6506	1.0000	27.000	0.466
2	-6.6914	0.7351	1.8531	0.001	0.467
3	-9.1393	0.6830	2.5311	0.717	0.468
4	-8.5224	0.7969	2.3602	3.129	0.469
5	-8.4805	0.7359	2.3486	0.028	0.469
6	-9.0920	0.8495	2.5180	0.096	0.470
7	-8.5053	0.7094	2.3555	253.263	0.471
8	-3.2433	0.6999	0.8982	5.718	0.472
9	-1.2866	0.4397	0.3563	0.003	0.473
10	-1.4492	0.3404	0.4013	29.160	0.474

Uncorrected			Corrected			Calculation		
θ_{lab}	$A_y(\theta_{lab})$	$\Delta A_{y\,lab}$	$\theta_{c.m.}$	$A_y(\theta_{c.m.})$	$\Delta A_{y\,c.m.}$	$A_y(\theta_{c.m.})$	Dev.	χ^2
22.0	-0.109	0.022	21.8	-0.113	0.023	-0.093	-0.020	0.81
26.0	-0.144	0.027	25.4	-0.148	0.029	-0.125	-0.022	0.61
30.0	-0.150	0.015	28.8	-0.156	0.016	-0.173	0.016	1.06
32.0	-0.200	0.035	30.6	-0.223	0.039	-0.209	-0.014	0.13
35.0	-0.211	0.046	33.8	-0.317	0.056	-0.295	-0.023	0.17
40.0	0.043	0.065	41.6	0.172	0.088	0.171	0.001	0.00
45.0	0.114	0.036	46.5	0.127	0.039	0.115	0.013	0.10
50.0	0.049	0.022	50.9	0.047	0.024	0.065	-0.018	0.58
55.0	0.052	0.026	55.4	0.051	0.027	0.024	0.027	1.01
60.0	-0.036	0.035	60.0	-0.040	0.037	-0.018	-0.022	0.35
65.0	-0.066	0.028	64.7	-0.065	0.030	-0.074	0.008	0.08
70.0	-0.158	0.051	69.4	-0.168	0.058	-0.159	-0.009	0.02
75.0	-0.246	0.068	74.1	-0.309	0.086	-0.299	-0.010	0.01
80.0	-0.154	0.086	79.4	-0.347	0.110	-0.337	-0.010	0.01
85.0	0.393	0.089	86.0	0.668	0.125	0.625	0.043	0.12
90.0	0.520	0.086	91.2	0.626	0.100	0.664	-0.038	0.15
95.0	0.457	0.079	95.7	0.508	0.086	0.519	-0.012	0.02
100.0	0.359	0.069	100.4	0.399	0.075	0.346	0.053	0.50
105.0	0.059	0.054	105.1	0.075	0.059	0.143	-0.068	1.34
110.0	-0.039	0.066	109.8	-0.026	0.070	-0.119	0.093	1.74
115.0	-0.474	0.078	114.5	-0.524	0.088	-0.466	-0.057	0.43
120.0	-0.597	0.087	119.5	-0.770	0.101	-0.793	0.023	0.05
125.0	-0.378	0.121	124.9	-0.521	0.141	-0.510	-0.011	0.01
130.0	0.165	0.096	130.1	0.265	0.112	0.300	-0.035	0.10
135.0	0.865	0.273	135.0	1.000	0.243	0.686	0.314	1.67
140.0	0.425	0.098	139.8	0.566	0.115	0.606	-0.039	0.12
145.0	0.098	0.102	144.8	0.131	0.114	0.129	0.003	0.00
152.0	-0.389	0.112	151.9	-0.484	0.124	-0.488	0.004	0.00

^{120}Sn NEUTRON ELASTIC SCATTERING ANALYZING POWERS

Neutron Energy ± Energy Spread 9.906 ± 0.232 MeV
Excitation Energy (J^{π}) 0.000 MeV (0^+)

Normalization ± Calibration Error 1.00 ± 0.030
Chi-square/degree-of-freedom 0.374

f-Value	B_f	ΔB_f	Ratio	F-Value	F-Test
1	-6.3331	0.4890	1.0000	28.000	0.466
2	-10.7357	0.5991	1.6952	0.000	0.466
3	-13.9687	0.6166	2.2057	0.505	0.467
4	-12.2837	0.6702	1.9396	0.013	0.468
5	-12.0130	0.6000	1.8969	4.870	0.469
6	-12.0291	0.5881	1.8994	0.242	0.469
7	-11.8564	0.4380	1.8721	99.519	0.470
8	-5.6132	0.4144	0.8863	12.112	0.471
9	-2.6081	0.2562	0.4118	12.607	0.472
10	-1.8721	0.2226	0.2956	127.176	0.473

Uncorrected			Corrected			Calculation		
θ_{lab}	$A_y(\theta_{lab})$	$\Delta A_{y\,lab}$	$\theta_{c.m.}$	$A_y(\theta_{c.m.})$	$\Delta A_{y\,c.m.}$	$A_y(\theta_{c.m.})$	Dev.	χ^2
20.0	-0.111	0.007	20.0	-0.116	0.007	-0.110	-0.006	0.70
22.0	-0.093	0.022	21.9	-0.096	0.023	-0.128	0.032	1.93
26.0	-0.141	0.031	25.4	-0.144	0.033	-0.171	0.028	0.72
30.0	-0.222	0.026	28.9	-0.232	0.029	-0.239	0.007	0.06
32.0	-0.240	0.031	30.6	-0.262	0.035	-0.288	0.026	0.54
35.0	-0.265	0.044	33.9	-0.432	0.061	-0.406	-0.027	0.19
40.0	-0.001	0.011	41.4	0.126	0.017	0.130	-0.004	0.06
45.0	0.069	0.037	46.5	0.084	0.041	0.091	-0.007	0.03
50.0	0.045	0.008	50.6	0.045	0.009	0.038	0.007	0.57
55.0	-0.023	0.029	55.3	-0.026	0.031	-0.014	-0.012	0.15
60.0	-0.112	0.049	60.0	-0.116	0.053	-0.064	-0.052	0.98
65.0	-0.148	0.037	64.6	-0.154	0.041	-0.121	-0.034	0.68
70.0	-0.180	0.010	69.5	-0.193	0.012	-0.194	0.001	0.00
75.0	-0.229	0.063	74.0	-0.305	0.081	-0.256	-0.049	0.37
80.0	0.066	0.022	79.8	0.063	0.034	0.054	0.009	0.07
85.0	0.500	0.028	85.6	0.688	0.048	0.699	-0.011	0.05
90.0	0.558	0.061	90.9	0.658	0.071	0.639	0.018	0.07
95.0	0.349	0.069	95.7	0.388	0.077	0.492	-0.103	1.83
100.0	0.313	0.072	100.3	0.347	0.078	0.332	0.016	0.04
105.0	0.163	0.053	105.0	0.192	0.056	0.138	0.053	0.89
110.0	-0.121	0.066	109.7	-0.110	0.072	-0.125	0.015	0.04
115.0	-0.436	0.078	114.5	-0.497	0.089	-0.493	-0.004	0.00
120.0	-0.663	0.067	119.5	-0.888	0.085	-0.839	-0.048	0.32
125.0	-0.294	0.109	125.0	-0.390	0.133	-0.424	0.033	0.06
130.0	0.249	0.094	130.2	0.359	0.113	0.335	0.023	0.04
135.0	0.491	0.119	135.0	0.638	0.139	0.634	0.004	0.00
140.0	0.424	0.074	139.8	0.548	0.083	0.536	0.012	0.02
145.0	0.001	0.079	144.7	0.028	0.090	0.060	-0.032	0.13
152.0	-0.498	0.088	151.9	-0.606	0.097	-0.624	0.018	0.03

^{120}Sn NEUTRON ELASTIC SCATTERING ANALYZING POWERS

Neutron Energy ± Energy Spread 13.894 ± 0.155 MeV
Excitation Energy (J^{π}) 0.000 MeV (0^+)

Normalization ± Calibration Error 1.00 ± 0.030
Chi-square/degree-of-freedom 1.450

ℓ-Value	B_ℓ	ΔB_ℓ	Ratio	F-Value	F-Test
1	-2.7761	0.4779	1.0000	29.000	0.466
2	-2.3571	0.5743	0.8491	1.000	0.466
3	-6.2069	0.5740	2.2358	0.606	0.466
4	-9.1513	0.6180	3.2965	1.747	0.467
5	-11.3628	0.6053	4.0931	4.302	0.468
6	-10.2751	0.6168	3.7013	4.028	0.469
7	-10.2348	0.5258	3.6868	5.150	0.469
8	-6.5394	0.4840	2.3556	15.395	0.470
9	-3.0487	0.3721	1.0982	32.017	0.471
10	-1.7321	0.3521	0.6239	6.262	0.472
11	-1.6693	0.2127	0.6013	3.167	0.473
12	-1.4146	0.1802	0.5096	36.246	0.474

Uncorrected			Corrected			Calculation		
θ_{lab}	$A_y(\theta_{lab})$	ΔA_{ylab}	$\theta_{c.m.}$	$A_y(\theta_{c.m.})$	$\Delta A_{yc.m.}$	$A_y(\theta_{c.m.})$	Dev.	χ^2
20.0	-0.083	0.005	19.7	-0.090	0.006	-0.081	-0.009	1.98
22.0	-0.062	0.018	21.6	-0.066	0.019	-0.094	0.028	2.26
26.0	-0.108	0.017	24.9	-0.113	0.018	-0.123	0.010	0.28
30.0	-0.059	0.032	28.4	-0.062	0.038	-0.165	0.103	7.18
35.0	0.026	0.030	34.7	0.031	0.043	0.051	-0.020	0.21
40.0	0.245	0.072	41.6	0.347	0.097	0.376	-0.029	0.09
45.0	0.278	0.036	45.9	0.312	0.039	0.285	0.027	0.48
50.0	0.276	0.046	50.3	0.307	0.051	0.258	0.049	0.92
55.0	0.245	0.067	55.0	0.277	0.073	0.239	0.038	0.28
60.0	0.076	0.053	59.6	0.084	0.060	0.147	-0.063	1.09
65.0	-0.157	0.041	64.5	-0.181	0.047	-0.147	-0.034	0.52
70.0	-0.340	0.089	69.4	-0.515	0.137	-0.612	0.098	0.51
75.0	-0.272	0.092	74.8	-0.519	0.126	-0.750	0.231	3.33
80.0	0.123	0.104	80.7	0.238	0.126	0.517	-0.279	4.91
85.0	0.569	0.079	85.9	0.779	0.098	0.697	0.082	0.69
90.0	0.232	0.073	90.8	0.291	0.082	0.255	0.036	0.19
95.0	-0.074	0.057	95.5	-0.095	0.062	-0.144	0.049	0.63
100.0	-0.361	0.046	100.2	-0.424	0.051	-0.422	-0.002	0.00
105.0	-0.525	0.052	104.8	-0.605	0.058	-0.549	-0.056	0.91
110.0	-0.532	0.092	109.5	-0.594	0.100	-0.524	-0.070	0.49
115.0	-0.285	0.075	114.2	-0.305	0.088	-0.372	0.066	0.57
120.0	-0.194	0.063	120.0	-0.163	0.079	-0.166	0.003	0.00
125.0	-0.115	0.061	125.9	-0.148	0.072	-0.147	-0.001	0.00
130.0	-0.078	0.053	130.6	-0.080	0.059	-0.031	-0.050	0.72
135.0	0.098	0.045	135.1	0.117	0.052	0.091	0.026	0.26
140.0	0.141	0.050	139.5	0.204	0.057	0.169	0.035	0.37
145.0	-0.045	0.060	144.2	0.060	0.067	0.068	-0.008	0.01
150.0	-0.682	0.139	149.6	-0.886	0.164	-0.688	-0.198	1.46
155.0	-0.827	0.148	155.2	-1.000	0.148	-0.946	-0.054	0.13

^{116}Sn NEUTRON ELASTIC SCATTERING ANALYZING POWERS

Neutron Energy ± Energy Spread 13.894 ± 0.155 MeV
Excitation Energy (J^{π}) 0.000 MeV (0^{+})

Normalization ± Calibration Error 1.00 ± 0.030

Uncorrected			Corrected		
θ_{lab}	$A_y(\theta_{lab})$	$\Delta A_{y\,lab}$	$\theta_{c.m.}$	$A_y(\theta_{c.m.})$	$\Delta A_{y\,c.m.}$
22.0	-0.075	0.023	21.5	-0.080	0.025
30.0	-0.075	0.049	28.6	-0.100	0.055
40.0	0.232	0.080	41.6	0.282	0.098
50.0	0.293	0.044	50.5	0.306	0.048
60.0	0.160	0.071	59.7	0.203	0.077
70.0	-0.359	0.107	69.5	-0.493	0.132

^{120}Sn NEUTRON INELASTIC SCATTERING ANALYZING POWERS

Neutron Energy ± Energy Spread 9.906 ± 0.232 MeV
Excitation Energy (J^{π}) 1.171 MeV (2^{+})

Normalization ± Calibration Error 1.00 ± 0.030

Uncorrected			Corrected		
θ_{lab}	$A_y(\theta_{lab})$	$\Delta A_{y\,lab}$	$\theta_{c.m.}$	$A_y(\theta_{c.m.})$	$\Delta A_{y\,c.m.}$
40.0	-0.007	0.057	40.6	-0.015	0.064
50.0	0.091	0.073	50.4	0.097	0.079
70.0	0.057	0.075	70.0	0.062	0.083
80.0	-0.144	0.092	80.0	-0.174	0.104
85.0	-0.020	0.157	85.0	-0.040	0.175

^{120}Sn NEUTRON INELASTIC SCATTERING ANALYZING POWERS

Neutron Energy ± Energy Spread 9.906 ± 0.232 MeV
Excitation Energy (J^{π}) 2.400 MeV (3^{-})

Normalization ± Calibration Error 1.00 ± 0.030

Uncorrected			Corrected		
θ_{lab}	$A_y(\theta_{lab})$	$\Delta A_{y\,lab}$	$\theta_{c.m.}$	$A_y(\theta_{c.m.})$	$\Delta A_{y\,c.m.}$
40.0	0.016	0.049	40.4	0.017	0.054
50.0	-0.018	0.063	50.3	-0.025	0.069
70.0	0.097	0.042	70.2	0.108	0.047
80.0	0.126	0.036	80.2	0.142	0.041
85.0	-0.043	0.065	85.1	-0.045	0.072

APPENDIX D.

POLYETHYLENE CORRECTION FACTORS

D.1 Introduction

One of the parameters required in the normalization of $\sigma(\theta)$ data taken by the neutron time-of-flight group at TUNL is the polyethylene correction factor which is designated as $PCF(\theta_H)$ in equation 4.2. The $PCF(\theta_H)$ factor is used to correct $Y_H(\theta_H)$, the hydrogen yield from the difference spectra of the normalization measurements at angle θ_H, for efficiency, attenuation, finite geometry, and multiple scattering effects. The calculation of the $PCF(\theta_H)$ factors is done by using the Monte Carlo code EFFIGY15. The $PCF(\theta_H)$ factor is simply the ration of the known $\sigma(\theta)$ for hydrogen to the calculated yield from EFFIGY15 at the angle the normalization measurements were made θ_H.

As stated in Chapter 2, the difference spectra from the normalization measurements are calculated from in spectra taken using a polyethylene sample ($(CH_2)_n$) and from out spectra taken using a carbon sample. An example of a hydrogen difference spectrum is shown in figure D.1, together with the polyethylene in and carbon out spectra used to determine it.

The θ_H angle is the angle for which the resolution of the hydrogen peak and the elastic and inelastic (Q = -4.44 MeV) scattering carbon peaks is optimum for the incident neutron energy of the experiment. For the usual energies at which $\sigma(\theta)$ data for neutron scattering are taken at TUNL, the θ_H angles are 35° for 8 MeV, 32° for 10 MeV, 30° for 12 MeV, 28° for 14 MeV and 25° for 17 MeV.

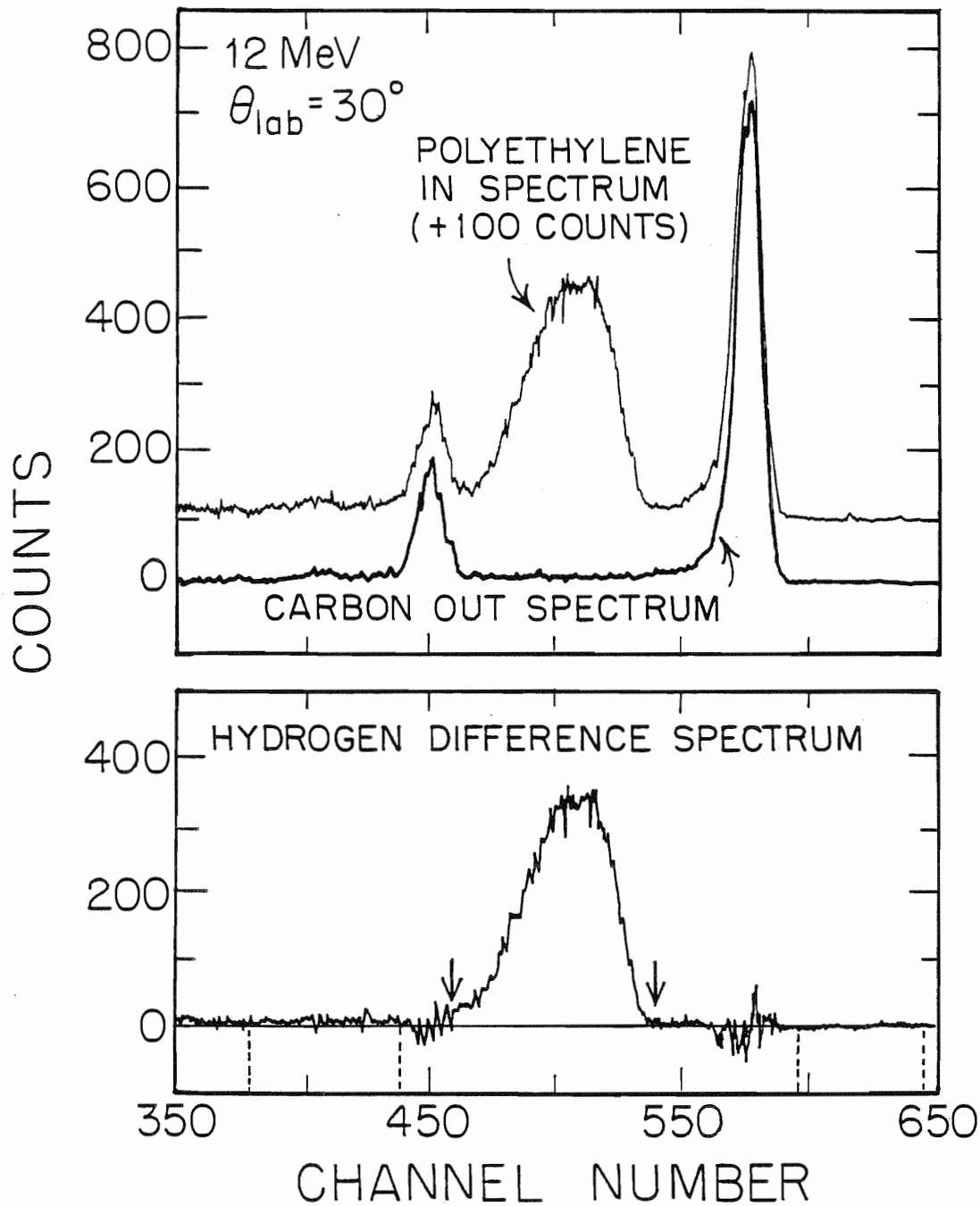

Figure D.1. Polyethylene in, carbon out, and hydrogen difference spectra for the right detector at 12 MeV and $\theta_{lab} = 30°$.

D.2 Calculation

It is not necessary to calculate the PCF(θ_H) factors every time experiments are done, but only to have a table of precalculated values since the $\sigma(\theta)$ measurements are usually performed at standard energies (8, 10, 12, 14, and 17 MeV) and since the θ_H angles and the physical parameters of the polyethylene and carbon samples and the gas cells are known. The procedure for the calculation is given in the users manual for EFFIGY15.

From 1979 to the present (1986), three polyethylene samples and two carbon samples have been used. The old and new large polyethylene samples have been paired with a large carbon sample and a small polyethylene sample has been paired with a small carbon sample. The old large polyethylene sample was used prior to November of 1980. The new large polyethylene sample has been in use since November of 1980. Note that the polyethylene and carbon samples are matched so that they both have approximately the same number of hydrogen atoms. The physical parameters for the polyethylene and carbon samples are given in table D-1. Note also that gas cell C has been used only with the new large polyethylene sample and gas cell B has been used with all three polyethylene samples.

Historical note, the new large polyethylene sample was made after the old large polyethylene sample was damaged when -- in an effort to save time in switching from a $A_y(\theta)$ experiment to a $\sigma(\theta)$ experiment -- an attempt was made to use gas cell B in a $\sigma(\theta)$ experiment. The sample was damaged when, due to a lack of air cooling, the epoxy seals for the tantalum end cap of gas cell B melted causing the end cap to fall off, and thus exposing the sample to the deuteron beam (i.e., there is now a large hole in the old sample).

TABLE D-1

Parameters for the Polyethylene and Carbon Samples

Parameter		Polyethylene			Carbon	
		Large New*	Large Old**	Small	Large	Small
mass+ (g)		3.373	3.410	0.721	2.913	0.561
diameter (cm)		1.435	1.430	0.592	0.954	0.405
height (cm)		2.279	2.314	2.791	2.376	2.542
volume++ (cm^3)		3.680	3.713	0.763	1.694	0.324
number of nuclei: ($\times 10^{23}$ nuclei)	C	1.448	1.464	0.309	1.461	0.281
	H	2.897	2.928	0.619		
density of nuclei: ($\times 10^{22}$ nuclei/cm^3)	C	3.936	3.943	4.056	8.621	8.673
	H	7.871	7.886	8.112		

* The new large polyethylene sample has been in use since November of 1980.

** The old large polyethylene sample was in use prior to November of 1980.

\+ The masses have been corrected for the masses of the air displaced by the samples on the scale in the weighing process.

++ The volumes have been corrected for the holes in the samples for the wires.

Note that chemical composition of polyethylene is taken to be $(CH_2)_n$.

The cross section library for the EFFIGY15 calculations contained the Hopkins and Breit hydrogen values (Yale phase shifts) (Hopkins 1971) and the $\sigma(\theta)$ data for carbon from 9 to 15 MeV of Glasgow (Glasgow 1976) and below 9 MeV and above 15 MeV values from ENDF/B-V. The total cross sections for hydrogen and carbon are from ENDF/B-V. The source reaction cross section library used the $\sigma(\theta)$ values for the $D(d,n)^3He$ reaction measured by M. Drosg (Drosg 1978).

Briefly, at energy, the procedure for calculating the $PCF(\theta_H)$ values is to run EFFIGY15 in its two element mode using the parameters for one of the polyethylene samples to generate calculated in spectra. Then, the code is run in its one element mode using the parameters of the matching carbon sample to generate calculated out spectra. The calculated out spectra are then subtracted from the calculated in spectra to obtain the calculated difference spectra. These calculated difference spectra are examined to determine window setting for the hydrogen peaks. The windows are then put into the input data set for the polyethylene sample, and the code is run again in the two element mode. However, this time it is also run in the subtraction mode. The code uses the calculated out spectra from a binary data file to calculate difference spectra from newly calculated in spectra. Then, the code sums the counts in the window settings to determine the calculated yield for hydrogen. The calculated yield for hydrogen is then used to calculate the ratio of the known $\sigma(\theta)$ to the calculated yield.

Values of $PCF(\theta_H)$ are tabulated in table D-2 for the new large polyethylene/carbon pair for measurements using gas cells A and C. No values are given for the old large polyethylene/carbon pair for an obvious reason. No values are given for the small polyethylene/carbon pair, since they have not been in recent use. This is because, due to their size, the

TABLE D-2

PCF(θ_H) Values for the New Large Polyethylene and Carbon Samples[a)]

En(MeV)	θ_H	PCF(θ_H)
	Gas Cell B (2.0 bar)	
8	35°	1.247 ± 0.017
10	32°	1.211 ± 0.016
12	30°	1.219 ± 0.016
14	28°	1.219 ± 0.017
	Gas Cell C (2.0 bar)	
8	35°	1.233 ± 0.016
10	32°	1.195 ± 0.016
11	29°	1.200 ± 0.016
12	30°	1.190 ± 0.016
14	28°	1.189 ± 0.016
17	25°	1.194 ± 0.018
	Gas Cell C (7.9 bar)	
17	25°	1.195 ± 0.018

a) The distance from the end of the gas target to the center of the scattering sample is 9.2 cm for these calculations. Note that the end of the gas target is not the outside end wall of the gas cell, it is the inside end wall of the gas cell.

counting rates for this pair are too low and because of the difficulty of obtaining successive measurements with this pair that are in agreement. The values given for the new polyethylene/carbon pair are the averages from several calculations in which the starting random number seeds were changed and the flight path of the detector was varied from 4 to 6 m.

The uncertainties quoted in table D-2 were determined from combining in quadrature the statistical uncertainties for the calculated yields, the uncertainties for the $\sigma(\theta)$ values for hydrogen, and uncertainties for the $\sigma(\theta)$ values for the $^{2}H(d,n)^{3}He$ reaction. The statistical uncertainties, in principle, can be made zero by running the code for enough neutron histories. For the calculations presented here, the statistical uncertainties (including an addition factor due to the dispersion in the values that were averaged) are all less that 0.25%. The uncertainties for the $\sigma(\theta)$ values for hydrogen are about 1.3%. Note that the $\sigma(\theta)$ for hydrogen used to calculate the $PCF(\theta_H)$ factor exactly cancels with the value in the $\sigma(\theta)$ data normalization calculations, so that the $\sigma(\theta)$ for hydrogen are only really needed to calculate the yields in EFFIGY15. For the $\sigma(\theta)$ values for the $^{2}H(d,n)^{3}He$ reaction, there is a cancellation to first order between the values used in calculating the $PCF(\theta_H)$ values and the values used in calculating corrections to $\sigma(\theta)$ data. For these $\sigma(\theta)$, maximum uncertainties of 25% of the uncertainties in the $\sigma(\theta)$ values tabulated by Drosg are used.

The contributions to the overall uncertainties due to uncertainties in the σ_T for hydrogen and carbon are negligible, since these values are used in calculating the transmissions through the scattering samples. For the transmissions calculated (90% or higher), there would have to be uncertainties greater than 15% in the σ_T to effect the $PCF(\theta_h)$ values.

Finally, there are negligible contributions to the overall uncertainties in the $\sigma(\theta)$ values for carbon, since for the worse case at 17 MeV multiple scatterings involving scattering from carbon only contribute about 2% of the counts in the region of the calculated hydrogen peak.

APPENDIX E.

EFFICIENCY DATA TABULATIONS

Tabulations of the efficiency data, which are presented in chapter 3, are given in this appendix. The data are shown in figures 3.6 and 3.7 for the right and left detectors, respectively. Definitions for terms used throughout this appendix are:

E_n = incident neutron energy.

$\varepsilon(E_n)_{exp}$ = measured efficiency at energy E_n.

$\Delta\varepsilon_{exp}$ = relative uncertainty in $\varepsilon(E_n)_{exp}$ in percent.

The calculations of the relative and normalization uncertainties are discussed in chapter 3.

The scintillator vessels for the right and left detectors of the neutron time-of-flight spectrometer are 4.45 and 6.35 cm in radius, respectively; both are 5.08 cm thick. The vessel for the right detector is filled with NE-218 liquid organic scintillator and coupled to a Phillips 58-DVP photomultiplier tube; that for the left detector is filled with NE-213 and coupled to a Amperex XP-2041 photomultiplier tube.

DATA SET 1: EFFICIENCY DATA FOR THE RIGHT DETECTOR

0.50×Cs Energy Bias

Normalization Uncertainty 4.11%
Proton Bias Energy 1.30 ± 0.15 MeV

E_n	$\varepsilon(E_n)_{exp}$	$\Delta\varepsilon_{exp}$	E_n	$\varepsilon(E_n)_{exp}$	$\Delta\varepsilon_{exp}$	E_n	$\varepsilon(E_n)_{exp}$	$\Delta\varepsilon_{exp}$
2.04	0.2588	1.26	9.98	0.2008	1.26	13.97	0.1804	1.54
2.15	0.2625	1.32	10.17	0.2034	0.86	14.16	0.1805	1.65
2.26	0.2775	1.31	10.36	0.2049	1.18	14.54	0.1781	1.87
2.55	0.3054	1.56	10.55	0.2008	1.18	14.73	0.1804	1.98
2.93	0.2986	1.55	10.74	0.1962	1.18	14.92	0.1804	2.10
3.14	0.2797	2.11	10.93	0.1950	1.18	15.11	0.1789	2.17
3.39	0.2974	1.49	11.13	0.1903	1.16	15.30	0.1752	2.24
3.94	0.2747	1.45	11.32	0.1914	1.18	15.48	0.1713	2.31
4.59	0.2820	1.34	11.51	0.1900	1.18	15.67	0.1728	2.38
5.31	0.2674	1.34	11.70	0.1893	1.18	15.86	0.1734	2.45
6.08	0.2488	1.31	11.89	0.1808	1.18	16.05	0.1758	2.52
6.86	0.2458	1.34	12.08	0.1804	1.18	16.24	0.1720	2.59
7.24	0.2355	1.55	12.27	0.1856	1.18	16.43	0.1773	2.66
7.61	0.2275	1.58	12.46	0.1837	1.18	16.62	0.1789	2.73
8.26	0.2289	1.36	12.65	0.1816	1.18	16.80	0.1770	2.80
8.77	0.2158	1.27	12.84	0.1812	1.18	16.99	0.1783	2.89
8.82	0.2157	1.26	13.03	0.1798	1.18	17.18	0.1692	3.02
9.02	0.2109	1.26	13.22	0.1828	1.25	17.37	0.1671	3.11
9.21	0.2057	1.22	13.40	0.1834	1.32	17.56	0.1668	3.20
9.59	0.1988	1.26	13.59	0.1821	1.39	17.75	0.1620	3.28
9.79	0.2028	0.89	13.78	0.1845	1.46	17.93	0.1585	3.38

DATA SET 1: EFFICIENCY DATA FOR THE RIGHT DETECTOR

1.0×Cs Energy Bias

Normalization Uncertainty 4.11%
Proton Bias Energy 2.00 ± 0.10 MeV

E_n	$\varepsilon(E_n)_{exp}$	$\Delta\varepsilon_{exp}$	E_n	$\varepsilon(E_n)_{exp}$	$\Delta\varepsilon_{exp}$	E_n	$\varepsilon(E_n)_{exp}$	$\Delta\varepsilon_{exp}$
2.04	0.0369	1.29	9.79	0.1788	0.90	14.16	0.1537	1.65
2.15	0.0585	1.67	9.98	0.1765	1.27	14.54	0.1489	1.87
2.26	0.0824	1.63	10.17	0.1755	0.87	14.73	0.1495	1.99
2.55	0.1392	1.83	10.36	0.1783	1.18	14.92	0.1465	2.10
2.93	0.1687	1.90	10.55	0.1766	1.18	15.11	0.1471	2.17
3.14	0.1984	1.79	10.74	0.1710	1.19	15.30	0.1476	2.24
3.39	0.2099	1.58	10.93	0.1693	1.19	15.48	0.1450	2.31
3.65	0.2201	1.20	11.32	0.1636	1.19	15.67	0.1451	2.38
3.94	0.2112	1.48	11.51	0.1625	1.19	15.86	0.1445	1.73
4.59	0.2311	1.33	11.70	0.1617	1.19	16.05	0.1469	1.78
5.31	0.2273	1.34	11.89	0.1595	1.19	16.24	0.1460	1.83
6.08	0.2184	1.32	12.08	0.1575	1.19	16.43	0.1486	1.88
6.86	0.2128	1.35	12.27	0.1615	1.19	16.62	0.1466	1.93
7.24	0.2062	1.11	12.46	0.1601	1.19	16.80	0.1477	1.98
7.61	0.2008	1.36	12.65	0.1584	1.19	16.99	0.1483	2.05
8.26	0.2029	1.43	12.84	0.1578	1.19	17.18	0.1443	2.15
8.77	0.1956	1.27	13.03	0.1552	1.19	17.37	0.1451	2.21
8.82	0.1951	1.27	13.22	0.1559	1.26	17.56	0.1458	2.27
9.02	0.1897	1.27	13.40	0.1550	1.33	17.75	0.1426	2.33
9.10	0.1973	1.20	13.59	0.1532	1.40	17.93	0.1398	3.40
9.21	0.1862	1.11	13.78	0.1535	1.47			
9.59	0.1783	1.28	13.97	0.1516	1.54			

DATA SET 1: EFFICIENCY DATA FOR THE RIGHT DETECTOR

2.0×Cs Energy Bias

Normalization Uncertainty 4.11%
Proton Bias Energy 3.10 ± 0.10 MeV

E_n	$\varepsilon(E_n)_{exp}$	$\Delta\varepsilon_{exp}$	E_n	$\varepsilon(E_n)_{exp}$	$\Delta\varepsilon_{exp}$	E_n	$\varepsilon(E_n)_{exp}$	$\Delta\varepsilon_{exp}$
3.14	0.0140	5.86	10.36	0.1531	1.19	14.54	0.1246	1.88
3.39	0.0382	2.76	10.55	0.1517	1.19	14.73	0.1251	1.99
3.65	0.0609	1.60	10.74	0.1474	1.19	14.92	0.1221	2.11
3.94	0.0869	1.73	10.93	0.1463	1.19	15.11	0.1222	2.18
4.59	0.1371	1.43	11.32	0.1416	1.19	15.30	0.1217	2.25
5.31	0.1572	1.41	11.51	0.1412	1.19	15.48	0.1190	2.32
6.08	0.1652	1.37	11.70	0.1408	1.19	15.67	0.1181	2.39
6.86	0.1688	1.40	11.89	0.1394	1.19	15.86	0.1166	1.74
7.24	0.1670	1.69	12.08	0.1371	1.19	16.05	0.1173	1.79
7.61	0.1599	1.41	12.27	0.1384	1.19	16.24	0.1155	1.84
8.26	0.1646	1.48	12.46	0.1378	1.19	16.43	0.1167	1.89
8.77	0.1610	1.30	12.65	0.1358	1.19	16.62	0.1143	1.94
8.82	0.1625	1.30	12.84	0.1351	1.19	16.80	0.1142	1.99
9.02	0.1597	1.30	13.03	0.1327	1.19	16.99	0.1133	2.06
9.10	0.1518	1.21	13.22	0.1324	1.27	17.18	0.1111	2.17
9.21	0.1553	1.15	13.40	0.1322	1.33	17.37	0.1103	2.22
9.59	0.1500	1.30	13.59	0.1306	1.40	17.56	0.1119	2.29
9.79	0.1533	0.91	13.78	0.1298	1.47	17.75	0.1098	2.35
9.98	0.1519	1.29	13.97	0.1282	1.55	17.93	0.1081	3.42
10.17	0.1504	0.88	14.16	0.1299	1.66			

DATA SET 1: EFFICIENCY DATA FOR THE RIGHT DETECTOR

3.0×Cs Energy Bias

Normalization Uncertainty 4.11%
Proton Bias Energy 4.00 ± 0.10 MeV

E_n	$\varepsilon(E_n)_{exp}$	$\Delta\varepsilon_{exp}$	E_n	$\varepsilon(E_n)_{exp}$	$\Delta\varepsilon_{exp}$	E_n	$\varepsilon(E_n)_{exp}$	$\Delta\varepsilon_{exp}$
3.94	0.0008	49.07	7.61	0.1277	1.71	9.59	0.1258	1.33
4.59	0.0387	2.29	8.26	0.1357	1.49	9.79	0.1305	0.93
5.31	0.0837	1.63	8.77	0.1333	1.32	9.98	0.1296	1.32
6.08	0.1118	1.47	8.82	0.1370	1.32	10.17	0.1277	1.32
6.86	0.1295	1.47	9.02	0.1357	1.32			
7.24	0.1309	1.79	9.21	0.1309	1.26			

DATA SET 1: EFFICIENCY DATA FOR THE RIGHT DETECTOR

4.0 × Cs Energy Bias

Normalization Uncertainty 4.11%
Proton Bias Energy 5.10 ± 0.10 MeV

E_n	$\varepsilon(E_n)_{exp}$	$\Delta\varepsilon_{exp}$	E_n	$\varepsilon(E_n)_{exp}$	$\Delta\varepsilon_{exp}$	E_n	$\varepsilon(E_n)_{exp}$	$\Delta\varepsilon_{exp}$
5.31	0.0118	3.72	10.93	0.1082	1.21	14.92	0.0983	2.12
6.08	0.0494	1.78	11.32	0.1064	1.21	15.11	0.0987	2.18
6.86	0.0805	1.62	11.51	0.1073	1.21	15.30	0.1004	2.25
7.24	0.0901	2.04	11.70	0.1079	1.20	15.48	0.0969	2.32
7.61	0.0918	1.56	11.89	0.1076	1.21	15.67	0.0959	2.39
8.26	0.1057	1.54	12.08	0.1062	1.21	15.86	0.0948	1.74
8.77	0.1074	1.37	12.27	0.1078	1.20	16.05	0.0951	1.79
8.82	0.1119	1.36	12.46	0.1079	1.20	16.24	0.0928	1.84
9.02	0.1129	1.35	12.65	0.1070	1.20	16.43	0.0933	1.89
9.10	0.1048	1.24	12.84	0.1071	1.20	16.62	0.0913	1.94
9.21	0.1164	1.18	13.03	0.1058	1.21	16.80	0.0907	2.00
9.59	0.1038	1.36	13.22	0.1058	1.28	16.99	0.0905	2.06
9.79	0.1094	0.95	13.40	0.1057	1.34	17.18	0.0880	2.19
9.98	0.1087	1.35	13.59	0.1051	1.41	17.37	0.0868	2.25
10.17	0.1081	0.90	13.78	0.1047	1.48	17.56	0.0884	2.31
10.36	0.1111	1.21	13.97	0.1037	1.56	17.75	0.0859	2.37
10.55	0.1100	1.21	14.16	0.1047	1.66	17.93	0.0861	3.45
10.74	0.1083	1.21	14.54	0.1006	1.89			

DATA SET 1: EFFICIENCY DATA FOR THE RIGHT DETECTOR

7.0 × Cs Energy Bias

Normalization Uncertainty 4.11%
Proton Bias Energy 8.20 ± 0.10 MeV

E_n	$\varepsilon(E_n)_{exp}$	$\Delta\varepsilon_{exp}$	E_n	$\varepsilon(E_n)_{exp}$	$\Delta\varepsilon_{exp}$	E_n	$\varepsilon(E_n)_{exp}$	$\Delta\varepsilon_{exp}$
10.17	0.0432	1.30	13.03	0.0648	1.24	15.86	0.0689	2.47
10.36	0.0452	1.29	13.22	0.0661	1.31	16.05	0.0684	2.54
10.55	0.0473	1.28	13.40	0.0671	1.37	16.24	0.0671	2.61
10.74	0.0500	1.28	13.59	0.0675	1.44	16.43	0.0668	2.69
10.93	0.0523	1.27	13.78	0.0681	1.51	16.62	0.0676	2.75
11.32	0.0567	1.26	13.97	0.0678	1.58	16.80	0.0677	2.82
11.51	0.0582	1.26	14.16	0.0684	1.69	16.99	0.0675	2.93
11.70	0.0596	1.25	14.54	0.0683	1.90	17.18	0.0650	3.13
11.89	0.0605	1.25	14.73	0.0681	2.02	17.37	0.0647	3.22
12.08	0.0601	1.25	14.92	0.0691	2.13	17.56	0.0657	3.31
12.27	0.0620	1.25	15.11	0.0687	2.20	17.75	0.0645	3.39
12.46	0.0633	1.24	15.30	0.0693	2.27	17.93	0.0633	3.49
12.65	0.0638	1.24	15.48	0.0684	2.34			
12.84	0.0643	1.25	15.67	0.0690	2.40			

DATA SET 2: EFFICIENCY DATA FOR THE RIGHT DETECTOR

0.50×Cs Energy Bias

Normalization Uncertainty 3.40%
Proton Bias Energy 1.30 ± 0.15 MeV

E_n	$\varepsilon(E_n)_{exp}$	$\Delta\varepsilon_{exp}$	E_n	$\varepsilon(E_n)_{exp}$	$\Delta\varepsilon_{exp}$	E_n	$\varepsilon(E_n)_{exp}$	$\Delta\varepsilon_{exp}$
7.26	0.2356	1.18	10.17	0.2071	1.21	13.03	0.1844	0.85
8.24	0.2211	0.60	11.13	0.1929	0.84	13.97	0.1788	1.10
9.21	0.2094	1.21	12.08	0.1877	1.21			

DATA SET 2: EFFICIENCY DATA FOR THE RIGHT DETECTOR

1.0×Cs Energy Bias

Normalization Uncertainty 3.40%
Proton Bias Energy 2.00 ± 0.10 MeV

E_n	$\varepsilon(E_n)_{exp}$	$\Delta\varepsilon_{exp}$	E_n	$\varepsilon(E_n)_{exp}$	$\Delta\varepsilon_{exp}$	E_n	$\varepsilon(E_n)_{exp}$	$\Delta\varepsilon_{exp}$
7.26	0.2061	1.19	10.17	0.1801	1.22	13.03	0.1565	0.86
8.24	0.1950	0.61	11.13	0.1703	0.85	13.97	0.1509	1.11
9.21	0.1889	1.22	12.08	0.1599	1.22			

DATA SET 2: EFFICIENCY DATA FOR THE RIGHT DETECTOR

2.0×Cs Energy Bias

Normalization Uncertainty 3.40%
Proton Bias Energy 3.10 ± 0.10 MeV

E_n	$\varepsilon(E_n)_{exp}$	$\Delta\varepsilon_{exp}$	E_n	$\varepsilon(E_n)_{exp}$	$\Delta\varepsilon_{exp}$	E_n	$\varepsilon(E_n)_{exp}$	$\Delta\varepsilon_{exp}$
7.26	0.1658	1.20	10.17	0.1541	1.23	13.03	0.1333	0.87
8.24	0.1580	0.61	11.13	0.1476	0.85	13.97	0.1275	1.11
9.21	0.1574	1.23	12.08	0.1389	1.23			

DATA SET 2: EFFICIENCY DATA FOR THE RIGHT DETECTOR

3.0×Cs Energy Bias

Normalization Uncertainty 3.40%
Proton Bias Energy 4.00 ± 0.10 MeV

E_n	$\varepsilon(E_n)_{exp}$	$\Delta\varepsilon_{exp}$	E_n	$\varepsilon(E_n)_{exp}$	$\Delta\varepsilon_{exp}$	E_n	$\varepsilon(E_n)_{exp}$	$\Delta\varepsilon_{exp}$
7.26	0.1305	1.21	10.17	0.1313	1.24	13.03	0.1193	0.88
8.24	0.1296	0.62	11.13	0.1282	0.86	13.97	0.1142	1.12
9.21	0.1319	1.25	12.08	0.1226	1.24			

DATA SET 2: EFFICIENCY DATA FOR THE RIGHT DETECTOR

4.0×Cs Energy Bias

Normalization Uncertainty 3.40%
Proton Bias Energy 5.10 ± 0.10 MeV

E_n	$\varepsilon(E_n)_{exp}$	$\Delta\varepsilon_{exp}$	E_n	$\varepsilon(E_n)_{exp}$	$\Delta\varepsilon_{exp}$	E_n	$\varepsilon(E_n)_{exp}$	$\Delta\varepsilon_{exp}$
7.26	0.0900	1.24	10.17	0.1097	1.26	13.03	0.1054	0.89
8.24	0.1011	0.64	11.13	0.1097	0.87	13.97	0.1018	1.13
9.21	0.1076	1.27	12.08	0.1065	1.25			

DATA SET 2: EFFICIENCY DATA FOR THE RIGHT DETECTOR

7.0×Cs Energy Bias

Normalization Uncertainty 3.40%
Proton Bias Energy 8.20 ± 0.10 MeV

E_n	$\varepsilon(E_n)_{exp}$	$\Delta\varepsilon_{exp}$	E_n	$\varepsilon(E_n)_{exp}$	$\Delta\varepsilon_{exp}$	E_n	$\varepsilon(E_n)_{exp}$	$\Delta\varepsilon_{exp}$
8.24	0.0028	1.71	11.13	0.0538	0.92	13.97	0.0660	1.16
9.21	0.0214	1.67	12.08	0.0589	1.33			
10.17	0.0391	1.44	13.03	0.0645	0.93			

DATA SET 1: EFFICIENCY DATA FOR THE LEFT DETECTOR

0.35×Cs Energy Bias

Normalization Uncertainty 4.11%
Proton Bias Energy 1.20 ± 0.15 MeV

E_n	$\varepsilon(E_n)_{exp}$	$\Delta\varepsilon_{exp}$	E_n	$\varepsilon(E_n)_{exp}$	$\Delta\varepsilon_{exp}$	E_n	$\varepsilon(E_n)_{exp}$	$\Delta\varepsilon_{exp}$
2.04	0.2555	1.47	4.59	0.2784	1.36	9.02	0.2015	1.28
2.15	0.2639	1.34	5.31	0.2595	1.32	9.21	0.1984	0.87
2.26	0.2657	1.36	6.08	0.2418	1.04	9.40	0.1940	1.28
2.55	0.2801	1.50	6.86	0.2269	1.39	9.59	0.1935	1.28
2.93	0.2691	1.98	7.61	0.2185	1.37	9.79	0.1937	1.28
3.14	0.2997	1.73	8.32	0.2081	1.35	9.98	0.1932	1.28
3.39	0.3023	1.63	8.77	0.2099	1.27			
3.94	0.2793	1.60	8.82	0.2075	1.28			

DATA SET 1: EFFICIENCY DATA FOR THE LEFT DETECTOR

1.0×Cs Energy Bias

Normalization Uncertainty 4.11%
Proton Bias Energy 2.03 ± 0.10 MeV

E_n	$\varepsilon(E_n)_{exp}$	$\Delta\varepsilon_{exp}$	E_n	$\varepsilon(E_n)_{exp}$	$\Delta\varepsilon_{exp}$	E_n	$\varepsilon(E_n)_{exp}$	$\Delta\varepsilon_{exp}$
2.04	0.0023	3.35	10.36	0.1632	1.30	14.54	0.1394	1.95
2.15	0.0397	1.92	10.55	0.1618	1.29	14.73	0.1381	2.07
2.26	0.0602	1.82	10.74	0.1592	1.30	14.92	0.1366	2.18
2.55	0.1119	1.99	10.93	0.1574	1.30	15.11	0.1356	2.35
2.93	0.1476	2.05	11.13	0.1548	1.30	15.30	0.1357	2.42
3.14	0.1830	1.84	11.32	0.1548	1.30	15.48	0.1354	2.47
3.39	0.2013	1.63	11.51	0.1517	1.30	15.67	0.1354	2.54
3.94	0.2020	1.47	11.70	0.1491	1.30	15.86	0.1363	2.60
4.59	0.2242	1.35	11.89	0.1501	1.30	16.05	0.1372	2.67
5.31	0.2172	1.37	12.08	0.1471	1.30	16.24	0.1400	2.72
6.08	0.2089	0.96	12.27	0.1472	1.30	16.43	0.1408	2.79
6.86	0.1976	1.39	12.46	0.1455	1.30	16.62	0.1424	2.85
7.61	0.1888	1.41	12.65	0.1449	1.30	16.80	0.1397	2.92
8.32	0.1829	1.40	12.84	0.1417	1.30	16.99	0.1415	3.00
8.77	0.1876	1.28	13.03	0.1395	1.31	17.18	0.1416	3.08
8.82	0.1829	1.30	13.22	0.1400	1.37	17.37	0.1392	3.18
9.02	0.1800	1.30	13.40	0.1398	1.43	17.56	0.1392	3.27
9.21	0.1783	0.88	13.59	0.1399	1.50	17.75	0.1379	3.35
9.40	0.1752	1.29	13.78	0.1391	1.58	17.93	0.1379	3.44
9.59	0.1739	1.29	13.97	0.1397	1.65	18.12	0.1380	3.53
9.79	0.1714	1.29	14.16	0.1403	1.75			
9.98	0.1686	1.30	14.35	0.1371	1.85			

DATA SET 1: EFFICIENCY DATA FOR THE LEFT DETECTOR

2.2 × Cs Energy Bias

Normalization Uncertainty 4.11%
Proton Bias Energy 3.20 ± 0.10 MeV

E_n	$\varepsilon(E_n)_{exp}$	$\Delta\varepsilon_{exp}$	E_n	$\varepsilon(E_n)_{exp}$	$\Delta\varepsilon_{exp}$	E_n	$\varepsilon(E_n)_{exp}$	$\Delta\varepsilon_{exp}$
3.14	0.0002	509.42	10.93	0.1344	1.32	14.73	0.1145	2.08
3.39	0.0140	6.48	11.13	0.1334	1.32	14.92	0.1092	2.20
3.94	0.0589	2.40	11.32	0.1326	1.32	15.11	0.1113	2.27
4.59	0.1137	1.64	11.51	0.1314	1.32	15.30	0.1124	2.33
5.31	0.1393	1.45	11.70	0.1312	1.32	15.48	0.1089	2.52
6.08	0.1511	1.15	11.89	0.1289	1.32	15.67	0.1089	2.59
6.86	0.1517	1.48	12.08	0.1261	1.32	15.86	0.1073	2.65
7.61	0.1457	1.46	12.27	0.1262	1.32	16.05	0.1059	2.72
8.32	0.1460	1.42	12.46	0.1249	1.32	16.24	0.1092	2.76
8.77	0.1499	1.31	12.65	0.1241	1.32	16.43	0.1086	2.84
8.82	0.1489	1.33	12.84	0.1229	1.33	16.62	0.1077	2.91
9.02	0.1449	1.33	13.03	0.1215	1.33	16.80	0.1055	2.97
9.21	0.1428	0.89	13.22	0.1174	1.39	16.99	0.1061	3.05
9.40	0.1416	1.33	13.40	0.1187	1.45	17.18	0.1055	3.13
9.59	0.1411	1.33	13.59	0.1180	1.52	17.37	0.1036	3.23
9.79	0.1411	1.32	13.78	0.1169	1.59	17.56	0.1036	3.32
9.98	0.1401	1.32	13.97	0.1166	1.66	17.75	0.1043	3.40
10.36	0.1373	1.32	14.16	0.1152	1.78	17.93	0.1035	3.45
10.55	0.1362	1.32	14.35	0.1162	1.88	18.12	0.1029	3.57
10.74	0.1348	1.32	14.54	0.1149	1.99			

DATA SET 1: EFFICIENCY DATA FOR THE LEFT DETECTOR

3.3 × Cs Energy Bias

Normalization Uncertainty 4.11%
Proton Bias Energy 4.40 ± 0.10 MeV

E_n	$\varepsilon(E_n)_{exp}$	$\Delta\varepsilon_{exp}$	E_n	$\varepsilon(E_n)_{exp}$	$\Delta\varepsilon_{exp}$	E_n	$\varepsilon(E_n)_{exp}$	$\Delta\varepsilon_{exp}$
4.59	0.0078	8.70	9.79	0.1145	1.36	12.46	0.1086	1.35
5.31	0.0467	1.95	10.36	0.1134	1.36	12.65	0.1076	1.35
6.08	0.0835	1.34	10.55	0.1130	1.36	12.84	0.1070	1.35
6.86	0.1038	1.60	10.74	0.1119	1.35	13.03	0.1062	1.35
7.61	0.1076	1.55	10.93	0.1121	1.35	13.22	0.1028	1.42
8.32	0.1146	1.48	11.13	0.1121	1.35	13.40	0.1048	1.48
8.77	0.1194	1.35	11.32	0.1120	1.35	13.59	0.1041	1.54
8.82	0.1183	1.37	11.51	0.1119	1.35	13.78	0.1035	1.61
9.02	0.1163	1.37	11.70	0.1123	1.35	13.97	0.1036	1.67
9.21	0.1152	0.91	11.89	0.1102	1.35	14.16	0.1023	1.79
9.40	0.1146	1.37	12.08	0.1089	1.35			
9.59	0.1143	1.36	12.27	0.1092	1.35			

DATA SET 1: EFFICIENCY DATA FOR THE LEFT DETECTOR

4.7 × Cs Energy Bias

Normalization Uncertainty 4.11%
Proton Bias Energy 5.80 ± 0.10 MeV

E_n	$\varepsilon(E_n)_{exp}$	$\Delta\varepsilon_{exp}$	E_n	$\varepsilon(E_n)_{exp}$	$\Delta\varepsilon_{exp}$	E_n	$\varepsilon(E_n)_{exp}$	$\Delta\varepsilon_{exp}$
6.08	0.0133	3.06	11.51	0.0929	1.38	14.92	0.0894	2.22
6.86	0.0414	2.21	11.70	0.0933	1.38	15.11	0.0880	2.30
7.61	0.0599	1.82	11.89	0.0920	1.38	15.30	0.0857	2.52
8.32	0.0780	1.61	12.08	0.0927	1.38	15.48	0.0854	2.59
8.77	0.0868	1.42	12.27	0.0926	1.38	15.67	0.0835	2.65
8.82	0.0868	1.45	12.46	0.0916	1.38	15.86	0.0829	2.71
9.02	0.0866	1.44	12.65	0.0919	1.38	16.05	0.0840	1.96
9.21	0.0876	0.94	12.84	0.0912	1.38	16.24	0.0830	2.01
9.40	0.0879	1.43	13.03	0.0912	1.38	16.43	0.0850	2.89
9.59	0.0891	1.42	13.22	0.0901	1.44	16.62	0.0846	2.96
9.79	0.0896	1.41	13.40	0.0880	1.51	16.80	0.0853	3.01
9.98	0.0906	1.41	13.59	0.0899	1.57	16.99	0.0819	3.09
10.36	0.0899	1.41	13.78	0.0906	1.63	17.18	0.0825	3.18
10.55	0.0906	1.40	13.97	0.0888	1.72	17.37	0.0815	3.26
10.74	0.0901	1.40	14.16	0.0904	1.82	17.56	0.0800	3.37
10.93	0.0910	1.39	14.35	0.0897	1.92	17.75	0.0797	3.45
11.13	0.0917	1.39	14.54	0.0856	2.02	17.93	0.0803	3.54
11.32	0.0925	1.39	14.73	0.0869	2.13	18.12	0.0807	3.62

DATA SET 1: EFFICIENCY DATA FOR THE LEFT DETECTOR

9.0 × Cs Energy Bias

Normalization Uncertainty 4.11%
Proton Bias Energy 10.3 ± 0.10 MeV

E_n	$\varepsilon(E_n)_{exp}$	$\Delta\varepsilon_{exp}$	E_n	$\varepsilon(E_n)_{exp}$	$\Delta\varepsilon_{exp}$	E_n	$\varepsilon(E_n)_{exp}$	$\Delta\varepsilon_{exp}$
10.36	0.0010	9.78	13.03	0.0323	1.73	15.67	0.0466	2.85
10.55	0.0023	5.88	13.22	0.0325	1.77	15.86	0.0465	2.89
10.74	0.0043	4.07	13.40	0.0357	1.78	16.05	0.0468	2.09
10.93	0.0064	3.31	13.59	0.0364	1.83	16.24	0.0471	2.12
11.13	0.0088	2.85	13.78	0.0376	1.87	16.43	0.0489	3.06
11.32	0.0118	2.51	13.97	0.0405	1.90	16.62	0.0496	3.11
11.51	0.0148	2.27	14.16	0.0406	2.01	16.80	0.0485	3.18
11.70	0.0177	2.12	14.35	0.0423	2.09	16.99	0.0496	3.24
11.89	0.0198	2.03	14.54	0.0432	2.18	17.18	0.0479	3.34
12.08	0.0226	1.94	14.73	0.0439	2.26	17.37	0.0486	3.42
12.27	0.0261	1.85	14.92	0.0431	2.37	17.56	0.0499	3.50
12.46	0.0270	1.83	15.11	0.0443	2.43	17.75	0.0497	3.58
12.65	0.0294	1.78	15.30	0.0459	2.48	17.93	0.0496	3.66
12.84	0.0307	1.76	15.48	0.0461	2.78	18.12	0.0493	3.75

DATA SET 2: EFFICIENCY DATA FOR THE LEFT DETECTOR

0.50×Cs Energy Bias

Normalization Uncertainty 3.40%
Proton Bias Energy 1.50 ± 0.15 MeV

E_n	$\varepsilon(E_n)_{exp}$	$\Delta\varepsilon_{exp}$	E_n	$\varepsilon(E_n)_{exp}$	$\Delta\varepsilon_{exp}$	E_n	$\varepsilon(E_n)_{exp}$	$\Delta\varepsilon_{exp}$
7.26	0.2115	1.19	10.17	0.1776	0.87	13.03	0.1603	0.87
8.24	0.1965	0.87	11.13	0.1702	1.23	13.97	0.1556	0.91
9.21	0.1796	0.71	12.08	0.1643	0.87			

DATA SET 2: EFFICIENCY DATA FOR THE LEFT DETECTOR

1.0×Cs Energy Bias

Normalization Uncertainty 3.40%
Proton Bias Energy 2.20 ± 0.15 MeV

E_n	$\varepsilon(E_n)_{exp}$	$\Delta\varepsilon_{exp}$	E_n	$\varepsilon(E_n)_{exp}$	$\Delta\varepsilon_{exp}$	E_n	$\varepsilon(E_n)_{exp}$	$\Delta\varepsilon_{exp}$
7.26	0.1893	1.20	10.17	0.1628	0.87	13.03	0.1403	0.88
8.24	0.1766	0.88	11.13	0.1543	1.23	13.97	0.1358	0.91
9.21	0.1651	0.72	12.08	0.1456	0.87			

DATA SET 2: EFFICIENCY DATA FOR THE LEFT DETECTOR

2.0×Cs Energy Bias

Normalization Uncertainty 3.40%
Proton Bias Energy 3.20 ± 0.15 MeV

E_n	$\varepsilon(E_n)_{exp}$	$\Delta\varepsilon_{exp}$	E_n	$\varepsilon(E_n)_{exp}$	$\Delta\varepsilon_{exp}$	E_n	$\varepsilon(E_n)_{exp}$	$\Delta\varepsilon_{exp}$
7.26	0.1552	1.21	10.17	0.1418	0.88	13.03	0.1221	0.89
8.24	0.1445	0.89	11.13	0.1364	1.24	13.97	0.1164	0.92
9.21	0.1397	0.72	12.08	0.1288	0.88			

DATA SET 2: EFFICIENCY DATA FOR THE LEFT DETECTOR

3.0 × Cs Energy Bias

Normalization Uncertainty 3.40%
Proton Bias Energy 4.20 ± 0.15 MeV

E_n	$\varepsilon(E_n)_{exp}$	$\Delta\varepsilon_{exp}$	E_n	$\varepsilon(E_n)_{exp}$	$\Delta\varepsilon_{exp}$	E_n	$\varepsilon(E_n)_{exp}$	$\Delta\varepsilon_{exp}$
7.26	0.1223	1.22	10.17	0.1213	0.89	13.03	0.1094	0.89
8.24	0.1192	0.91	11.13	0.1189	1.26	13.97	0.1050	0.92
9.21	0.1176	0.73	12.08	0.1145	0.89			

DATA SET 2: EFFICIENCY DATA FOR THE LEFT DETECTOR

4.0 × Cs Energy Bias

Normalization Uncertainty 3.40%
Proton Bias Energy 5.30 ± 0.15 MeV

E_n	$\varepsilon(E_n)_{exp}$	$\Delta\varepsilon_{exp}$	E_n	$\varepsilon(E_n)_{exp}$	$\Delta\varepsilon_{exp}$	E_n	$\varepsilon(E_n)_{exp}$	$\Delta\varepsilon_{exp}$
7.26	0.0829	1.26	10.17	0.1013	0.91	13.03	0.0967	0.90
8.24	0.0921	0.93	11.13	0.1013	1.27	13.97	0.0939	0.93
9.21	0.0957	0.75	12.08	0.0994	0.90			

DATA SET 2: EFFICIENCY DATA FOR THE LEFT DETECTOR

7.0 × Cs Energy Bias

Normalization Uncertainty 3.40%
Proton Bias Energy 8.23 ± 0.10 MeV

E_n	$\varepsilon(E_n)_{exp}$	$\Delta\varepsilon_{exp}$	E_n	$\varepsilon(E_n)_{exp}$	$\Delta\varepsilon_{exp}$	E_n	$\varepsilon(E_n)_{exp}$	$\Delta\varepsilon_{exp}$
8.24	0.0003	12.92	11.13	0.0413	1.44	13.97	0.0571	0.97
9.21	0.0108	1.25	12.08	0.0500	0.98			
10.17	0.0282	1.12	13.03	0.0545	0.97			

LIST OF REFERENCES

Allen 1977 — B.J. Allen, A.R. de L. Musgrove, J.W. Boldemen, and R.L. Macklin, "Valence Neutron Capture in ^{54}Fe," Nuclear Physics A283 (1977) 37-44.

Antolkovic 1983 — B. Antolkovic, I. Slaus, D. Plenkovic, P. Macq, and J.P. Meulders, "Study of the Reaction $^{12}C(n,3\alpha)n$ from Threshold to E_n = 35 MeV," Nuclear Physics A394 (1983) 87-108.

Batty 1968 — C.J. Batty, B.E. Bonner, E. Friedman, C. Tschalär, L.E. Williams, A.S. Clough, and J.B. Hunt, "Excitation of Isobaric Analogue States in (p,n) Reactions at 30 and 50 MeV and the Isospin Dependence of the Optical Model," Nuclear Physics A116 (1968) 643-672.

Becchetti 1969 — F.D. Becchetti, Jr., and G.W. Greenlees, "Nucleon-Nucleus Optical-Model Parameters; A > 40, E < 50 MeV," Physical Review 182 (1969) 1190-1209.

Beverly 1972 — W.B. Beverly, "Muse: A Multiple Scattering Effect Code for Infinite Slabs," Ballistic Research Laboratory Report BRL-1588 (1972).

Beyerle 1981 — A.G. Beyerle, "Double Differential Continuum Neutron Scattering Cross Sections in Iron and Nickel for Incident Energies of 7.5, 10, and 12 MeV," Ph.D. Dissertation, North Carolina State University, 1981.

Browne 1978 — E. Browne, J.M. Dairiki, R.E. Doebler, A.A. Shihab-Eldin, L.J. Jardine, J.K. Tuli, and A.B. Buyrn, Table of Isotopes, 7th ed., edited by C.M. Lederer and V.S. Shirley (John Wiley and Sons, Inc.; New York; 1978).

Bucher 1973 — W. Bucher, C. Hollandsworth, and R. Lamoreaux, "On The Measurement Of The Small-Angle Scattering Of Fast Neutrons," Nuclear Instruments And Methods 111 (1973) 237-249.

Bucher 1975a — W.P. Bucher and C.E. Hollandsworth, "Small-Angle Scattering of 7-14-MeV Neutrons by Pb and U," Physical Review Letters 35 (1975) 1419-1422.

Bucher 1975b — W.P. Bucher, C.E. Hollandsworth, and J.E. Youngblood, "Neutron Cross Sections for Small-Angle Elastic Scattering from Nitrogen and Oxygen," Ballistic Research Laboratory Report BRL-1795 (1975).

Byrd 1978 — R.B. Byrd, "Isospin in (p,n) Reactions Between Mirror Nuclei: The Lane Model and Comparisons between Polarizations and Analyzing Powers," Ph.D. Dissertation, Duke University, 1978.

Byrd 1983 — R.B. Byrd, "JANECOR," unpublished, and private communications, Duke University and Triangle Universities Nuclear Laboratory, Durham, North Carolina, 1983.

Christy 1973 — A. Christy and O. Häusser, "Quadrupole Moments of Nuclear Excited States Measured by the Reorientation Effect in Coulomb Excitation," Nuclear Data Tables A11 (1973) 281-98.

de Boer 1968 — J. de Boer and J. Eichler, "The Reorientation Effect," in Advances in Nuclear Physics (Plenum Press, New York, 1968) Vol. 1 1-65.

Delaroche 1976 — J.P. Delaroche, Ch. Lagrange, and J. Salvy, "The Optical Model with Particular Consideration of the Coupled-Channel Optical Model," Nuclear Theory in Neutron Nuclear Data Evaluation (Vienna: IAEA, 1976) Vol. 1 251-312.

Delaroche 1982 — J.P. Delaroche, S.M. El-Kadi, P.P Guss, C.E. Floyd, and R.L. Walter, "Elastic and Inelastic Scattering of Neutrons from ^{54,56}Fe and ^{63,65}Cu (II). Scattering and nuclear structure effects from coupled channels calculations," Nuclear Physics A390 (1982) 541-560.

Delaroche 1983 — J.P. Delaroche, C.E. Floyd, P.P Guss, R.C. Byrd, K. Murphy, G. Tungate, and R.L. Walter, "Complex Spin-Orbit Potential for $^{208}Pb(n,n)^{208}Pb$ at 10 MeV," Physical Review C28 (1983) 1410-1413.

Dietze 1982 — G. Dietze and H. Klein, "NRESP4 and NEFF4 Monte Carlo Codes for the Calculation of Neutron Response Functions and Detection Efficiencies for NE-213 Scintillator Detectors," Physikalisch-Technische Bundesanstalt Report ND-22 (1982).

Drosg 1972 — M. Drosg, "Accurate Measurement of the Counting Efficiency of a NE-213 Neutron Detector between 2 and 26 MeV," Nuclear Instruments And Methods 105 (1972) 573-584.

Drosg 1978 — M. Drosg, "Unified Absolute Differential Cross Sections for Neutron Production by the Hydrogen Isotopes for Charged-Particle Energies Between 6 and 17 MeV," Nuclear Science and Engineering 67 (1978) 190-220.

El-Kadi 1981 — S.M. El-Kadi, "Neutron Elastic And Inelastic Scattering Studies On ^{54}Fe, ^{56}Fe, ^{63}Cu, And ^{65}Cu," Ph.D. Dissertation, Duke University, 1981.

El-Kadi 1982 — S.M. El-Kadi, C.E. Nelson, F.O Purser, R.L. Walter, A. Beyerle, C.R. Gould, and L.W. Seagondollar, "Elastic and Inelastic Scattering of Neutrons from $^{54,56}Fe$ and $^{63,65}Cu$ (I). Measurements from 8 to 14 MeV and a Spherical Optical Model Analysis," Nuclear Physics A390 (1982) 509-540.

ENDF/B-V — Tabulations issued in July of 1979 of neutron scattering data and evaluations for energies upto 20 MeV from the National Neutron Cross Section Center located at Brookhaven National Laboratory, Upton, New York.

Etemad 1973 — M.A. Etemad, "Neutron Elastic Scattering Measurements At 7.0 MeV," Aktiebolaget Atomenergi Report AE-482 (1973).

Ferrer 1977 — J.C. Ferrer, J.D. Carlson, and J. Rapaport, "Neutron Elastic Scattering at 11 MeV and the Isospin Dependence of the Neutron-Nucleus Optical Potential," Nuclear Physics A275 (1977) 325-341.

Floyd 1981 — C.E. Floyd, Jr., "Scattering of Polarized Fast Neutrons from ^{9}Be, ^{54}Fe, ^{65}Cu, and ^{208}Pb: The Determination of the Spin-Orbit Interaction," Ph.D. Dissertation, Duke University, 1981.

Floyd 1983 — C.E Floyd, P.P Guss, R.C. Byrd, K. Murphy, R.L. Walter, and J.P. Delaroche, "Spin-Orbit Potential Properties Derived from Measurements of Analyzing Powers for Neutron Scattering from ^{54}Fe and ^{65}Cu," Physical Review C28 (1983) 1498-1503.

Foster 1971 — D.G. Foster, Jr., and D.W. Glasgow, "Neutron Total Cross Sections, 2.5-15 MeV. I. Experimental," Physical Review C3 (1971) 576-603.

Fulmer 1962 — C.B. Fulmer, "Elastic Scattering of Protons by Single Isotopes," Physical Review 125 (1962) 631-638.

Gammel 1963 — J.L. Gammel, "The n-p Total and Differential Cross Sections in the Energy Range 0-40 MeV," in Fast Neutron Physics Part II: Experiments and Theory, edited by J.B. Marion and J.L. Fowler (Interscience Publishers, New York, 1963) 4 2185-2226.

Garber 1976 — D.I. Garber and R.R. Kinsey, "Neutron Cross Sections: Curves," Brookhaven National Laboratory Report BNL-325 2 (1976).

Glasgow 1976 — D.W. Glasgow, F.O. Purser, H. Hogue, J.C. Clement, K. Stelzer, G. Mack, J.R. Boyce, D.H. Epperson, S.G. Buccino, P.W. Lisowski, S.G. Glendinning, E.G. Bilpuch, H.W. Newson, and C.R. Gould, "Differential Elastic and Inelastic Scattering of 9- to 15-MeV Neutrons from Carbon," Nuclear Science and Engineering 61 (1976) 521-533.

Glendinning 1980 — S.G. Glendinning, "Elastic and Inelastic Neutron Scattering Cross Sections for ^{10}B, ^{11}B, and ^{16}O," Ph.D. Dissertation, Duke University, 1980.

Guss 1982a — P.P Guss, "Elastic and Inelastic Neutron Scattering Cross Sections and Analyzing Powers for ^{58}Ni, ^{60}Ni, ^{116}Sn, and ^{120}Sn," Ph.D. Dissertation, Duke University, 1982.

Guss 1982b — P.P Guss, C.E. Floyd, K. Murphy, C.R. Howell, R.S. Pedroni, G.M. Honoré, H.G. Pfützner, G. Tungate, R.C. Byrd, R.L. Walter, and J.P. Delaroche, "Spin-Orbit Deformations Deduced from Analyzing Powers for Inelastic Neutron Scattering from ^{54}Fe, ^{56}Fe, ^{58}Ni, ^{60}Ni, ^{120}Sn, and ^{208}Pb," Physical Review C25 (1982) 2854-2857.

Guss 1985 — P.P. Guss, R.C. Byrd, C.E. Floyd, C.R. Howell, K. Murphy, G. Tungate, R.S. Pedroni, and R.L. Walter, "Cross Sections and Analyzing Powers for Fast-Neutron Scattering to the Ground and First Excited States of ^{58}Ni and ^{60}Ni," Nuclear Physics A438 (1985) 187-211.

Guss 1986 — P.P. Guss et al. to be published 1986.

Hansen 1985 — L.F. Hansen, F.S. Dietrich, B.A. Pohl, C.H. Poppe, and C. Wong, "Test of Microscopic Optical Model Potentials for Neutron Elastic Scattering at 14.6 MeV Over a Wide Mass Range," Physical Review C31 (1985) 111-119.

Hodgson 1971 — P.E. Hodgson, Nuclear Reactions and Nuclear Structure), (Clarendon Press, Oxford, 1971).

Hogue 1977a — H.H. Hogue, "Elastic and Inelastic Scattering of Fast Neutrons by 6LI, ^{7}Li, ^{9}Be, and ^{12}C," Ph.D. Dissertation, Duke University, 1977.

Hogue 1977b — H.H. Hogue, "EFFIGY" and various notes, unpublished, and private communications, Duke University and Triangle Universities Nuclear Laboratory, Durham, North Carolina, 1977-82.

Holmqvist 1971 — B. Holmqvist and T. Wiedling, "Optical Model Analyses of Experimental Fast Neutron Elastic Scattering Data," Aktiebolaget Atomenergi Report AE-430 (1971).

Honoré 1983 — G.M. Honoré and R.C. Byrd, "Jane User's Manual," unpublished, Duke University and Triangle Universities Nuclear Laboratory, Durham, North Carolina, 1983.

Honoré 1986a — G.M. Honoré, "Neutron Scattering Cross Section and Analyzing Power Measurements for ^{40}Ca and ^{89}Y and Comprehensive Optical Model Analyses," Ph.D. Dissertation, Duke University, 1986,

Honoré 1986b — G.M. Honoré, W. Tornow, C.R. Howell, R.S. Pedroni, R.C. Byrd, R.L. Walter, and J.P. Delaroche, "Coupled-Channel Analysis of Nucleon Scattering from ^{40}Ca up to 80 MeV," Physical Review C33 (1986) 1129-1140.

Hopkins 1971 — J.C. Hopkins and G. Breit, "The ^{1}H(n,n)^{1}H Scattering Observables Required for High-Precision Fast-Neutron Measurements," Nuclear Data Tables A9 (1971) 137-145.

Howell 1984 — C.R. Howell, "Neutron Scattering from ^{28}Si and ^{32}S: Cross Sections and Analyzing Powers from 8 to 40 MeV," Ph.D. Dissertation, Duke University, 1984.

Jeukenne 1976 — J.-P. Jeukenne, A. Lejeune, and C. Mahaux, "Many-Body Theory of Nuclear Matter," Physics Reports (Section C of Physics Letters) 25C (1976) 83-174.

Jeukenne 1977 — J.-P. Jeukenne, A. Lejeune, and C. Mahaux, "Optical-Model Potential in Finite Nuclei from Reid's Hard Core Interaction," Physical Review C16 (1977) 80-96.

Kinney 1970 — W.E. Kinney, "Finite-Sample Corrections to Neutron Scattering Data," Nuclear Instruments and Methods 83 (1970) 15-28.

Lagrange 1982 — Ch. Lagrange and A. Lejeune, "Phenomenological and Microscopic Optical Model Analyses of the Interaction of Low-Energy Nucleons with ^{93}Nb," Physical Review C25 (1982) 2273-2291.

Larson 1980 — D.C. Larson, D.M. Hetrick, and J.A. Harvey, "Comparison of the Neutron Total Cross Section Measurements with Optical Model Predictions from 2 to 80 MeV," Bulletin of the American Physical Society 25 (1980) 543; and a private communication to R.L. Walter.

LeVine 1981 — M.J. LeVine, E.K. Warburton, and D. Schwalm, "Static Quadrupole Moments for the 2^+ States of ^{54,56,58}Fe," Physical Review C23 (1981) 244-252.

Lisowski 1973 — P.W. Lisowski, "The Transfer Polarization of the D(d,n)^{3}He Reaction and the Scattering of Polarized Neutrons from ^{4}He and ^{3}He," Ph.D. Dissertation, Duke University, 1973.

Lisowski 1975 — P.W. Lisowski, R.L. Walter, C.E. Busch, and T.B. Clegg, "Polarization Transfer in the ^{2}H($\vec{d}$,$\vec{n}$)^{3}He Reaction at $\theta = 0^\circ$," Nuclear Physics A242 (1975) 298-308.

Luttinger 1961 — J.M. Luttinger, "Fermi Surface and Some Simple Equilibrium Properties of a System of Interacting Fermions," Physical Review 121 (1961) 942-949.

Mahaux 1982 — C. Mahaux and H. Ngo, "Polarization and Correlation Contributions to the Shell-Model Potential in ^{40}Ca and ^{208}Pb," Nuclear Physics A578 (1982) 205-236.

Marion 1968 — J.B. Marion and F.C. Young, Nuclear Reaction Analysis: Graphs and Tables, (North-Holland, Amsterdam, 1968), pp. 134-135.

Mellema 1983a — S.H. Mellema, "Microscopic and Collective Model Analysis of Nucleon Scattering from ^{54,56}Fe," Ph.D. Dissertation, Ohio University, 1983.

Mellema 1983b — S.H. Mellema, R.W. Finlay, F.S. Dietrich, and F. Petrovich, "Microscopic and Conventional Optical Model Analysis of Fast Neutron Scattering from ^{54,56}Fe," Physical Review C28 (1983) 2267-2277.

Mughabghab 1973 — S.F. Mughabghab and D.I. Garber, "Neutron Cross Sections: Resonance Parameters," Brookhaven National Laboratory Report BNL-325 1 (1973).

Ohlsen 1973 — G.G. Ohlsen and P.W. Keaton, Jr., "Techniques for Measurement of Spin-$\frac{1}{2}$ and Spin-1 Polarization and Analyzing Tensors," Nuclear Instruments And Methods 109 (1973) 41-59.

Pedroni 1984 — R.S. Pedroni, "EFFIGY15" and "EFFIGY15 Manual," unpublished, Duke University and Triangle Universities Nuclear Laboratory, Durham, North Carolina, 1984.

Perey 1983 — C.M. Perey, J.A. Harvey, R.L. Macklin, F.G. Perey, and R.R. Winters, "Resonance Parameters of ^{60}Ni+n from Measurements of Transmission and Capture Yields from 1 to 450 KeV," Physical Review C27 (1983) 2556-2586.

Rapaport 1979 — J. Rapaport, V. Kulkarni, and R.W. Finlay, "A Global Optical-Model Analysis of Neutron Scattering Data," Nuclear Physics A330 (1979) 15-28.

Raynal 1972 — J. Raynal, "Spin-Orbit Interaction in Inelastic Nucleon Scattering," in The Structure of Nuclei, IAEA Report Number IAEA-SMR-8/8 (Vienna, 1972) pp.75-116.

Raynal 1979 — J. Raynal, Private communication to R.L. Walter; see also Raynal 1972.

Rosen 1965 — L. Rosen, J.G. Beery, A.S. Goldhaber, and E.H. Auerbach, "Elastic Scattering of 10.5- and 14.5-MeV Polarized Protons from Nuclei and the Optical Model Potential at Intermediate Energies," Annals of Physics 34 (1965) 96-152.

Satchler 1980 — G.R. Satchler, Introduction to Nuclear Reactions, (John Wiley and Sons, New York,1980).

Satchler 1983 — G.R. Satchler, Direct Nuclear Reactions, (Clarendon Press, Oxford, 1983).

Schwandt 1982 — P. Schwandt, H.O. Meyer, W.W. Jacobs, A.D. Bacher, S.E. Vigdor, M.D. Kaitchuck, and T.R. Donoghue, "Analyzing Power of Proton-Nucleus Elastic Scattering between 80 and 180 MeV," Physical Review C26 (1982) 55-64.

Serber 1947 — R. Serber, "The Production of High Energy Neutrons by Stripping," Physical Review 72 (1947) 1008-1016.

Sheldon 1981 — Private communication to R.L. Walter.

Smith 1984 — A.B. Smith, P.T. Guenther, and J.F. Whalen, "The Optical Model of Few-MeV Neutron Elastic Scattering from Z = 39 to 51 Targets," Nuclear Physics A415 (1984) 1-29.

Tamura 1965 — T. Tamura, "Analyses of the Scattering of Nuclear Particles by Collective Nuclei in Terms of the Coupled-Channel Calculation," Reviews of Modern Physics 37 (1965) 679-708.

Walter 1985 — R.L. Walter and P.P Guss, "A Global Optical Model for Neutron Scattering for A $\geq$ 3 and 10 MeV $\leq$ E $\leq$ 80 MeV," in Nuclear Data for Basic and Applied Science, (Santa Fe 1985) in press.

Winters 1985 — R.R. Winters, C.H. Johnson, and A.D. MacKellar, "Optical Model for Low-Energy neutrons on ^{60}Ni," Physical Review C31 (1985) 384-391.

Wick 1949 — G.C. Wick, "A Theorem on Cross Sections," Physical Review 75 (1949) 1459-1460.

Wong 1972 — C. Wong, J.D. Anderson, J.W. McClure, B.A. Pohl, and J.J. Wesolowski, "Measurements and Optical-Model Analyses of Quasielastic (p,n) Reactions," Physical Review C5 (1972) 158-163.

Woye 1980 — E. Woye and W. Tornow, "JANE," unpublished, Physikalisches Institut der Universität Tübingen, Tübingen, West Germany and Duke University and Triangle Universities Nuclear Laboratory, Durham, North Carolina, 1980.

Yamanouti 1980 — Y. Yamanouti, J. Rapaport, S.M. Grimes, V. Kulkarni, R.W. Finlay, D. Bainum, P. Grabmayr, and G. Randers-Pehrson, "Elastic and Inelastic Scattering of 24 MeV Neutrons from Even Isotopes of Ni," Nuclear Cross Sections for Technology: Proceedings of the International Conference, edited by J.L. Fowler, C.H. Johnson, and C.D. Bowman (U.S. Government Printing Office; Washington, D.C.; 1980) (NBS Special Publication 594) 146-149.

BIOGRAPHY

Ronald Scott Pedroni

Born:	January 30, 1956
	Jacksonville, Florida
Education:	Jacksonville University, B.A. 1978
Positions:	Teaching Assistant, Duke University 1978-79
	Research Assistant, Duke University 1979-86
Honorary Societies:	Phi Kappa Phi, Sigma Pi Sigma
Professional Societies:	American Physical Society

PUBLICATIONS:

1. "Elastic and Inelastic Neutron Cross Sections for Boron-10 and Boron-11," S.G. Glendinning, S. El-Kadi, C.E. Nelson, R.S. Pedroni, F.O. Purser, R.L. Walter, A.G. Beyerle, C.R. Gould, L.W. Seagondollar and P. Thambidurai, Nuclear Science and Engineering 80 (1982) 256-262.

2. "Neutron Elastic and Inelastic Scattering Cross Sections for Carbon-13 Between 10 and 18 MeV," J.H. Davé, C.R. Gould, L.W. Seagondollar, C.R. Howell, R.S. Pedroni, F.O. Purser and R.L. Walter, Nuclear Science and Engineering 80 (1982) 388-392.

3. "Analyzing Power Measurements for $^{2}H(\vec{n},n)^{2}H$ Scattering at 10 MeV Compared to Few-Nucleon Calculations and Data for $^{2}H(\vec{p},p)^{2}H$ Scattering," W. Tornow, C.R. Howell, R.C. Byrd, R.S. Pedroni and R.L. Walter, Physical Review Letters 49 (1982) 312-315.

4. "Spin-Orbit Deformations Deduced from Analyzing Powers for Inelastic Neutron Scattering from ^{54}Fe, ^{56}Fe, ^{58}Ni, ^{60}Ni, ^{120}Sn, and ^{208}Pb," P.P. Guss, C.E. Floyd, K. Murphy, C.R. Howell, R.S. Pedroni, G.M. Honoré, H.G. Pfützner, G. Tungate, R.C. Byrd, R.L. Walter and J.P. Delaroche, Physical Review C25 (1982) 2854-2857.

5. "Measurements of Analyzing Power for $^{2}H(\vec{n},n)^{2}H$ Scattering at 14.1 MeV and Comparisons to $^{2}H(\vec{p},p)^{2}H$," W. Tornow, R.C. Byrd, C.R. Howell, R.S. Pedroni and R.L. Walter, Physical Review C27 (1983) 2439-2442.

6. "Cross Sections and Analyzing Powers for Fast-Neutron Scattering to the Ground and First Excited States of ^{58}Ni and ^{60}Ni," P.P. Guss, R.C. Byrd, C.E. Floyd, C.R. Howell, K. Murphy, G. Tungate, R.S. Pedroni, R.L. Walter, J.P. Delaroche and T.B. Clegg, Nuclear Physics A438 (1985) 187-211.

ABSTRACTS:

1. "Differential Cross Sections and Analyzing Powers for the Elastic Scattering of Neutrons from ^{93}Nb," R.S. Pedroni, G.M. Honoré, C.R. Howell, P.P. Guss, K. Murphy, R.C. Byrd, G. Tungate and R.L. Walter, Bulletin of the American Physical Society 27 (1982) 722.

2. "Differential Cross Section and Analyzing Power for the Scattering of 17MeV Neutrons from ^{54}Fe and ^{58}Ni," R.S. Pedroni, C.R. Howell, G.M. Honoré, H.G. Pfützner, M.L. Roberts, R.C. Byrd and R.L. Walter, Bulletin of the American Physical Society 28 (1983) 998.

3. "Analyzing Powers for the Inelastic Scattering of Neutrons from ^{54,56}Fe and ^{58,60}Ni," R.S. Pedroni, R.C. Byrd, J.P. Delaroche, P.P Guss, G.M. Honoré, C.R. Howell, H.G. Pfützner, G. Tungate, and R.L. Walter, Bulletin of the American Physical Society 30 (1985) 797.

CO-AUTHORED ABSTRACTS:

1. "Neutron Elastic and Inelastic Scattering from ^{63}Cu, ^{65}Cu, ^{54}Fe and ^{56}Fe Between 8 and 14 MeV," S. El-Kadi, A. Beyerle, C. Gould, A. McDermott, R. Pedroni, P. Thambidurai, C.E. Nelson, F.O. Purser, W. Seagondollar and R.L. Walter, Bulletin of the American Physical Society 24 (1979) 866.

2. "Neutron Scattering Analyzing Powers and Cross Sections for Nickel," P.P Guss, C.E. Floyd, G. Tungate, R. Pedroni, R.C. Byrd, J.-P. Delaroche, T.B. Clegg and R.L. Walter, Bulletin of the American Physical Society 26 (1981) 623.

3. "Neutron Elastic Scattering from 1P-Shell Nuclei Between 10-15 MeV," J.H. Davé, C.R. Gould, L.W. Seagondollar, S.G. Glendenning, C.R. Howell, R.S. Pedroni, F.O. Purser and R.L. Walter, ibid., p. 551.

4. "Neutron Scattering from ^{116,120}Sn," P.P. Guss, G. Tungate, C.E. Floyd, R. Pedroni, K. Murphy, R.C. Byrd, R.L. Walter, T.B. Clegg and J.P. Delaroche, ibid., p. 1139.

5. "Scattering of 10-MeV Polarized Neutrons from Deuterons," W. Tornow, C.R. Howell, R.S. Pedroni, G.M. Honoré, R.C. Byrd and R.L. Walter, Bulletin of the American Physical Society 27 (1982) 543.

6. "Spin-Orbit Deformations Deduced from Analyzing Powers for Inelastic Neutron Scattering from ^{54}Fe, ^{56}Fe, ^{58}Ni, ^{60}Ni, ^{120}Sn and ^{208}Pb," P.P. Guss, C.E. Floyd, K. Murphy, C.R. Howell, R.S. Pedroni, G.M. Honoré, H.G. Pfützner, G. Tungate, R.C. Byrd, R.L. Walter and J.P. Delaroche, ibid., p. 542.

7. "Analyzing Power and Differential Cross Section Measurements for Neutron Elastic and Inelastic Scattering from Silicon," C.R. Howell, R.S. Pedroni, G.M. Honoré, K. Murphy, R.C. Byrd, G. Tungate and R.L. Walter, ibid., p. 722.

8. "The Scattering of Neutrons from Deuterons at 14 MeV," W. Tornow, R.C. Byrd, C.R. Howell, G.M. Honoré, R.S. Pedroni and R.L. Walter, ibid., p. 700.

9. "Scattering of 17-MeV Polarized Neutrons," C.R Howell, R.S. Pedroni, G.M. Honoré, H.G. Pfützner, R.C. Byrd and R.L. Walter, Bulletin of the American Physical Society 28 (1983) 736.

10. "Elastic and Inelastic Scattering of Neutrons at Small Angles," R.E. Anderson, C.R. Gould, B.C. Karp, K.E. Nash, R.S. Pedroni, H.G. Pfützner and R.L. Walter, ibid., p. 648.

11. "Differential Cross Sections and Analyzing Powers for the Elastic Scattering of Neutrons from ^{89}Y," G.M. Honoré, R.S. Pedroni, C.R. Howell, H.G. Pfützner, P.P. Guss, K. Murphy, R.C. Byrd, G. Tungate and R.L. Walter, Bulletin of the American Physical Society ibid., p. 736.

12. "Analyzing Powers and Differential Cross Sections for Elastic and Inelastic Neutron Scattering from Silicon," C.R. Howell, R.S. Pedroni, G.M. Honoré, H.G. Pfützner, R.C. Byrd and R.L. Walter, Bulletin of the American Physical Society 29 (1984) 637.

13. "Differential Cross Sections and Analyzing Powers for the Scattering of Neutrons from Calcium," G.M. Honoré, C.R. Howell, R.S. Pedroni, H.G. Pfützner, R.C. Byrd, R.L. Walter, J.P. Delaroche and W. Tornow, ibid., p. 638.

14. "Neutron Scattering from Sulfur Between 8 and 40 MeV," C.R. Howell, R.S. Pedroni, G.M. Honoré, H.G. Pfützner, R.C. Byrd and R.L. Walter, ibid., p. 1037.